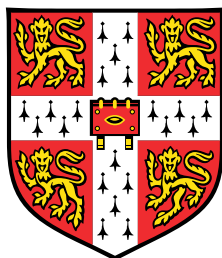


Investigating the atmospheric composition and climate response to mitigation: a methane emissions-driven approach



Zofia Staniaszek

Department of Chemistry
University of Cambridge

This thesis is submitted for the degree of
Doctor of Philosophy

Selwyn College

August 2023

Declaration

This thesis is the result of my own work and includes nothing which is the outcome of work done in collaboration except as declared in the Acknowledgements and specified in the text. I further state that no substantial part of my thesis has already been submitted, or, is being concurrently submitted for any such degree, diploma or other qualification at the University of Cambridge or any other University or similar institution except as declared in the Preface and specified in the text. It does not exceed the prescribed word limit for the relevant Degree Committee.

Zofia Staniaszek

Acknowledgements

Firstly, I'd like to thank my supervisors, Prof Alex Archibald and Dr Paul Griffiths for their invaluable guidance, feedback and support throughout my PhD. Thank you for your generosity with your time, adapting your support to my needs, especially through lockdowns and changing working patterns. I'm grateful to Alex for his active role in leading and normalising conversations around mental health in the group.

Special thanks to Dr Gerd Folberth and Dr Fiona O'Connor for developing and sharing the methane emissions-driven configuration of UKESM1 that underpins this work, and for our collaborations throughout my PhD. Dr Luke Abraham has been very generous in his help with a range of issues. Thanks to Dr Steve Turnock and Dr Chris Smith for their advice as part of the Methane Pledge project.

My PhD was funded as part of the NERC C-CLEAR doctoral training programme. I'm thankful to have had the funding to attend training and conferences throughout my PhD. Thanks to Kathleen and my DTP cohort for all the support right at the beginning.

Thank you to everyone in Union Road and especially the G6 crew - I'm so grateful to have made friendships that will last beyond the PhD. To James, Matt and Johnny, thanks for all of your help in the early stages of my PhD, and for managing to somehow avoid hitting me with the tennis ball (iykyk). Michelle, Seb and Lorrie, thanks for being such great company in the office - I'm so glad we managed to fulfil the office rearrangement of our dreams. Finally, thanks so much to Lorrie, Print, Megan, May and Selena for keeping me company in the last few months of writing up.

The last few years have been pretty rough, but in difficult moments it genuinely helped me to think about writing these acknowledgements, and think of all the people I am so grateful to have in my life.

I wouldn't have started, continued, or finished this PhD without CUDT and the dance community in Cambridge. To all of my previous dance partners (and successful conversion to friends): the huge number of hours I've spent training with you in freezing badminton courts, boiling squash courts and everything in between have been the best

times. Anjali, we've grown so much since Beginners, thanks for sticking around for the whole time! Carrie, thanks for being equally technique-obsessed and for all of our endless hours of training and same-sex wins! And June, for continuing our streak, getting us to the A team and Inter final at IVDA and so much more. Thank you both for making the best dance thruple anyone could wish for, for all your kindness and understanding in back pain times and for helping me get through it. During a PhD, not many people cheer and give you a hi-five when you get something right - but David Mallabone does in dance lessons. Usually my favourite hour of the week, they've brought me so much joy. Thank you for challenging me and teaching me how to become a better dancer, and the unwavering encouragement throughout my time here. To all the CUDT dancers over the years who have made training and competitions so fun - there are too many of you to name but I appreciate all of you! Finally, thanks to all of the XS dancers for welcoming me into the XS family in the last year.

To all of the Matts Saints/Canada squad, I'm so grateful to call you my friends. Thank you for all the laughs, lockdown dinners, celebrations, as well as being there for the bad times with all the check-ins, chats, hugs and picking me up off the floor (metaphorically and literally) when I was down. Jack, thanks for moving back to Cambridge so we could share some more life crises. Ben, I'm so glad we had each other for company in our semi non-functional lockdown times. I don't know what I would do without all our chats, cute whimsical times and memes. Will, thanks for all the fun, kindness and support over the years.

I've very grateful to have access to the University Counselling Service and the DRC which have helped me to manage my mental and physical health. My incredible mentor Elizabeth has taught me so much. Thank you to Colleen, my physio, for understanding my needs and for helping me improve and manage. Thanks to the online disability community (and meme pages) for teaching me so much and helping me to feel less alone with my health issues.

To my family, especially Emi and Mama, there are too many things to mention here - thanks for always being there for me. More specifically, thanks to Mama for your help with proof-reading this thesis.

Publications

Staniaszek, Zosia, Paul T Griffiths, Gerd A Folberth, Fiona M O'Connor, N Luke Abraham, and Alexander T Archibald (2022). “The role of future anthropogenic methane emissions in air quality and climate”. In: *NPJ Clim Atmos Sci* 5.1, pp. 1–8

Folberth, G. A., Zosia Staniaszek, AT Archibald, N Gedney, PT Griffiths, CD Jones, FM O'Connor, RJ Parker, AA Sellar, and A Wiltshire (2022). “Description and Evaluation of an Emission-Driven and Fully Coupled Methane Cycle in UKESM1”. In: *J. Adv. Model Earth Syst.*, e2021MS002982

Abstract

Methane is the second most important greenhouse gas after carbon dioxide, and also plays a central role in the chemistry of the atmosphere. The combination of its shorter lifetime and higher effectiveness as a greenhouse gas makes it an attractive option for near-term mitigation of climate change. Methane is also a key tropospheric ozone precursor: ozone is a greenhouse gas, and acts as an air pollutant in the troposphere. Therefore, mitigation of methane has both climate and air quality benefits.

A new configuration of the UK Earth System Model, UKESM1-ems, has been developed with a updated methane treatment. Methane emissions are input directly, rather than prescribing a global surface concentration. This thesis focuses on UKESM1-ems and the new capabilities it provides: a more process-based treatment of methane; simulating feedbacks in the methane cycle, and the ability to directly perturb methane emissions.

When compared to the previous, concentration-driven model, UKESM1-ems simulates the methane distribution with a better correlation compared to observations, including an improved latitudinal distribution, interhemispheric gradient and vertical gradient. The observed trend in methane over time is also reproduced, combining the methane emissions inputs, online wetland emissions and online chemistry and transport to simulate the methane mixing ratio. The modelled absolute methane mixing ratio is lower than observations: this is likely due to an underestimate in methane emissions, within the current large uncertainty range for emissions.

Experiments following different emissions pathways are explored using UKESM1-ems. Firstly, an idealised scenario where all anthropogenic methane emissions are removed instantaneously, to attribute the role of future anthropogenic methane. Methane declines to below pre-industrial levels within 12 years and global surface ozone decreases to levels seen in the 1970s. By 2050, 690,000 premature deaths per year and 1 degree of warming can be attributed to anthropogenic methane.

Secondly, the same low-methane scenario is used, with perturbed nitrogen oxide (NO_x) and carbon monoxide (CO) emissions, to investigate their impact on the atmospheric

oxidising capacity and test the hydroxyl (OH) relationship to NO_x and CO. The effect of methane on NO_x is also explored. Decreased methane emissions perturb both the NO/NO_2 ratio and the partitioning between NO_x and reservoir species, leading to increased NO_x in low-methane scenarios.

Finally, a Global Methane Pledge scenario is simulated. This pledge aims to reduce methane emissions by 30% globally by 2030, compared to 2020 values. The new ability of UKESM1-ems to mask emissions from different countries is used to implement this scenario and study regional impacts. The global mean methane mixing ratio decreases by 13% compared to 2020 levels. The expected temperature benefit (0.2°C) following this scenario is not seen in this experiment - this signal is too small and is within the noise and interannual variability of UKESM1-ems. There are global benefits for air quality, with ozone concentrations and population exposure to ozone decreasing in all countries. Global Methane Pledge member countries, where emissions reductions take place, see greater local air quality benefits than non-member countries.

Contents

Abbreviations	xiv
List of Figures	xvii
List of Tables	xxii
1 Introduction	1
1.1 Changes in climate	1
1.1.1 Climate forcings	4
1.1.2 Climate feedbacks	6
1.2 Methane in the atmosphere	7
1.2.1 Methane sources	8
1.2.2 Methane sinks	10
1.2.3 Methane lifetime	12
1.2.4 Chemistry of methane and related species	13
1.2.5 Methane feedbacks in the Earth system	16
1.2.6 Radiative forcing of methane	19
1.3 Methane treatment in chemistry-climate models	19
1.4 Future methane scenarios	21

<i>CONTENTS</i>	xi
1.4.1 Methane mitigation	23
1.5 Thesis outline	25
2 Description and evaluation of the UKESM1-ems model	27
Abstract	28
2.1 Introduction	29
2.2 Model description	31
2.2.1 UK Earth System Model (UKESM1-conc)	31
2.2.2 Emissions-driven UKESM1	32
2.2.3 Running UKESM1-ems experiments	36
2.3 Comparing UKESM1-ems and UKESM1-conc	37
2.3.1 Methane mixing ratio	37
2.3.2 Methane lifetime	39
2.3.3 CH ₄ + OH reaction flux	41
2.3.4 Ozone	42
2.4 OH multi-model comparison	44
2.5 Model evaluation against observations	46
2.5.1 NOAA observation data	47
2.5.2 Methane mixing ratio comparison	48
2.5.3 Interhemispheric gradient of methane and CO	51
2.5.4 Latitudinal distributions of CH ₄ and CO	54
2.6 Vertical profile evaluation	60
2.6.1 ATom observation data	60

2.6.2	Comparison between modelled and observed profiles	61
2.7	Summary	64
3	Attributing the role of future anthropogenic methane emissions	67
	Abstract	68
3.1	Introduction	69
3.2	Experiment setup	69
3.3	The impacts of ZAME on atmospheric composition	70
3.4	The impacts of ZAME on climate	75
3.5	Comparison with AerChemMIP	78
3.6	Discussion	80
3.7	Summary	86
4	Exploring the sensitivity to NO_x, methane and CO in UKESM1-ems	87
	Abstract	88
4.1	Introduction	89
4.2	Experiment setup	94
4.3	Methane and CO response	96
4.4	How does methane affect NO _x ?	97
4.4.1	Changes in NO/NO ₂ ratio	99
4.4.2	Changes in NO _x sources and sinks	102
4.5	OH sensitivity to NO and CO emissions	107
4.5.1	Methane lifetime	114
4.5.2	OH, CO, NO _x and methane relationship	116

<i>CONTENTS</i>	xiii
4.6 Summary	118
5 Modelling the Global Methane Pledge	121
Abstract	122
5.1 Introduction	123
5.2 Experiment setup	126
5.3 Atmospheric composition response	131
5.3.1 Ozone response	135
5.3.2 Reaction fluxes	139
5.4 Health impacts	142
5.5 Radiative forcing and temperature response	144
5.5.1 Radiative forcing estimates	146
5.6 Summary	148
6 Conclusions and future work	151
6.1 Future work	155
A Appendices	159
A.1 Data and code availability	159
A.2 Methane Pledge countries	160
A.3 Experiment suite IDs used in this thesis	161
Bibliography	190

Abbreviations

ACCMIP	Atmospheric Chemistry and Climate Model Intercomparison Project (part of CMIP5)
AerChemMIP	Aerosols Chemistry Model Intercomparison Project (part of CMIP6)
ATom	NASA's Atmospheric Tomography mission
CLE	Current legislation scenario, chapter 5
CMIP5	Fifth Coupled Model Intercomparison Project
CMIP6	Sixth Coupled Model Intercomparison Project
COP	Conference of Parties (of the UN Framework Convention on Climate Change)
CTM	Chemistry Transport Model
ERF	Effective radiative forcing
ESM	Earth system model
GFDL-AM4.1	Geophysical Fluid Dynamics Laboratory Atmospheric Model
GISS	Goddard Institute for Space Studies model

GMP	Global Methane Pledge
GMST	Global mean surface temperature
GWP	Global warming potential
IPCC	International Panel on Climate Change
JAMSTEC ACTM	Japan Agency for Marine-Earth Science and Technology Atmospheric Chemistry Transport Model
JULES	Joint UK Land Environment Simulator
LBC	Lower boundary condition
NH	Northern hemisphere
NOAA CMDL	National Oceanic & Atmospheric Administration, Climate Monitoring and Diagnostics Laboratory
PI	Pre-industrial, 1850 and before
RCP	Representative Concentration Pathways (from CMIP5)
RMSE	Root mean square error
SH	Southern hemisphere
SLCFs	Short lived climate forcers
SSPs	Shared Socio-economic Pathways (from CMIP6)
UKCA	UK Chemistry and Aerosol Model
UKCA	United Kingdom Chemistry and Aerosol model
UKESM1	UK Earth System Model (version 1.0)
UKESM1-conc	UK Earth System Model, concentration-driven
UKESM1-ems	UK Earth System Model, emissions-driven

UNFCCC	United Nations Framework Convention on Climate Change
VOCs	Volatile organic compounds
ZAME	Zero anthropogenic methane emissions scenario
NO _x	nitrogen oxides, NO and NO ₂
NO _y	sum of all nitrogen oxides and oxidised odd-nitrogen species
CH ₄	methane
CO	carbon monoxide
CO ₂	carbon dioxide
HNO ₃	nitric acid
HO _x	OH and HO ₂
JO ¹ D	rate constant for photolysis of ozone to form JO ¹ D
MCF	methyl chloroform
MeOO	methyl peroxy radical
O ¹ D	excited odd oxygen radical
O ³ P	odd oxygen radical
O ₃	ozone
OH	hydroxyl radical
RO ₂	peroxy radicals

List of Figures

1.1	Changes in global surface temperature between 1900-2100.	2
1.2	Energy balance of the atmosphere.	3
1.3	Effective radiative forcings and global temperature changes from emitted gases.	5
1.4	Observed changes in methane mixing ratios over time	7
1.5	The global methane budget for 2008-2017.	9
1.6	Wetland methane emissions in different future scenarios.	18
1.7	Methane emissions trajectories in the SSP scenarios.	22
1.8	Maximum technically feasible reductions for methane emissions.	24
2.1	Schematic of the structure of the UK Earth System model.	31
2.2	Methane emissions in UKESM1-ems.	33
2.3	Annual mean methane mixing ratio in UKESM1-conc and UKESM1-ems.	38
2.4	Residual surface exchange flux needed to resolve methane bias in UKESM1-ems.	38

2.5	Comparison of historical trends in methane lifetime, OH and CH ₄ + OH flux between UKESM1-ems and UKESM1-conc.	40
2.6	Comparison of historical trends in ozone and JO(¹ D) between UKESM1-ems and UKESM1-conc.	43
2.7	Inter-model comparison of OH distribution for the period 2000-2009.	45
2.8	Locations of methane measurements from the NOAA ESRL GMD Carbon Cycle Cooperative Air Sampling Network.	47
2.9	Number of NOAA CMDL measurement stations in each model latitude band.	48
2.10	Methane trends over time for UKESM1-ems and NOAA observations.	49
2.11	Observed and modelled interhemispheric gradient of methane over time.	52
2.12	Observed and modelled interhemispheric gradient of CO over time.	54
2.13	Spatial distribution of annual mean methane mixing ratios over time for observations and UKESM1-ems.	55
2.14	Latitudinal distribution of methane concentration in UKESM1-ems, UKESM1-conc and observations for 2000-2009.	57
2.15	Latitudinal distribution of the difference between modelled and observed methane mixing ratios over time.	57
2.16	Latitudinal distribution of CO mixing ratio over time for UKESM1-ems.	58
2.17	Latitudinal distribution of the difference between modelled and observed CO mixing ratios over time.	59
2.18	Map showing paths of ATom flight campaigns.	61
2.19	Vertical profiles of methane mixing ratio for UKESM1-conc and UKESM1-ems in 2000.	62

3.1	Methane emissions inputs and the resulting surface methane concentrations in UKESM1-ems	71
3.2	Atmospheric composition changes over time in the zero anthropogenic methane scenario (ZAME) from 2015-2050.	72
3.3	Physical climate changes associated with the zero anthropogenic methane scenario (ZAME).	76
3.4	Comparison of ZAME and AerChemMIP ozone and temperature changes with respect to methane concentration.	79
3.5	Schematic of the relevant reactions linking methane, HO _x and NO _x	82
3.6	Changes in HO ₂ and OH/HO ₂ ratio over time for ZAME and SSP3-7.0.	83
3.7	NO and NO ₂ evolution over time and zonal decadal mean difference plots for 2040-2050.	84
4.1	Schematic describing the NO _x -NO _y system, with sources, reservoirs and sinks for NO _x and NO _y	90
4.2	CO and NO emissions in SSP3-7.0 and SSP1-2.6.	95
4.3	Methane and CO response in SSP3-7.0, ZAME and lowCO/NO _x scenarios.	97
4.4	NO _x response in SSP3-7.0, ZAME and lowCO/NO _x scenarios.	98
4.5	NO mixing ratio difference between high (SSP3-7.0) and low (ZAME) methane scenarios.	100
4.6	NO ₂ mixing ratio difference between high (SSP3-7.0) and low (ZAME) methane scenarios.	101
4.7	Mixing ratios and fluxes affecting the NO/NO ₂ ratio.	103

4.8	Tropospheric annual mean concentration over time for NO_y species.	105
4.9	Tropospheric NO_y concentration over time and the percentage of NO_y present as NO_x	106
4.10	Global tropospheric mean OH concentration over time in the SSP3-7.0, ZAME and lowCO/ NO_x scenarios.	108
4.11	OH zonal mean difference between the low emissions scenarios and the baselines (SSP3-7.0 and ZAME).	109
4.12	Percentage OH zonal mean difference for 2025-2029 between the low emissions scenarios and the baselines (SSP3-7.0 and ZAME).	110
4.13	Ozone mixing ratio differences between high (SSP3-7.0) and low (SSP1-2.6) NO_x scenarios.	112
4.14	$\text{HO}_2 + \text{NO}$ flux difference between high (SSP3-7.0) and low (SSP1-2.6) NO_x scenarios.	113
4.15	Evolution of methane lifetime with respect to OH in the SSP3-7.0, ZAME and lowCO/ NO_x scenarios.	115
4.16	Relationship between the tropospheric mean OH concentration and the sources of NO_x , CO and methane.	117
5.1	Methane emissions in CMIP6, ECLIPSE, CLE and GMP scenarios.	127
5.2	Methane emissions in the Global Methane Pledge (GMP) scenario	130
5.3	Methane response in the Global Methane Pledge (GMP) scenario	131
5.4	Atmospheric composition changes over time for the CLE and GMP scenarios.	133
5.5	Ozone response in the Global Methane Pledge (GMP) scenario	136

5.6	Tropospheric ozone column and zonal means in the GMP and CLE scenarios.	137
5.7	Reaction fluxes affecting tropospheric ozone production in GMP and CLE scenarios.	141
5.8	Ozone exposure in the CLE and GMP scenarios.	143
5.9	Temperature response in the Global Methane Pledge scenario.	145

List of Tables

2.1	Metrics for model evaluation and reasoning for their inclusion in this analysis.	30
2.2	Comparison of methane emissions and sink terms between the UKESM1-ems and top-down (TD) and bottom-up (BU) estimates. . . .	35
4.1	Outline of the CO and NO _x mitigation experiments.	95
5.1	Methane pledge experiments and associated methane emissions.	129
5.2	Countries with the highest ozone and ozone changes in the GMP and CLE scenarios (this is the same for both).	138
5.3	Mortality related to long-term ozone exposure in the GMP and CLE scenarios.	144
A.1	Countries not signed up to the Global Methane Pledge as of March 2023	160
A.2	Model experiments used in this thesis	161

Chapter 1

Introduction

1.1 Changes in climate

Human influence on climate was first hypothesised in the 19th century, when it was discovered that emitted gases had a warming – or greenhouse – effect on the atmosphere and Earth, by trapping outgoing thermal radiation (Wayne 2006). Carbon dioxide (CO₂) and methane (CH₄) are two examples of greenhouse gases. Observations of CO₂ starting in the 1950s and continuing up to the present day have shown an increasing trend (Keeling et al. 2001). Long-term temperature measurements have shown that the climate is changing and global mean temperatures are increasing (Callendar 1938; Hawkins et al. 2013). The Intergovernmental Panel on Climate Change (IPCC) was established to provide assessments on the changing climate, and with each assessment the link between human activity and changes in climate has been strengthened: the most recent assessment states that *‘human activities, principally through emissions of greenhouse gases, have unequivocally caused global warming’* (IPCC 2023).

Fig 1.1 shows a visualisation of the warming over time using the climate stripes, from 1900 to the present day and into the future up to 2100. Global surface temperatures have reached 1.1 °C above pre-industrial levels (2011-2020 average, compared to 1850-1900, IPCC (2023)). Fig 1.1 also shows the differences in temperature experienced by

selected generations depending on when they were born, and therefore also the climate impacts they experience, such as extreme weather events (e.g. Thiery et al. (2021)). This highlights the speed of this temperature change, and also motivates action to mitigate climate change, to secure the futures of current and future generations.

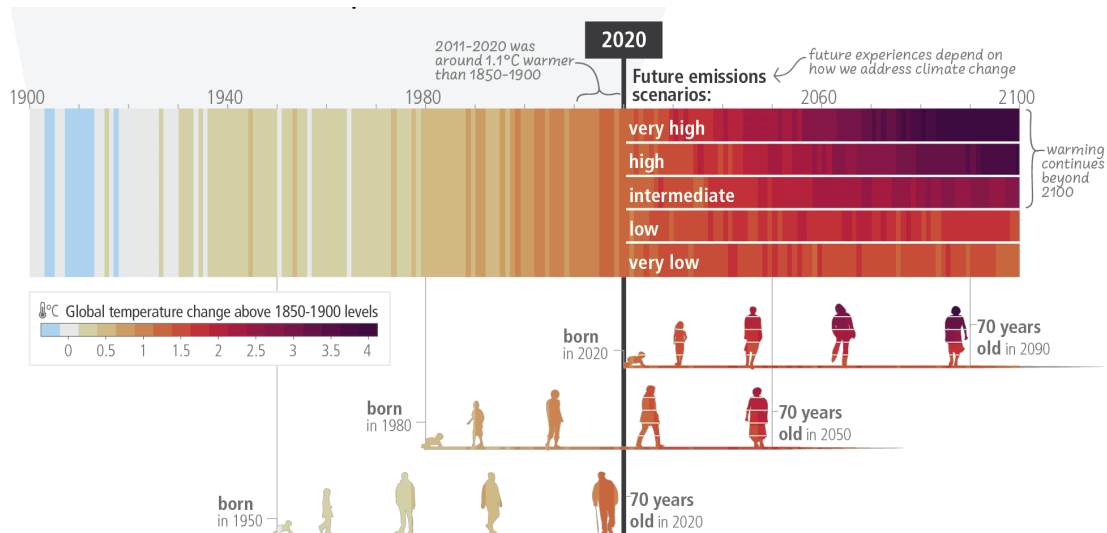


Figure 1.1: Observed (1900–2020) and projected (2021–2100) changes in global surface temperature (relative to 1850–1950) shown as ‘climate stripes’. Different future temperature scenarios are shown: very low (SSP1-1.9), low (SSP1-2.6), intermediate (SSP2-4.5), high (SSP3-7.0) and very high (SSP5-8.5). The temperatures and therefore climate impacts experienced by three representative generations are shown below (born in 1950, 1980 and 2020). Figure from IPCC AR6 Synthesis Report (Summary for Policymakers Fig 1).

The atmospheric temperature is controlled by the balance of incoming solar radiation and outgoing thermal and shortwave radiation, shown in Fig 1.2. Some of the incoming solar radiation is reflected by clouds and the Earth’s surface: this reflectivity is known as the albedo. The remaining solar radiation is absorbed by the surface and re-emitted as thermal radiation. Some of the thermal radiation is emitted into space, and some is trapped by greenhouse gases in the atmosphere, leading to a warming effect. Increasing the albedo cools the atmosphere - one example of this is after a volcanic eruption, when ash clouds block solar radiation from reaching the surface. Conversely, increas-

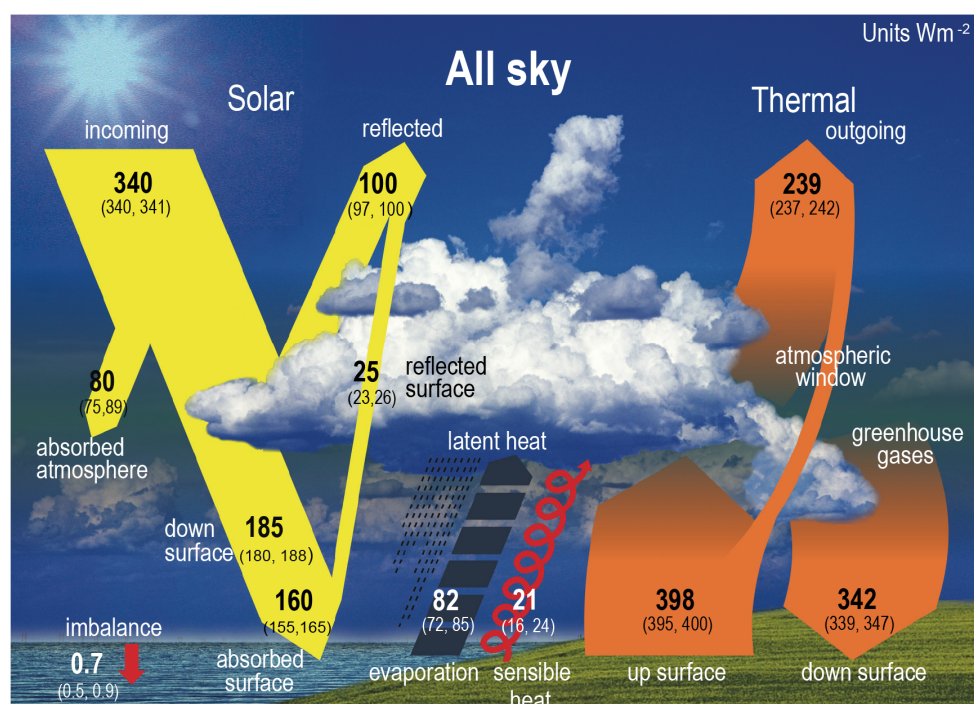


Figure 1.2: Balance of incoming solar radiation (in yellow) and outgoing thermal radiation (in orange) demonstrating cloud and surface albedo, and the greenhouse effect. Figure from IPCC AR6 WGI (Fig 7.2).

ing greenhouse gas concentrations traps more radiation in the atmosphere, and leads to warming.

The impact of a greenhouse gas on the Earth's energy balance is quantified by its radiative forcing. A forcing is the change in energy flux at the top of the atmosphere resulting from a perturbation, measured in W m^{-2} . The net effect of a greenhouse gas is to increase the energy flux towards the surface, and reduce the energy flux to the top of the atmosphere, leading to warming, defined as a positive forcing. The resulting temperature change, ΔT , can be approximated using the equation below, where ΔF is the forcing and λ is the climate sensitivity parameter (Ramaswamy et al. 2019). Therefore, the radiative forcing is a useful metric to compare the climate impacts of different atmospheric components and their changes over time.

$$\Delta F = \lambda \Delta T \quad (1.1)$$

The Paris Agreement is a legally binding international treaty on climate change. Its goal is to limit global warming in the 21st century to well below 2°C above pre-industrial levels, and make efforts to stay below 1.5°C (UNFCCC 2015). The Agreement outlines goals for a peak and subsequent decline in greenhouse gas emissions as soon as possible, informed by results from the IPCC (IPCC 2013). With current estimates for greenhouse gas emissions in 2030, it is likely that the 1.5°C threshold will be exceeded in the 21st century (IPCC 2023). However, concerted and sustained mitigation action to reduce greenhouse gas emissions would lead to a slowdown in global warming in the next couple of decades. The annual conference of parties (COP) of the UN Framework Convention on Climate Change (UNFCCC) provides an opportunity to review progress in meeting climate goals.

1.1.1 Climate forcings

Climate forcings are gases or aerosols that are radiatively active, or have an indirect impact on the radiative balance. Fig 1.3 shows the contribution of different emitted components to the change in global temperature, and their effective radiative forcing (ERF). The ERF is the radiative forcing with rapid adjustments taken into account (such as cloud changes), and is more representative of the overall climate response to a perturbation (Forster et al. 2016).

Carbon dioxide is the most important greenhouse gas and climate forcing, with an estimated radiative forcing of 2.16 [1.90 to 2.41] W m⁻² (IPCC 2021b). Reducing CO₂ emissions and limiting the total amount of CO₂ in the atmosphere are required to mitigate global warming and climate change.

CO₂ and nitrous oxide (N₂O) are both long-lived greenhouse gases, with atmospheric lifetimes of around 100 years or more. Decreasing their emissions, while necessary, will

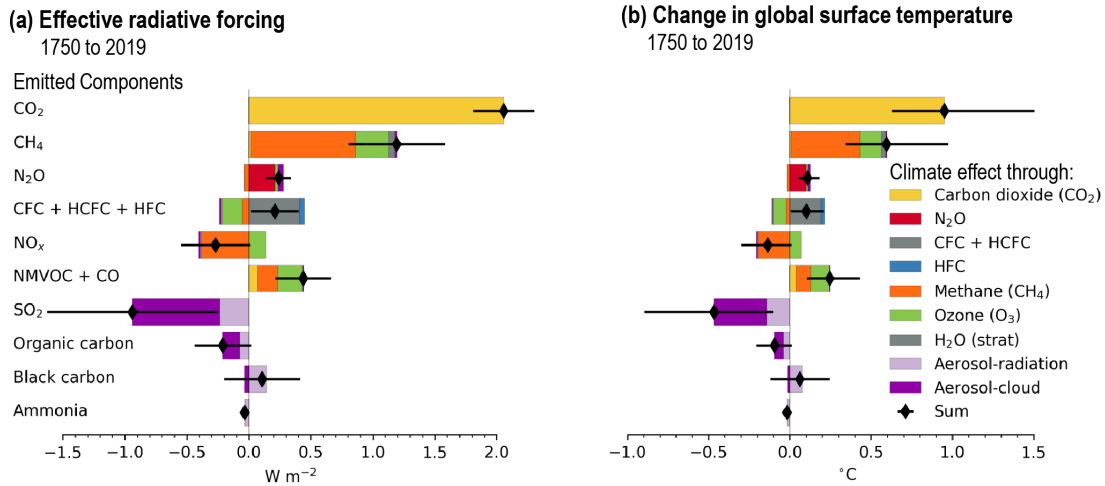


Figure 1.3: Contribution of different emitted gases to effective radiative forcing (ERF, left) and global temperature increase (right). Figure from IPCC AR6 WGI Technical Summary (Fig 15).

reduce their atmospheric concentrations slowly: over many decades or centuries. By contrast, short-lived climate forcers (SLCFs) have much shorter lifetimes (from hours to months, up to a decade). They tend to be more potent climate forcers, but are present in much lower concentrations than CO₂. SLCFs are often also air pollutants, and include methane, ozone, black carbon and hydrofluorocarbons. SLCF mitigation can provide near-term climate benefits due to their short atmospheric lifetime and high radiative efficiency: benefits may be seen on a decadal timescale (Shindell et al. 2017a; Shoemaker et al. 2013; Cain et al. 2022). Reducing emissions of SCLFs, especially methane, decreases the likelihood of overshooting the 1.5 degree threshold, and reduces the need for future net negative CO₂ emissions (IPCC 2022; Rogelj et al. 2018).

Methane is the second most important greenhouse gas, after carbon dioxide. Per molecule, methane is a much more effective greenhouse gas than CO₂, because methane molecules absorb in a part of the infrared spectrum that is not saturated at current levels (Etminan et al. 2016). The radiative forcing of methane can be approximated by a quadratic dependence on its concentration, whereas that of CO₂ has a weaker, logarithmic dependence (Meinshausen et al. 2020; Etminan et al. 2016). The overall climate impact of methane is lower than that for CO₂ because it is present in much

lower concentrations, and has a shorter lifetime. The IPCC estimate for the effective radiative forcing for methane is 1.19 [0.81 to 1.58] W m^{-2} , with a corresponding contribution of 0.65 [0.36-1.02] $^{\circ}\text{C}$ to global surface temperature increase (see Fig 1.3, IPCC (2021b)).

1.1.2 Climate feedbacks

The Earth system consists of many interconnected systems and processes occurring in the land, atmosphere and ocean. These connections and feedbacks between processes make it hard to predict what will happen when one thing changes in the system, or when many things change at the same time.

A positive feedback acts to amplify the original effect of a change, while a negative feedback acts to counteract the initial change. An example of a positive feedback is the ice-albedo feedback. Ice is a very reflective surface, and reflects more solar radiation than land or water. If warmer temperatures cause ice to melt, and ice cover to decrease, the ocean area will reflect less radiation and absorb more (see Fig 1.2). This leads to more warming, and in turn to more ice melting, amplifying the effect of the initial warming.

Another example is the water vapour feedback. Water vapour is a greenhouse gas, but unlike CO_2 , its concentration is determined by the atmospheric temperature: air at a higher temperature holds more water. Increasing global temperatures from emitted greenhouse gases (e.g. CO_2 , methane) lead to increased water vapour concentrations, which trap more radiation and lead to additional warming.

We use models as tools to help simulate these Earth system processes. These range in complexity from simplified energy balance models, to fully-coupled Earth system models (ESMs). To understand the full complexity of the Earth system it is useful to compare multiple models which may have different strengths and weaknesses. The main mechanism for this are the Coupled Model Intercomparison Projects (CMIP5, CMIP6, etc), which inform the IPCC report cycle. Collated results from these models are used

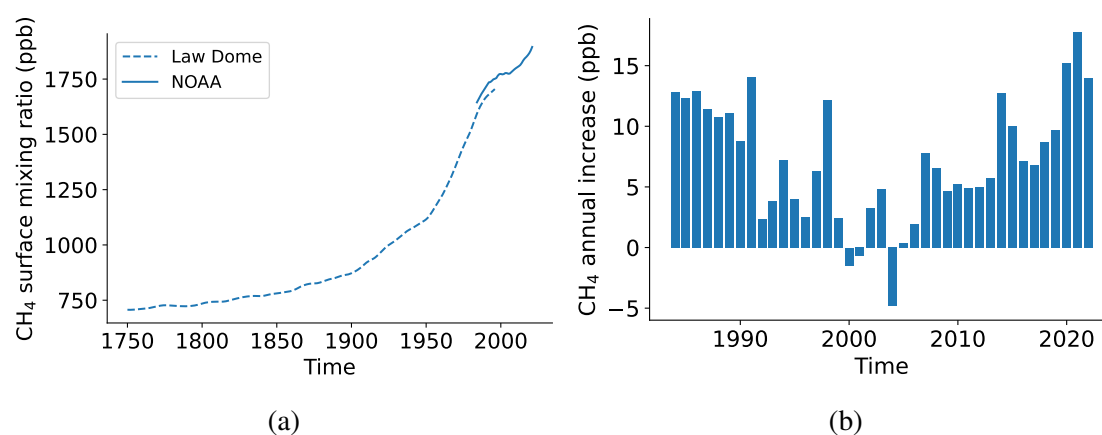


Figure 1.4: (a) Observed methane concentrations from 1750 to present day, from firn air, ice cores and flask samples (Etheridge et al. 1998; Rubino et al. 2019; Lan et al. 2022). Note that the Law Dome and NOAA measurements are consistent: the slight offset is due to the interhemispheric gradient in methane- the Law Dome measurements are from the southern hemisphere. (b) Observed annual change in global mean surface mixing ratio from 1985 to 2022 (Lan et al. 2022).

to improve the scientific understanding of climate change, and inform policy for climate mitigation.

1.2 Methane in the atmosphere

The amount of methane in the atmosphere has more than doubled since pre-industrial times (see Fig 1.4a). This increase can be attributed to anthropogenic (human-derived) emissions of methane since the industrial revolution, continuing up to the present day. Methane has been measured at a range of sites globally since the 1980s (Dlugokencky (2020), shown in Fig 2.8), and since 2009 using satellites to provide a global picture of methane distribution over time (Palmer et al. 2021; Hu et al. 2018; Butz et al. 2011). Data from ice cores can also be used, to probe methane concentrations before direct measurements were available (Law Dome data in Fig 1.4a, Etheridge et al. (1998)).

Methane concentrations have shown an increasing trend since measurements started, but this paused between 1999-2007, known as the hiatus period. The annual change in observed methane can be seen in Fig 1.4b, including the hiatus period, characterised by the low and negative values. After 2007, the annual increase resumed and has reached record levels in recent years (Nisbet et al. 2019). Overall, the methane surface mixing ratio has increased from around 700 ppb in 1750 to 1922 ppb in April 2023 (IPCC 2021b; Dlugokencky 2020).

1.2.1 Methane sources

The total amount of methane in the atmosphere (the methane burden) and its rate of change are controlled by the sources and sinks of methane. These are difficult to estimate directly, because many of the sources and sinks are diffuse, and methane is well-mixed due to its long lifetime relative to the timescale for atmospheric mixing. The magnitudes of the sources and sinks can be estimated by combining independent emissions and sink components (a bottom-up approach) or by using an inversion model, constrained by atmospheric measurements (a top-down approach). Saunio et al. (2020) collated currently available emissions inventories from top-down and bottom-up models to diagnose the methane budget for the 2000-2009 decade, and for the more recent period 2008-2017, shown in Fig 1.5.

Wetlands are the largest natural source of methane, estimated at 149 [102-182] Tg yr⁻¹ for 2008-2017 (Saunio et al. 2020). The remainder of the natural contributions include inland waters, geological sources, wild animals and termites, and combine to 222 [143-306] Tg yr⁻¹ (Saunio et al. 2020). Anthropogenic sources over the same time period account for approximately 50% of methane emissions: 128 [113-154] Tg yr⁻¹ from fossil fuels, 206 [191-223] Tg yr⁻¹ from agriculture and waste and 30 [26-40] Tg yr⁻¹ from biomass and biofuel burning (Saunio et al. 2020). There is some interannual variability in these source terms, for example due to differences in anthropogenic activity, biomass burning activity, and seasonal wetland extent.

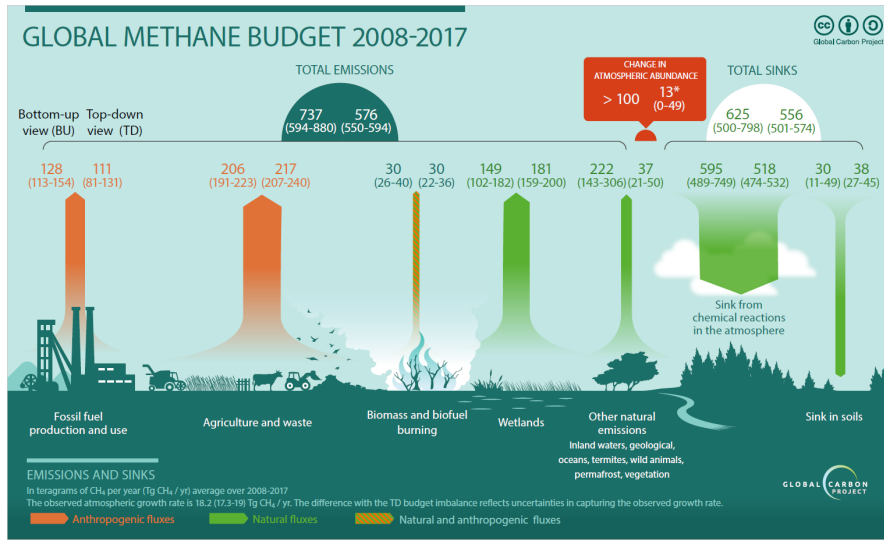


Figure 1.5: The global methane budget for 2008-2017. Top-down and bottom-up estimates are shown. Upwards arrows show anthropogenic and natural emissions emissions (in orange and green respectively). Downwards arrows show the methane sinks. Figure from Saunio et al. (2020).

Methane emitted from wetlands is produced by microbes. The flux of methane emitted depends on the microbial process rates, the balance between methane-destroying and methane-generating activity, and the waterlogged area, or wetland extent (Gedney et al. 2004). The flux, F_{CH_4} can be parametrised by equation 1.2 (Gedney et al. 2004).

$$F_{CH_4} = f_{wet} k_{CH_4} C_{eff} Q_{10}(T) \quad (1.2)$$

$$Q_{10}(T) = Q_{10}(T_0)^{T/T_0} \quad (1.3)$$

f_{wet} is the wetland area fraction, k_{CH_4} is a global constant, C_{eff} is a parameter for microbial substrate availability. $Q_{10}(T)$ is a temperature dependent factor (relative to reference temperature T_0): increases in temperature lead to increased methane production via higher microbial process rates (Christensen et al. 2003). This equation can be used to calculate wetland emissions fluxes and their evolution over time, for example in the Joint UK Land Environment Simulator (JULES), a land surface model. The mag-

nitude and location of wetland emissions varies year-on-year due to meteorology (e.g. through the amount and location of rainfall), and will also change over longer timescales with climate, as temperature and precipitation patterns change.

These relationships suggest a positive wetland-climate feedback: methane emissions from wetlands cause an increase in methane mixing ratio, increasing its radiative forcing effect, increasing temperature, thus increasing wetland emissions further (Zhang et al. 2023; Gedney et al. 2019; Cao et al. 1998). For example, Christensen et al. (2003) estimated that 2 °C of warming over northern wetlands would lead to a 45% increase in methane emissions from wetlands. The potential for wetland feedbacks and the implications are discussed further in section 1.2.5.

1.2.2 Methane sinks

The dominant sink for methane in the atmosphere is its reaction with the hydroxyl radical, OH (reaction 1.4). This reaction accounts for 90% of the global methane sink (Kirschke et al. 2013). OH is the dominant tropospheric oxidant and reacts with most pollutants. Its high reactivity means that direct measurements of OH concentration represent a very localised area and its chemistry (e.g. Stone et al. (2012)). Therefore, to constrain the global mean OH concentration and trends, it is necessary to use a proxy: a trace gas whose primary reaction is with OH and whose emissions are known (Montzka et al. 2011). The tracer methylchloroform (MCF) has been used for this purpose: measurements of MCF over time combined with emissions inventories for MCF are used to estimate the OH sink strength (Prinn et al. 1995; Krol et al. 1998; Montzka et al. 2011).



The remaining 10% of methane is oxidised via several routes. Methane reacts with chlorine (Cl) radicals in the troposphere through reaction 1.5. This occurs especially in polluted areas of the northern hemisphere, and over the Southern Ocean, in total comprising $\sim 2.5\%$ of global methane oxidation (Wang et al. 2019; Hossaini et al. 2016). $O(^1D)$, an excited oxygen atom formed via photolysis of ozone or oxygen, also reacts with methane in the stratosphere (reaction 1.6). Methane can also be photolysed in the stratosphere (reaction 1.7). Finally, there is a terrestrial sink for methane: methanotrophic bacteria in aerated soils convert methane to CO_2 (reaction 1.8) (Smith et al. 2000).

The atmospheric methane growth rate is determined by the size of the imbalance between the total global methane source and global sink. This is represented in equation 1.9, where the rate of change of methane mixing ratio, $\frac{d[CH_4]}{dt}$, is determined by the total methane emissions (*Emissions*) and the sink term for methane, shown as a first-order loss, $-k'[CH_4]$ (Holmes 2018). Equation 1.10 shows this first-order loss term as a sum of the individual sink terms discussed in the previous paragraphs, with rate constants k_x .

$$\frac{d[CH_4]}{dt} = Emissions - k'[CH_4] \quad (1.9)$$

$$\begin{aligned} \frac{d[CH_4]}{dt} = E - k_{CH_4+OH}[CH_4][OH] - k_{CH_4+Cl}[CH_4][Cl] \\ - k_{soil}[CH_4] - k_{strat}[CH_4] \end{aligned} \quad (1.10)$$

Increases in the methane growth rate can be caused by an increase in emissions, a decrease in sink strength, or a combination of sink and source strength changes. For example, after the methane hiatus period in 1999-2006, the growth rate increased. Reasons for this observed trend have been hypothesised, but with no consensus in the literature. For example, Kirschke et al. (2013) suggested that the renewed growth is due to increased wetland and fossil fuel emissions, while Turner et al. (2017) argue that it may be due to a decrease in methane emissions, offset by a larger decrease in the OH sink strength. One of the limitations in attributing these changes is the difficulty in quan-

tifying the methane sink, i.e. OH and its trend. Observationally constraining the OH concentration often relies on methylchloroform (MCF) measurements. This is becoming increasingly difficult over time due to decreasing MCF concentration and a higher uncertainty in its budget (Naus et al. 2021). In recent years satellite observations have also been used to provide insights into the methane growth rate. Several studies have shown that the high methane growth rate in the last couple of years can be attributed to increased biogenic methane emissions, especially over Eastern Africa (Feng et al. 2023; Nisbet et al. 2019; Lunt et al. 2019).

1.2.3 Methane lifetime

The methane lifetime is a metric used to represent the residence time for methane, or the timescale for methane oxidation in the atmosphere. Methane lifetime, τ , is defined as the methane burden (m , in Tg), divided by the sum of the different loss processes for methane (L_x , in Tg yr⁻¹), as shown in the equation below (Holmes 2018). The methane burden is the total mass of methane in the atmosphere, and the loss processes represent each of the methane sinks (see equations 1.4-1.8). The loss processes can also be represented by first-order loss frequencies, in yr⁻¹, from equation 1.10. The result of equation 1.11 gives a methane lifetime in years.

$$\begin{aligned} \tau &= \frac{m}{L} = \frac{m}{L_{OH} + L_{Cl} + L_{soil} + L_{strat}} \\ &= \frac{1}{k'} = \frac{1}{k_{CH_4+OH}[OH] + k_{CH_4+Cl}[Cl] + k_{soil} + k_{strat}} \end{aligned} \quad (1.11)$$

The methane lifetime is not an observable quantity: it requires measurements or estimates of the atmospheric methane burden and the global methane sink. Chemistry-climate models, Earth system models or top-down observational inversion methods can be used to calculate the chemical sink for methane (mainly due to OH oxidation) and therefore derive a methane lifetime. Prather et al. (2012) calculated the contribution of methane oxidation by OH to the methane lifetime as 11.2 ± 1.3 years. The life-

times with respect to chlorine, stratospheric loss and soil uptake are much longer (150, 200 and 120 years respectively, Myhre et al. (2013) and Prather et al. (2012)), showing that oxidation by OH is the dominant sink for methane. All of these sinks combined give an overall atmospheric lifetime for methane. Based on top-down models, this was estimated as 9.7 ± 1.1 years by the IPCC in their most recent assessment (IPCC 2021a).

The methane lifetime gives an indication of the oxidative capacity of the atmosphere. Changes in methane lifetime are driven by factors that affect OH (including methane itself), and trends in OH are associated with trends in methane lifetime (John et al. 2012; Stevenson et al. 2020). The methane lifetime can also be affected by k_{OH} , the rate constant for the $\text{CH}_4 + \text{OH}$ reaction, which increases with temperature (Burkholder et al. 2020; Atkinson et al. 2004).

The methane lifetime is an important factor in the climate warming impact of methane (see section 1.1.1). A longer methane lifetime means an increased methane residence time in the atmosphere, over which it has a warming effect. The lifetime also gives an indication of how long it would take for methane concentrations and burden to decrease if methane emissions decreased or stopped - in this case around a decade. This highlights methane's role as a short-lived climate forcer and the opportunity for observable mitigation efforts on a relatively short timescale (compared to CO_2) (e.g. Shindell et al. (2017a) and Shoemaker et al. (2013)).

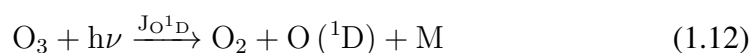
1.2.4 Chemistry of methane and related species

Methane plays a central role in the chemistry of the atmosphere (Crutzen 1973; Seinfeld et al. 2016). Through its reaction with OH (reaction 1.1), methane affects many other processes and species, including ozone (O_3), nitrogen oxides ($\text{NO}_x = \text{NO} + \text{NO}_2$), carbon monoxide (CO) and other volatile organic compounds (VOCs).

Ozone is an important gas: it is both a climate forcer and an air pollutant (Monks et al. 2015). Ozone in the stratosphere prevents harmful UV radiation reaching the surface. However, tropospheric ozone near the surface leads to poor air quality and negative impacts on human health, crops and ecosystems.

Ozone production occurs when VOCs are oxidised in the presence of NO_x (Crutzen 1973). Therefore, NO_x and VOCs (including methane and CO) are known as ozone precursors. The emissions of these precursors through anthropogenic activities has increased the tropospheric ozone burden since pre-industrial times, although the spatial distribution of ozone is very heterogeneous (IPCC 2021a; Tarasick et al. 2019).

Ozone can be photolysed at wavelengths below 310nm to form excited O atoms, $\text{O} (^1\text{D})$, with a photolysis rate constant of $J_{\text{O}^1\text{D}}$ (see equation 1.12). Most $\text{O} (^1\text{D})$ in the troposphere is quenched to ground state $\text{O} (^3\text{P})$ (reaction 1.13), but a small fraction reacts with water via reaction 1.14, to form OH (Levy 1971). This reaction is the primary source for OH in the troposphere (Lelieveld et al. 2016).



Ozone is both a product of methane oxidation, and also affects methane through its role in the production of OH, which goes on to destroy methane. This is one of the ways in which methane affects its own lifetime (see section 1.2.5). Therefore, ozone affects methane and vice versa.

Stratospheric ozone decreased over the second half of the 20th century due to widespread use of ozone depleting substances (Stolarski et al. 1992). This means that more photons with shorter wavelengths reached the troposphere, increasing $J_{\text{O}^1\text{D}}$ and therefore OH production, reducing the methane lifetime. Conversely, future stratospheric ozone recovery is likely to increase the methane lifetime, by reducing $J_{\text{O}^1\text{D}}$ (Voulgarakis et al. 2013).

Nitrogen oxides, NO_x , play several important roles in atmospheric chemistry. Tropospheric sources of NO_x include anthropogenic emissions (combustion, biomass burning), and natural emissions (lightning and soil emissions) (Logan 1983). These sources

are spatially heterogeneous: at the surface in urban areas combustion emissions dominate, whereas lightning is the main NO_x source in the tropical upper troposphere. NO_x has a short lifetime (\sim days) so its spatial distribution is also very heterogeneous. NO_x is an ozone precursor; the reactions of NO_x with VOCs are key to photochemical production of ozone (Crutzen 1979). NO_x also influences OH by contributing to its secondary source, via radical recycling (Lelieveld et al. 2016).

Carbon monoxide is an important species when considering methane chemistry. CO and methane share some of the same primary sources, such as use of fossil fuels, incomplete combustion and biomass burning (Holloway et al. 2000). Oxidation of methane and other VOCs leads to secondary CO production (Levy II 1972). Analogous to methane, reaction with OH accounts for 90-95% of the sink for CO (Holloway et al. 2000), so the burdens and lifetimes of methane and CO are closely coupled. Gaubert et al. (2017) found that the 20 % decrease in CO emissions between 2002 and 2013 led to an 8 % decrease in methane lifetime, via decreased depletion of OH. Therefore, CO also has an indirect radiative forcing impact via its effect on methane (and ozone) concentrations.

Methane, CO and OH are closely linked via the $\text{CH}_4/\text{CO} + \text{OH}$ sink reactions, and the secondary production of CO from methane. This CH_4 -CO-OH system can be described using the time-dependent equations for the concentrations of CO, CH_4 and OH (equations 1.15-1.17, Prather (1994) and Prather (1996)). The S_x terms represent source terms: emissions for CO and CH_4 , and production of OH (mainly through reaction 1.4). The reactions included here are those of OH with CH_4 and CO, as well as an OH + X reaction, where X represents all other sinks for OH (Prather 1994).

$$\frac{d[\text{CH}_4]}{dt} = S_{\text{CH}_4} - k_{\text{CH}_4+\text{OH}}[\text{CH}_4][\text{OH}] \quad (1.15)$$

$$\frac{d[\text{CO}]}{dt} = S_{\text{CO}} - k_{\text{CO}+\text{OH}}[\text{CO}][\text{OH}] + k_{\text{CH}_4+\text{OH}}[\text{CH}_4][\text{OH}] \quad (1.16)$$

$$\frac{d[\text{OH}]}{dt} = S_{\text{OH}} - k_{\text{X}+\text{OH}}[\text{OH}][\text{X}] - k_{\text{CO}+\text{OH}}[\text{CO}][\text{OH}] - k_{\text{CH}_4+\text{OH}}[\text{CH}_4][\text{OH}] \quad (1.17)$$

This simplified scheme (equations 1.15-1.17) represents the coupling between CO, CH₄ and OH. It can be used to estimate what would happen, for example, following a perturbation in methane emissions, S_{CH_4} (e.g. Heimann et al. (2020)). The resulting increase in methane concentration affects both OH and CO, and therefore also has a feedback on methane. Note that these equations don't include the impact of changes in methane on S_{OH} via ozone as discussed above. This and more methane feedbacks are discussed further in the next section.

1.2.5 Methane feedbacks in the Earth system

Methane self-feedback via oxidation

Methane has an important self-feedback via its main sink: the reaction with OH. The concentration of OH determines the residence time of methane in the atmosphere, or the methane lifetime. The first-order effect of increasing methane emissions is to increase methane concentrations. The increased methane concentration leads to more reaction with OH, and decreases OH concentration. This is the second-order effect, or feedback – having less OH decreases the strength of the sink for methane, so methane concentrations increase further. The resulting concentration increase is proportionally higher than the increase in methane emissions. These interactions between OH and methane are described by the equations 1.15-17, (Prather 1994).

The methane self-feedback can be quantified by the feedback factor, f . This is the ratio between the emissions change and the resulting concentration increase, or equivalently, the increase in methane lifetime (τ) resulting from a change in burden (Holmes 2018). Equation 1.18 shows how the feedback factor can be calculated using the changes in τ , loss frequency (k) and the methane burden (m), following an emissions perturbation. Previous studies have calculated $f \sim 1.3-1.4$ (Holmes 2018; Thornhill et al. 2021b; Fiore et al. 2009). Therefore, for an increase in emissions by 10 %, the expected increase in methane concentration would be 13-14 %. The feedback factor is not an observable parameter, but comparison between modelled values gives a useful indication of the feedback strength in different models.

$$f = \frac{1}{1 + R} \quad R = -\frac{d \ln \tau}{d \ln m} = \frac{d \ln k}{d \ln m} \quad k = \frac{1}{\tau} \quad (1.18)$$

Factors that lead to a greater increase in methane concentration for a given perturbation in methane emissions increase the methane self-feedback strength. These increase the impact that methane has on its own sink. One example is a larger methane burden, which leads to a lower global mean OH concentration, which is more affected by changes in methane emissions.

Factors that decrease the methane self-feedback include those that decrease the influence of methane on the OH concentration. An increased CO burden leads to more reaction of OH with CO, so a smaller proportion of OH oxidises methane. Increases in humidity or lightning NO_x can lead to increased OH concentrations, through the O(1D) + H₂O reaction (1.14), and by secondary production of OH respectively (Levy 1971; Labrador et al. 2004). In both of these examples, a given increase in methane emissions affects the global OH concentration less, leading to a weaker self-feedback.

Methane-climate feedbacks

Increased natural methane emissions from wetlands have the potential to act as a positive methane-climate feedback to future warming (Melton et al. 2013). In model experiments, natural methane emissions are often presumed to be constant over the 21st century, due to large uncertainties in their future evolution (Zhang et al. 2017; He et al. 2020), and model limitations (e.g. CMIP6, Thornhill et al. (2021a)). In reality, the natural methane emissions vary over time due to changes in CO₂, temperature and precipitation, as shown for different climate scenarios in Fig 1.6 (Kleinen et al. 2021).

Zhang et al. (2017) calculated an increase in global mean temperature of 0.04-0.14K from the inclusion of wetland feedbacks over the 21st century, relative to the RCP scenarios (used in CMIP5). They estimated increases in wetland methane emissions of between 29% and 97% by 2100 (for the lowest and highest future warming scenarios

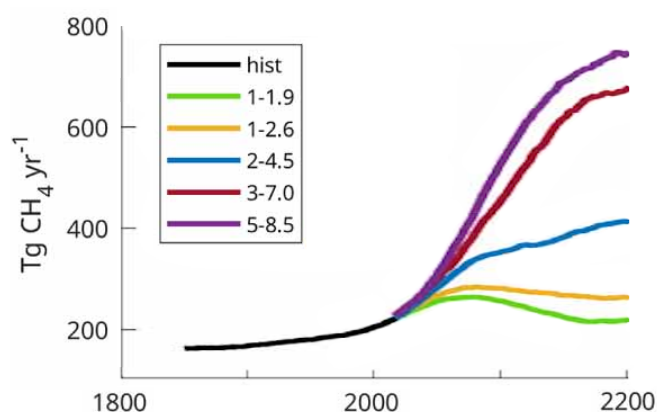


Figure 1.6: Wetland methane emissions over time for different future warming scenarios in CMIP6, from the lowest warming scenario (SSP1-1.9) to the highest warming scenario (SSP5-8.5). Figure from Kleinen et al. (2021) (Fig A5).

respectively). While the largest cause for the increased wetland emissions is likely to be increased CO_2 concentrations (via changes in the net primary productivity of wetlands), there is also an impact from increased temperature, which would form a wetland methane-climate feedback (Melton et al. 2013). Earth system models with interactive wetland components are needed to model this effectively (e.g. Gedney et al. (2004) and Melton et al. (2013)).

Other potential positive feedbacks exist within the methane system that may become more significant in the future. Increased temperatures causing widespread permafrost thaw may lead to increased methane emissions, and further increases in temperature (Dean et al. 2018; Treat et al. 2013). Although much less likely, a similar mechanism can be envisaged for methane hydrates in the ocean (Ruppel et al. 2017; Archer et al. 2009). These mechanisms are only likely to happen over very long timescales, but they may represent tipping points for the climate system, where small perturbations could lead to rapid large scale changes at a critical point (Lenton et al. 2019; Dean et al. 2018).

1.2.6 Radiative forcing of methane

Methane has a radiative impact both directly through its action as a greenhouse gas, and indirectly, through its effect on other radiatively-active compounds (Etminan et al. 2016). This is shown in Fig 1.3, where the CH₄ bar is composed of contributions from methane, ozone and stratospheric water vapour. The indirect mechanisms include: formation of ozone via methane oxidation, stratospheric water vapour changes, and the self-feedback of methane on its own lifetime. In total, the IPCC estimate of the methane (emissions-based) effective radiative forcing is 1.19 [0.81 to 1.58] W m⁻², (IPCC 2021a).

Ozone has an estimated effective radiative forcing of 0.47 [0.24 to 0.71] W m⁻² (IPCC 2021a). A proportion of this can be attributed to the ozone produced by methane oxidation. This was estimated by Thornhill et al. (2021b) as 0.14 ± 0.03 W m⁻² of the (stratospherically adjusted) radiative forcing for ozone.

1.3 Methane treatment in chemistry-climate models

Chemistry-climate models are a tool used to simulate the atmosphere and Earth system. These models have varying levels of complexity, for example in the number of chemical reactions they include. The newest generation of models are Earth system models (ESMs, e.g. Sellar et al. (2019), Kelley et al. (2020), and Dunne et al. (2020)). These simulate different systems such as the atmosphere, ocean and land, and the interactions between them, to form the full Earth system. There is often a compromise between detailed inclusion of processes and the resulting time and computational expense required to perform complicated calculations. ESMs output a large amount of data, including meteorology and distributions of chemical and aerosol species.

The current treatment of methane in most chemistry-climate models is to prescribe a time-varying lower boundary condition (LBC) (e.g. Lamarque et al. (2010) and Voulgarakis et al. (2013)). The methane surface mixing ratio is set to a fixed value annually across the globe. This was the approach used by all models in CMIP6 (Eyring et al.

2016). The previous approach, used by some CMIP5 models, fixed the methane mixing ratio globally across all model levels (e.g. Voulgarakis et al. (2013)). These approaches are justified by the long lifetime of methane, which means it is well-mixed throughout the troposphere. However, the use of an LBC means that methane mixing ratios are underestimated in the northern hemisphere and overestimated in the southern hemisphere. The surface model level can act as a source or a sink to buffer the methane concentration at the surface in a non-physical way. The LBC also puts limitations on the feedbacks that can be simulated in the system. For example, wetland emissions that vary with temperature and wetland extent cannot couple into the methane cycle.

A new generation of Earth system models are now being developed with methane emissions instead of a lower boundary condition. In these models, the emissions are input from inventories and/or interactive emissions within the model itself. He et al. (2020) extended the standard version of the Geophysical Fluid Dynamics Laboratory Atmospheric Model (GFDL-AM4.1) to use methane emissions instead. While this is emissions-driven, it is not interactive: the wetland emissions are climatological monthly means, with no interannual variability, limiting the feedbacks that can be modelled.

A fully interactive methane configuration of the UK Earth System Model (UKESM1-ems) was developed by Folberth et al. (2022) and is evaluated in Chapter 2. This is the first emissions-driven Earth system model that also has online wetland emissions. The methane concentration at the surface is determined by the emissions and sinks, instead of an LBC. UKESM1-ems includes interactive wetland emissions, which are output by the Joint UK Land Environment Simulator (JULES) model (Clark et al. 2011). These wetland emissions vary with temperature and wetland extent, so are dependent on meteorology and climate. The anthropogenic emissions used are from the CMIP6 inventory and vary spatially and temporally (Hoesly et al. 2018; Gidden et al. 2019). UKESM1-ems is the basis of the work and experiments in this thesis.

Emissions-driven models are constrained by the availability of accurate inputs, or emissions, as well as the model's ability to simulate the oxidative capacity of the atmosphere. Different emissions inventories are available based on varying assumptions, including magnitude and location of emissions, usually based on sector and country emissions (e.g Höglund-Isaksson et al. (2020) and McDuffie et al. (2020)). The main inventories used

and the differences between their historical emissions are shown in Fig 1.7 (Sauniois et al. 2020). The model results from these emissions inputs are likely to vary depending on which inventory is chosen. In an emissions-driven system, the methane mixing ratio is determined by the relative strength of the emissions compared to the model sinks. The simulated OH distribution also affects the methane mixing ratio and burden, and vice versa. This contrasts to an LBC system in which the mixing ratio is set.

1.4 Future methane scenarios

In the climate modelling community, a range of Shared Socioeconomic Pathways (SSPs) were created using a set of socioeconomic assumptions, for use in future projections. These give a broad spectrum of potential future trajectories (Eyring et al. 2016). The scenarios involve assumptions about population growth, economic growth, international cooperation, technological advancement and energy demand (Riahi et al. 2017). Each scenario has a consistent story within which these parameters are defined.

SSP1 is the most optimistic in terms of social development: it includes reduced inequality, successful international cooperation and large technological advances, with an environmental priority (Van Vuuren et al. 2017). SSP5 involves high economic growth in a fossil fuel driven economy (Kriegler et al. 2017). There are five scenarios in total, and SSPs 2-4 are intermediate scenarios.

In CMIP6, the SSPs were matched up with radiative forcings for 2100 to complement the previous scenarios used in CMIP5 (O'Neill et al. 2016). Not all of the target radiative forcings are achievable for all of the defined SSPs. For example, limiting SSP3 to 1.26 W m^{-2} of forcing is unfeasible, due to high greenhouse gas emissions, limited technology and high pressures on land use for a large population (Riahi et al. 2017). The core scenarios for CMIP6 span a range of socioeconomic pathways and radiative forcings. Some of these scenarios (e.g. SSP5-8.5) are helpful in illustrating a world to be avoided, as a motivation for climate policies, while others (e.g. SSP1-2.6) are aspirational trajectories we can aim for to limit climate impacts.

The methane trajectories for the SSPs in CMIP6 are determined by the changes in source strengths for the different scenarios. Fig 1.7b shows the methane trajectory for each SSP scenario. SSP3-7.0 has the most extreme methane trajectory, with an almost linear increase throughout the 21st century (Gidden et al. 2019). This is due to high fossil fuel and coal usage. By contrast, SSP1-2.6 involves major methane reductions, resulting from the move away from fossil fuels. Methane emissions also decrease in scenarios where public health is a priority, e.g. SSP5-8.5 (Riahi et al. 2017), since targeting methane as an ozone precursor is effective in improving air quality (Staniaszek et al. 2022; Shindell et al. 2021; Shindell et al. 2017a; West et al. 2012).

Since the hiatus period in 2000-2007, there has been strong growth in atmospheric methane (Nisbet et al. 2019). 2020, 2021 and 2022 were all record breaking years in terms of annual increase in observed atmospheric methane, with 15, 18 and 14 ppb annual increases respectively (Lan et al. 2022). While overall in terms of greenhouse gas emissions, we are currently on a trajectory in line with SSP2-4.5 (UNFCCC 2021), for methane the current trends are consistent with the most carbon-intensive projections, such as SSP3-7.0 (see Fig 1.7, (Saunois et al. 2020)).

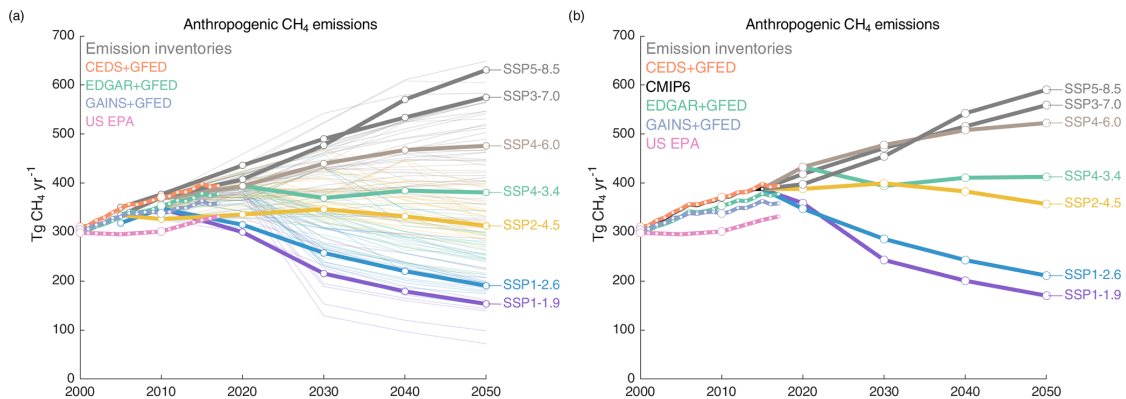


Figure 1.7: Methane emissions trajectories for the historical period and the SSP scenarios. Historical emissions estimates from different inventories are shown. Note that the US EPA estimate is a projection from 2005 onwards. On the left are unharmonised emissions, showing that the current trend is consistent with the high methane scenarios. On the right are the harmonised emissions used as inputs for CMIP6. Figure from Saunois et al. (2020) (Fig 2).

1.4.1 Methane mitigation

At the time of writing, over 125 countries (representing 50% of anthropogenic methane emissions) have signed up to the Global Methane Pledge (globalmethanepledge.org), and there is extensive potential for mitigation (Shindell et al. 2017b; Nisbet et al. 2020; Shindell et al. 2021; Höglund-Isaksson et al. 2020). The goal of the Pledge is to reduce methane emissions globally by 30% by 2030, relative to 2020 levels.

The opportunities for methane mitigation vary by sector and region (IPCC 2022; Shindell et al. 2021), see Fig 1.8. Currently available measures could reduce methane emissions by 45% by 2030, and 54% by 2050, relative to the current trajectory (estimated by Shindell et al. (2021) and Höglund-Isaksson et al. (2020) respectively). The sector with the largest mitigation potential is oil and gas, through measures such as leakage detection and repair. According to the Global Methane Assessment, up to 80% of oil and gas emissions can be prevented at low or no cost (Shindell et al. 2021). Methane emissions from waste and wastewater can also be mitigated to a large extent using available technologies, such as separation and biogas recovery. Opportunities for methane mitigation in the agriculture sector are much more limited and uncertain, and may be reliant on newer technologies (Nisbet et al. 2020).

Many studies have highlighted the significant co-benefits of methane mitigation for both climate and air quality (e.g. Fiore et al. (2008), Stohl et al. (2015), Allen et al. (2021), Shindell et al. (2005), and Shindell et al. (2021)). Allen et al. (2021) used the SSP experiments from AerChemMIP to isolate the methane-only contribution of SLCF mitigation from a high methane scenario (SSP3-7.0) level down to SSP1-2.6 levels. They showed that by 2050, the global mean atmospheric methane concentration decreases by 26%, resulting in a 9.7% decrease in surface ozone concentrations, and a temperature decrease of 0.39 ± 0.05 K, compared to SSP3-7.0. Shindell et al. (2021) explored a methane concentration reduction of 30% compared to present day (2015) using an ensemble of models. They attributed a global population-weighted ozone exposure decrease of 2-2.5 ppb, and a temperature decrease of 0.18 ± 0.02 K to the methane change. Ocko et al. (2021) found that a quarter of a degree of warming could be avoided by 2050 by implementing currently available methane mitigation technologies. Abernethy

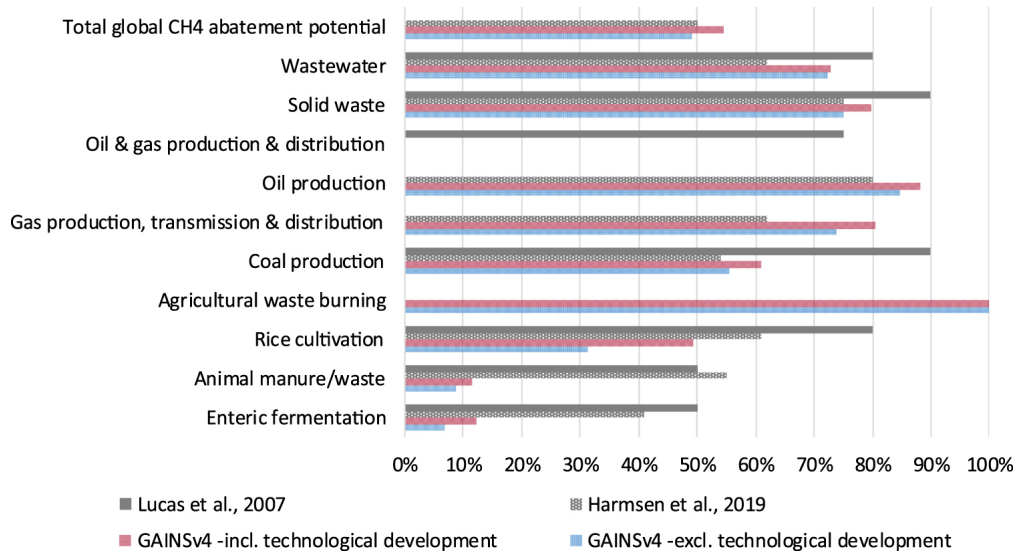


Figure 1.8: Maximum technically feasible reductions for methane emissions by sub-sector, calculated by Harmsen et al. (2019) and Lucas et al. (2007) and in the GAINsv4 model. Figure from Höglund-Isaksson et al. (2020) (Fig 13).

et al. (2021) explored methane removal scenarios using UKESM1-ems, with different removal amounts and rates. They estimated that every petagram of methane removed leads to a 0.21 ± 0.04 K decrease in global mean surface temperature and a 1.0 ± 0.2 ppb decrease in global mean surface ozone concentration.

While the link between methane mitigation and climate and air quality benefits is established, these studies have all been done with concentration-driven models (with the exception of Abernethy et al. (2021)). In these models, methane emissions reductions are applied globally rather than at the locations of the sector and country emissions. Updated studies with emissions-driven models would provide a more complete picture, with non-uniform methane emissions interacting with non-uniform oxidant fields. As discussed in section 1.3, the use of a lower boundary condition also limits the feedbacks that can be simulated, in particular the methane self-feedback. The inclusion of this feedback would ensure that the methane cycle is more fully represented in the mitigation experiments, and would likely lead to a more accurate representation of the evolution of methane and methane lifetime over time.

1.5 Thesis outline

The aims of this thesis are to evaluate and explore the new capability of the methane emissions-driven configuration of UKESM1. I test out this new configuration, which is a key development that will be integrated into the next generation of Earth system models.

Showcasing the new state-of-the art methane treatment in Earth system modelling, I simulate the atmospheric impacts of methane mitigation in a model with a fully-represented methane cycle. This shows the central role of methane in atmospheric chemistry and the widespread impacts of methane changes on composition and climate. I show the advantages of simulating the full methane cycle - being able to explain composition changes and the underlying processes more comprehensively.

This work exhibits a new tool for evaluating methane mitigation methods, which can be used to underpin policy decisions in climate and air quality, both globally and on a regional scale.

Chapter 2 introduces UKESM1-ems, the Earth system model used throughout this thesis. It includes a description of UKESM1-ems, and evaluation of the model performance against previous model versions and observations.

In Chapter 3, an attribution experiment is explored where anthropogenic methane is removed from 2015 onwards (up to 2050) in a zero anthropogenic methane emissions (ZAME) experiment. The climate and composition impacts of this large scale change are studied.

Chapter 4 takes the ZAME experiments further, implementing CO and NO_x emissions reductions down to SSP1-2.6 levels. The aim of this chapter is to better understand the relationships between CO, NO_x, OH and methane in UKESM1-ems.

In Chapter 5, UKESM1-ems is used for a mitigation experiment based on the Global Methane Pledge, up to 2030 and beyond. The potential impacts on climate and air quality of a full realisation of the Methane Pledge are explored.

Chapter 6 concludes this thesis with a summary of the outcomes as well as areas for future work.

Chapter 2

Description and evaluation of the UKESM1-ems model

Abstract

The emissions-driven configuration of the UK Earth System Model (UKESM1-ems) represents an improvement in the representation of methane processes in the atmosphere in chemistry-climate models. The emissions-based approach leads to an improvement in the simulation of methane distribution in the atmosphere. This is shown through improvements in simulating the interhemispheric gradient, latitudinal distribution and vertical profile of methane, compared to the previous model configuration, which uses a lower boundary condition. These metrics are evaluated with a view to using UKESM1-ems for mitigation experiments, to understand the strengths and limitations of this model.

I compare UKESM1-ems against observations for the 1985-present period and show that the model reproduces the trends observed in methane mixing ratios over this time period, suggesting that the processes causing the recent trends are captured in the model. UKESM1-ems underestimates the absolute mixing ratios by around 10%, likely due to missing methane emissions inputs, and an overestimate of OH in the model.

Some of my work in this chapter was included in the publication ‘Description and Evaluation of an Emission-Driven and Fully Coupled Methane Cycle in UKESM1’, see Folberth et al. (2022). My role in this included analysis of historical simulations, comparison with observations, writing the corresponding sections and reviewing the manuscript in collaboration with the co-authors.

2.1 Introduction

This chapter introduces the UK Earth System Model (version 1.0), both in its standard release configuration (UKESM1-conc) as well as the methane emissions-driven configuration (UKESM1-ems), which is the focus of this work. Section 2.2 describes both models and the emissions used.

At the start of this project, UKESM1-ems was still in development. Before starting any experiments it was necessary to understand how the model performs both compared to the previous configuration, and against observations. This model evaluation is the focus of the rest of the chapter: section 2.3 and 2.4 compare historical simulations for UKESM1-conc and UKESM1-ems; section 2.5 compares UKESM1-ems against observed historical methane mixing ratios; and section 2.6 compares the modelled methane vertical profiles with flight data. Finally, section 2.7 summarises the model evaluation and highlights further areas to explore.

UKESM1-ems represents an upgrade in the treatment of methane in Earth system models to a more realistic process-based approach, with explicit sources and sinks, described further in section 2.2.2. Table 2.1 outlines the metrics I've used for the evaluation of UKESM1-ems in the following sections. Each metric provides a different perspective on methane and other relevant compounds in the Earth system.

These metrics are explored with a view to using UKESM1-ems for the attribution and mitigation experiments in Chapters 3-5, and studying the atmospheric composition and climate impacts of imposed emissions changes. This evaluation will help to understand the strengths and potential limitations of using UKESM1-ems moving forward, and give a better idea of its capabilities, which will be helpful for designing experiments.

Metric	Why is this important?
Methane mixing ratio	A measure of atmospheric concentration of methane, independent of pressure. Both the absolute concentration and trends are important for climate and atmospheric composition.
Methane burden	The total amount of methane in the atmosphere, usually in Tg. Used to calculate methane lifetime.
Methane lifetime	Combines the methane burden and the flux through the $\text{CH}_4 + \text{OH}$ reaction to give an indication of the timescale for methane destruction by OH in the atmosphere. This determines the residence time of methane in the atmosphere and therefore also its radiative impacts.
Interhemispheric gradient	The difference between northern and southern hemispheric methane mixing ratios, it is affected by methane emissions, oxidation of methane and transport through the atmosphere. Also gives an indication for the timescale of northern hemisphere emissions propagating into the southern hemisphere/background mixing ratio.
Latitudinal distribution	A more detailed spatial view of methane sources and sinks to identify where emissions or sinks could be missing or too high.
Vertical profile	An indication of mixing time in the troposphere and stratosphere and the vertical distribution of sources and sinks.
OH concentration and distribution	OH is the primary atmospheric oxidant and these metrics give an indication of the oxidative capacity of the atmosphere. Strongly affects the lifetime of many VOCs including methane and CO.
CO mixing ratio and distribution	CO is closely linked to methane via its oxidation by OH, and is also a product of methane oxidation. Provides further information on the coupling between OH and methane.
Ozone	Important for air quality and also a greenhouse gas. Responds to changes in methane and OH and so is important to simulate for methane mitigation experiments.

Table 2.1: Metrics for model evaluation and reasoning for their inclusion in this analysis.

2.2 Model description

2.2.1 UK Earth System Model (UKESM1-conc)

The UK Earth System Model (version 1.0, UKESM1) is the basis of the experiments in this thesis and is a key Earth System Model (ESM) used in CMIP experiments. UKESM1 is described in Sellar et al. (2019) and focuses on modelling processes directly, where possible, rather than prescribing parameters from external sources. A series of component models representing different parts of the Earth system couple together to form UKESM1, as shown in Fig 2.1. The United Kingdom Chemistry and Aerosol model (UKCA) simulates the atmospheric composition (Archibald et al. 2020a). The Joint UK Land Environment Simulator (JULES) simulates land processes (Clark et al. 2011).

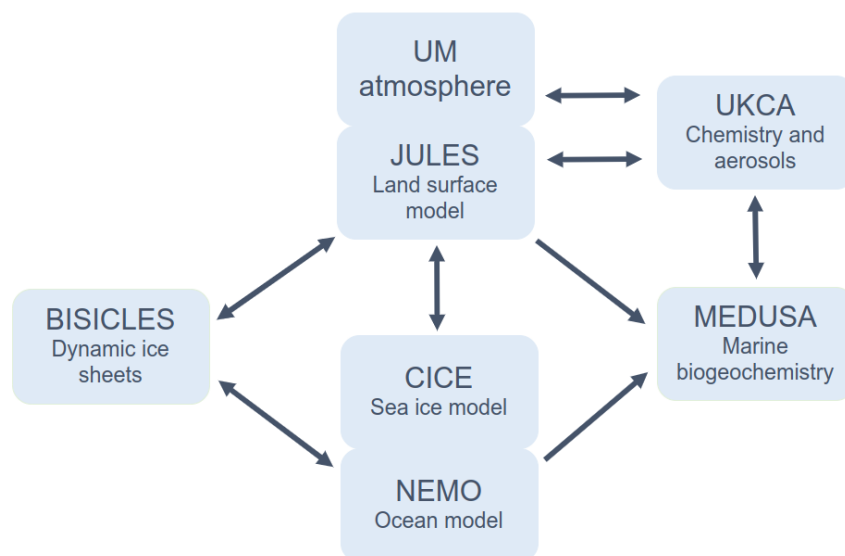


Figure 2.1: Schematic of the structure of the UK Earth System model, showing its component models and how they couple with each other.

The standard configuration of UKESM1 simulates methane using a prescribed methane mixing ratio at the surface (a lower boundary condition). These mixing ratios are derived from external models and are applied globally: the methane is spatially invariant at

the surface but changes over time. Methane emissions from wetlands are simulated in JULES, but are diagnostic only and don't influence the modelled methane mixing ratio. This configuration of UKESM1 is hereafter referred to as UKESM1-conc. The model resolution used throughout this work is N96 (1.25 x 1.875 degrees), and the model height is 85 km (85 unevenly spaced vertical levels). The chemistry scheme used in UKCA here is StratTrop (Archibald et al. 2020a).

2.2.2 Emissions-driven UKESM1

The emissions-driven UKESM1 configuration (hereafter referred to as UKESM1-ems) represents the state-of-the-art in chemistry-climate modelling in terms of methane (Folberth et al. 2022). The main difference compared to UKESM-conc is the inclusion of explicit emissions sources for methane at the surface, instead of a prescribed mixing ratio. A more detailed UKESM1-ems model description can also be found in Folberth et al. (2022), section 2.

Methane emissions

The different sources of methane are included in UKESM1-ems separately based on: availability of emissions inventories, ability to directly simulate the emission processes within the model, and uncertainty in emissions magnitude and variability. The methane emissions are inputs into the model, with the exception of wetland emissions, which are calculated online.

The anthropogenic and biomass burning emissions used are from CMIP6 inventories (Hoesly et al. 2018; Van Marle et al. 2017). Anthropogenic emissions include those from fossil fuel use, agriculture, waste and other human activities. Biomass burning emissions are currently prescribed in UKESM1-ems, but there is work taking place to include interactive biomass and wildfire emissions in future versions of UKESM1-ems (Folberth et al. 2022).

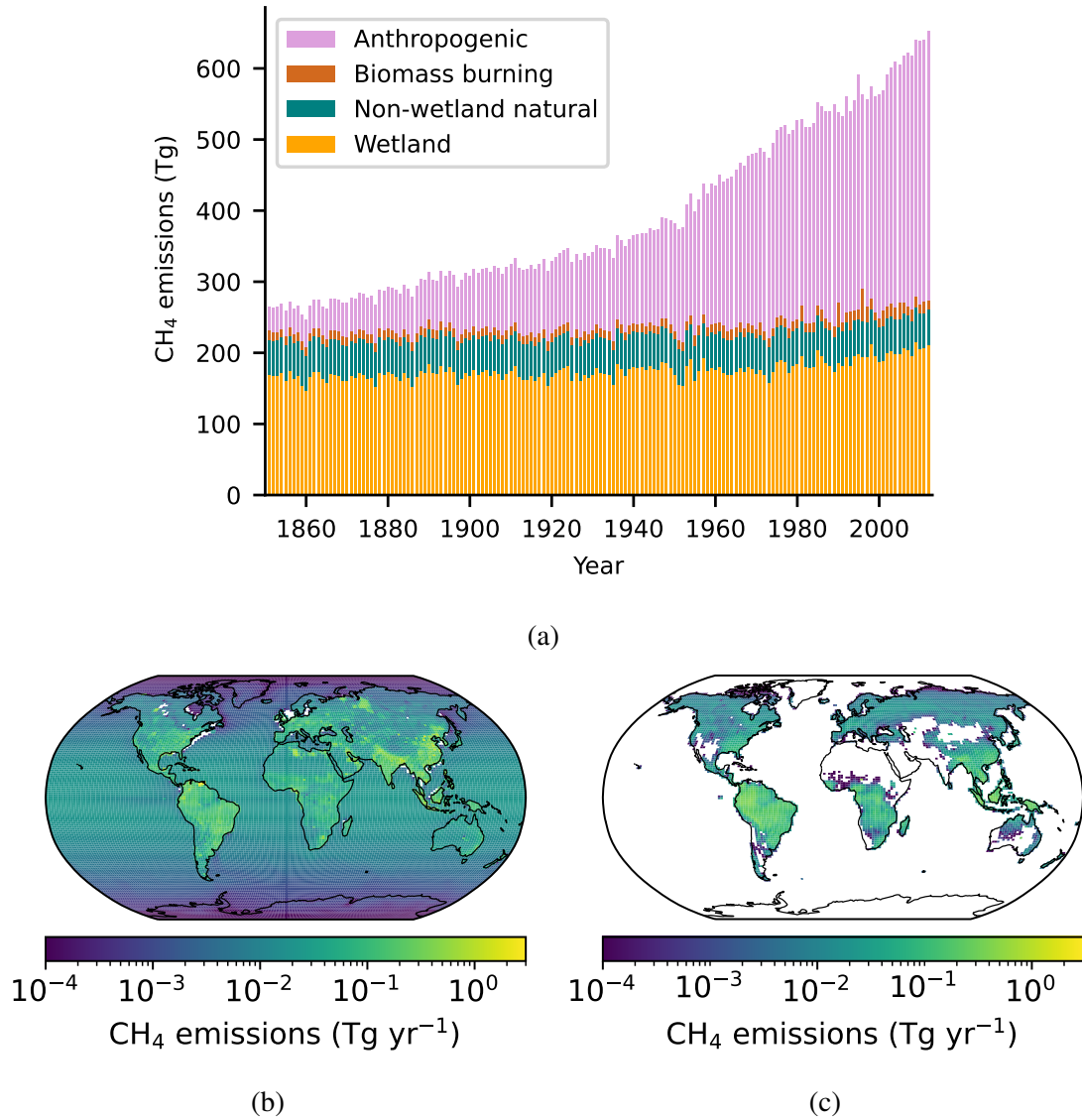


Figure 2.2: Methane emissions in UKESM1-ems. Anthropogenic and biomass burning emissions are from the CMIP6 inventory (Gidden et al. 2019), wetland emissions are calculated in the model interactively using JULES (Clark et al. 2011), and non-wetland natural emissions are based on (Fung et al. 1991). (a) Emissions used in the historical experiments. (b) 2000-2009 decadal mean distribution of non-wetland methane emissions used as model input for UKESM1. (c) 2000-2009 decadal mean distribution of wetland methane emissions.

Wetland emissions of methane are simulated using JULES, using the parametrisation described in section 1.2.1. While in UKESM1-conc these are diagnostic only, in UKESM1-ems the JULES wetland scheme couples into UKCA; the wetland emissions are interactive. The overall methane production from wetlands depends on temperature, substrate availability and wetland extent, which is affected by precipitation (Gedney et al. 2019). Folberth et al. (2022) and Gedney et al. (2019) compared the wetland fraction simulated by JULES against observation-based estimates (from Davidson et al. (2018) and Zhang et al. (2021)), and found that it compared well spatially and temporally. The global total wetland area was within the observational spread (Gedney et al. 2019). The modelled wetland emissions in UKESM1-ems are in good agreement with top-down and bottom-up estimates from Saunio et al. (2020) and Kirschke et al. (2013) (see first line in Table 2.2). The uncertainty in each of these wetland emissions estimates is very high (between 20-50% of the total wetland emissions). This is one of the major uncertainties in the methane budget and represents a large uncertainty in the methane emissions in UKESM1-ems, which can propagate through to the methane mixing ratio and burden. The JULES model and wetland emissions outputs are not evaluated further here, but are acknowledged as a potential source of error.

The magnitude of the non-wetland natural emissions sources of methane is also highly uncertain due to the dispersed nature of the sources (Saunio et al. 2020). In UKESM1-ems, these emissions are prescribed at 50 Tg per year: 20 Tg from ocean sources, 20 Tg from termites and 10 Tg from hydrates, corresponding to results from Fung et al. (1991). These are assumed to be constant over time, due to absence of better understanding.

Figure 2.2a shows the methane emissions UKESM1-ems over the historical period, including the relative magnitudes of the different methane sources. While wetland, biomass burning and non-wetland natural emissions remain relatively constant over time, anthropogenic methane emissions have steadily increased since the pre-industrial era and now make up the majority of methane emissions. Figure 2.2 also shows the regional distribution of methane emissions used in UKESM1-ems for 2000-2009. Anthropogenic emissions are mainly located in the northern hemisphere and correspond to industrialised areas. Wetland emissions are highest around the tropics and are distributed more evenly between the hemispheres.

	UKESM1-ems	2000-2009 decadal means in Tg(CH ₄) per year			
		Kir-BU	Kir-TD	Sau-BU	Sau-TD
Sources					
Wetlands	197	217 [177-284]	175 [142-208]	147 [102-179]	180 [153-196]
Anthropogenic	333	331 [304-368]	335 [273-409]	334 [321-358]	332 [312-347]
Wildfires	11	3[1-5]	n/a	n/a	n/a
Termites	20	11 [2-22]	n/a	9 [3-15]	n/a
Oceanic sources	21	18 [2-40]	n/a	13 [9-22]	n/a
Methane hydrates	9	6[2-9]	n/a	0	n/a
Sinks					
Total chemical loss	549	604 [483-738]	518 [510-538]	595 [489-749]	505 [459-516]
Tropospheric OH	525	528 [454-617]	n/a	553 [476-677]	n/a
Tropospheric O(1D)	1	n/a	n/a	n/a	n/a
Stratospheric OH, O(1D)	23	51 [16-84]	n/a	31 [12-37]	n/a
Tropospheric Cl	n/a	25 [13-37]	n/a	11 [1-35]	n/a
Soil uptake	31	28 [9-47]	32 [26-42]	30 [11-49]	34 [27-41]
Overall budget					
Sum of sources	591	678 [542-852]	548 [526-569]	703 [566-842]	547 [524-560]
Sum of sinks	580	632 [592-785]	540 [514-560]	625 [500-798]	540 [486-556]
Imbalance	11	46	3 [-4-19]	78	3 [-10-38]
Atmospheric growth	9.3	n/a	6	n/a	5.8 [4.9-6.6]

Table 2.2: Comparison of methane emissions and sink terms between the UKESM1-ems model (values from Folberth et al. (2022)) and the top-down (TD) and bottom-up (BU) estimates from Saunio et al. (2020) and Kirschke et al. (2013). Decadal averages for 2000-2009 are shown in Tg (CH₄) per year. Uncertainties are reported as the [min-max] range from the included studies. Note that for the BU estimates not all sources are included, notably non-wetland natural emissions.

Methane sinks

The photochemical sinks for methane are simulated in UKCA. This includes the reaction with OH, which is the dominant sink for methane, and stratospheric loss. The reaction with chlorine radicals is not included in UKCA. In UKESM1-conc, there is no soil sink for methane. In UKESM1-ems, the methane surface removal process is

included via surface dry deposition. The size of the sinks in UKESM1-ems are in very good agreement with the bottom-up estimates from Saunio et al. (2020), shown in Table 2.2 (Folberth et al. 2022).

2.2.3 Running UKESM1-ems experiments

When I started this project, the methane emissions-driven configuration of UKESM1 was still in development stages, and not widely available in the standard release versions of UKESM1. UKESM1-ems was developed by Gerd Folberth at the MetOffice, who provided the historical, SSP3-7.0 and an SSP1-2.6 experiments used for the data analysis in this chapter. These were run on the MetOffice internal supercomputer. I accessed the data from these experiments via the MetOffice MASS storage archive, and used the JASMIN UK collaborative data analysis facility to convert the data and perform the analysis.

For my own experiments in Chapters 3-5, I ran UKESM1-ems on the Monsoon2 high-performance computer. This included experiment design, creating emissions inputs files, running extra baseline and spin-up runs, and setting up an experiment for each scenario and its ensemble members. In this case, as is standard practice when using UKESM1, the different ensemble members are started off in 2015 from different historical experiments (which end in 2014). These historical experiments are started from slightly different points in the pre-industrial climatology in UKESM1-ems, to give an approximation of the model spread in a given scenario.

For the experiments in this thesis, UKESM1-ems with a coupled atmosphere-ocean was used. At its fastest on Monsoon2, experiments run at a rate of around 10 model years per week, assuming no issues with the machine (of which there have been several over the course of my PhD). As expected with these kind of experiments, a large part of the model running included troubleshooting and solving problems when they arose.

2.3 Comparing UKESM1-ems and UKESM1-conc

In this section, UKESM1-ems is compared with UKESM1-conc over the historical period (1850-2015). My aim is to understand the similarities and differences between UKESM1-ems and UKESM1-conc - one of the CMIP6 models, which represent the current widely-used standard in chemistry-climate modelling. The differences between the two models can be attributed to the differing methane treatments: emissions-driven and concentration-driven. Here I explore the differences in methane mixing ratio, lifetime and ozone between the two models.

2.3.1 Methane mixing ratio

UKESM-ems and UKESM-conc show good agreement in annual mean methane mixing ratio up to 1920, where they start to diverge (see Fig 2.3). UKESM1-conc has a higher mixing ratio for the remainder of the time period up to 2015. This divergence coincides with anthropogenic emissions becoming a major methane source: by 1950, anthropogenic emissions surpass natural emissions (see Fig 2.2a). The rate of increase in mean mixing ratio is higher in 1950-1980 for both experiments, and flattens again after 1980. These profiles are consistent with the JAMSTEC ACTM simulations and measurements (direct and from ice cores) for the 1910-2010 time period (Ghosh et al. 2015).

Methane bias in the emissions-driven model

By the end of the historic period, the methane mixing ratio simulated by UKESM1-ems is approximately 150ppb lower than in UKESM1-conc (8%, year 2014). The bias relative to observations is discussed in section 2.5. In their emissions-driven model, Heimann et al. (2020) found a similar low bias of 190 ppb, or 11% (year 2000). In both cases the low bias can be attributed to either an insufficient source strength for methane i.e. too low emissions, or too large a tropospheric methane sink, largely based on the OH concentration. This low bias in methane has knock-on effects on other atmospheric

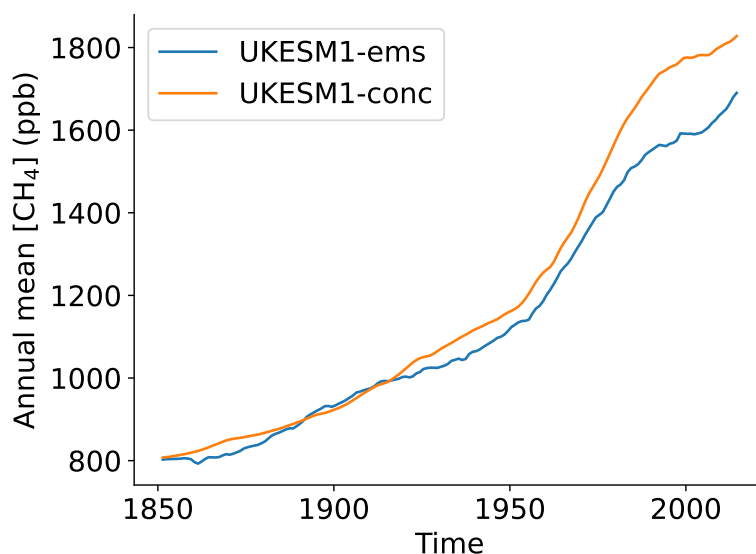


Figure 2.3: Annual mean methane mixing ratio over time since 1850 for UKESM1-conc (in orange) and UKESM1-ems (in blue).

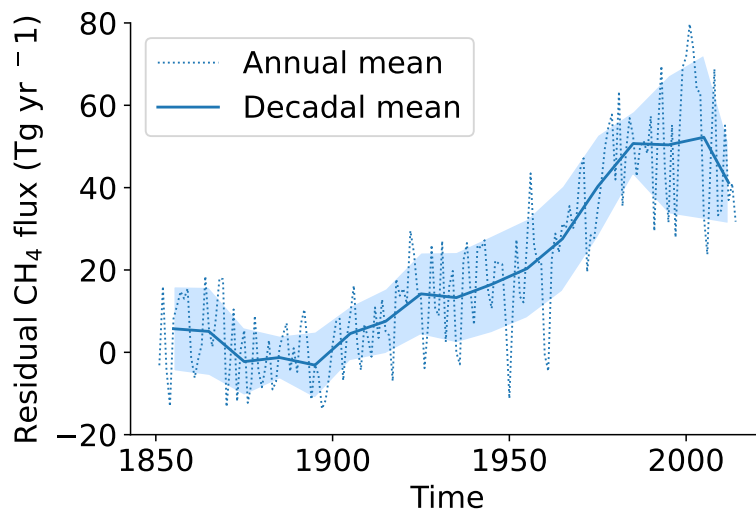


Figure 2.4: Time series of the annual (dotted line) and decadal average (solid line) total residual surface exchange flux needed to reconcile the difference in surface methane mixing ratio between UKESM1-ems and UKESM1-conc, from pre-industrial to present day (1850-2015), in $\text{Tg}(\text{CH}_4) \text{yr}^{-1}$. The envelope shows 1σ around the decadal means.

components through methane chemistry and radiative effects: this is explored in the sections below.

To quantify the possible missing emissions, Folberth et al. (2022) calculated the residual methane surface flux required to reconcile the difference in modelled mixing ratio, shown in Fig 2.4. This decadal mean residual flux is around 50 ± 20 Tg in the decade 2000-2009. A missing source of this magnitude is within the uncertainty limits for the emissions estimates from both anthropogenic sources (333 Tg, 15%) and wetland sources (197 Tg, 20%). Missing emissions are also consistent with a recent study suggesting that anthropogenic methane emissions estimates are too low, based on re-evaluation of pre-industrial ice-core records (Hmiel et al. 2020).

2.3.2 Methane lifetime

The methane lifetime is a measure of the oxidative capacity of the atmosphere. In this work, the methane lifetime with respect to tropospheric OH is calculated, using the whole atmosphere burden of methane (m) and the tropospheric CH_4 -OH flux (L_{OH}) - see equation 2.1 (Prather et al. 2012). The lifetime is primarily affected by the product of methane concentration, $[\text{CH}_4]$, the OH concentration, $[\text{OH}]$, and the $\text{CH}_4 + \text{OH}$ rate constant ($k_{\text{CH}_4+\text{OH}}$, which has a strong temperature dependence (Atkinson et al. 2004)). These concentrations are not independent and are also affected by other variables such as the CO and O_3 concentrations. The methane lifetime is also an important metric in comparing different chemistry-climate models and their oxidising capacity.

$$\tau_{OH} = \frac{m}{L_{OH}} = \frac{m}{k_{\text{CH}_4+\text{OH}} [\text{OH}][\text{CH}_4]} \quad (2.1)$$

The methane lifetime as a function of time over the historical period is shown in Fig 2.5a, for UKESM1-ems and UKESM1-conc. From 1850 to 1920 the methane lifetime increased steadily in both experiments, correlated with an increase in methane mixing ratio (Fig 2.3). After 1920, the methane lifetimes start to diverge, likely due to the

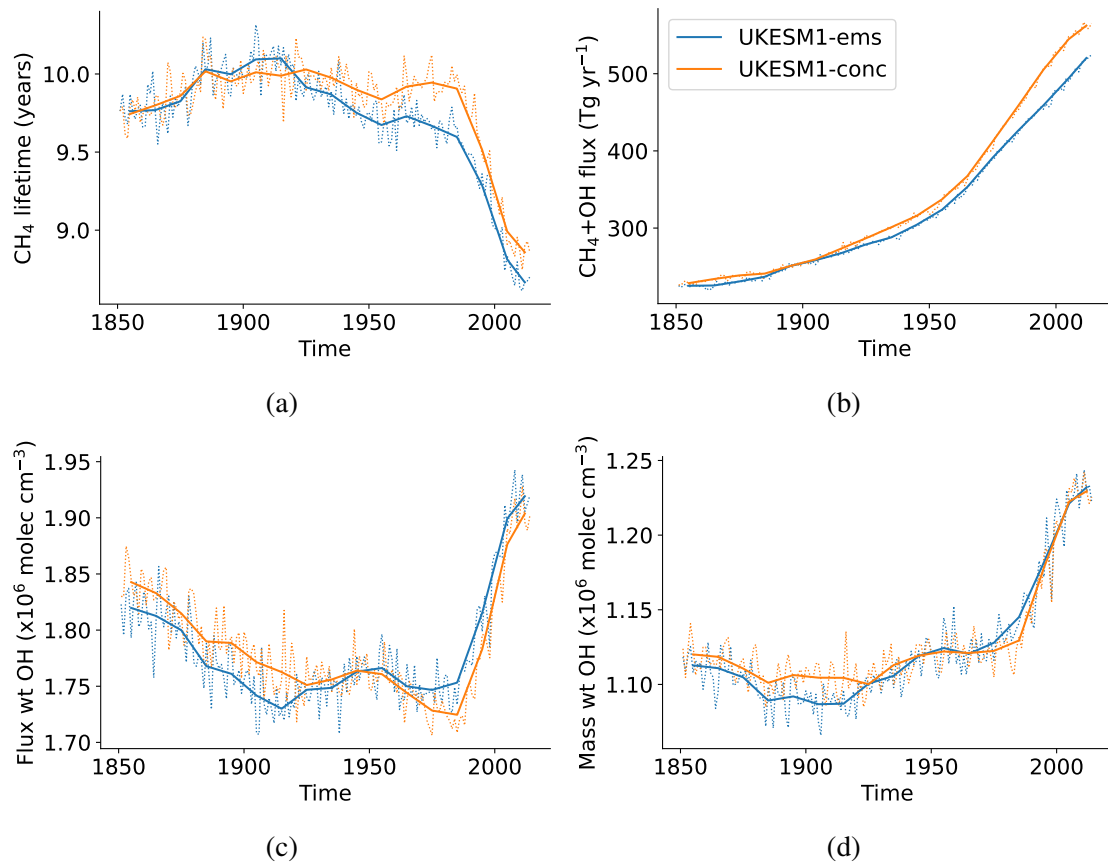


Figure 2.5: Comparison of historical trends between UKESM1-ems (in blue) and UKESM1-conc (in orange): annual means (dotted lines) and decadal means (solid lines). (a) Methane lifetime, calculated as the total atmospheric methane burden divided by the tropospheric $\text{CH}_4 + \text{OH}$ reaction flux. (b) Flux through the $\text{CH}_4 + \text{OH}$ reaction over time. (c,d) OH tropospheric mean concentration, calculated using CH_4 -reaction-weighting and airmass-weighting respectively (see (Lawrence et al. 2001)).

arising anomaly in methane mixing ratio. The UKESM1-conc methane lifetime remains fairly constant, with a small decrease up to 1980, whereas the UKESM1-ems methane lifetime decreases steadily from 1920. Between 1980 and 2015, the lifetime in both decreases by around $\sim 10\%$.

For the ACCMIP experiments in CMIP5, Naik et al. (2013) calculated a multi-model mean reduction in methane lifetime between 1850 and 2000 of $2.0 \pm 8.8\%$. The reductions observed in UKESM1-ems and UKESM1-conc are 12% and 10% respectively,

greater than this multi-model upper bound estimate. The methane lifetime between 1980 and 2000 decreased by 8.2% in UKESM1-ems and 9.3% in UKESM1-conc, compared to a $4.3 \pm 1.9\%$ decrease in ACCMIP. Naik et al. (2013) attributed the decrease in lifetime to climate warming and an increase in OH. The multi-model experiments were timeslice simulations, where the system is in steady state. UKESM1-ems and UKESM1-conc are transient integrations, in which methane is unlikely to be in steady state, which may contribute to the discrepancy between the calculated lifetimes.

2.3.3 CH₄ + OH reaction flux

The methane concentration, OH concentration and the temperature dependence of the CH₄ + OH rate constant all affect the CH₄ + OH reaction flux (calculated as $k_{CH_4+OH} [OH][CH_4]$). Since the flux and the methane burden are used to calculate the methane lifetime (see Equation 2.1), the changes in all of these quantities can be used to explain the trends in methane lifetime over time.

Figs 2.5c,d show the CH₄-reaction-weighted and airmass-weighted tropospheric means of OH respectively, as recommended by Lawrence et al. (2001). This enables comparison with a range of studies - the weighting used has a large impact on the calculated tropospheric mean. The CH₄-reaction-weighted OH gives an indication of OH changes that affect the CH₄ + OH reaction flux. Further discussion on the trends in OH can be found in section 2.4.

Fig 2.5b shows a steadily increasing CH₄ + OH reaction flux over time. However, the increase in flux-weighted OH mixing ratio between 1910-1950, and decrease up to 1980 (Fig 2.5c) are not replicated in the CH₄ + OH flux trend, suggesting that changes in OH do not have a significant effect on the flux trend in this time period. Between 1910-1980, the dominant drivers of methane lifetime change are likely to be the increasing methane concentration over time and the increasing temperature. After 1980, the growth rate in methane mixing ratio decreases and flattens (see Fig 2.3), corresponding to a reversal in trend and a large increase in OH (Fig 2.5c). Meanwhile, the CH₄ + OH reaction flux continues to increase, decreasing the methane lifetime over this period (see Fig 2.5a).

After 1920, the methane lifetime in UKESM1-conc is longer than in UKESM1-ems, despite the larger $\text{CH}_4 + \text{OH}$ flux, which is the main sink term. The larger methane burden in UKESM1-conc outweighs the difference in flux terms (see equation in section 2.3.2).

The $\text{CH}_4 + \text{OH}$ flux trend can help to explain the drivers behind changes in the methane burden over time. The rate of change of methane burden is controlled by production (P) and loss (L) terms, shown in equation 2.2. P represents methane emissions. L is equivalent to the $\text{CH}_4 + \text{OH}$ flux (Fig 2.5b), assuming the other sinks are negligible in comparison (Prather et al. 2012). During the hiatus period (1999-2006), the rate of change of methane burden over time is zero: P and L must be balanced for this to occur.

$$\frac{d[\text{CH}_4]}{dt} = P - L \quad (2.2)$$

Fig 2.5b shows that L continues to increase throughout the hiatus period, which suggests that P must also be increasing at the same rate so that $\frac{d[\text{CH}_4]}{dt} = 0$. After 2007 the loss rate continues to increase. This suggests that the renewed growth rate is due to (larger) increases in the source strength (Kirschke et al. 2013) such that $\frac{d[\text{CH}_4]}{dt} > 0$, rather than a decrease in the sink strength, as suggested by Turner et al. (2017).

2.3.4 Ozone

The impact on ozone following a change in methane emissions is an important parameter for methane mitigation experiments. One of the main benefits of methane emissions reductions is through air quality benefits from reducing ozone concentrations. Therefore, it is important to understand if and how ozone differs between emissions-driven and concentration-driven models.

The annual mean surface ozone mixing ratio in UKESM1-ems is lower for the entire period from pre-industrial times to the present day (see Fig 2.6a). The increased difference between UKESM1-ems and UKESM1-conc after around 1950 is consistent with

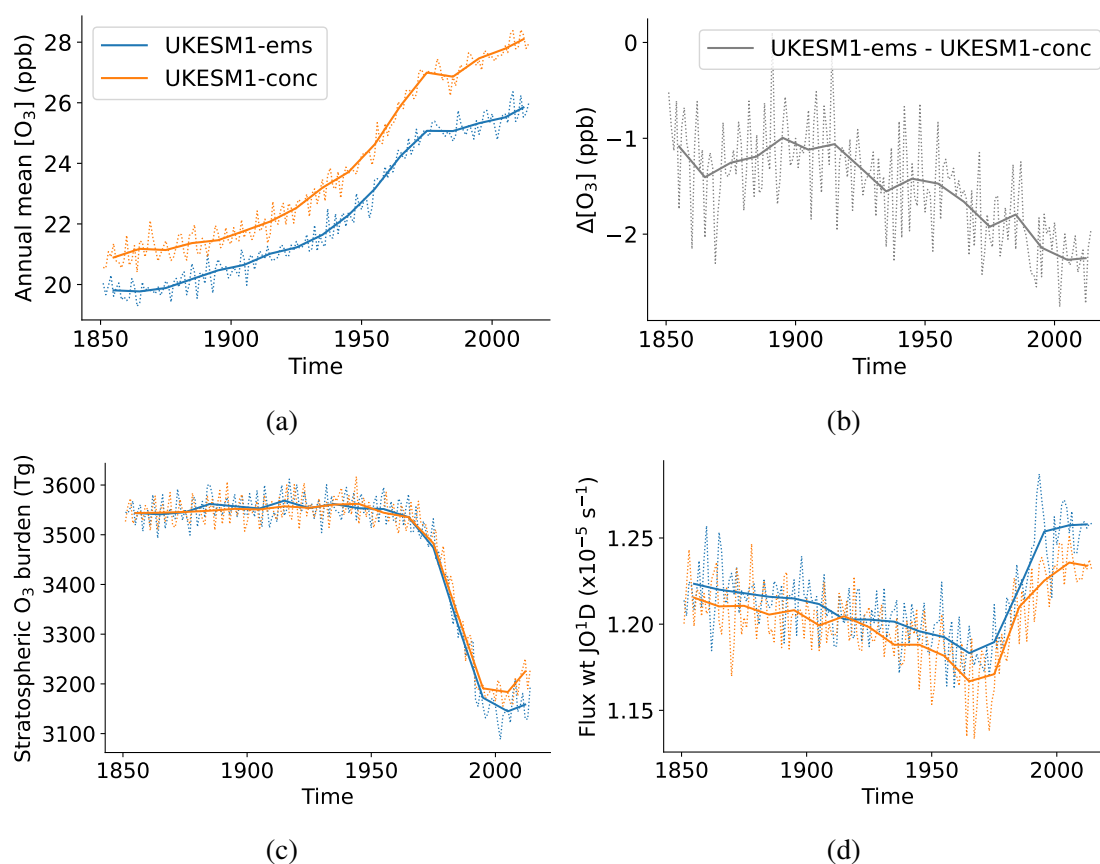


Figure 2.6: (a) 1850-2014 modelled historical annual mean surface ozone concentrations, for UKESM1-ems (blue) and UKESM1-conc (orange): annual means (dotted lines) and decadal means (solid lines). (b) Difference (UKESM1-ems - UKESM1-conc) in modelled surface ozone concentration. (c) 1850-2014 modelled historical stratospheric ozone concentrations (d) 1850-2014 modelled historical JO(¹D).

the lower methane concentration in UKESM1-ems (Fig 2.3). The difference in ozone between UKESM1-conc and UKESM1-ems in 1850-1950 is more surprising (Fig 2.6b). The global mean methane mixing ratios are very similar (see Fig 2.3), but the ozone difference may be attributable to the heterogeneous methane distribution in UKESM1-ems. Ozone production is a very localised process, and higher or lower methane concentrations in certain areas are likely to affect the local ozone production, leading to a difference in the global mean ozone concentration. To test this I looked at all of the ozone budget terms and calculated the total tropospheric ozone production and loss in

UKESM1-ems and UKESM1-conc. The total ozone production is lower in UKESM1-ems than in UKESM1-conc. The loss terms are dependent on the amount of ozone burden - in steady state, when production decreases then loss will also decrease. Overall, it is likely that the differences in ozone stem from lower ozone production in UKESM1-ems.

Another explanation for the difference in tropospheric ozone between UKESM1-ems and UKESM1-conc could be a difference in stratospheric ozone, and JO^1D . Ozone is exchanged between the stratosphere and troposphere, so the stratosphere can be a source for tropospheric ozone. Stratospheric ozone also affects the JO^1D flux, which in turn affects photolysis rates in the troposphere and therefore the amount of ozone. The stratospheric ozone burden in UKESM1-ems matches that of UKESM1-conc closely (see Fig 2.6c). The rapid decrease in stratospheric ozone after the 1960s can be clearly seen following the widespread use of ozone-depleting substances, with signs of recovery from the 1990s onwards. The JO^1D fluxes for UKESM1-ems and UKESM1-conc are very similar for the whole time period, although with high interannual variability (Fig 2.6d). From these I conclude that the difference in pre-industrial ozone is not due to a difference in JO^1D flux, or ozone transported from the stratosphere, and instead from changes in the production terms as suggested above.

2.4 OH multi-model comparison

In this section I explore the changes in OH over time in UKESM1-ems and UKESM1-conc, and also compare the OH distribution in these models to the multi-model ensemble from ACCMIP, and an observationally-constrained estimate from Spivakovsky et al. (2000). The modelled OH distribution has a large impact on methane, and most other atmospheric chemistry species, so understanding it is important for experiments going forward.

The magnitude and distribution of OH concentrations are both important in defining the oxidative capacity of the atmosphere. Trends in the hydroxyl (OH) concentration over

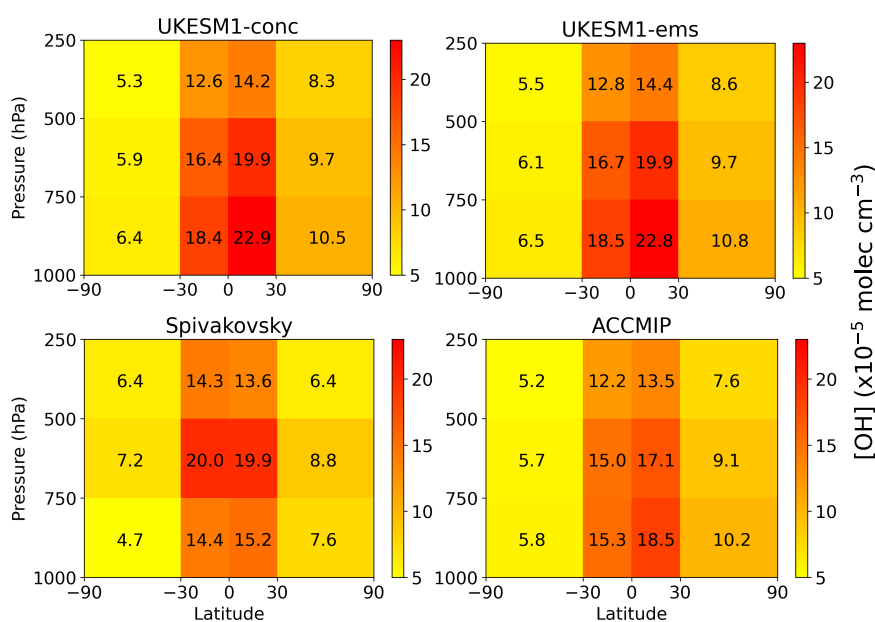


Figure 2.7: Comparison of OH distribution for the period 2000-2009 between UKESM1-ems (Folberth et al. 2022), UKESM1-conc (Archibald et al. 2020a), ACCMIP (Naik et al. 2013) and Spivakovsky (Spivakovsky et al. 2000) results. The OH concentration is air-mass weighted. The troposphere is split into 12 latitude and altitude areas of approximately equal mass, as in Lawrence et al. (2001).

time are affected by many factors including temperature, CO concentrations, methane, VOC emissions and NO_x emissions.

Weighting the OH mixing ratio by the $\text{CH}_4 + \text{OH}$ reaction flux shows the OH concentration where the methane oxidation happens: at the surface, and in the tropics. Between 1850 and 1920, the flux weighted OH concentration decreases (Fig 2.5c) corresponding to the increase in methane mixing ratio (Fig 2.3). After 1920, increasing ozone precursor emissions, which act to increase ozone and therefore OH, act against the continued increase in methane to give no net trend in OH (Stevenson et al. 2020). The increase in tropospheric mean OH in UKESM1-ems and UKESM1-conc between 1980 and 2014 (8%) is consistent with the multi-model results from AerChemMIP (9%, Stevenson et al. (2020)).

The OH distribution can be split into latitude and altitude regions according to Lawrence et al. (2001) to enable comparison between models, and against observation-based reference levels. These estimates were computed using a photochemical box model and atmospheric measurement constraints of ozone, CO, NO_x, hydrocarbons, water vapour, temperature and other parameters (Spivakovsky et al. 2000). OH is highest in the tropical troposphere (1000-500hPa, 30S-30N), as shown by the red and dark orange areas in Fig 2.7. There is generally good agreement between UKESM1-ems and the UKESM1-conc and ACCMIP models. The 2005-2014 decadal tropospheric mean OH concentration for ACCMIP is $1.11 \pm 0.16 \times 10^6$ (Archibald et al. 2020a): UKESM1-ems and UKESM1-conc both lie within this range (both 1.23×10^6 , mass-weighted).

In terms of the effect of methane treatment on OH, there are no significant differences between the UKESM1-ems and UKESM1-conc OH distributions. The OH concentration is higher near the surface in the tropics for both UKESM1 models compared to the ACCMIP average and the observation-based estimate (Fig 2.7 bottom left (Spivakovsky et al. 2000)). Naik et al. (2013) found that the ensemble of 17 CMIP5 models consistently simulated higher OH concentrations in the northern hemisphere, with interhemispheric ratios of 1.28 ± 0.1 (for 2000). Observation based estimates predict no gradient, or a reversed gradient in OH (0.88 ± 0.3 , Prinn et al. (2001)). UKESM1 also overestimates the interhemispheric gradient in OH compared to Spivakovsky et al. (2000) and Prinn et al. (2001). This is consistent with the CMIP5 models and affects the distribution of the OH sink, and therefore the distribution of methane.

2.5 Model evaluation against observations

In section 2.3, the model performance of UKESM1-ems was compared with another model (UKESM1-conc). In this section, results from UKESM1-ems are compared against sampled surface methane mixing ratios, to see how well the model performs against observations.

2.5.1 NOAA observation data

Background concentration data is necessary for analysis of long-term methane trends and evaluation of model performance. Measurements from close to point sources such as wetlands and landfills are not suitable for this purpose, as these do not represent the background (well-mixed) methane concentration. Also, the model would not be able to capture these real world small-scale variations due to its coarse resolution.

Surface methane concentrations from the NOAA ESRL GMD Carbon Cycle Cooperative Air Sampling Network (Lan et al. 2022) were used as the observation dataset for the historical global methane distribution. Monthly data are available from 1985, from flask samples of air collected at the stations shown in Fig 2.8 (Lan et al. 2022).

The stations shown in Fig 2.8 were mapped onto the N96 model grid (with resolution $1.25^\circ \times 1.875^\circ$) to enable comparison between model and observations. The latitudinal

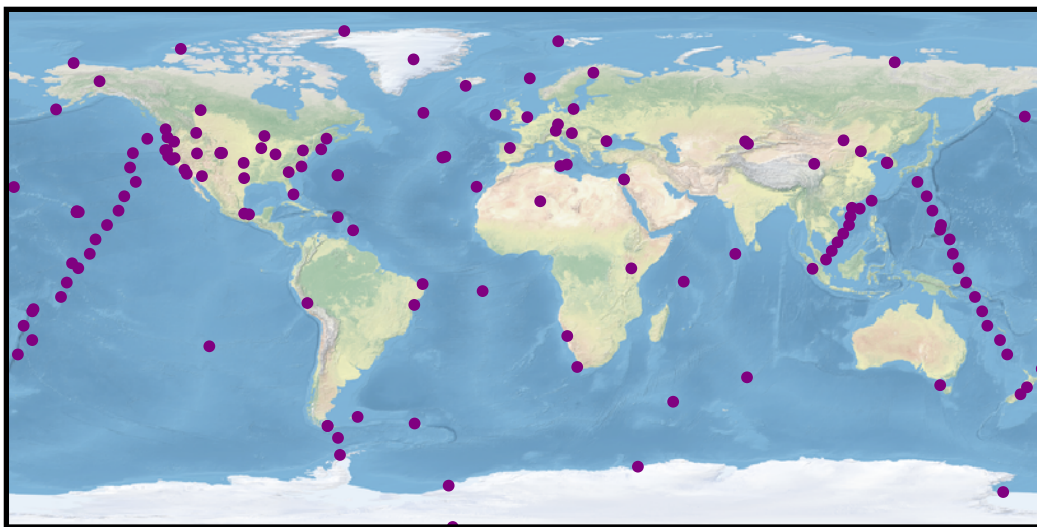


Figure 2.8: Locations of methane measurements from the NOAA ESRL GMD Carbon Cycle Cooperative Air Sampling Network. Measurements were obtained via surface flasks, for the 1985-2019 period. Not all stations have data for the whole period, and some are single measurements from ship cruises (Lan et al. 2022).

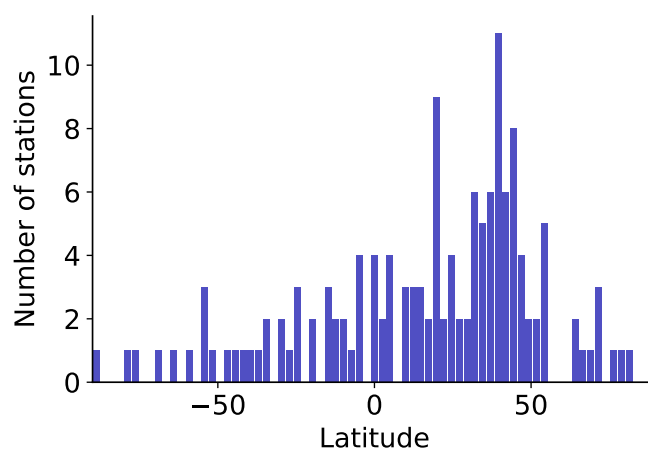


Figure 2.9: Number of NOAA CMDL measurement stations in each model latitude band over the time period 1985-2018. Note not all stations were measuring over the whole period.

resolution of UKESM1 is 1.25° (around 140km) - Fig 2.9 shows the number of stations in each model latitude band. The mean observed CH_4 surface mixing ratio for each model latitude band was calculated. The dataset covers the whole latitude range, with a higher density of stations in the northern hemisphere, but fewer measurement stations at high latitudes.

The latitude-binned observational data were interpolated in latitude and time using the SciPy 2D cubic interpolation method (Virtanen et al. 2020) to give a 144 latitude x 192 longitude observational dataset for 1985-2018, for direct comparison with the N96 UKESM1-conc and UKESM1-ems experiments. The historical UKESM1-ems run finishes in 2014, so the first three years of the SSP3-7.0 scenario were used in addition to the historical scenario to provide a dataset spanning the same time period as the observation dataset.

2.5.2 Methane mixing ratio comparison

UKESM1-conc, UKESM1-ems and observations all show an increase in methane surface mixing ratio of ~ 200 ppb over the 1985-2018 time period (see Fig 2.10a). Indirect

methane concentration data from before this period is available from ice cores, but is not studied here (Etheridge et al. 1998).

The UKESM1-conc methane trend is consistent with the observations (r squared = 0.96), with an underestimate of 10 ± 1 ppb (2005-2014 mean). In this model the surface methane concentration is prescribed. The lower boundary condition imposes a non-physical buffer to the methane concentration, so it is difficult to explain an underestimate in methane concentration using physical processes in the model i.e. the balance between sources and sinks. MAGICC is the model used to convert between emissions and concentrations to create the LBC inputs in CMIP6 (used in UKESM1-conc) (Meinshausen et al. 2011). A difference in the magnitude and distribution of OH between MAGICC and UKESM1-conc could explain the small difference in methane surface mixing ratio.

Most of the historic methane trend is captured in UKESM1-ems, with a correlation with the observations of 0.83 ± 0.06 . The model successfully replicates the hiatus period in 1999-2006 with constant global methane burden (Kirschke et al. 2013). In UKESM1-ems, the methane mixing ratio is determined by the relative magnitudes of the sources

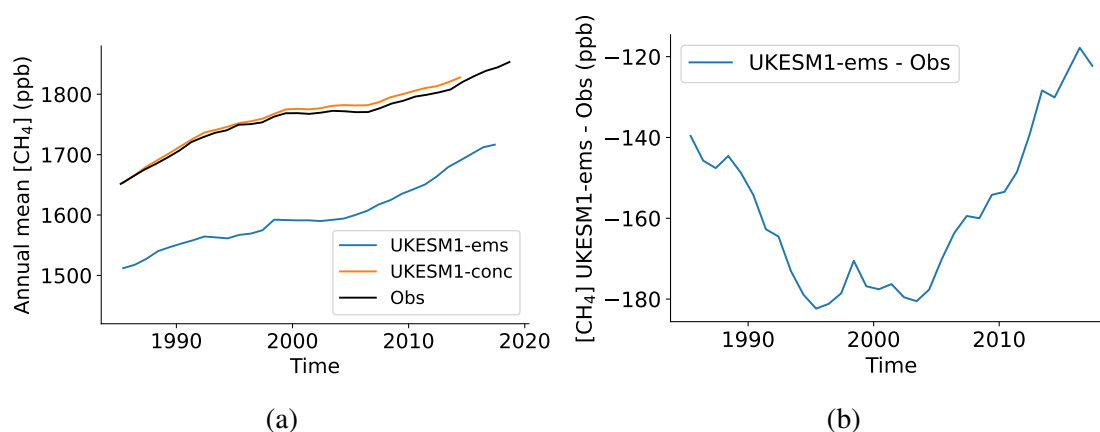


Figure 2.10: (a) Annual mean methane mixing ratio over time for 1985-2018. Observations from the NOAA CMDL network are shown in black, UKESM1-ems in blue and UKESM1-conc in orange. (b) Bias in the annual mean methane concentration of UKESM1-ems compared to NOAA CMDL observations. Corresponds to the blue - black curves in (a).

and sinks. This means the processes that caused the hiatus are included in the model: whether that means changes to natural or anthropogenic methane emissions (Zhang et al. 2022; Kirschke et al. 2013), or changes in the OH sink, or both (Turner et al. 2017).

However, the bias in UKESM1-ems with respect to observations (see Fig 2.10b) is around -130 ppb, which corresponds to approximately 8% of the observed methane mixing ratio (in 2014). There is a higher mismatch in the period between 1995-2003, when the anomaly is around 180 ppb. This could reflect a larger missing source of methane emissions in the CMIP6 inventory during this time.

The distribution of OH in UKESM1-conc and UKESM1-ems is very similar, but the more spatially heterogeneous distribution of methane in UKESM1-ems means that the distribution of methane oxidation may be different. The effect of an overestimate of OH in the northern hemisphere (Naik et al. 2013) is likely to be similar for UKESM1-conc and UKESM1-ems, and so does not explain the increased bias in UKESM1-ems. The remaining bias in UKESM1-ems may be due to underestimates in methane sources: the emissions in this configuration are not optimised with respect to observations. Transport between methane sources and areas of high methane oxidation rate may also have an effect.

Other emissions-driven models also underestimate methane, or require emissions optimisation to achieve parity with observed methane concentrations. Dalsøren et al. (2016) used the Oslo CTM3 global chemical transport model (CTM) to study the evolution of methane from 1970 to 2012. They used an emissions-driven configuration with emissions from EDGAR v4.2 and Bousquet et al. (2011), and simulated an increase in surface methane mixing ratio from 1984-2012 of around 180 ppb, but also underestimated the absolute concentrations by 5 % across this period. They attributed this to overestimates in the OH sink, and using emissions inventories optimised to a different OH distribution to the one modelled. He et al. (2020) developed an emissions-driven configuration of the GFDL-AM4.1 chemistry-climate model. They simulated the methane mixing ratio time series compared to the NOAA observations with a root mean square error (RMSE) of 10.4-11.6 ppb, which they attribute to emissions optimisation undertaken for wetland and anthropogenic emissions.

UKESM1-ems captures the trend of methane over time, and predicts the methane mixing ratio within $\sim 10\%$ of the observed values. This suggests that the model successfully simulates the main factors controlling the methane concentration. The emissions in UKESM1-ems are not optimised, and the OH is not prescribed, so there are more free running parameters than in the models discussed above, which leads to a potential for an increased bias with respect to observations.

2.5.3 Interhemispheric gradient of methane and CO

The interhemispheric gradient is the difference in surface methane mixing ratio between the northern and southern hemispheres (NH and SH), measured in parts per billion (ppb). This gradient is positive and arises from the geographical imbalance of sources and sinks. Most methane sources are land-based (see section 1.2.1). The northern hemisphere has a much greater land mass, so accounts for the dominant source of methane. This is mainly an anthropogenic effect: in the pre-industrial simulation there is a much lower interhemispheric gradient (Etheridge et al. 1998), because the natural sources are more balanced between the hemispheres.

In general, chemistry-climate models are likely to underestimate the interhemispheric gradient for methane. Rates of methane destruction due to OH are greatest in the tropics, where the water vapour, sunlight and temperature conditions are most favourable. The observed NH/SH OH ratio is approximately 0.89 (Wolfe et al. 2019; Prinn et al. 2001), so the actual sink for methane may be greater in the southern hemisphere. However, as discussed in previous sections, models generally overestimate the OH interhemispheric ratio, with a greater proportion of OH in the northern hemisphere (Naik et al. 2013). This leads to more destruction of methane in the northern hemisphere and a smaller simulated interhemispheric gradient.

In this work, the gradient is calculated by taking the difference in mean methane surface concentration between 45°N - 90°N and 45°S - 90°S . These areas represent the highest and lowest concentrations of methane in the troposphere respectively. Compared to using the difference between the hemispheric mean (0 - 90°N and 0 - 90°S), this method

gives a reduced uncertainty, as the modelled and measured methane concentrations are more spatially uniform at high latitudes. The ratio between the 45°N-90°N and 45°S-90°S mean mixing ratios is also shown (in Fig 2.11b), to enable comparison with the OH interhemispheric ratios.

UKESM1-conc simulates a methane interhemispheric gradient of zero, so UKESM1-ems represents a large improvement in model skill. The observed and modelled gradients are shown in Fig 2.11, as well as the interhemispheric ratio. The observed interhemispheric ratio is fairly constant over time, with some inter-annual variability. In UKESM1-ems, the methane interhemispheric gradient is lower than the observed gradient; methane is more evenly distributed between the hemispheres. This underestimate is consistent with the inferred model overestimate of OH in the northern hemisphere (see section 2.4). Another explanation for the difference in gradients is an underestimate of methane emissions in UKESM1-ems in the northern hemisphere. This could be from wetland emissions, which have a high uncertainty, or an underestimate in anthropogenic emissions as suggested by Hmiel et al. (2020).

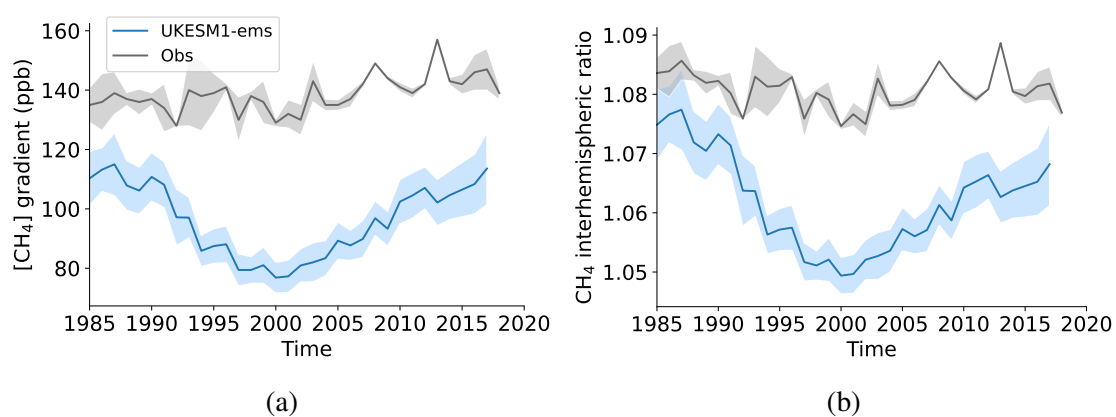


Figure 2.11: Interhemispheric gradient of methane over time. NOAA CMDL observations are shown in black and UKESM1-ems in blue. (a) Mean methane concentration in 45N - 90N minus the mean in 45S - 90S. (b) Ratio between the 45N - 90N mean and the 45S - 90S mean.

Comparison with CO interhemispheric gradient

There is strong coupling between methane and CO in the atmosphere and so I also consider the CO interhemispheric gradient in this section. CO is the main sink for OH (39%, Lelieveld et al. (2016)) - the drivers of methane interhemispheric gradient, such as OH concentrations and methane emissions, also affect the CO gradient. There are also independent sources of CO, including biomass burning and oxidation of non-methane VOCs (NMVOCs), which would affect the CO gradient but not methane. Grant et al. (2010) found that secondary production of CO via oxidation of methane and NMVOCs corresponds to around 60% of the total CO source, with methane oxidation accounting for 28%.

Qualitatively, UKESM1-ems successfully captures the factors which affect the interannual variability in the CO interhemispheric gradient. The UKESM1-ems and observed gradients share similar features such as peaks around 1998 and 2004, which are not seen in the methane interhemispheric gradients. This represents an improvement on the modelled CO gradient in UKESM1-conc.

Both UKESM1-ems and the observations show a decreasing trend in interhemispheric gradient over time, consistent with decreasing northern hemisphere CO emissions (Jiang et al. 2017) (see Fig 2.12). The UKESM1-ems interhemispheric CO gradient is approximately 30 ppb lower than the observed gradient throughout the time period studied. This is consistent with an underestimate in methane emissions in the northern hemisphere (and therefore lower modelled methane interhemispheric gradient, Fig 2.11), leading to less secondary CO production there. An overestimate of OH in the northern hemisphere would affect both CO and CH₄ gradients in the same way, leading to a lower gradient in UKESM1-ems. However, the trends in the modelled CH₄ and CO gradients are different: a decline and then increase for methane and a steady decrease for CO. Overall, the differences between the observed and modelled gradients are likely a combination of different biases in methane emissions, CO emissions and OH concentrations.

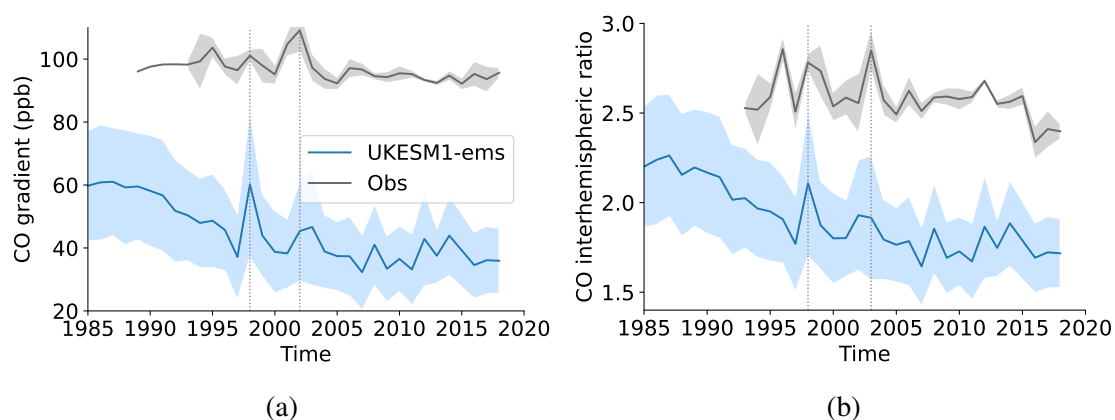


Figure 2.12: Interhemispheric gradient of CO over time. NOAA CMDL observations are shown in black and UKESM1-ems in blue. (a) Mean methane concentration in 45N - 90N minus the mean in 45S - 90S. (b) Ratio between the 45N - 90N mean and the 45S - 90S mean.

2.5.4 Latitudinal distributions of CH₄ and CO

The UKESM1-ems spatial distribution of methane is more homogeneous than the observed distribution. The interhemispheric gradient alone does not give a full picture of the spatial distribution. Fig 2.13 shows the latitudinal variation of methane with time for observations and UKESM1-ems. The dominant trend seen in Figs 2.13a and b is the increase in methane concentration over time at all latitudes. There is also latitudinal variation, with higher concentrations in the northern hemisphere for all years (causing the interhemispheric gradient).

To isolate the variation with respect to latitude, the data in Figs 2.13a, b were normalised to the 90°S value for each year (representative of the background methane concentration). This is shown in Fig 2.13c and d. The greater areas of light green and yellow in the NH observations highlight the larger interhemispheric gradient compared to UKESM1-ems, as seen in Fig 2.11.

The location and strength of the methane sources in UKESM1-ems could be improved with respect to observations. For example, there is an area of high methane concentration in the observations at $\sin(\text{latitude}) = 0.75$, which corresponds to around 50°N, from

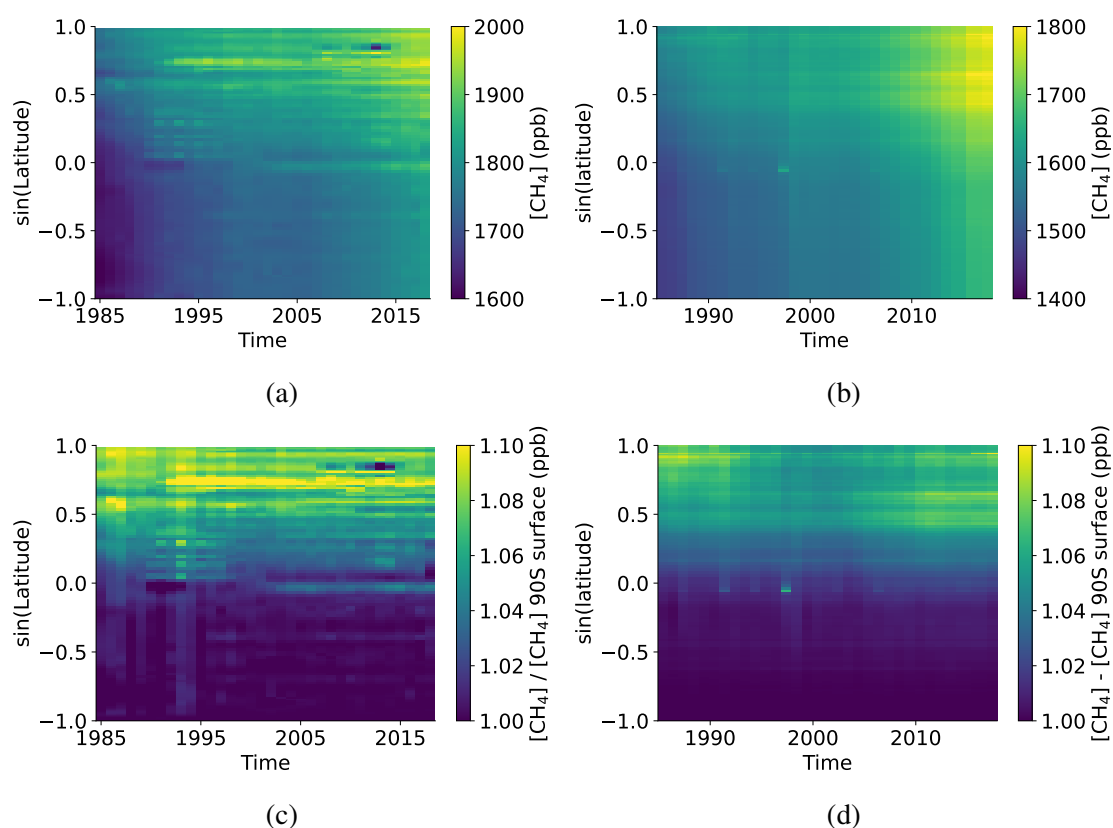


Figure 2.13: Spatial distribution of annual mean methane mixing ratios over time for (a,c) (interpolated) observations and (b,d) UKESM1-ems. (a,b) show absolute mixing ratios: the scales are offset by 200 ppb to enable comparison of the spatial distribution without the bias in concentration. (c,d) show the latitudinal variation in methane concentration, detrended from the background increase in methane over time. Methane at each latitude was normalised to the 90°S value for each year i.e. $[\text{CH}_4] / [\text{CH}_4]_{90S}$.

around 1990. This is likely due to a methane source rather than a localised difference in sinks. This latitude corresponds to Europe and North America, and the timing corresponds to the increase in usage of natural gas, of which these regions accounted for over 50% (in 2000, EIA (2012)).

One of the limitations of the observational dataset is that some of the latitudes correspond to only one measurement station, especially in the southern hemisphere (see Fig 2.9). Stations may be influenced by local sources and sinks, which creates a possibil-

ity for large uncertainties in the measured zonal mean methane concentration at that latitude. This is another possible explanation for the large methane anomaly at 50°N: proximity of a station to a methane source (there are only two stations at this latitude, see Fig 2.9). The area of high methane concentration around the equator, from 2004, in the observations, corresponds to one latitude band that contains two stations, and so this zonal mean may also be influenced by local sources such as biomass burning.

Decadal average latitudinal profiles for years 2000-2009 are shown in Fig 2.14. For comparison purposes, the y-axes differ by 200 ppb to offset the bias in UKESM1-ems. The maximum interhemispheric gradient is 106 ppb for UKESM1-ems for 2000-2009, with a decadal average global mean surface methane mole fraction of 1592 ppb. Heimann et al. (2020) reported an interhemispheric gradient of 104 ppb with global mean mole fraction of 1590 ppb, for 2000-2005, from their BASE experiment, which is comparable to UKESM1-ems. The maximum observed gradient is 209 ppb with a global mean mole fraction of 1805 ppb. The observed methane profiles are far more variable in the northern hemisphere than in UKESM1-ems; localised peaks in methane concentration are much shallower in UKESM1-ems. Overall, moving from the concentration-driven to emissions-driven model represents an improvement in the model skill in simulating the global methane distribution.

The improvement in model skill from UKESM1-conc to UKESM1-ems can be seen clearly when considering all latitudes over time. Fig 2.15 shows the difference between modelled and observed methane concentration for UKESM1-ems and UKESM1-conc over latitude and time. The results are normalised to the background concentration (90S), to take into consideration the UKESM1-ems model bias, as well as the change in methane over time. Both models replicate the uniform distribution in the southern hemisphere. UKESM1-conc shows a significant low bias in methane in the northern hemisphere due to the latitudinally invariant lower boundary condition. UKESM1-ems shows a smaller bias in the northern hemisphere. As previously mentioned, there is a greater difference at around 50°N, corresponding to high methane concentrations in the observations, such that UKESM1-ems gives an underestimate in this region.

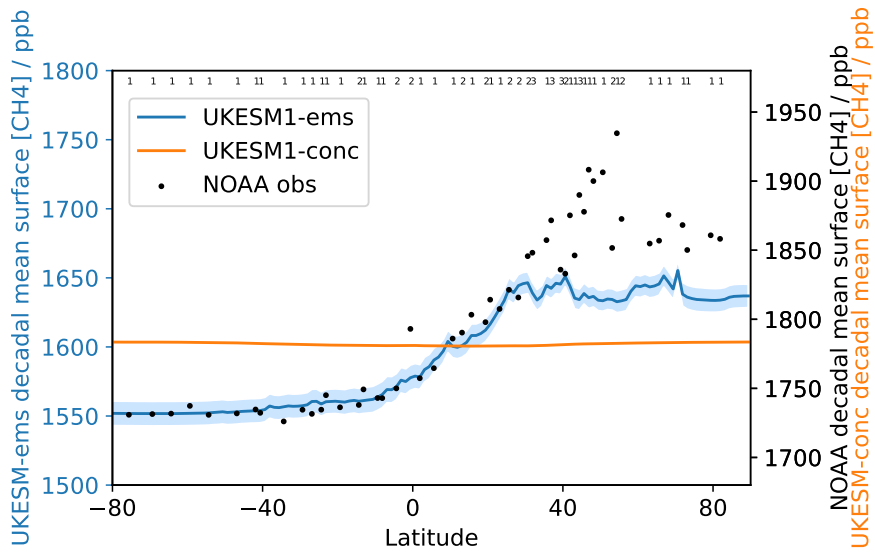


Figure 2.14: Latitudinal distribution of methane concentration in UKESM1-ems (blue), UKESM1-conc (orange) and observations (black) (Dlugokencky 2020) for 2000-2009. The numbers along the top indicate the number of data points/stations for each latitude contributing to the observation data.

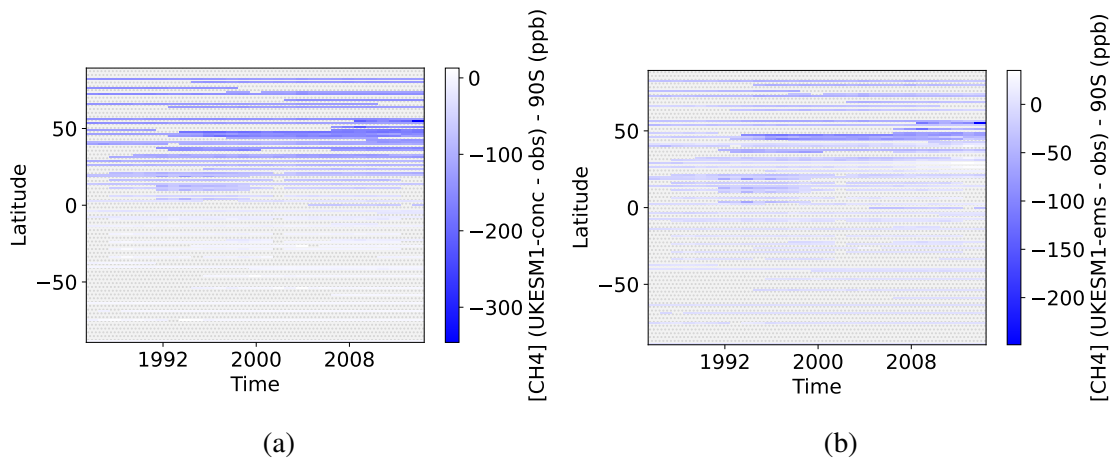


Figure 2.15: Difference between the modelled and observed annual mean methane mixing ratio, with respect to the methane concentration at 90°S, for (a) UKESM1-conc and (b) UKESM1-ems.

Comparison with CO distribution

This section considers the CO distribution over latitude and time. Intense tropical biomass burning events can cause large peaks in CO and therefore affect its latitudinal distribution. Such events, exacerbated by the extreme ENSO event of 1997/1998, caused a maximum in CO consistent in the emissions inventories considered by Granier et al. (2011). Novelli et al. (2003) estimated that the CO source from biomass burning was 45-80% higher than the annual average, corresponding to an extra 225-400 Tg of excess CO released. This was mainly in Indonesia in Sept-Nov 1997 (Duncan et al. 2003), but extreme fire events also occurred in the boreal forests in 1998 (Yurganov et al. 2004). This is consistent with the simulated UKESM1-ems mixing ratios for these years: the large anomaly in CO concentration in 1997 and the increase in the tropics and northern hemisphere in 1998 (see Fig 2.16). The observations also show a widespread increase in CO mixing ratio in 1998, but the measurements of CO at equatorial latitudes did not start until 2004 so the large peak in the tropics is not observed in this dataset (Lan et al. 2022).

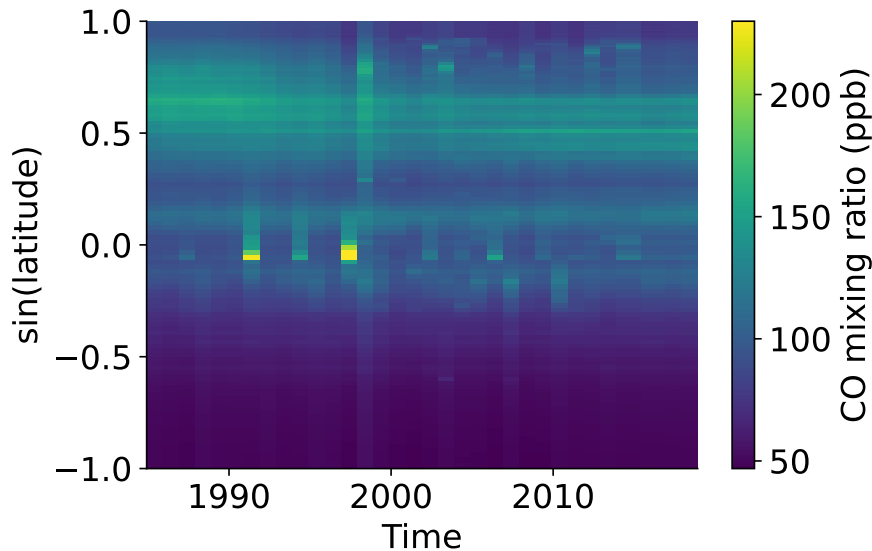


Figure 2.16: Latitudinal distribution of CO mixing ratio over time for UKESM1-ems. The colour bar saturates at 230 ppb, which only affects the peak at the equator in 1998 (exceeds 500 ppb).

CO emissions affect the methane profile: increased CO reduces the OH sink, resulting in a higher methane concentration. The 1998 CO increase most likely leads to the uptick in the methane concentration profile around 1999 (seen most clearly in UKESM1-ems, Fig 2.13b). The CO distribution also shows maxima at the equator in 1991, 1994 and 2006 (2.16), which are also likely to be associated with large-scale biomass burning events (Van Marle et al. 2017) and also affect methane concentrations.

In contrast to the methane anomaly, there is no latitudinally uniform bias with respect to observations in the simulated CO mixing ratios. Fig 2.17 shows the difference in CO surface concentrations between the observed and UKESM1-ems/UKESM1-conc results. Similar to the methane anomaly (Fig 2.15), CO is underestimated from around 50N to 90N. This may be due to insufficient sources of methane and CO, or other VOCs, leading to not enough secondary production of CO, as explored by Heimann et al. (2020). Many other models also show a similar underprediction at northern high latitudes (Naik et al. 2013; Stein et al. 2014). CO in the tropics is overestimated in UKESM1-ems and UKESM1-conc, except in the area around 30N from 1990-2000. This overestimation may be due to an overestimate of CO biomass burning emissions. The UKESM1-conc and UKESM-ems CO concentrations are consistent with observations at southern mid to high latitudes.

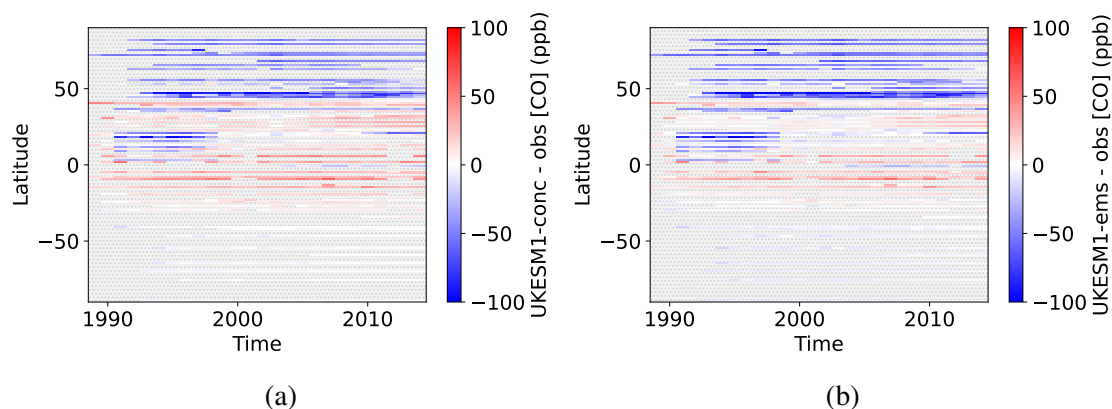


Figure 2.17: Difference between the modelled and observed annual mean CO mixing ratio over time for (a) UKESM1-conc and (b) UKESM1-ems.

A low bias in CO would be consistent with the low biased methane in UKESM1-ems. However, very similar CO anomalies are seen in UKESM1-conc, where the methane surface concentrations are much more consistent with observations. This suggests that the biases in CO are not due to methane related processes. Folberth et al. (2022) suggested that other processes in the atmosphere are likely to affect the CO distribution, for example loss of HO₂ on aerosols.

2.6 Vertical profile evaluation

In this section, the variation of methane with altitude was studied to gain a better understanding of methane vertical profiles, how these may differ between concentration and emissions-driven models, and whether UKESM1-ems gives better agreement compared to observations. UKESM1-ems is compared with UKESM1-conc, and against flight observations from the surface up to 12km (Wofsy et al. 2018).

2.6.1 ATom observation data

NASA's Atmospheric Tomography mission (ATom) provides a global dataset of greenhouse gas measurements, including methane, from 2016-2018 (Wofsy et al. 2018). The flight paths of the NASA-DC-8 aircraft are shown in Fig 2.18. Measurements were taken continuously while profiling from 0.2 - 12 km altitude (shown in purple shading). This dataset spans the entire latitude range of the atmosphere and samples mainly the Atlantic and Pacific free troposphere. Over three years, data was sampled in all four seasons. This provides a background methane concentration dataset, away from land-based sources. More information, and data for other species, can be found at <https://espo.nasa.gov/atom/content/ATom> (last access: Aug 2023).

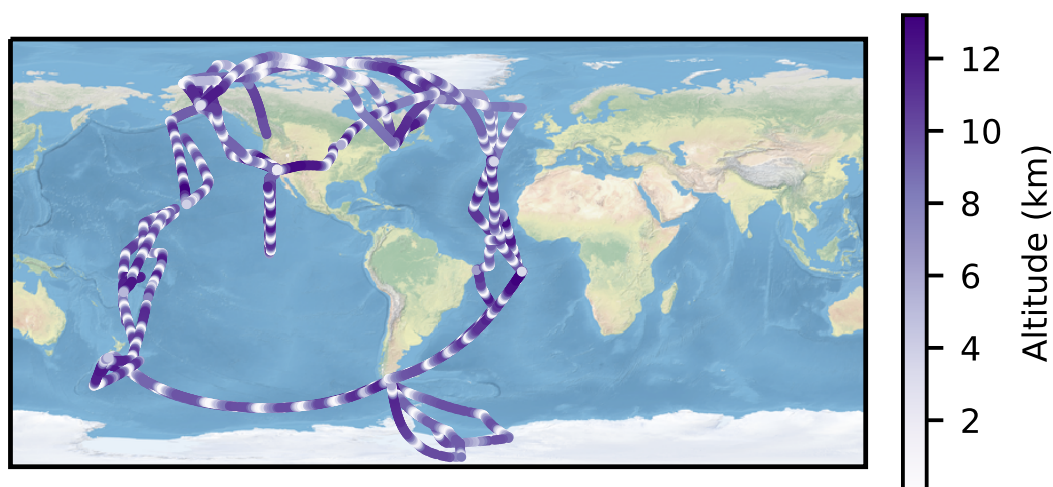


Figure 2.18: Paths of ATom flight campaigns from 2016 - 2018 using the NASA-DC-8 aircraft. The shading in purple shows altitude, profiled from 0.2 - 12 km.

2.6.2 Comparison between modelled and observed profiles

Tropospheric and interhemispheric transport timescales are much shorter than the methane lifetime with respect to oxidation by OH, so methane is fairly well-mixed between hemispheres and throughout the troposphere (Prather 2007). The mixing ratio is a useful metric here, because it is independent of the decreasing pressure with altitude: a decreasing mixing ratio means there is a sink for methane, and an increase corresponds to a source. In general, the mixing ratio of methane is highest at the surface, where the sources are, and decreases with altitude. Methane enters the stratosphere at the tropical tropopause and is transported upwards and polewards via the Brewer-Dobson circulation (Brewer 1949). Due to oxidation in the stratosphere, the methane mixing ratio decreases as the air moves polewards. Therefore, the stratospheric methane mixing ratio is expected to be lower than the tropospheric methane mixing ratio.

Here I consider the methane vertical profile for six latitude bands: 90-60°S, 60-30°S, 30°S-0, 0-30°N, 30-60°N and 60-90°N. The variation of annual mean methane mixing ratio with altitude in each band is shown in Fig 2.19. The values were normalised to the

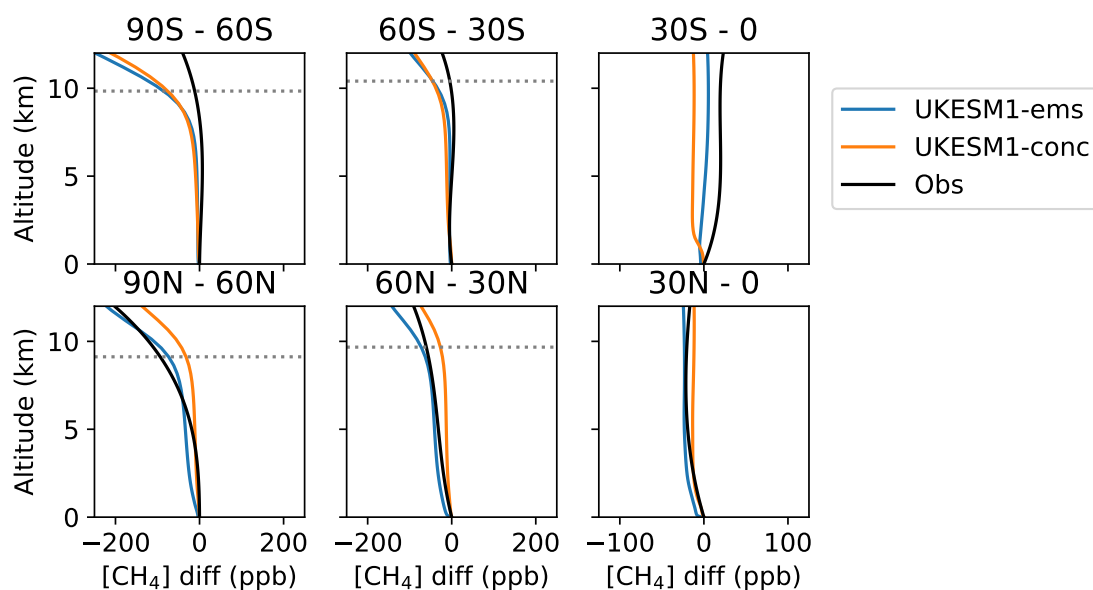


Figure 2.19: Vertical profiles of methane mixing ratio for UKESM1-conc (in orange) and UKESM1-ems (in blue) experiments in the year 2000, scaled to the surface methane concentration each latitude band. Observations from the ATom dataset are shown in black. The altitude corresponding to 125 ppb of ozone is marked by the dotted lines, which is used as an indication of the tropopause height. Note the x axis for the tropical latitudes (right hand side) is half the scale.

surface methane mixing ratio in each latitude band. This enables easier comparison between different model and observation years, as well as removing latitudinal differences in surface methane concentration, to focus on the vertical profiles. For the observations, a polynomial fit was calculated for the data points in each latitudinal band to give a vertical profile. For the model data, the profile shown is the mean methane mixing ratio at each altitude.

In the tropics (30°S-30°N), UKESM1-ems and UKESM1-conc both simulate a vertical profile consistent with the observations. The methane mixing ratio is almost invariant throughout the measurement range (0-12km). The tropopause in the tropics is above the measurement range, so only tropospheric methane, which is well-mixed, is sampled there.

The 30°S-0 observed methane profile (top right panel in Fig 2.19) shows a slight increase in methane with altitude between 0 and 5 km, which is also reproduced in UKESM1-ems. This is surprising since all of the methane sources are land-based, and means that the methane increase with altitude is likely due to transport from other areas of the troposphere. UKESM1-ems captures some of this increase, whereas UKESM1-conc does not.

In the lower and mid troposphere, methane is well mixed and shows little variation with altitude: this is seen in the observations and reproduced by both UKESM1-ems and UKESM1-conc. In the southern extratropics, the concentration and emissions-driven models show very similar profiles, with modelled methane decreasing at a faster rate with altitude than in the observations. In the northern extratropics, the difference in methane surface mixing ratio is larger between UKESM1-ems and UKESM1-conc (see Fig 2.14). There, the methane mixing ratio drops off at a lower altitude, and/or at a greater rate in UKESM1-ems compared to UKESM1-conc. This is despite these experiments having the same chemistry and transport, and the same tropopause levels (marked in dotted lines, showing the altitude of $[O_3] = 125$ ppb), which are expected to be the primary drivers of differences in vertical profile.

The preindustrial vertical profiles for UKESM1-ems and UKESM1-conc are almost identical - when there is a much smaller difference in the modelled latitudinal distribution of methane. At high latitudes (60-90°S and 60-90°N), the emissions-driven methane drops off more quickly with altitude than in the concentration-driven model, as seen in Fig 2.19 for the present day.

Given that UKESM1-ems and UKESM1-conc have the same chemistry, transport and tropopause levels, it was initially expected that the vertical profiles for methane in these models would be identical. This suggests that the methane emissions-driven treatment in some way affects the stratospheric transport. The difference between models is more pronounced where there is a less uniform latitudinal distribution of methane simulated in UKESM1-ems (i.e. in the present day).

Overall, UKESM1-ems shows improvement over UKESM1-conc in simulating the vertical profiles of methane in the northern extratropics compared to observations, and performs similarly in the tropics and southern extratropics.

2.7 Summary

This chapter introduced the models used throughout this work: UKESM1-ems and UKESM1-conc (Sellar et al. 2019; Folberth et al. 2022). The first section includes a model description for both the standard, concentration-driven configuration, and the methane emissions-driven configuration. The main updates required for UKESM1-ems were the implementation of emissions at the surface instead of a lower boundary condition, coupling wetland emissions from JULES into UKCA, and the inclusion of the methane soil sink.

UKESM1-ems improves upon the skill of UKESM1-conc in modelling the global distribution of methane, by simulating its sources and sinks directly. These improvements are particularly seen in the interhemispheric gradient, and latitudinal distribution of methane.

UKESM1-ems successfully reproduces the trend in methane mixing ratio from 1850 to present day, including the methane hiatus period. From around 1920 onwards there is an increasing low bias in methane compared to UKESM1-conc (which is very similar to observations). By 2014 there is a 150 ppb (8%) low bias in the methane mixing ratio of UKESM1-ems relative to observations (Lan et al. 2022). This is likely to be a combination of too low methane emissions and too strong a methane sink (OH concentration). These factors also contribute to a decreased interhemispheric gradient and lower northern hemisphere methane in UKESM1-ems compared to observations.

The emissions-driven treatment of methane causes a difference in simulated preindustrial ozone concentration between UKESM1-ems and UKESM1-conc - the ozone concentration in UKESM1-ems is lower. Here UKESM1-ems may represent an improve-

ment in the process-based representation of ozone production: with a heterogeneous distribution of methane leading to a differences in local ozone production.

The OH distribution and trend over time are similar in UKESM1-ems and UKESM1-conc, and are also consistent with other modelled OH distributions in CMIP6 models. Compared to observationally-constrained estimates, all models overestimate OH in the northern hemisphere. This is likely to affect the simulated methane distribution in UKESM1-ems.

UKESM1-ems simulates the vertical profiles for methane better than UKESM1-conc. Methane is invariant with altitude in the troposphere, where it is well-mixed, and then the mixing ratio decreases in the upper troposphere and above the tropopause due to sinks in the stratosphere. In the southern hemisphere, in UKESM1-ems and UKESM1-conc, the methane decreases with altitude more rapidly than in the observed vertical profile. In the northern hemisphere extratropics, UKESM1-ems more closely matches the observed vertical profile, compared to UKESM1-conc. The difference in methane distribution between the concentration and emissions driven models likely leads to changes in the vertical profile, and leads to an improvement in simulating the vertical profile in UKESM1-ems.

Overall, UKESM1-ems represents an improvement in the capability for modelling methane. The strengths highlighted in this chapter include the ability to change methane emissions on a global and regional scale, compared to using a lower boundary condition. The trends in methane are simulated successfully, and there is an improved modelled latitudinal distribution. This shows the suitability for using UKESM1-ems in experiments looking at changes in methane emissions over time. The main limitation is the low-bias in methane concentrations with respect to observations, which will be taken into consideration going forward.

Chapter 3

Attributing the role of future anthropogenic methane emissions

Abstract

Mitigation of greenhouse gas emissions is crucial for achieving the goals of the Paris climate agreement. One key gas is methane, whose representation in most climate models is limited by using prescribed surface concentrations. Here I use the new, methane emissions-driven configuration of the UK Earth System Model (UKESM1-ems) and simulate a zero anthropogenic methane emissions scenario (ZAME) in order to (i) attribute the role of anthropogenic methane emissions on the Earth system and (ii) bracket the potential for theoretical maximum mitigation.

I find profound, rapid and sustained impacts on atmospheric composition and climate, compared to a counterfactual projection (SSP3-7.0, the ‘worst case’ scenario for methane). In ZAME, methane declines to below pre-industrial levels within 12 years and global surface ozone decreases to levels seen in the 1970s. By 2050, 690,000 premature deaths per year and 1 degree of warming can be attributed to anthropogenic methane in SSP3-7.0. This work demonstrates the significant maximum potential of methane emissions reductions, and their air-quality co-benefits, but also reiterates the need for action on carbon dioxide (CO₂) emissions. I show that a methane emissions-driven treatment is essential for simulating the full Earth system impacts and feedbacks of methane emissions changes.

This chapter was published in *npj Climate and Atmospheric Science* (Staniaszek et al. 2022). My role in this was the experimental design, model runs, data analysis and writing, with discussions and advice from my co-authors.

3.1 Introduction

The previous chapter outlines the emissions-driven configuration of UKESM1, and evaluates its performance in the historical time period. UKESM1-ems provides a new capability to change methane emissions interactively, rather than being constrained by a lower boundary condition. This capability is used in this chapter to explore the role of anthropogenic methane in the Earth system in a future climate scenario. The changes in atmospheric composition and climate attributable to anthropogenic methane emissions are quantified.

The methods used for this attribution experiment are introduced in section 3.2. The impacts of methane emissions on climate and composition are investigated in sections 3.3 and 3.4 respectively. In section 3.5 the results from this emissions reduction experiment are compared to those from other studies, such as AerChemMIP. The discussion (section 3.6) focuses on the atmospheric chemistry response to methane mitigation, and how the use of an emissions-driven model affects the model response. The results are summarised in section 3.7.

3.2 Experiment setup

SSP3-7.0 was used as the underlying, or counterfactual scenario. It has the most extreme future methane trajectory in CMIP6 (Gidden et al. 2019), but one in which the simulated methane concentrations match the recent trends in methane observations (see Fig 3.1b). In this attribution study, the use of SSP3-7.0 also provides an estimate of the maximum impact attributable to future anthropogenic methane emissions.

To simulate the effects of zero anthropogenic methane, I instantaneously removed all anthropogenic methane emissions from 2015 onwards. The remaining emissions are from wetlands, biomass burning and non-wetland natural emissions (see Fig 3.1a). This scenario is hereafter referred to as ZAME.

The experiments were run with a fully coupled atmosphere-ocean at N96 resolution, from 2015 to 2050. Three ensemble members each were run for the counterfactual and ZAME scenarios, continuing from one of three different historical realisations. These are shown in the figures in lighter colours, with the ensemble mean in the darker colour.

I examine these methane emissions reductions not as a feasible strategy, but to show the effect of anthropogenic methane in the counterfactual SSP3-7.0 scenario, via the impacts of maximum theoretical emission mitigation. I aim to highlight the importance of limiting further methane increases and the significant maximum potential of emissions reductions.

Several studies have explored the impacts of stopping methane emissions, usually in conjunction with carbon dioxide in order to calculate the warming commitment associated with zero anthropogenic emissions (ZEC) e.g. Palazzo Corner et al. (2023) and Matthews et al. (2012). Solomon et al. (2010) performed an experiment where anthropogenic methane emissions were zeroed out instantaneously using an intermediate complexity climate model (BERN2.5CC EMIC). They found that the warming impacts of anthropogenic methane persist long after emissions and concentrations have decreased, with over 20% of the warming still present 50 years after cessation of emissions. Here, I am able to represent the Earth system response to zero anthropogenic methane emissions more fully through: the direct representation of methane emissions (rather than assuming a fixed methane lifetime), the inclusion of methane's feedback on its own lifetime, a full chemistry scheme, and the inclusion of interactive wetlands. This is likely to result in a more rapid decrease in methane concentration than previous studies due to the self-feedback as described in section 1.2.5, which will also likely affect the temperature response.

3.3 The impacts of ZAME on atmospheric composition

In the ZAME scenario, (following the cessation of anthropogenic methane emissions, Fig 3.1a), surface methane decreases globally with an e-folding timescale of 6.55 ± 0.06 years, and reaches below pre-industrial levels by 2030 (i.e. within 15 years; see

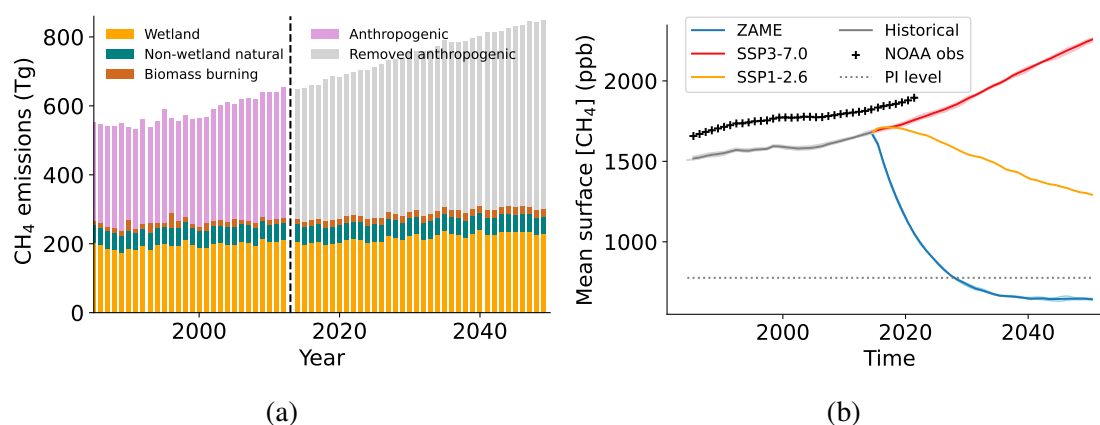


Figure 3.1: Methane emissions inputs and the resulting surface methane concentrations in UKESM1-ems (a) Methane emissions used as inputs into UKESM1-ems for 1985 - 2050, from Gidden et al. (2019). The emissions are split into sectors: interactive wetland emissions (orange), non-wetland natural (green), biomass burning (dark orange), anthropogenic (pink), and removed anthropogenic in the zero anthropogenic methane emissions scenario (ZAME, grey). (b) Methane surface concentrations from 1985-2050. Historical model concentrations are in dark grey and observations (Dlugokencky, NOAA/GML (gml.noaa.gov/ccgg/trends_ch4/)) are shown by crosses. Three future scenarios are shown: ZAME (blue), SSP3-7.0 (red) and SSP1-2.6 (orange). The pre-industrial (PI) level is shown by the dotted line. The fainter coloured lines show the three individual ensemble members and the darker line shows the ensemble mean, for SSP3-7.0 and ZAME.

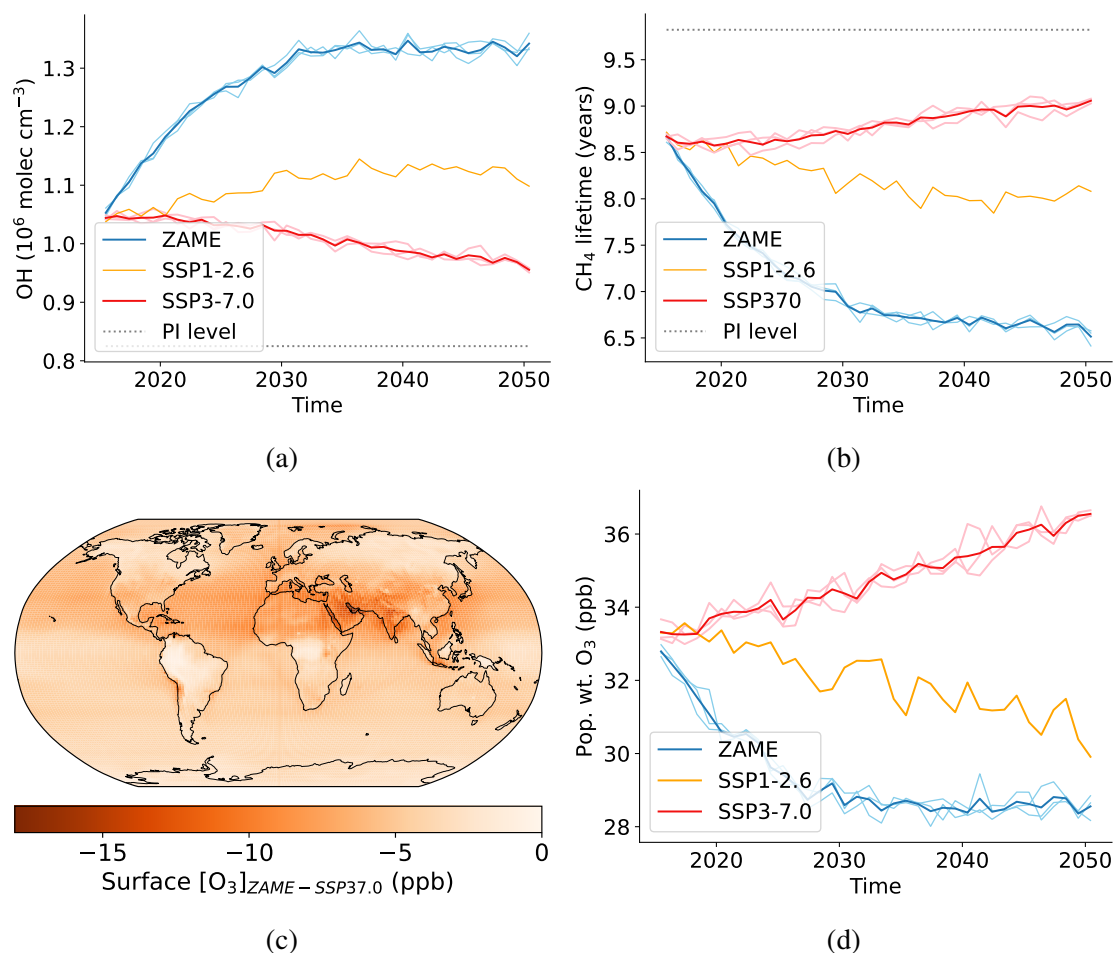


Figure 3.2: Atmospheric composition changes over time in the zero anthropogenic methane scenario (ZAME) from 2015-2050. The SSP3-7.0 scenario is shown in red, ZAME in blue, SSP1-2.6 in orange and pre-industrial values in dotted grey. The fainter coloured lines show the three individual ensemble members and the darker line shows the ensemble mean, for SSP3-7.0 and ZAME. (a) Global mean (airmass-weighted) tropospheric OH concentration. (b) Methane lifetime, defined as total atmosphere burden divided by $\text{CH}_4 + \text{OH}$ flux in the troposphere. (c) Decadal mean (2040-2050) change in surface ozone concentrations in ZAME compared to SSP3-7.0. (d) Population-weighted surface ozone concentration. Population datasets are based on the the underlying SSP scenarios (O'Neill et al. 2016). The tropopause is defined as a $[\text{O}_3] = 125 \text{ ppb}$ surface.

Fig 3.1b). The whole atmosphere methane burden declines to below pre-industrial levels within 12 years, stabilising at 1775 ± 15 Tg, 71% below the counterfactual in 2050.

Commensurate with the decrease in methane, levels of OH increase. OH is the main component of the atmosphere's oxidising capacity, and determines the methane lifetime, but itself is controlled by the amount of methane and other reactive gases in the atmosphere (Naik et al. 2013). The magnitude of the OH sink decreases in ZAME due to the changes in methane: directly via reduction of the $\text{CH}_4 + \text{OH}$ reaction, and indirectly due to decreases in secondary production of carbon monoxide (CO), the other major OH sink. As a result, the global mean surface OH concentration increases over time in ZAME (see Fig 3.2a). It reaches a new constant level of $1.34 \pm 0.01 \times 10^6$ molec cm^{-3} by 2035 (after 20 years), more than 30% higher than the present-day period. This represents a change unprecedented over the historic period (1850-2014) (Stevenson et al. 2020) and drives the rapid decrease in the lifetime of methane.

Methane is an important precursor for tropospheric ozone (Fiore et al. 2008). This relationship holds well in the ZAME scenario: tropospheric ozone is significantly reduced, globally. In SSP3-7.0, the population-weighted surface ozone concentration increases linearly from 2015 to 2050, reaching 35.32 ± 0.07 ppb (9.4% higher than 2014, Fig 3.2d). In ZAME, the surface ozone concentration decreases rapidly in the first decade, then stabilises to a new steady-state value of 27.8 ± 0.5 ppb (13.9 % below 2014) up to 2050. This corresponds to historical global population-weighted ozone levels from the 1970s (simulated with UKESM1.0). The population data used are consistent between the simulations (from SSP3 in 2050 (Jones et al. 2016)), so the differences stem from the regional surface ozone changes.

In SSP3-7.0, the area-weighted surface ozone concentration remains constant over the time period of the experiment. However, the population-weighted concentration increases (Fig 3.2d), showing that the proportion of the population living in high-ozone areas increases in the counterfactual. In ZAME, both the population-weighted and the area-weighted ozone concentrations decrease.

The largest ozone reductions in ZAME occur in the Northern Hemisphere tropics (see Fig 3.2c), in regions associated with the highest tropospheric ozone precursor emissions

(Griffiths et al. 2021; Archibald et al. 2020b). These are populous regions, such as over India, implying methane emissions have an important role in air quality and human health in these regions.

To quantify the air quality impacts of anthropogenic methane, I calculated the long-term ozone-related mortality for SSP3-7.0 and ZAME for 2050, according to the method in Malley et al. (2017). The relationship between the change in mortality, $\Delta Mort$, and the change in ozone exposure, ΔO_3 (relative to a minimum threshold) is shown in equation 3.1. y_0 is the baseline mortality rate and β is a constant representing the association between long-term ozone concentration and mortality. The global average mortality data for cardiovascular and respiratory diseases comes from the Global Burden of Disease database for 2015 (Murray et al. 2020) (<http://ghdx.healthdata.org/gbd-results-tool>). The uncertainty limits quoted were derived from the uncertainty of the mortality rate. The 2050 population estimates for SSP3 are from Jones et al. (2016), and the population age distribution data was estimated by the UN population division for 2050 (<https://population.un.org/wpp/DataQuery/>). This is the same method as used in Shindell et al. (2021), but here global average mortality was used, where they use country-specific mortality.

$$\Delta Mort = y_0(1 - \exp^{-\beta\Delta O_3})Pop \quad (3.1)$$

There are clear links between short-term ozone exposure and mortality, however the impact of long-term exposure on mortality is less well studied, and the use of different ozone exposure metrics makes comparison between studies challenging ((Europe 2013; Huangfu et al. 2020)). Sun et al. (2022) showed that the method from Malley et al. (2017) used a high mortality rate and therefore gave an upper estimate of the mortality. Here I have used the upper and lower limits of this mortality rate (or hazard ratio) to provide some indication of uncertainty for this calculation. Remaining uncertainty in my estimates is likely due to the use of global mortality rate instead of country-specific rates, due to time and data constraints.

According to the above method, the ozone associated with anthropogenic methane is responsible for 690,000 premature deaths per year (456,000 - 910,000, lower and upper bounds of mortality rate) in 2050: 43% from respiratory causes and 57% from cardiovascular causes. This corresponds to around 1270 annual deaths per million tonnes (Tg) of methane emissions, or 65% higher total (ozone related) deaths per year compared to ZAME. This figure is lower than the results from the recent Global Methane Assessment (GMA) report (Shindell et al. 2021) (~1400 fewer deaths per Tg CH₄ mitigated). This may be due to the use of global average instead of country-specific mortality, which is likely to lead to an underestimate in deaths attributed to methane via ozone. However, the air quality impacts as predicted by UKESM1-ems are consistent with those from LBC models, and emphasise the opportunities for action on air quality via methane mitigation.

The ozone response to decreased future methane emissions is highly dependent on the underlying scenario. Up to 2050 and beyond, SSP3-7.0 has high emissions of CO, nitrogen oxides (NO_x), and volatile organic compounds (VOCs), all of which are precursors for ozone formation. At the opposite end of the spectrum, CO, NO_x and VOC emissions decrease substantially in SSP1-2.6 (Gidden et al. 2019). Therefore, anthropogenic methane emissions (reductions) in SSP1-2.6 would have a different impact on ozone. Up to 2050, ZAME gives greater ozone decreases than SSP1-2.6 (see Fig 3.2d): the large decrease in methane counteracts the much higher ozone precursor emissions. While the ZAME ozone trend stabilises in the mid 21st century, the ozone concentration in SSP1-2.6 continues to decrease, highlighting the importance of concerted ozone precursor emissions reductions.

3.4 The impacts of ZAME on climate

The global mean surface temperature (GMST) increase is substantially reduced in ZAME, compared with the counterfactual – in good agreement with other studies (Shindell et al. 2021; Allen et al. 2021), and in spite of no change to CO₂. The GMST diverges from the SSP3-7.0 trajectory within a decade of zero anthropogenic methane emissions. Over a 10-20 year time horizon (near-term), the reduction in methane and

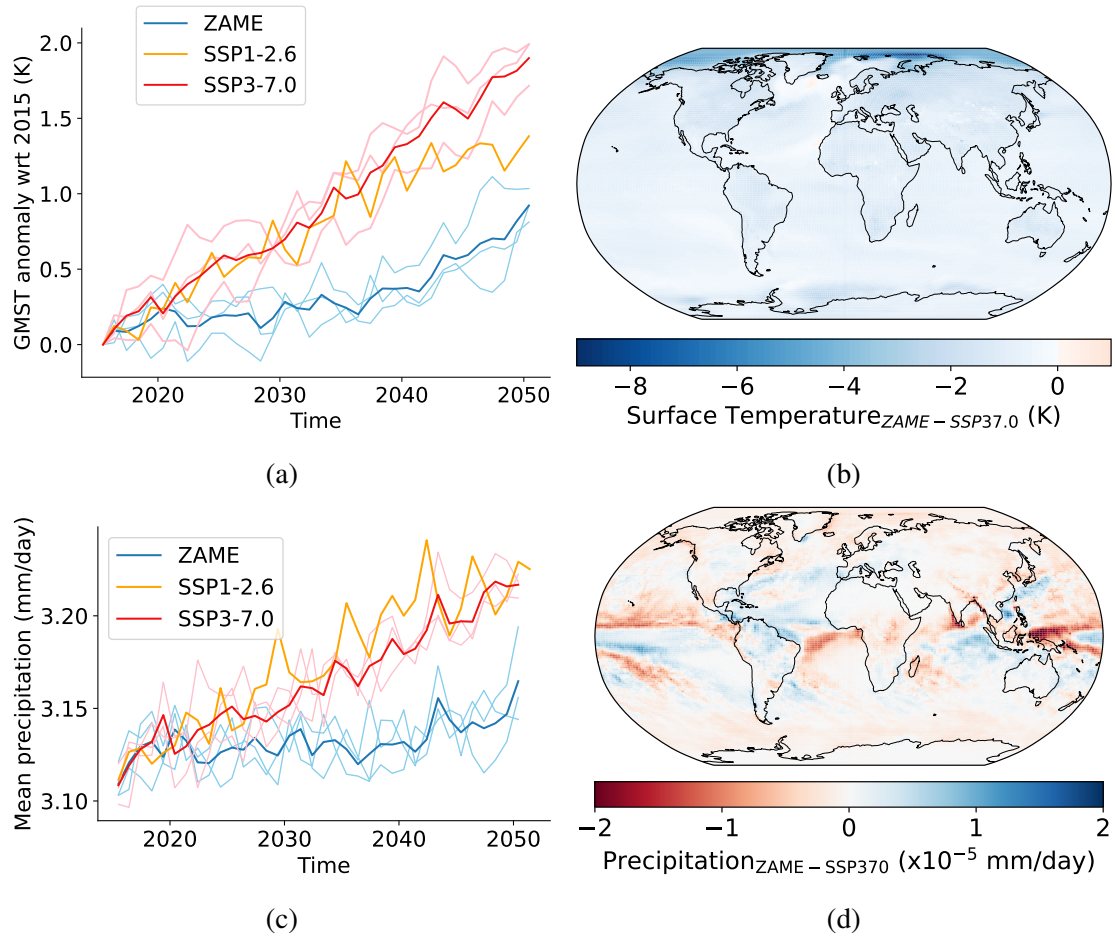


Figure 3.3: Physical climate changes associated with zero anthropogenic methane (ZAME), compared to SSP3-7.0 and SSP1-2.6. ZAME is shown in blue, SSP3-7.0 in red and SSP1-2.6 in orange. The fainter coloured lines show the three individual ensemble members and the darker line shows the ensemble mean, for SSP3-7.0 and ZAME. (a) Global mean surface temperature (GMST) anomaly with respect to 2015 values, for 2015-2050. (b) Global surface temperature difference for 2040-2050: ZAME - SSP3-7.0. (c) Global mean precipitation for 2015-2050. (d) 2040-2050 decadal average precipitation in ZAME compared to SSP3-7.0. Red areas correspond to where there is less precipitation in ZAME than SSP3-7.0.

its indirect effects (O'Connor et al. 2021) counterbalance other climate forcings (such as carbon dioxide), so overall there is little temperature change. While the methane concentration stabilises, the other greenhouse gas concentrations continue to increase, leading to increasing temperatures after 2035. Over a 20+ year time horizon (the long-term), there is a sustained reduction in the rate of temperature increase: 0.045 (0.036-0.059) K per year in 2035-2050 in ZAME compared to 0.059 (0.055-0.063) K per year in the counterfactual. The evolution of temperature beyond 2050 is beyond the scope of this study, so it is unknown whether the ZAME scenario would have a permanently lower rate of temperature increase, or whether it would converge towards the SSP3-7.0 trajectory (as the time since the methane perturbation increases).

By 2050, anthropogenic methane in SSP3-7.0 causes 0.96 ± 0.09 K more warming compared to ZAME (Fig 3.3a). Considering the 2040-2050 period (Fig 3.3b), the temperature increase is globally uniform, except for in the Arctic, where Arctic amplification is seen in SSP3-7.0. This highlights that anthropogenic methane has the greatest impact in some of the regions most susceptible to climate change. The processes contributing to the amplification include feedbacks related to sea ice change, and ocean and atmospheric heat transport (IPCC 2021a): ESMs such as UKESM1-ems enable these to be simulated.

Between 2015 to 2050 alone, SSP3-7.0 leads to almost 2 degrees of warming in UKESM1-ems (see Fig 3.3a) - the entirety of the temperature limit compared to pre-industrial levels set in the Paris agreement (UNFCCC 2015). The total temperature increase (pre-industrial to 2050) in SSP3-7.0 is 2.82 ± 0.12 K. The ZAME experiment shows that one degree of this warming (or one third of the SSP3-7.0 total temperature increase to 2050) can be attributed to the effects of future anthropogenic methane emissions. This further highlights the potential of methane emissions reductions for climate mitigation (Shoemaker et al. 2013; Shindell et al. 2017a; Ocko et al. 2021; Shindell et al. 2021) but shows that even the zero methane scenario breaches 1.5 degrees, and underscores the necessity of CO₂ mitigation.

Mirroring the changes in global temperature, removing anthropogenic methane emissions results in a decrease in total precipitation by 2050, and a slowed rate of increase in precipitation compared to the counterfactual (Fig 3.3c). By 2040-2050, ZAME re-

sults in a small but statistically significant reduction in the rate of precipitation (globally averaged) of 0.061 ± 0.013 mm per day, or 1.9% less. Unlike surface temperature, the spatial distribution of precipitation change is non-uniform, as shown in Fig 3.3d. The largest changes occur in the tropics, in the Maritime Continent, a region of greatest precipitation in UKESM1.0 and observations (Sellar et al. 2019).

3.5 Comparison with AerChemMIP

Use of a methane emissions-driven configuration may cause a difference in the model's temperature sensitivity with respect to methane (the level of warming for a change in mixing ratio). I analysed the global mean surface temperature sensitivity to methane concentration changes, using the $\Delta\sqrt{[\text{CH}_4]}$ relationship from Etminan et al. (2016). I compared my results to the work of Allen et al. (2021), who analysed a similar pair of AerChemMIP model experiments based on the SSP3-7.0 scenario. Unlike ZAME, these experiments were based on models using methane lower boundary conditions, and simulated smaller methane reductions.

As expected, the GMST response to methane emissions is larger in ZAME than in the AerChemMIP simulations, as shown in Fig 3.4a. The response in ZAME (orange cross in Fig 3.4a) is also greater than would be expected based on extrapolation of the AerChemMIP multi-model ensemble (MME) results (blue shaded area in Fig. 3.4a). However, the ZAME results are consistent with an extrapolation of the UKESM1.0 experiment in Allen et al. (2021) (green cross and dotted line in Fig. 3.4a). This most likely reflects a higher sensitivity of GMST to CH_4 in the underlying UKESM1.0 model compared to the AerChemMIP MME, rather than a GMST sensitivity difference between the LBC and emissions-driven model configurations. This is consistent with O'Connor et al. (2021), who found a higher present-day effective radiative forcing for methane in UKESM1.0 than in other models considered, which is expected to correlate to a larger GMST response.

Figure 3.4b compares the ozone response in the ZAME scenario with the AerChemMIP MME. As with GMST, the ZAME simulation represents a greater reduction in O_3 than

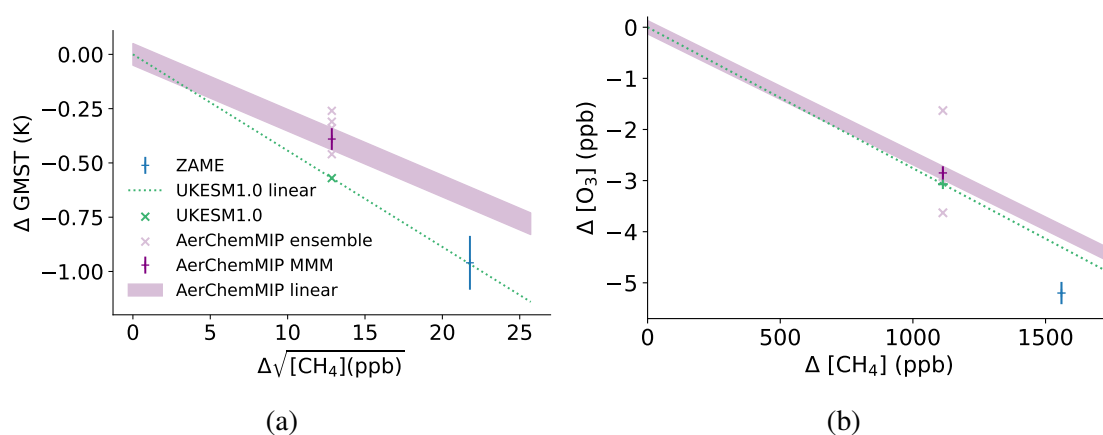


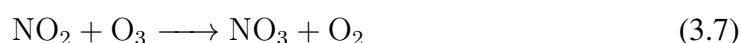
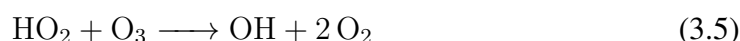
Figure 3.4: Comparison of ZAME and AerChemMIP ozone and temperature changes with respect to methane concentration. AerChemMIP results are shown in purple, the UKESM ensemble member in green and ZAME in blue. Linear trends are extrapolated to test linearity of ZAME with respect to AerChemMIP. (a) Difference in global mean surface temperature (ΔGMST) vs the difference in square root of methane concentration ($\Delta \sqrt{[\text{CH}_4]}$) for 2015-2050, according to the relationship between methane concentration and radiative forcing (Etminan et al. 2016). (b) Difference in ozone concentration ($\Delta [\text{O}_3]$) vs difference in methane concentration ($\Delta [\text{CH}_4]$) between 2015 and 2050. Error bars represent the standard error.

in the AerChemMIP study. As before, the ZAME results (orange cross in Fig. 3.4b) were compared with the extrapolation of the MME relationship ($\Delta[\text{O}_3] / \Delta[\text{CH}_4]$), and the UKESM1.0 simulation that was used in deriving the MME relationship (green cross in Fig. 3.4b). Although there is more variability in the AerChemMIP MME relationship for $\Delta[\text{O}_3] / \Delta[\text{CH}_4]$ than $\Delta\text{GMST} / \Delta[\text{CH}_4]$, the results from the ZAME simulation are a clear outlier, compared with both the MME and extrapolation of the UKESM-1 simulations. This could be due to extrapolation of the large change in emissions resulting in a non-linear response, but previous work with similar magnitude changes has shown that the $\Delta[\text{O}_3] / \Delta[\text{CH}_4]$ is linear (Fiore et al. 2008). I hypothesise that this result is driven by the use of CH_4 emissions – rather than a lower boundary condition, as used by all the models in the AerChemMIP study (Allen et al. 2021) and the recent GMA study (Shindell et al. 2021). I suggest that UKESM1-ems more faithfully simulates the O_3 response possible under extreme methane mitigation.

3.6 Discussion

Methane plays a central role in the chemistry of the atmosphere. Through a cascade of chemical reactions (3.2-3.9), perturbations to methane affect many species and result in numerous feedbacks. The chemistry scheme in UKESM1-ems allows us to model these effects.

Simple models of methane chemistry (Prather 2007; Rigby et al. 2017; Turner et al. 2017) fail to capture the effects of methane oxidation on HO_x and NO_x . Figure 3.5 shows the methane chemical-cascade simulated in UKESM1-ems. Under ZAME, the total methane emissions are reduced by approximately 60% (relative to 2015), decreasing methane concentrations globally. Methane is a source for secondary production of carbon monoxide (CO): this production is reduced, so the CO concentration decreases.



Reaction of CO with OH (reaction 3.3) is the main formation pathway for HO₂ (Seinfeld et al. 2016). The decrease in CO in ZAME (due to less secondary production, and higher OH) leads to less production of HO₂, and therefore lower modelled concentrations of HO₂ (see Fig 3.6a). Reaction with CO and CH₄ (reactions 3.2 and 3.3) are the main sink pathways for OH. With both species depleted, the sink for OH decreases, leading to an increase in OH. The decrease in HO₂ and the increase in OH both contribute to increasing the OH/HO₂ ratio, which increases by 16 % by 2050 in ZAME (see 3.6b).

The reduction in HO₂ slows production of O₃. By 2050, ozone in ZAME is much lower than in SSP3-7.0 (see Fig 3.2d). The HO₂ + NO reaction flux (the primary source of tropospheric ozone) (reaction 3.6) decreases (15 % by 2050) and so results in an ozone decrease. Secondly, the flux through the HO₂ + O₃ reaction increases (reaction 3.5), which depletes ozone. Both of these flux changes result in decreased ozone concentrations. Counter-intuitively, the HO₂ + O₃ flux increases despite decreases in both HO₂ and O₃. The origin of the drivers behind this have not been determined but will be the focus of future work. The mechanisms behind ozone changes from methane emissions reductions are investigated further in Chapter 5.

Finally, I consider the response of NO_x, which may be expected to be small, because NO_x emissions are unchanged in ZAME. However, the NO_x concentrations are higher (3.7), which implies that the overall NO_x lifetime has increased. The decrease in HO₂

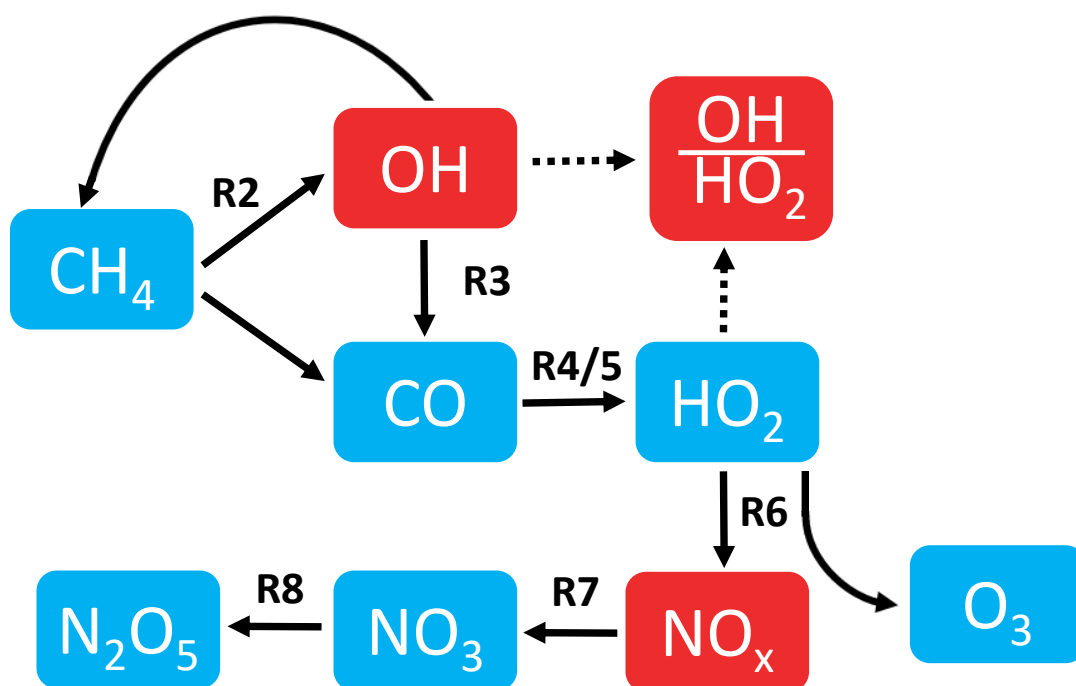


Figure 3.5: Schematic of the relevant reactions linking methane, HO_x and NO_x. Species that decrease in ZAME are labelled in blue, and those that increase in red. Solid arrows represent reactions, with labels referencing the relevant reactions (3.2-3.8). The dashed arrows show how OH and HO₂ both contribute to the OH/HO₂ ratio. This is a simplified schematic of a more complex system which includes more feedbacks, such as between HO_x, NO_x and ozone.

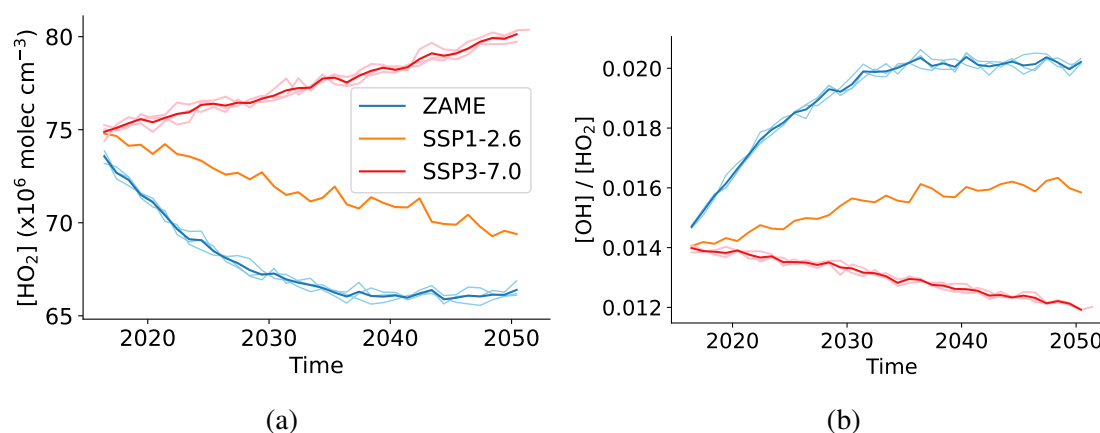


Figure 3.6: (a) Mass-weighted tropospheric mean HO₂ concentration over time, (b) OH/HO₂ ratio over time for ZAME and SSP3-7.0. ZAME results are shown in blue, and SSP3-7.0 in red.

means less NO is destroyed via reaction 3.6, so the NO concentration increases. NO₃ is produced via the reaction of NO₂ with O₃ (3.7). With less O₃, less NO₃ is produced and so the steady state concentration of NO₃ is lower. NO₃ and NO₂ react together to form the reservoir species, N₂O₅ (reaction 3.8). With less NO₃, less N₂O₅ is produced, and this sink pathway for NO₂ is lower, resulting in higher NO₂ concentrations. Nitric acid (HNO₃), the other reservoir species for NO_x, formed via reaction 3.9, increases slightly, but this reaction is very buffered and so large changes aren't seen. Overall, these responses indicate a strong coupling between NO_x and HO_x in the model (Holmes 2018). This makes attribution of the driving factors difficult in a small set of experiments, but it shows that there are strong feedbacks present that aren't able to be represented in simpler models. The coupling between NO_x and methane in ZAME and SSP3-7.0 is studied further in section 4.4.

Although the methane emissions in ZAME are similar to pre-industrial levels, the burden equilibrates to levels significantly below these (Fig 3.1). This reflects the very different atmospheric oxidising capacity simulated in ZAME (Fig 3.2a). The oxidising capacity is mainly controlled by the amount of OH in the atmosphere, which is controlled by the balance of sources and sinks. OH is much higher in future scenarios than in the pre-industrial atmosphere, due to the reduction of the OH sinks (via CH₄ and

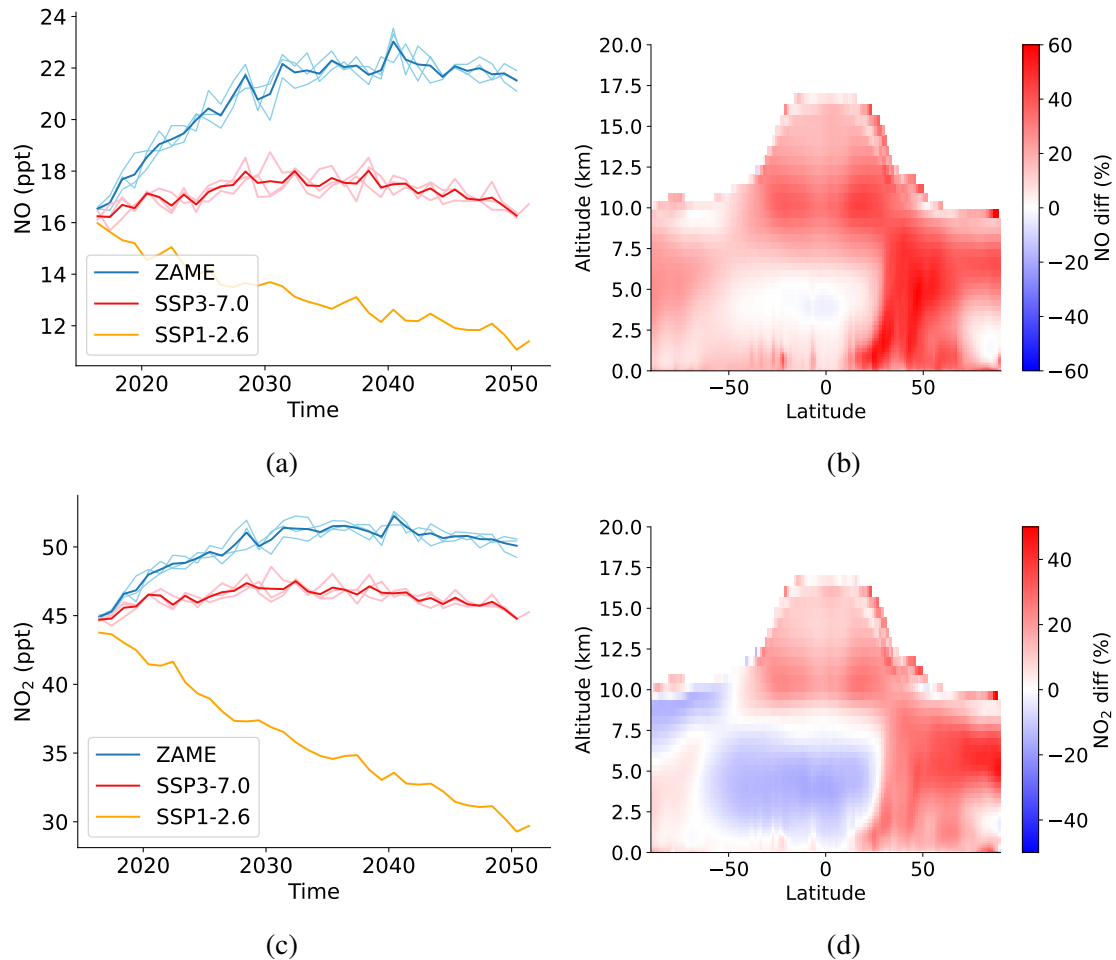


Figure 3.7: NO and NO₂ evolution over time and zonal decadal mean difference plots for 2040-2050. (a) and (c) show NO and NO₂ trends respectively over time in SSP3-7.0 (red) and ZAME (blue). (b) and (d) show the decadal (2040-2050) zonal mean percentage difference in NO and NO₂ mixing ratio between SSP3-7.0 and ZAME. This is calculated as ZAME - SSP3-7.0, so red areas show where [NO] or [NO₂] is higher in ZAME compared to SSP3-7.0, and blue areas show where it has decreased.

CO) described above and an increase in water vapour (H_2O), which is a feedback of the future climate change. Increasing H_2O leads to an increase in the probability of $\text{O}(^1\text{D})$ reacting with water (formed from O_3) to form HO_x . This in turn depletes more CH_4 and CO , leading to a further decreases in the OH sink.

I argue that the change in methane burden reflects the state dependence of the methane self-feedback process. I capture these effects and the knock-on impacts more fully in the emissions-driven simulations: by including CH_4 emissions directly, and having a fully interactive chemistry scheme with HO_x and NO_x coupling (unlike simpler emission driven models e.g., Hayman et al. (2021), Rigby et al. (2017), and Turner et al. (2017)). I argue that this self-feedback process is also not accurately simulated in surface concentration-driven methane models, including those that have participated in CMIP6 and sub-projects like AerChemMIP (Collins et al. 2017) (which use an LBC). The strength of the self-feedback varies across the globe (Holmes 2018). The interaction of the non-uniform methane emissions in UKESM1-ems with areas of high and low feedback strength is more representative of the physical Earth system, compared to an LBC model, where the surface methane concentrations are globally invariant. Calculation of the LBC trajectory from emissions requires intermediate, lower complexity models, with assumptions about methane lifetime and therefore oxidising capacity. There is also a non-physical adjustment process at the lower boundary due to the fixed surface methane concentration. The climate feedbacks on natural methane sources are also not considered in these LBC projects (Kleinen et al. 2021), but are enabled here.

Failure to capture these feedbacks accurately will affect the atmospheric composition response to methane emissions changes. These emissions changes, with the self-feedback enabled, result in an increase in an oxidising capacity (see OH in Fig 3.2a) that is simulated to be unprecedented over the last 150 years. Using the emissions-driven model avoids the use of an intermediate model, the non-physical adjustment process at the surface, and any effects on OH that these have.

3.7 Summary

In summary, I have shown that with the cessation of anthropogenic methane emissions, the methane burden can decrease to below pre-industrial levels within 15 years. In the SSP3-7.0 scenario, 1 degree of future warming can be attributed, directly and indirectly, to the methane concentration change resulting from the anthropogenic methane emissions. Reduction in the methane source leads to large scale changes in atmospheric composition, increasing the oxidising capacity of the atmosphere to levels not seen in the last 150 years.

In the future zero anthropogenic methane emissions scenario, surface ozone concentrations are greatly reduced, showcasing the air quality (and therefore human health) impacts of anthropogenic methane in the counterfactual scenario. I calculate that $\sim 690,000$ premature deaths (due to ozone) per year by 2050 are attributable to anthropogenic methane in the SSP3-7.0 scenario. Given my use of the highest emissions scenario for ozone precursors (SSP3-7.0), these estimates for the climate and ozone changes attributable to future anthropogenic methane represent the upper bound of its impact.

This work supports the growing literature of studies calculating significant co-benefits of methane action, such as the recent Global Methane Pledge. The use of methane emissions-driven Earth system models in follow-up studies is key to quantifying the full response of the Earth system to future methane changes, including the methane self-feedback and composition changes.

Chapter 4

Exploring the sensitivity to NO_x, methane and CO in UKESM1-ems

Abstract

The ZAME experiments in Chapter 3 showed the UKESM1-ems system response to methane emissions reductions. Here, I perform further experiments to better understand the coupling between methane, CO, NO_x and OH in UKESM1-ems, in particular looking at the impact of methane on NO_x, and the sensitivity of OH to CO and NO_x emissions.

Both the NO/NO₂ ratio and the total NO_x burden are affected by methane mitigation in UKESM1-ems. The increases in NO/NO₂ ratio are driven by decreases in ozone, MeOO + NO flux and HO₂ + NO flux. The total NO_x burden is affected through changes in the partitioning between NO_x and NO_y(=oxidised nitrogen species). In the low methane scenario there is less NO_y present in reservoir species (mainly MeONO₂ and NO₃), and more as active NO_x.

CO emissions mitigation decreases OH globally, while NO_x emissions reductions lead to increases in OH, mainly in the northern hemisphere. The impact of NO_x and CO emissions changes on OH were greater in the low-methane scenario. The relationship between OH, CO and NO_x derived in previous studies was also explored here, and I found that in these experiments the OH concentration is proportional to the ratio of the NO_x and CO+CH₄ burdens.

4.1 Introduction

In this chapter I further explore the relationships between CO, NO_x, methane and OH in UKESM1-ems. After the ZAME experiments described in Chapter 3, I wanted to study the coupling between these species in more detail. The aim is to provide a greater understanding of the emissions-driven model, in particular the factors affecting OH and NO_x. In this emissions-driven configuration, there are more feedbacks simulated than in the LBC model, with the methane concentrations responding in a more process-based way, affecting the methane lifetime, OH and ozone. These are central to the chemistry of the atmosphere and so also affect many other species.

As discussed in section 3.6, in the ZAME experiments, NO_x is affected by changes in methane emissions, even though NO_x emissions are unchanged. In Chapter 3 I hypothesised that the emissions-driven model may simulate stronger coupling between NO_x and methane than the concentration-driven models. In this chapter I go into more detail about the NO_x budget in UKESM1-ems, and how it is affected by methane changes, to look further at the drivers controlling NO_x.

NO_x is comprised of NO and NO₂, which form part of a chemical family. This is possible due to the fast interconversion between NO and NO₂, leading to a photostationary state, with a consistent ratio. The lifetime for conversion between them is on the order of minutes, and the reactions for their interconversion are shown below (Seinfeld et al. 2016).



The ratio of NO to NO₂ can be used as an indicator of the chemical state of the atmosphere (Seinfeld et al. 2016). Reactions 4.1 and 4.3 dictate the NO/NO₂ ratio in the absence of hydrocarbons. These two reactions are neutral in terms of ozone - with one ozone molecule effectively produced in reaction 4.1 and one used up in reaction 4.3 (Logan 1983). In the presence of hydrocarbons, such as methane, the reaction of NO with peroxy radicals (RO₂ species), with no ozone loss, leads to net ozone production, via the photolysis of NO₂ (reaction 4.1) (Crutzen 1979). All of the reactions above perturb the NO/NO₂ ratio, but do not change the total amount of NO_x (NO + NO₂) in the atmosphere.

To understand the NO_x budget, and what affects the total amount of NO_x in the atmosphere, the sources and sinks of NO_x must be considered. Emissions are the source of NO_x in the atmosphere. These occur at the surface, from fossil fuel use, biomass burning, and soils, and higher up in the atmosphere from aircraft. There is also a natural source of NO_x from lightning-induced fixation of atmospheric nitrogen (Schumann et al. 2007).

There are many sinks for NO_x in the atmosphere. NO and NO₂ can be oxidised via several different pathways to form compounds such as NO₃, RONO₂, N₂O₅, nitric acid (HNO₃) and peroxyacetyl nitrate species (PAN). NO_x and all of these oxidation products are collectively known as NO_y. NO_y compounds act as reservoirs or sinks of NO_x: they can be converted back to NO or NO₂, or removed from the atmosphere by reactions and physical removal. Fig 4.1 shows a schematic of the NO_x and NO_y sources, sinks and interconversion.

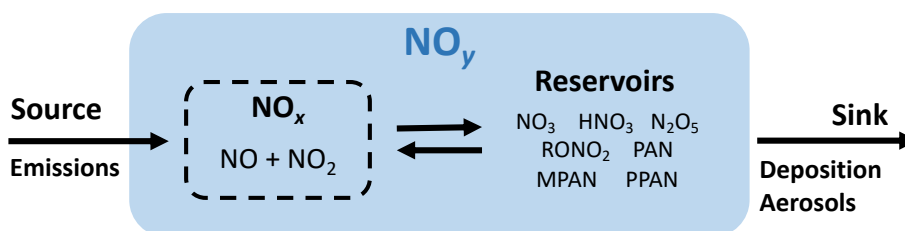
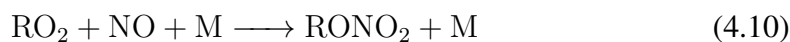
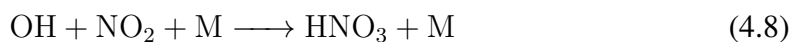
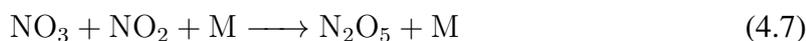


Figure 4.1: Schematic describing the NO_x-NO_y system, with sources, reservoirs and sinks for NO_x and NO_y.

HNO₃ is produced from the reaction of NO₂ with OH (reaction 4.8). N₂O₅ is formed from the reaction of NO₂ and NO₃. N₂O₅ also reacts with water on aerosols in a heterogeneous reaction to form HNO₃. Nitric acid is very soluble and is readily removed from the atmosphere through deposition: the formation of HNO₃ through these reactions is the major pathway for removal of NO_x from the atmosphere (Logan 1983).



The rate of change of NO_x is determined by the balance in sources, reaction to form NO_y reservoirs, and sinks (shown in Fig 4.1). Methane affects both the ratio of NO/NO₂, and the total amount of NO_x. The mechanisms for this are explored in this chapter, by considering the NO_y species, and looking at the fluxes for the above reactions.

Previous studies have analysed the effects of NO_x emissions perturbations on methane, ozone and climate. Stevenson et al. (2022) found that half of the observed methane growth rate between 2019 to 2020 could be explained by NO_x emissions reductions resulting from lockdowns (assumed to be 20 %). Fry et al. (2012) quantified the radiative forcing impacts of CO and NO_x emissions reductions (leading to a negative and positive forcing respectively). Both of these studies used the same set of chemistry transport models, from Task Force on Hemispheric Transport of Air Pollution (2010). These simulations used a methane LBC, and they diagnosed methane changes indirectly using the methane lifetime. While they simulated methane emissions perturbations (via changes in the LBC) these studies did not consider the impact of methane on NO_x.

CO is another species strongly coupled to methane. Reaction with CO is the major sink for OH in the troposphere (39% of total destruction, Lelieveld et al. (2016)). Therefore, changes in CO emissions affect the tropospheric OH concentration. Reductions in CO emissions lead to lower CO concentrations, reducing the sink strength for OH, causing an increase in OH concentrations. This has implications for the oxidative capacity of the atmosphere, and the lifetime of species such as methane. Any changes in OH caused by CO affect methane, and vice versa (Prather et al. 2012). Methane also affects the source of CO: methane oxidation is a secondary source for CO. This relationship can be described using the equations 1.15-1.17 in Chapter 1.

NO_x also affects OH production. Primary production of OH occurs via ozone photolysis and the reaction of O¹D + H₂O (Levy 1971). Ozone in the troposphere is produced via NO₂ photolysis; changes in NO_x affect ozone and therefore OH. NO_x also affects OH recycling, or secondary production of OH, which occurs when NO reacts with HO₂, re-forming OH (reaction 4.4). This process accounts for around 30% of OH production (Lelieveld et al. 2016), and is especially important at high latitudes, where there is less primary production of OH, due to lower photon flux and water vapour concentrations.

The relationship between OH, CO and NO_x has been formalised in several past studies. Wang et al. (1998) derived an expression for tropospheric OH concentration where [OH] is proportional to the ratio $S_N / S_C^{3/2}$ (equation 4.13). S_N is the source of NO_x and S_C is the source of hydrocarbons, approximated in that work as the source of CO. Decreasing CO reduces S_C , which leads to more OH by decreasing the sink, while decreasing NO_x reduces S_N , and decreases OH. The exponent of 3/2 accounts for non-linear feedbacks in the coupled chemistry between CO and OH. Dalsøren et al. (2006) used a weaker dependency of OH on the same ratio, with $[OH] \propto S_N / S_C$, in a 3D chemistry transport model.

$$[OH] \propto \frac{S_N}{S_C^{3/2}} \quad (4.13)$$

Naik et al. (2013) compared the historical OH changes over time relative to CO and NO_x concentrations for a range of CMIP5 models. They found a linear relationship between the absolute change in annual average tropospheric mean OH concentration from pre-industrial to present day (ΔOH), and the ratio of the change in tropospheric CO and NO_x burdens, ($\Delta\text{NO}_x / \Delta\text{CO}$). This is consistent with the relationship in Dalsøren et al. (2006). While the CO and NO_x emissions differences are consistent between the CMIP5 models, the changes in burden are not consistent, due to differences in chemical and physical schemes implemented in the models. Murray et al. (2021) tested the relationship in equation 4.13 in ACCMIP models and found that it explains intra-model variation in OH well, given the NO_x lifetime remains relatively constant. They showed that models generally disagree in their OH response to emissions changes, due to differences in VOC oxidation schemes and NO_x lifetimes, and found that changes in OH were better characterised by variations in the relative loss pathways of reactive nitrogen and carbon (CO + CH₄), $L_{\text{NO}_x} / L_C^{3/2}$. This is equivalent to the source ratio (at steady-state), but also takes into account the different chemistry schemes used by different models (where the same emissions give a different [OH]).

John et al. (2012) evaluated the influence of climate and emissions on OH and methane lifetime in a set of pre-industrial to present day CMIP5 experiments where selected forcings were kept at 1850 levels. They found that anthropogenic drivers were dominant in determining the methane lifetime trend over the historical period. They calculated the correlation coefficients for global annual mean OH vs methane burden, CO emissions, surface NO_x emissions and lightning NO_x emissions. In the historical simulation, the CO and NO_x emissions increase over time, while overall the tropospheric mean OH decreases. A strong anti-correlation is seen between CO emissions and OH concentration. The NO_x emissions increase over time would be expected to increase OH, however the opposite is seen, likely due to the effect of other anthropogenic emissions in this scenario, including CO. The ratio of CO to NO_x emissions was not studied here.

In this chapter, I consider CO, methane and NO_x mitigation experiments to unpick the relationship between methane and NO_x in UKESM1-ems.

CO mitigation is usually a by-product of mitigation of fossil fuels through measures to reduce methane and CO₂, rather than being directly targeted. Therefore, with targeted

measures to reduce emissions from fossil fuels (the sector with the most potential for abatement), CO emissions are also likely to decrease. CO emissions have been on a downward trend since the 1980s, and continue to decrease in all SSP scenarios except SSP3-7.0 (Gidden et al. 2019).

NO_x emissions decrease in most SSP scenarios due to air quality measures. In most of Europe and North America, NO_x emissions have peaked and are now decreasing due to emissions controls. The global emissions of NO_x are still increasing, mainly due to increasing industry and energy sectors in Asia, where emissions are still increasing and are likely to peak at a later date (Hoesly et al. 2018; Gidden et al. 2019).

Section 4.2 describes the experiments used in this chapter. Section 4.3 shows the methane, CO and NO_x responses to the emissions changes, and section 4.4 explores the mechanisms through which methane affects NO_x. Finally, section 4.5 looks at the impact of CO and NO_x on OH, and how well the relationship in equation 4.13 holds up in these experiments, with different CO and NO_x emissions.

4.2 Experiment setup

The ZAME and SSP3-7.0 scenarios from Chapter 3 were used as baselines for a further set of experiments. The focus of these was to probe the UKESM1-ems model system and processes, looking at coupling between CO, NO_x, methane and OH. The ZAME and SSP3-7.0 pair provide a high and low methane scenario. Within each of these, I implemented low CO and low NO_x emissions trajectories, to look at the system response to changes in CO and NO_x in different methane scenarios. All of the experiments used in this chapter are outlined in Table 4.1, and were run from 2015 up to 2030.

The low emissions trajectories for CO and NO_x follow the SSP1-2.6 pathway, and are shown in Fig 4.2. SSP1-2.6 is the one of the lowest emissions trajectories from CMIP6, and follows a ‘green growth’ scenario (Van Vuuren et al. 2017). By 2030, CO emissions in SSP1-2.6 are 32% lower than in SSP3-7.0, and NO_x emissions are 29% lower. These reductions are from measures targeted at reducing greenhouse gas emissions and

Scenario	CH ₄	CO	NO _x
SSP3-7.0	SSP3-7.0	SSP3-7.0	SSP3-7.0
SSP370lowCO	SSP3-7.0	SSP1-2.6	SSP3-7.0
SSP370lowNO _x	SSP3-7.0	SSP3-7.0	SSP1-2.6
ZAME	no anthro	SSP3-7.0	SSP3-7.0
ZAMElowCO	no anthro	SSP1-2.6	SSP3-7.0
ZAMElowNO _x	no anthro	SSP3-7.0	SSP1-2.6

Table 4.1: CO and NO_x mitigation experiments. All are based on the SSP3-7.0 scenario. In the ZAME scenarios the methane emissions are from natural and biomass burning sources only.

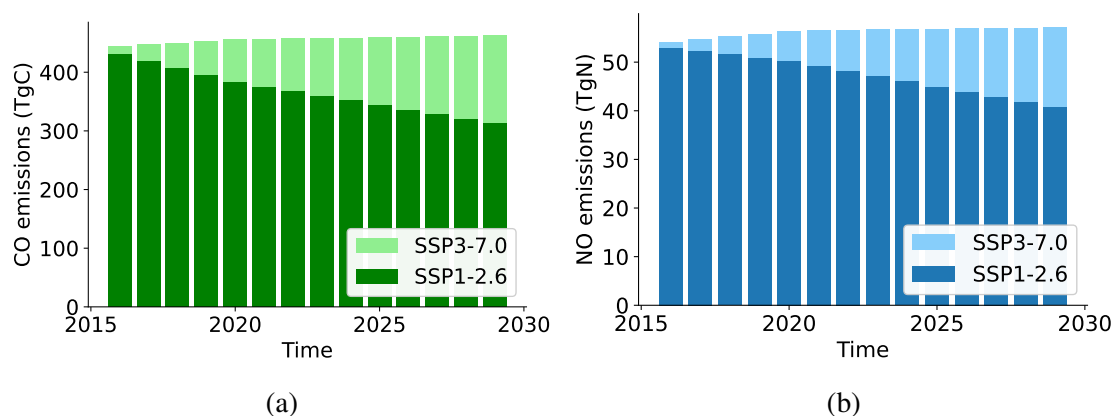


Figure 4.2: CO and NO emissions in SSP3-7.0 (lighter colours) and SSP1-2.6 (darker colours). SSP3-7.0 emissions are used in the baseline scenarios, and SSP1-2.6 CO and NO emissions are used in the lowCO and lowNO_x scenarios respectively.

improving air quality. All other emissions in these experiments are kept at SSP3-7.0 levels.

There is a natural source of NO_x emissions from lightning (around 10% of total NO_x emissions, (Murray 2016)), which is not changed directly here. In UKESM1-ems these NO_x emissions are simulated online and respond to changes in atmospheric variables such as convection and cloud top height according to Price et al. (1992). The NO_x emissions reductions here are implemented on the anthropogenic surface emissions only.

The experiments in Table 4.1 were run from 2015 up to 2030. There is one ensemble member for each low CO/NO_x experiment. SSP3-7.0 and ZAME both have three

ensemble members each, which through calculating an ensemble mean and spread is used to give an indication of whether the perturbations in the lowCO and lowNO_x experiments give results outside the baseline scenario. In the figures in this chapter, the lines labelled SSP3-7.0 and ZAME are the ensemble means (in darker orange and blue respectively) and the ensemble members contributing to the mean are shown, in lighter orange and blue.

4.3 Methane and CO response

In this section I present the results from the lowNO_x and lowCO experiments to show how reducing NO_x and CO emissions affects the methane mixing ratio and CO burden.

The surface mean methane mixing ratio response for the experiments in Table 4.1 is shown in Fig 4.3a. The main differences are between the ZAME and SSP3-7.0 scenarios, which have a large difference in methane emissions. The CO and NO_x emissions decreases do affect the methane mixing ratio - the resulting methane mixing ratios are just outside the ensemble mean for the ZAME and SSP3-7.0 scenarios, from around 2020 for low CO and around 2025 for low NO_x. Decreasing CO increases OH and therefore decreases methane mixing ratios, while decreasing NO_x decreases OH and increases methane mixing ratios. Overall, the methane response to these emissions changes is minimal and is not the focus of this chapter.

Fig 4.3b shows the tropospheric CO burden response to changing methane, CO and NO_x emissions. The large difference between SSP3-7.0 and ZAME comes from a reduction in the secondary production of CO via methane oxidation, and from higher OH concentrations in ZAME, leading to more destruction of CO. As expected, with lower primary CO emissions in the SSP370lowCO and ZAMElowCO experiments, the CO burden decreases over time. In the last three years of the time series, SSP370lowCO has a ~13% lower CO burden and ZAMElowCO has a ~17% lower CO burden, for the same CO emissions reduction. Decreasing CO emissions in ZAME has a larger impact on the CO burden, because primary CO emissions make up a greater proportion of the total CO source in ZAME. There is also a feedback effect via OH similar to the methane

self-feedback described in section 1.2.5. In ZAME, CO is responsible for a greater proportion of the sink for OH, so reducing CO emissions will lead to a proportionally larger increase in OH, which then reduces the CO burden further. Lower NO_x emissions have a similar impact on CO as they do for methane: reducing NO_x decreases OH, which increases the CO burden.

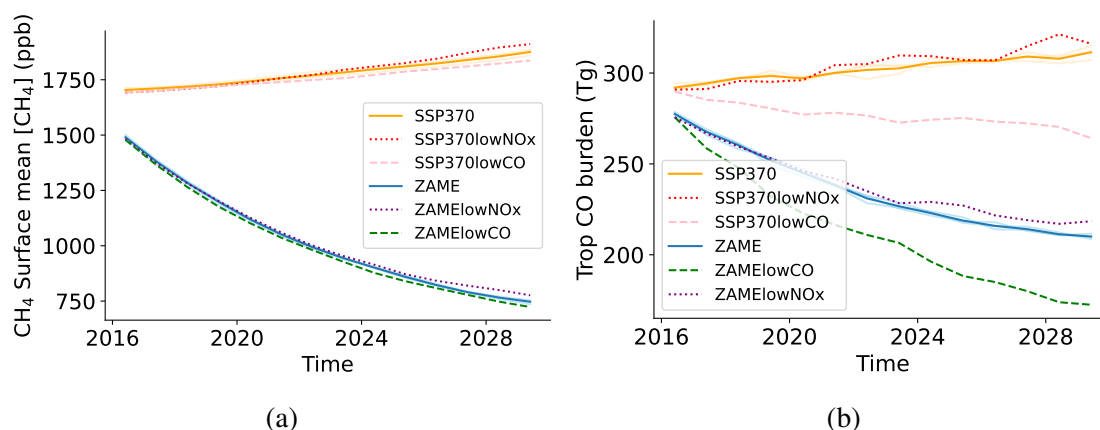


Figure 4.3: Methane and CO response in SSP3-7.0, ZAME (ensemble means) and lowCO/NO_x scenarios. (a) Methane annual mean surface mixing ratio. (b) Tropospheric CO burden.

4.4 How does methane affect NO_x?

The NO_x response to changes in methane in ZAME was one of the main motivations for doing these experiments: perturbing NO_x in a high and low methane scenario. In this section I consider two pairs of scenarios, one with high (SSP3-7.0) NO_x emissions: SSP3-7.0 and ZAME; and one with low (SSP1-2.6) NO_x emissions: SSP370lowNO_x and ZAMElowNO_x (see Table 4.1). In each of these pairs there is a high and low methane trajectory - this enables me to look at the response of NO_x to changes in methane.

Fig 4.4 shows the tropospheric average NO_x mixing ratios and burden from 2016 to 2030. The scenarios in orange and blue have the same (high) anthropogenic NO_x emissions, while the scenarios in dotted lines have the same (low) anthropogenic NO_x

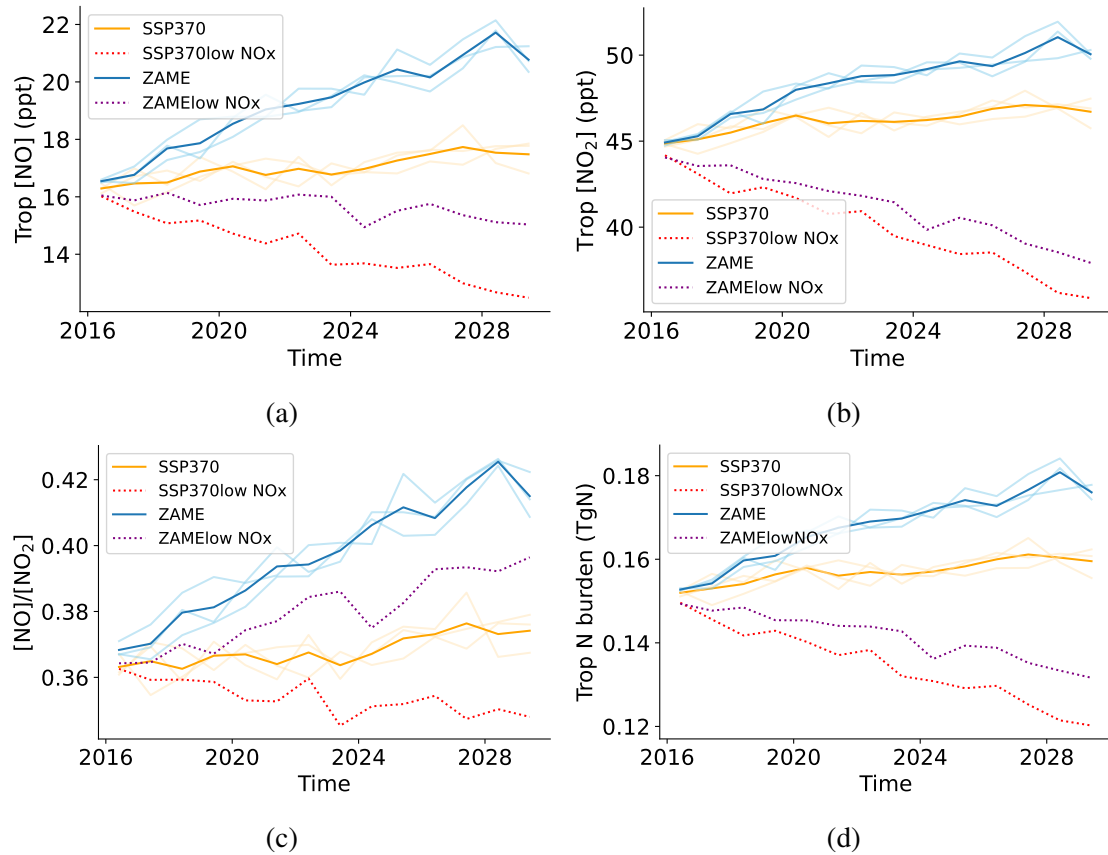


Figure 4.4: NO_x response in SSP3-7.0, ZAME and lowCO/NO_x scenarios. (a) NO tropospheric mean mixing ratio (b) NO₂ tropospheric mean mixing ratio. (c) NO_x tropospheric mean mixing ratio. (d) Total NO_x burden (NO+NO₂, TgN).

emissions. Panel (c) shows the NO/NO₂ ratio, ie. panels (a) divided by (b). With lower methane emissions, the NO_x mixing ratio and burden increases. This means that methane affects the source or sink terms of NO_x in UKESM1-ems. The NO/NO₂ ratio also changes with decreasing methane emissions, showing that methane also affects the photostationary state of NO/NO₂.

Fig 4.5 and Fig 4.6 show the zonal mean differences in NO and NO₂ respectively. The magnitude of the NO change is highest at the surface, corresponding to where the highest NO concentrations are (and emissions). NO₂ increases the most in the northern hemisphere and the tropical upper troposphere. When looking at the percentage difference, both NO and NO₂ show an increase in the northern hemisphere and in the tropical upper troposphere. These two regions have different chemical regimes, with the lower NH tropospheric region much more influenced by anthropogenic emissions, and with reservoir species such as N₂O₅ and NO₃. The tropical upper troposphere is likely to be more affected by lightning NO_x emissions. The high and low NO_x scenarios show very similar results, with slightly higher NO_x increases in the SSP3-7.0 NO_x scenario for the same change in methane emissions. The reasons behind these NO_x trends are explored in the next sections.

4.4.1 Changes in NO/NO₂ ratio

Firstly I consider the reactions that affect the NO/NO₂ ratio. These are reactions 4.1 to 4.5, which interconvert NO and NO₂. The NO₂ photolysis reaction is unlikely to be affected by changes in methane. However, NO + O₃ will be affected, because as seen in section 3.3, methane mitigation leads to a decrease in tropospheric ozone. Secondly, the HO₂ + NO reaction will be affected via the decrease in HO₂ described in section 3.6 (see Fig 3.6a). Finally, methane oxidation to form MeOO radicals (an RO₂ species) will affect the RO₂ + NO reaction. Taken together, decreasing ozone, HO₂ and RO₂ all favour NO over NO₂. These determine the ratio changes seen in Fig 4.4c, both in terms of comparison between experiments, and changes in ratio over time.

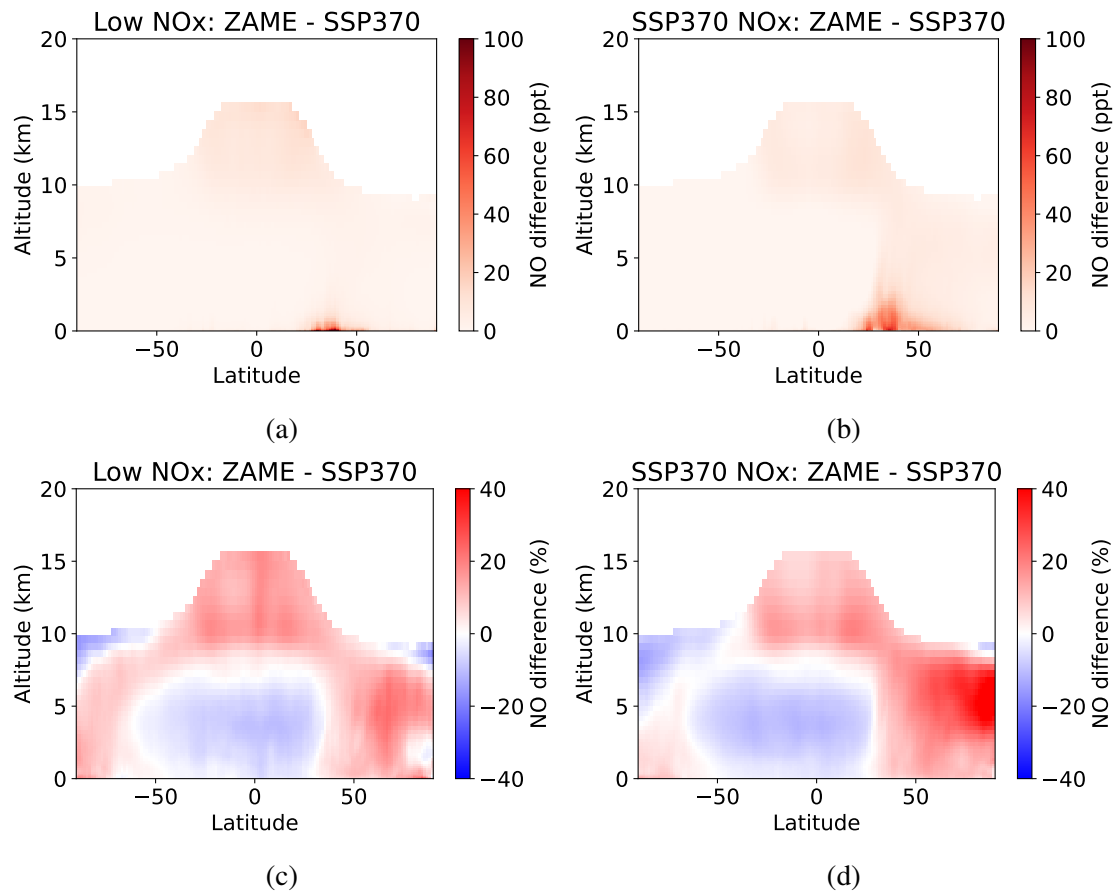


Figure 4.5: NO mixing ratio difference between high (SSP3-7.0) and low (ZAME) methane scenarios. (a,c) for a low (SSP1-2.6) NO_x state, (b,d) for a high (SSP3-7.0) NO_x state, in ppt (a,b) and percentage (c,d) terms.

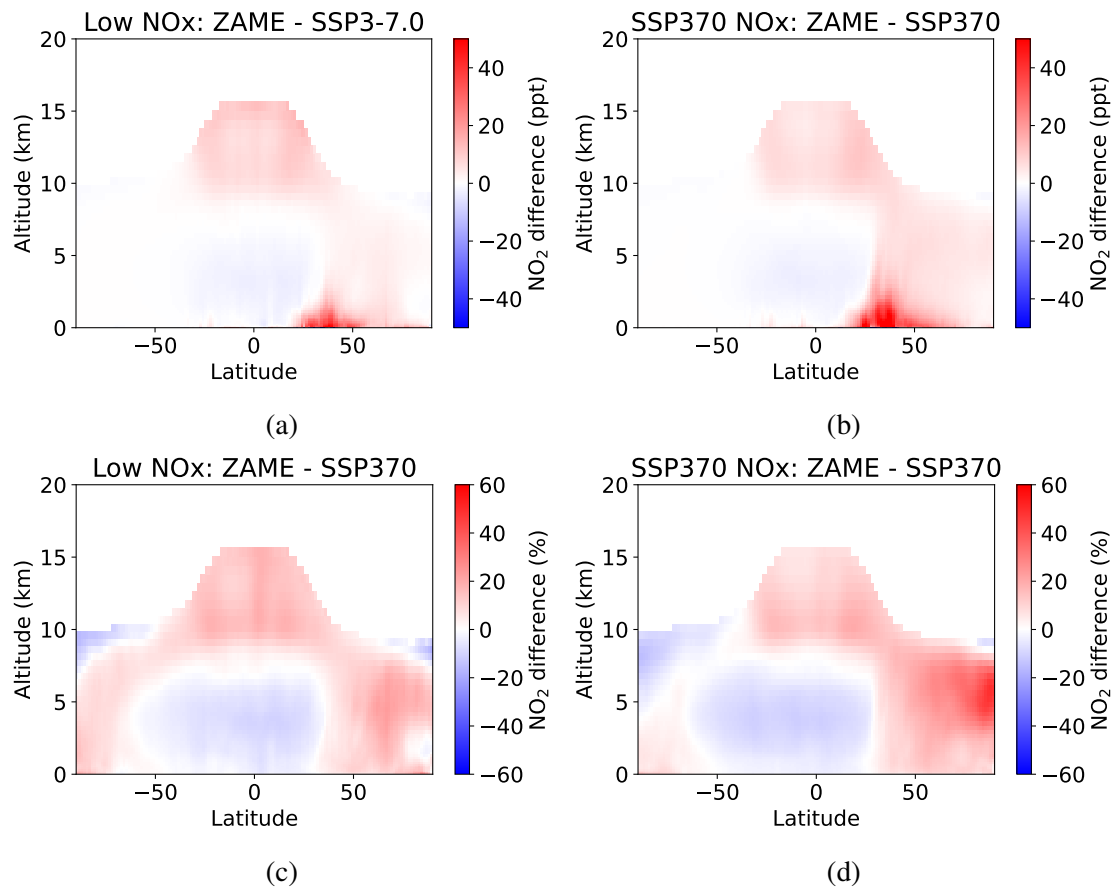


Figure 4.6: NO₂ mixing ratio difference between high (SSP3-7.0) and low (ZAME) methane scenarios. (a,c) for a low (SSP1-2.6) NO_x state, (b,d) for a high (SSP3-7.0) NO_x state, in ppt (a,b) and percentage (c,d) terms.

Assuming steady state for NO and NO₂ interconversion, I consider the steady state for NO₂, considering only the interconversion reactions between NO and NO₂ (4.1 to 4.5).

$$\begin{aligned} \frac{d[\text{NO}_2]}{dt} &= -J_{\text{NO}_2}[\text{NO}_2] + k_{\text{NO}+\text{O}_3}[\text{NO}][\text{O}_3] + k_{\text{HO}_2+\text{NO}}[\text{HO}_2][\text{NO}] \\ &\quad + k_{\text{RO}_2+\text{NO}}[\text{RO}_2][\text{NO}] \\ &= 0 \end{aligned} \quad (4.14)$$

$$\frac{[\text{NO}]}{[\text{NO}_2]} = \frac{k_1}{k_{\text{NO}+\text{O}_3}[\text{O}_3] + k_{\text{HO}_2+\text{NO}}[\text{HO}_2] + k_{\text{RO}_2+\text{NO}}[\text{RO}_2]} \quad (4.15)$$

When methane emissions and concentrations decrease, ozone, HO₂ and MeOO (an RO₂ species) all also decrease (Figs 3.2, 3.6a). These are all in the denominator in equation 4.15, so a decrease leads to an increase in the NO/NO₂ ratio. Fig 4.4c shows that the ratio is higher for the low methane scenarios compared to the SSP3-70 scenarios. Fig 4.7 shows the tropospheric ozone, MeOO + NO flux and HO₂ + NO flux. All three of these are lower in the ZAME/ZAMElowNO_x scenarios, and the difference gets larger over time. The zonal mean plots in Fig 4.7 show the distribution of the ozone and flux decreases: these are zonally uniform, consistent with a zonally uniform decrease in methane mixing ratio and oxidation, and tropospheric ozone. Decreasing ozone, HO₂ and MeOO all explain the increases in the NO/NO₂ ratio seen in Fig 4.4c between the SSP370 and ZAME scenarios (for high and low NO_x) and the increasing ratio over time in the low methane scenarios.

4.4.2 Changes in NO_x sources and sinks

Here I consider the tropospheric NO_x burden and investigate the causes of the change in NO_x over time, and the differences between the high and low methane scenarios.

The rate of change of NO_x over time depends on the sources and sinks of NO_x. The source includes both anthropogenic and natural emissions. In the experiments considered here, the anthropogenic NO_x emissions are the same in the compared scenarios

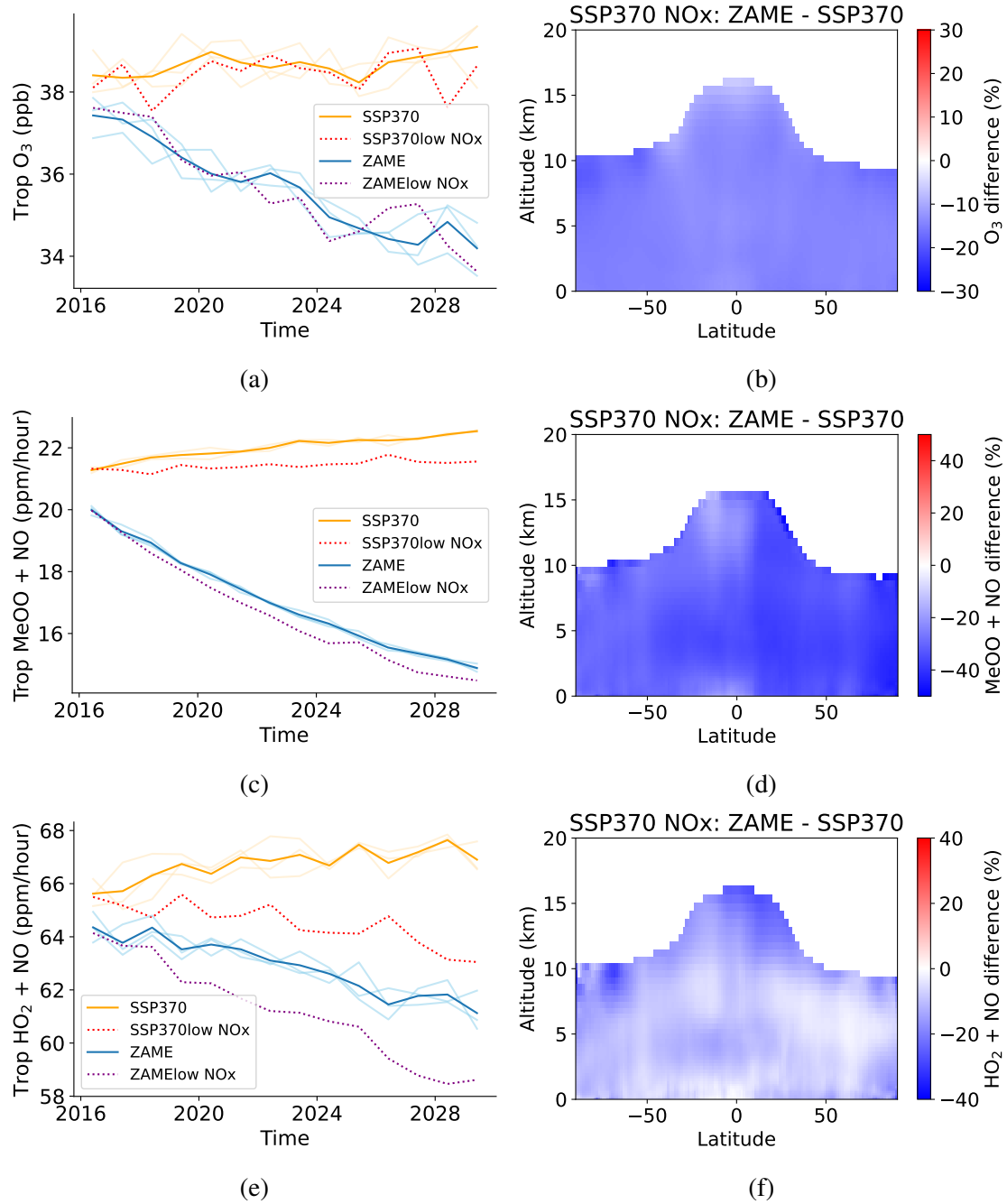


Figure 4.7: Mixing ratios and fluxes affecting the NO/NO₂ ratio, annual tropospheric mean and zonal mean over 2025-2029: (a, b) ozone mixing ratios. (c, d) MeOO + NO flux (e, f) HO₂ + NO flux.

(either high NO_x or low NO_x). The natural emissions from lightning are interactive in UKESM1-ems and vary based on factors such as convection and temperature (e.g. Barret et al. (2010) and Stockwell et al. (1999)). The lightning NO_x emissions in the scenarios studied in this chapter all show a high interannual variability and no significant differences between the low and high methane scenarios up to 2030. After 2030 there are larger differences between the ZAME and SSP3-7.0 scenarios, likely driven by the relative temperature decrease in the ZAME methane scenarios. However, there is still a large amount of noise, with the interannual variability in the emissions greater than the difference in emissions between the scenarios.

The rest of the emissions are input directly based on CMIP6 emissions: either SSP3-7.0 or SSP1-2.6 for the high and low NO_x trajectories respectively. These include surface and aircraft emissions. Therefore, these don't change between the high and low methane scenarios. Given this and the similar lightning NO_x emissions (to within interannual variability), it means that the NO_x changes are a result of NO_x reservoirs or sinks, and not a difference in emissions.

Given the same emissions, an increase in NO_x means that the lifetime of NO_x is longer in the low methane scenario - or there is a weaker sink for NO_x. To evaluate this, I looked at all of the available species of NO_y in UKESM1-ems. NO_y here includes the following: NO, NO₂, N₂O₅, HNO₃, NO₃, MPAN, PPAN, PAN and MeONO₂.

I found that HNO₃, N₂O₅ and PAN show no significant differences between the high and low methane scenarios (see Fig 4.8). There was also no difference in the total NO_y deposition. This is consistent with the HNO₃ results, since HNO₃ is the largest contributor to the deposition term.

Given the increase in NO₂, the NO₃ decrease in the low methane scenario (see Fig 4.8d) can be attributed to reduced ozone and less production of NO₃ through the reaction $\text{NO}_2 + \text{O}_3 \longrightarrow \text{NO}_3 + \text{O}_2$.

The tropospheric concentration of MeONO₂ is also much lower in the low methane scenarios, and decreases over time (see Fig 4.8c). MeONO₂ is formed via the reaction of MeOO with NO in the presence of a third body, M (4.11). The yield of MeONO₂

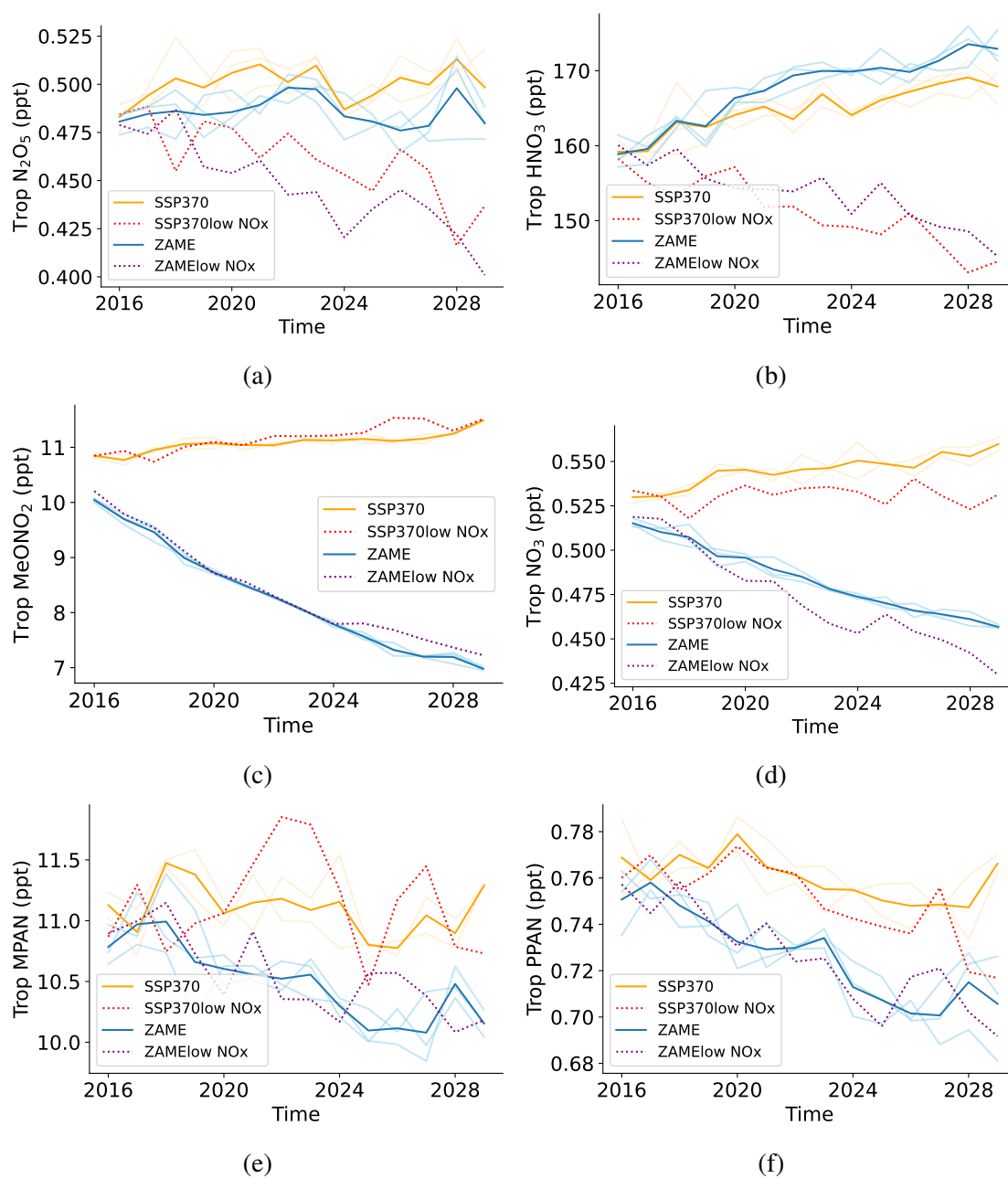


Figure 4.8: Tropospheric annual mean concentration over time for NO_y species (a) N₂O₅, (b) HNO₃, (c) MeONO₂, (d) NO₃, (e) MPAN, (f) PPAN.

from reaction 4.11 is small and highly uncertain (Atkinson et al. 2006). In the StratTrop chemistry scheme used here a yield of 0.1% is used. Archibald et al. (2007) assessed the contribution of MeO + NO₂ to MeONO₂ production and found this to be relevant only at very high levels of NO₂. In UKESM1, the sink for MeONO₂ is 96% photolysis, and so is largely independent of the scenario changes here - the MeONO₂ changes here are due to production. I have already discussed in the previous section that the MeOO concentration decreases due to less oxidation of methane (owing to the lower methane emissions). Therefore, there is also less formation of MeONO₂ in the lower methane scenarios. The concentrations of the reservoirs PPAN and MPAN are also lower in the low-methane scenarios (with a much smaller relative decrease compared to MeONO₂), although the mechanisms for this are unknown. The concentrations of these reservoir species are shown in Figs 4.8e, 4.8f.

Overall, in the low-methane scenarios, more N is present as NO_x species, and less in reservoir NO_y species. This is shown in Fig 4.9, with the percentage of NO_x in NO_y increasing over time, and more NO_x in the low-methane scenarios (ZAME and ZAMElowNO_x). In 2025-2029, NO_x comprises 18% and 16% in the ZAME and ZAMElowNO_x scenarios, compared to 17% and 15% in the corresponding high-methane scenarios. Given the deposition terms are very similar, the total amount of nitrogen atoms in the atmosphere is likely similar between the low and high methane scenarios, but more is in the active NO_x form in the low-methane scenarios.

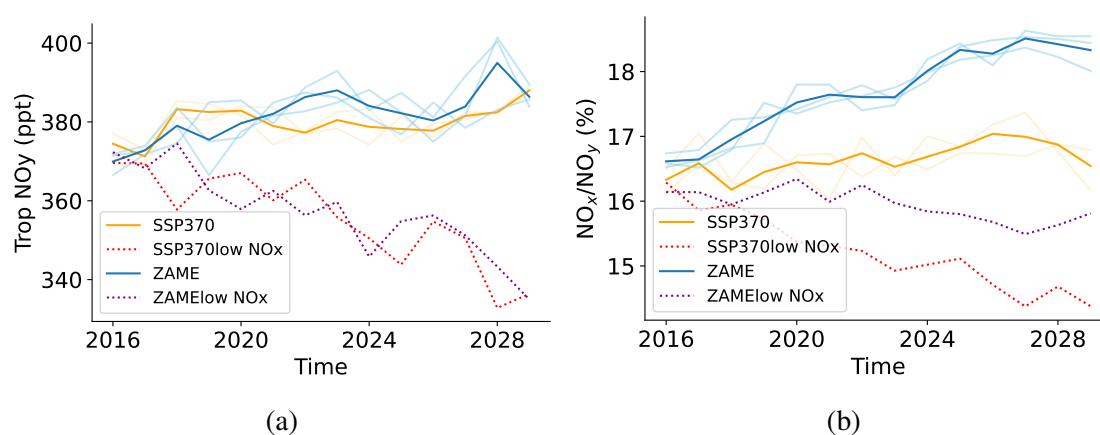


Figure 4.9: a) Tropospheric NO_y concentration over time. b) Percentage of NO_x=NO+NO₂ as a proportion of NO_y: (NO + NO₂) / NO_y.

4.5 OH sensitivity to NO and CO emissions

In this section I explore how changing CO and NO_x emissions affect OH, in a high (SSP3-7.0) and low (ZAME) methane state, using the experiments detailed in Table 4.1. In SSP3-7.0, the global mean tropospheric OH concentration remains fairly constant. In ZAME, OH increases corresponding to the decrease in methane, as described in section 3.3. I also show the impact of these emissions changes on methane lifetime.

The dashed lines in Fig 4.10 show the OH response to reduced CO emissions. In both the high and low methane cases, the resulting OH concentration is larger, as expected because CO is the main sink for OH. The percentage increase in OH in ZAME (in pink) is greater than in SSP3-7.0 (in green) - around 6% compared to 4%. The same reduction in CO emissions leads to a greater increase in OH, because in ZAME, CO accounts for a greater proportion of the total OH sink. So here we see a methane state dependence of the impact of CO emissions reductions.

The dotted lines in Fig 4.10 show the OH response to reduced NO_x. The NO_x perturbations have a smaller impact on OH than the CO emissions reductions. In the first half of this time series, in SSP3-7.0, the resulting OH concentration is within the model spread. In the ZAME_{lowNOx} experiment, the OH concentration decreases relative to the baseline much earlier than in SSP3-7.0. Overall, the NO_x reductions lead to a small decrease in OH, as expected due to the role of NO_x in ozone production (and therefore OH source), and OH recycling. The OH reduction due to NO_x in ZAME is larger than in SSP3-7.0, although in both the OH perturbation is much smaller and has a larger interannual variability than when changing CO emissions. In these experiments, the sensitivity of OH response to NO_x emissions in different methane states is lower and more uncertain than the state dependence of changes in CO emissions (see previous paragraph).

OH has a very short lifetime (~seconds) and therefore its distribution is not globally uniform. The tropospheric mean values give an idea of the changes in overall oxidising capacity: this is the sum of different regional changes. The zonal mean OH distribution

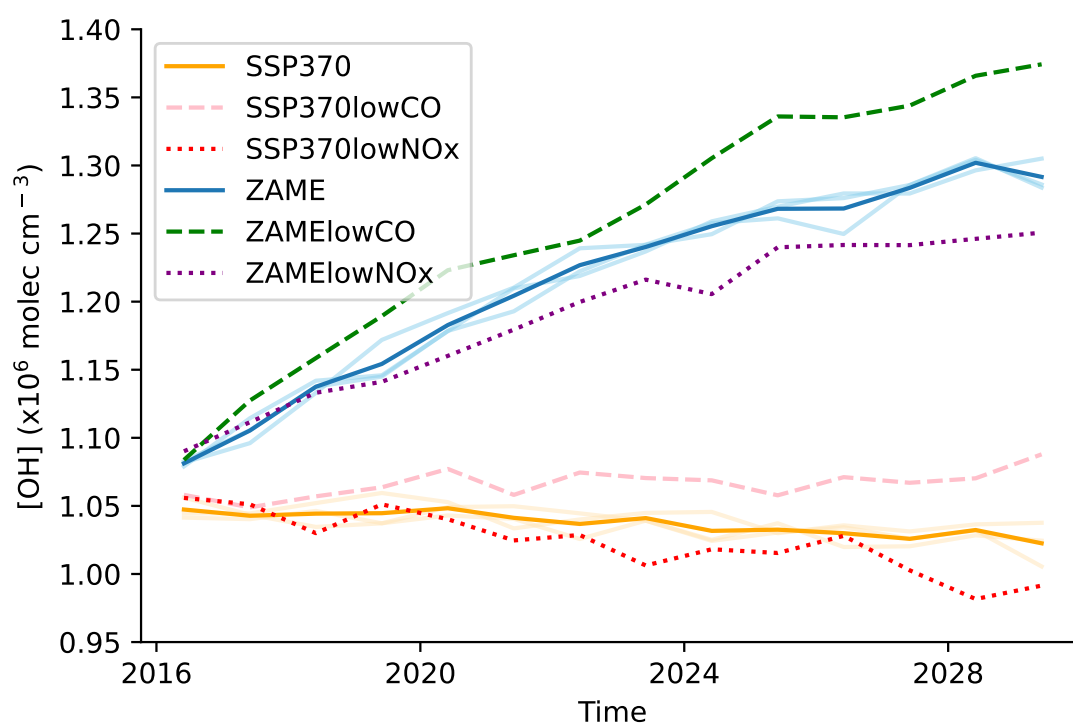


Figure 4.10: Global tropospheric mean OH concentration over time in the different scenarios described in Table 4.1. Dashed lines show lowCO scenarios and dotted lines show lowNO_x scenarios, for both SSP3-7.0 and ZAME baselines. The ensemble members for SSP3-7.0 and ZAME are shown in lighter colours, with the ensemble mean in the darker colours (orange and blue respectively). This is a measure of the uncertainty due to model spread.

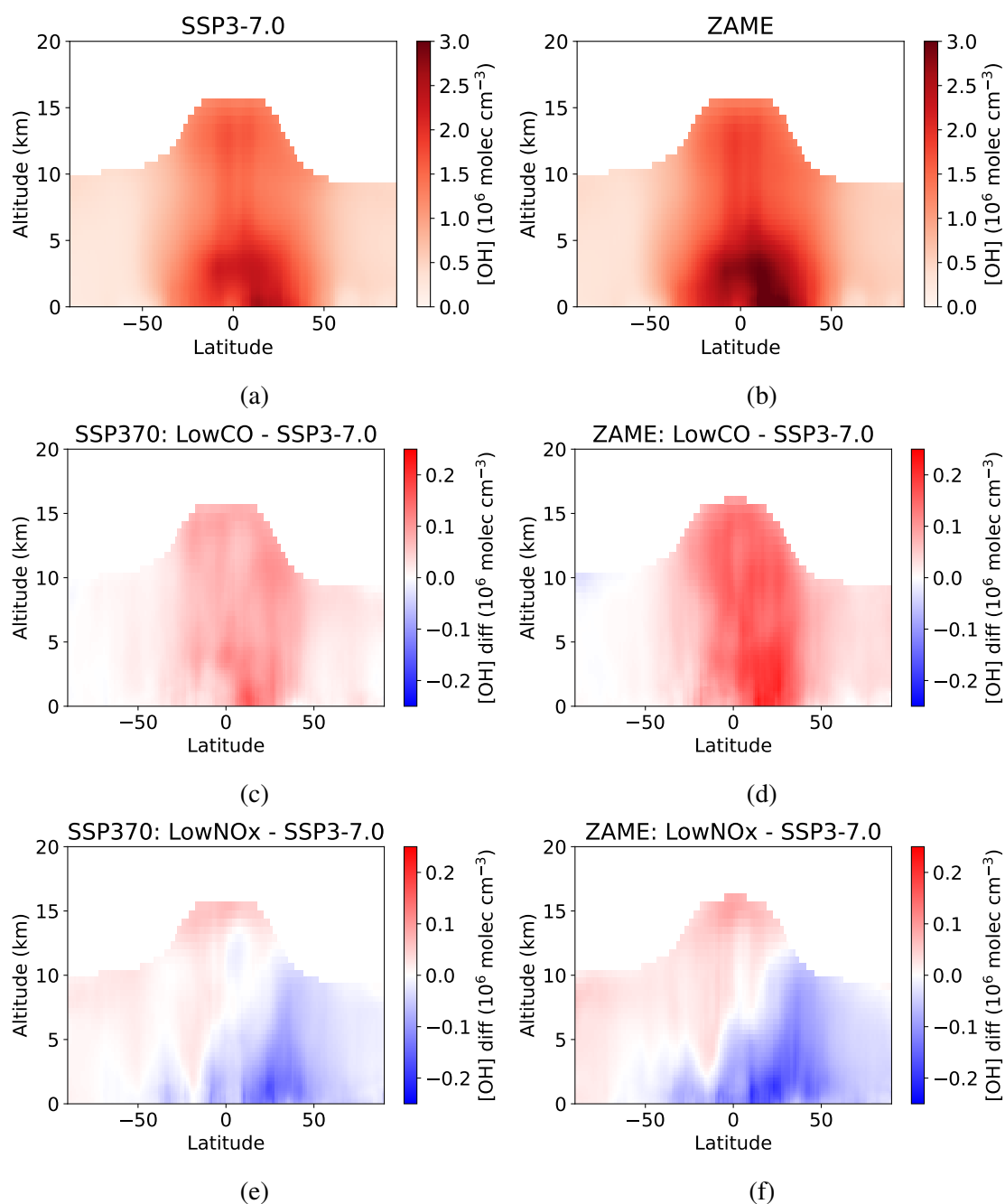


Figure 4.11: OH zonal mean difference for 2025-2029 between the low emissions scenarios and the baselines (SSP3-7.0 and ZAME). (a, b) OH zonal mean distribution in SSP3-7.0 and ZAME. (c, d) OH difference resulting from decreases in CO emissions in SSP3-7.0 and ZAME respectively. (e, f) OH difference resulting from decreases in NO_x emissions in SSP-3.70 and ZAME respectively.

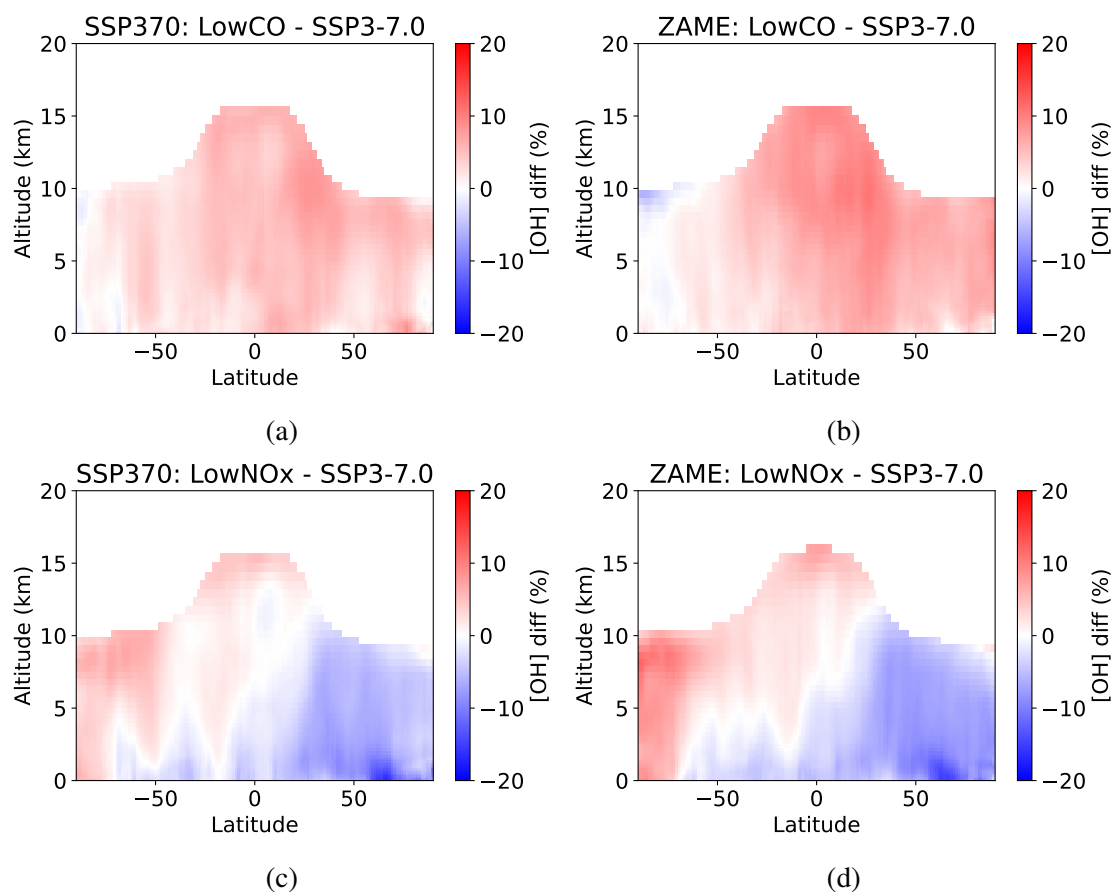


Figure 4.12: Percentage OH zonal mean difference for 2025-2029 between the low emissions scenarios and the baselines (SSP3-7.0 and ZAME). Same as Fig 4.11 but in percentage terms. (a, b) OH difference resulting from decreases in CO emissions in SSP3-7.0 and ZAME respectively. (c, d) OH difference resulting from decreases in NO_x emissions in SSP3-7.0 and ZAME respectively.

is shown in Figs 4.11a, b for SSP3-7.0 and ZAME. The highest OH concentration is in the tropics, in the lower troposphere.

CO and NO_x affect OH in different ways - the zonal distribution of their changes is also different, and shows the mechanism through which CO and NO_x affect OH. CO is relatively well-mixed in the troposphere, with a lifetime of around 2 months (Khalil et al. 1990). Therefore, decreasing CO emissions decreases CO concentrations globally. Less CO means less OH+CO reacting, and leads to more OH. Fig 4.11 c and d show the effect of CO emissions decreases on OH. OH decreases most where its concentration is highest: looking at a percentage difference shows that the decrease in OH is relatively uniform throughout the troposphere (see Fig 4.12).

NO affects OH via primary production of OH, and through radical recycling. NO₂ photolysis leads to ozone formation (reactions 4.1 and 4.2), which when photolysed forms O(¹D). A small proportion of this reacts with water to form OH (Levy 1971). Therefore, with lower NO_x concentrations, there is less ozone and the source for OH decreases. The secondary effect of NO_x is to recycle HO_x (convert HO₂ to OH), via the HO₂ + NO reaction, which forms OH and NO₂. This effectively increases the OH source by converting HO₂ to OH. NO_x has a much shorter lifetime than CO - between 1-2 days at the surface, up to 2 weeks in the upper troposphere (Seinfeld et al. 2016). Therefore NO_x concentrations are higher close to its sources, e.g. in urban areas and in the northern hemisphere. The zonal difference in OH between high and low NO_x scenarios shows a hemispheric difference: with a large decrease in OH in the northern hemisphere, which drives most of the global trend.

It is possible to isolate the two mechanisms by which NO_x affects OH. The impact on primary production of OH is via ozone. Fig 4.13 shows the zonal mean differences in ozone between the high and low NO_x experiments. The distribution of the ozone decrease is very similar to that of the OH decrease, for both SSP3-7.0 and ZAME. This makes sense because ozone is a precursor for OH. This likely explains most of the northern hemisphere OH decrease: a decrease in the primary source for OH.

The HO₂ + NO reaction is responsible for a similar amount of OH production as O(¹D) + H₂O (Lelieveld et al. 2016). I hypothesised that the changes in HO₂ + NO would have

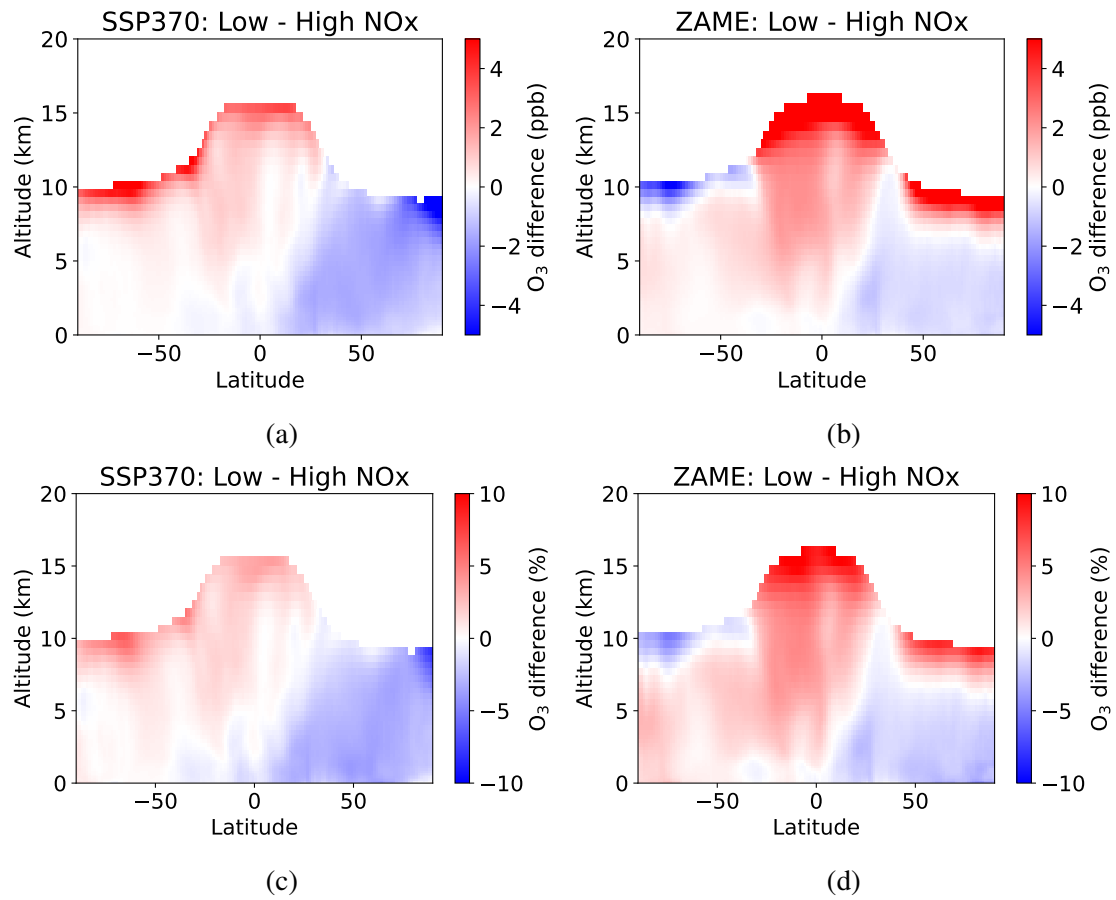


Figure 4.13: Ozone mixing ratio differences between high (SSP3-7.0) and low (SSP1-2.6) NO_x scenarios. (a,c) for a high (SSP3-7.0) methane state, (b,d) for a low (ZAME) methane state, in ppb (a,b) and percentage (c,d) terms.

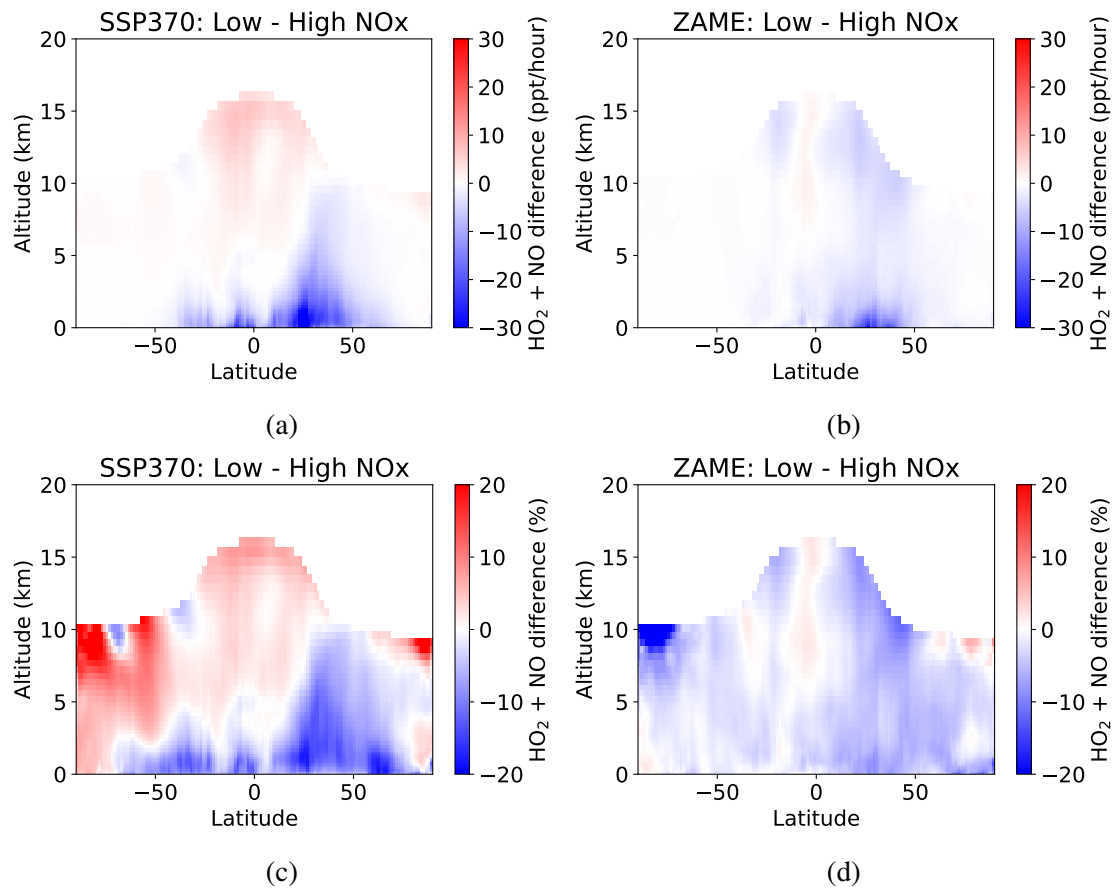


Figure 4.14: $\text{HO}_2 + \text{NO}$ flux difference between high (SSP3-7.0) and low (SSP1-2.6) NO_x scenarios. (a,c) for a high (SSP3-7.0) methane state, (b,d) for a low (ZAME) methane state, in ppt (a,b) and percentage (c,d) terms.

a greater impact in the northern hemisphere, due to less primary production of OH and higher NO_x emissions there. In SSP3-7.0, the zonal HO₂ + NO flux decrease is very similar to the OH decrease (Fig 4.11e compared to Fig 4.14c). There are large decreases in flux in the northern hemisphere, but the flux also decreases in the southern hemisphere low troposphere, with peaks extending up into the mid troposphere at around 0°, 30°S and 60°S (Fig 4.14c). These same peaks are seen in the OH distribution, suggesting that the change in HO₂ + NO flux contributes to the OH decrease, especially in the southern hemisphere. In ZAME, the HO₂ + NO flux decrease is much more hemispherically uniform, and both the absolute and percentage decreases are lower than in SSP3-7.0. The HO₂ concentrations in ZAME are lower than in SSP3-7.0 (by around 13% in 2030). Therefore, decreasing NO_x in ZAME has a smaller impact on the HO₂ + NO flux - there is a methane state dependence seen here via HO₂. In the low methane scenario, the influence of NO_x on OH via radical recycling is lower, and the main mechanism for NO_x affecting OH is likely through its primary production via ozone, as described in the previous paragraph.

Chua et al. (2023) used the GFDL-AM4.1 model to explore the drivers of historical tropospheric OH trends. They found that NO_x and methane were the most important factors in terms of driving global changes in OH, whereas CO had an impact regionally, but with increases and decreases in different areas cancelling out in the global average. In this study, methane, CO and NO_x all have an impact on the tropospheric mean OH concentration changes. In the time period considered by Chua et al. (2023), CO emissions don't change very much, whereas the 32% decrease simulated here has a much larger impact on OH. CO emissions have an impact globally, whereas NO_x affects OH most in the northern hemisphere.

4.5.1 Methane lifetime

The methane lifetime responds accordingly to the OH changes, with the low CO scenarios giving a shorter methane lifetime, and the low NO_x scenarios giving a longer lifetime (Fig 4.15). In these scenarios, the largest difference in methane lifetime comes from the changes in methane between SSP3-7.0 and ZAME, due to the large decrease in methane

burden, and its influence on OH, as discussed in section 3.3. The CO and NO_x emissions reductions are smaller than the methane emissions perturbation in ZAME, and they also only have a secondary impact on methane lifetime via changes in OH, rather than changing the methane burden directly. Therefore, a smaller change in methane lifetime in the lowNO_x and lowCO scenarios is as expected.

The dependence of methane lifetime on the CO and NO_x pathways affects the radiative impact of methane in different scenarios, by changing the residence time and therefore the time over which methane can act as a greenhouse gas. This highlights the limitations of assuming a constant methane lifetime over an extended time period, for example in Global Warming Potential calculations (which have well-documented limitations e.g. Fuglestvedt et al. (2003) and Shine (2009)), or in conversion of methane emissions to a lower boundary condition concentration.

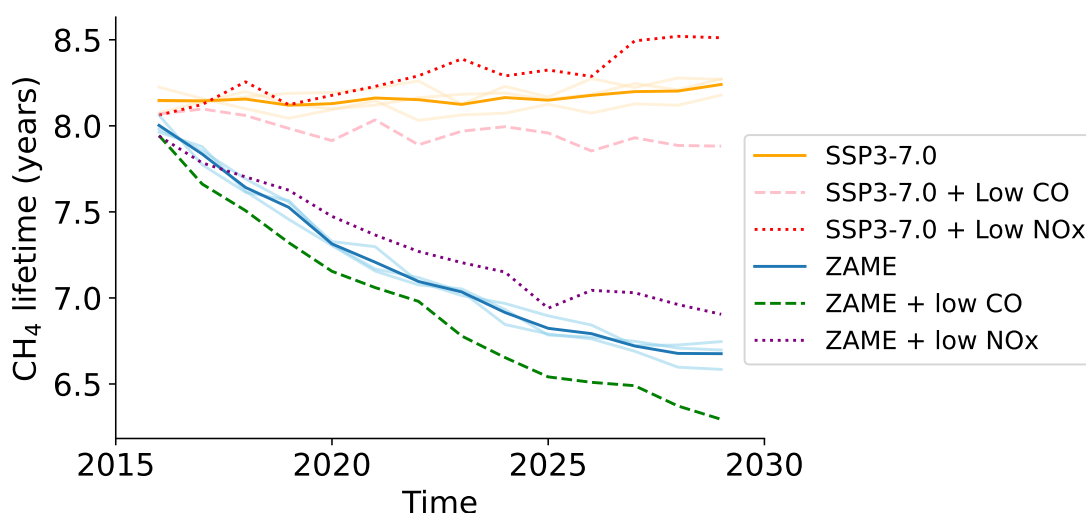


Figure 4.15: Evolution of methane lifetime with respect to OH in the different scenarios described in Table 4.1. Dashed lines show low CO scenarios and dotted lines show low NO_x scenarios, for both SSP3-7.0 and ZAME baselines. The ensemble members for SSP3-7.0 and ZAME are shown in lighter colours, with the ensemble mean in the darker colours (orange and blue respectively). This is a measure of the uncertainty due to model spread.

4.5.2 OH, CO, NO_x and methane relationship

As the results above have demonstrated, there is strong coupling between OH, CO, NO_x and methane. This is well established in the literature, and here specifically I explore the relationship between OH and the CO to NO_x ratio, to test which expression from the previous studies most faithfully represents the results from these experiments.

While Wang et al. (1998) use emissions to calculate the $S_N/S_C^{3/2}$ ratio, later studies have simplified this to the S_N/S_C ratio, or have used burdens instead of emissions (Dalsøren et al. 2006; Dalsøren et al. 2016; Naik et al. 2013). Using these experiments, with varying CO, NO_x and methane, I tested each of these relationships to see which was most representative for my data. Both assume that there are minimal changes in all VOCs except CO. This is not the case here (and arguably not the case over the last century or so as anthropogenic VOCs have changed significantly), since methane emissions increase in SSP3-7.0, and in ZAME the methane trends down to a new steady state, following the large decrease in emissions. Therefore, I included methane in the S_C term to take it into account - since it affects OH in a similar way that CO does.

Fig 4.16 shows the relationship between tropospheric mean OH and $S_N/S_C^{3/2}$, calculated using CO, CH₄ and NO_x emissions (4.16a and b) and burdens (4.16c and d). All experiments are plotted on the same axes in Fig 4.16a, and those for the SSP3-7.0 methane experiments in Fig 4.16b. The emissions relationship represents the system well for the SSP3-7.0 methane scenarios, with an r-squared correlation coefficient of 0.79. For the ZAME scenarios the emissions relationship does not hold.

One limitation in using emissions is the assumption that the emissions are proportional to the burden, or actual amount of CO/CH₄/NO_x in the atmosphere, which determines OH concentration. For small changes in emissions - where the system is not perturbed far from its steady state - this works well, such as in SSP3-7.0. However, in ZAME, the emissions change instantaneously at the start of the experiment. In 2015-2050, the emissions are very low, and don't change very much - $S_N/S_C^{3/2}$ in ZAME is fairly constant, in blue in Fig 4.16a. Meanwhile, the methane mixing ratio and burden are changing very rapidly to reach a new equilibrium, by around 2030. The OH concentration is determined by the methane mixing ratio and burden, which are decoupled from the

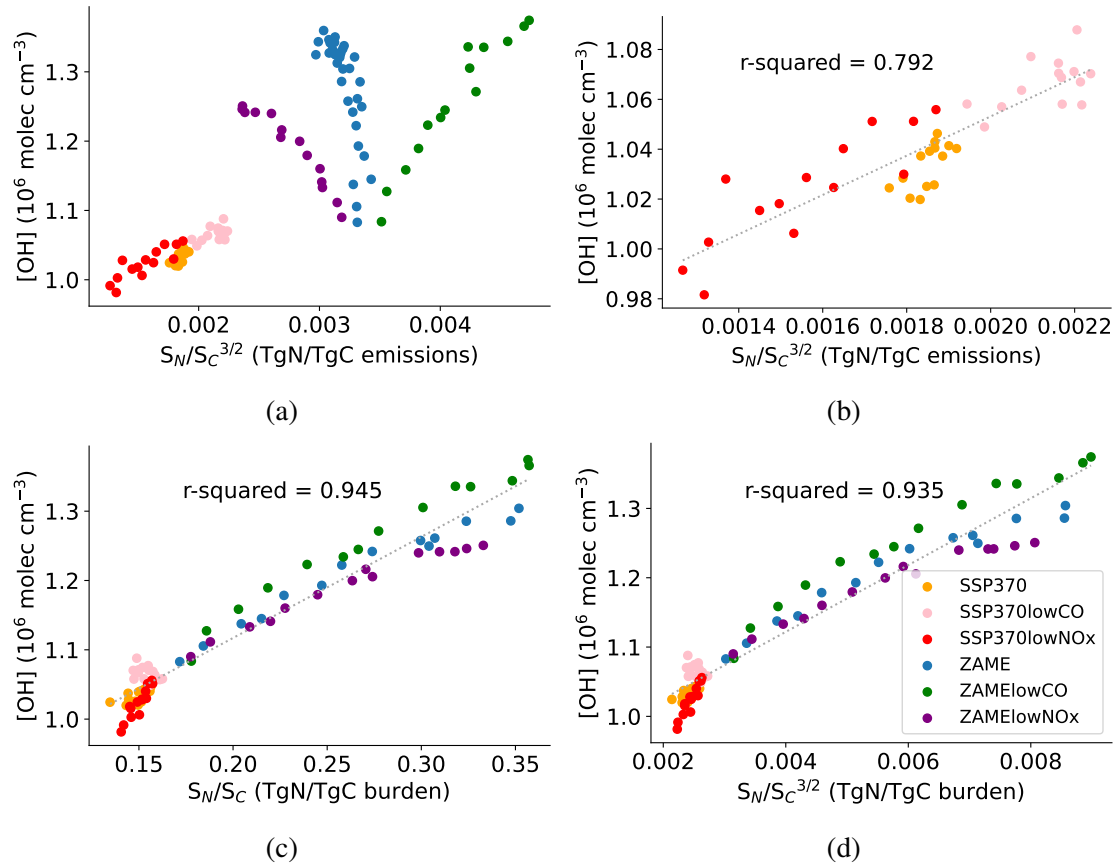


Figure 4.16: Relationship between the tropospheric mean OH concentration and the sources of NO_x , CO and methane. Each dot represents one year (annual average). Using $[\text{OH}] \propto S_N/S_C^{3/2}$ calculated using emissions, for (a) all experiments and (b) SSP3-7.0 methane experiments. Using S_N and S_C calculated as burdens for (c) $[\text{OH}] \propto S_N/S_C$ and (d) $[\text{OH}] \propto S_N/S_C^{3/2}$.

emissions, due to the large perturbation to the system in 2015. Methane is the greatest driver in OH concentration in the ZAME experiments, especially in the first 12 years, when burden decreases by 44%. After a time, (post 2030 onwards) the ZAME scenarios would reach a new equilibrium where the emissions do reflect the burden, and the resulting relationship between OH and $S_N/S_C^{3/2}$ would likely be similar to that in Fig 4.16b.

Using the burden ratio better represents the OH response to CO, CH₄ and NO_x changes in all experiments (see Fig 4.16c). The use of burdens instead of emissions allows for the inclusion of the methane effect on OH in the ZAME-based scenarios. The linear relationship from Dalsøren et al. (2016) (S_N/S_C) was used and compared against the more heavily carbon-emission-weighted relationship from Wang et al. (1998) ($S_N/S_C^{3/2}$). Both show good agreement when calculated using the burden, and the linear relationship performs slightly better (see Fig 4.16c, d).

While the Wang et al. (1998) relationship holds well for small changes in concentration (and emissions), it breaks down when the emissions and burden are not strongly correlated - i.e. when the system is perturbed far away from steady state. The burden relationship is more universally applicable to large emissions changes including methane. Both are extended here to include methane. This improvement is necessary for any scenarios where methane emissions change - which is nearly all CMIP6 scenarios.

4.6 Summary

My aim in this chapter was to better understand the coupling between CO, NO_x, methane and OH, and in particular to explain the changes in NO_x resulting from the zero anthropogenic methane emissions experiments in Chapter 3.

I found that decreasing methane emissions and therefore concentrations affects both the NO/NO₂ ratio and the total NO_x burden. With lower methane emissions, the NO/NO₂ ratio increases, due to less NO being converted to NO₂. This occurs via NO reacting with ozone, HO₂ and MeOO, which all decrease in the low-methane scenario.

The source for NO_x is consistent between the low and high methane scenarios considered here, so the changes in NO_x burden are related to the partitioning of NO_x into reservoirs, and its removal from the atmosphere via sinks. In the low methane scenario, less of the total nitrogen species are in reservoirs - more of NO_y is present as NO_x .

OH in UKESM1-ems responded to changes in NO_x and CO emissions as expected from the literature (e.g. John et al. (2012), Naik et al. (2013), and Stevenson et al. (2020)). CO mitigation acts to increase the amount of OH due to a reduction in the CO + OH sink. NO_x mitigation acts to decrease the amount of OH due to a decrease in tropospheric ozone, decreasing primary OH production, and through a decrease in radical recycling. The CO impacts are zonally uniform, with OH increasing globally, whereas the NO_x impacts on OH are located more in the northern hemisphere. This is consistent with the sources and lifetimes of CO and NO_x , where CO is well-mixed throughout the troposphere and NO_x concentrations are much higher closer to sources.

The derived relationship between OH and the CO to NO_x emissions ratio from Wang et al. (1998) was found to work well in the SSP3-7.0 scenario, where the changes in methane were moderate and the system was close to steady state. These are the conditions under which the relationship was derived. The ZAME scenario has very large changes in methane emissions and the system is perturbed far from equilibrium, so a relationship based on CO, methane and NO_x burdens (rather than emissions) was found to be more widely applicable. The burden relationship may also be more widely applicable across different models - where the emissions inputs for CO and NO_x are the same but they find different OH concentrations due to different chemistry schemes and NO_x lifetimes. The burden method is also likely to be more applicable over longer time periods, e.g. during large transitions in methane seen throughout the Holocene (Rubino et al. 2019; Rhodes et al. 2013).

Chapter 5

Modelling the Global Methane Pledge

Abstract

The Global Methane Pledge (GMP) was launched as part of COP26, with the aim of reducing global anthropogenic methane emissions by 30% by 2030, compared to 2020 levels. However, no exact policy was prescribed for how this would be achieved. UKESM1-ems was used to model a novel GMP scenario, using the new ability to change emissions and their spatial distribution. In this scenario, countries who signed up to the GMP undergo large methane emissions reductions, whilst non-GMP country emissions continue in line with current legislation. This scenario is used to quantify the potential temperature benefit from achieving the GMP, and investigate the drivers behind the ozone changes following methane mitigation. I also explore whether countries that reduce their methane emissions see local benefits through air quality improvements.

By 2040, the global mean surface methane mixing ratio decreases by 13% compared to 2020. This decrease is globally non-uniform, with greater decreases over countries where the methane emissions decrease. Ozone also decreases globally, leading to global air quality benefits and a reduction in ozone-related deaths (by 130 [-40-310] 000 deaths per year in 2049). Greater ozone benefits are seen in regions where methane emissions decrease, showing a local benefit to methane mitigation. UKESM1-ems does not show a significant decrease in global mean surface temperature in the GMP scenario; any signal from this methane perturbation is within the expected climate variability. Overall, following a trajectory in line with the Global Methane Pledge scenario would provide local air quality benefits in countries who reduce their methane emissions, but the likelihood of achieving and observing the quoted (in the GMP) 0.2°C temperature reduction remains unclear.

5.1 Introduction

The Global Methane Pledge was launched at COP26 in November 2021. Countries who sign up “agree to take voluntary actions to contribute to a collective effort to reduce global methane emissions at least 30 percent from 2020 levels by 2030” (globalmethanepledge.org). As of June 2023, 150 countries have signed up to the Pledge, covering around 50% of global anthropogenic methane emissions.

The 2021 Global Methane Assessment (Shindell et al. 2021) focused on the methane abatement potential in 2030, and was key in establishing the goals of the Global Methane Pledge. Shindell et al. (2021) collated results from several previous studies (Höglund-Isaksson et al. 2020; Harmsen et al. 2019; US EPA 2019; IEA 2020) and showed that ~ 125 Tg per year (30%) of anthropogenic methane emissions could be abated through existing methane-targeted control measures in the decade 2020-2030. Of these measures, 101 Tg/yr cost less than their estimated societal benefits (Shindell et al. 2021). These benefits include reduction in lost work hours due to heat exposure, and reduced ozone exposure leading to a decrease in Accident & Emergency (A&E) visits, hospitalization, and crop losses. Shindell et al. (2021) also estimated that behavioural changes, including reducing food loss and waste, shifting to healthier diets and improving livestock management could abate an additional 65-80 Tg/yr.

The short timescale and 2030 target was chosen since reducing methane emissions “is regarded as the single most effective strategy to reduce global warming in the near-term” (European Commission 2021). The main purpose of the Pledge so far has been to catalyse action around methane mitigation; there are currently no binding terms or reporting tasks directly associated with the Pledge. The Paris Agreement includes reporting of Nationally Determined Contributions (NDCs): a self defined climate pledge from each country, reported every five years, with a requirement for increasing ambition each round (UNFCCC 2015). Some countries cover methane under the umbrella of all greenhouse gases, and more are adding methane explicitly to their targets due to pressure from the Global Methane Pledge.

There are large variations in national targets for methane and the capability of different countries to reduce their methane emissions. For example, Canada has set a target of reducing emissions from the oil and gas sector by 75% by 2030, compared to 2012 values (Environment and Climate Change Canada, 2022). This is in line with the International Energy Agency's Net Zero roadmap for methane emissions from fossil fuels (75% decrease between 2020 and 2030, IEA (2021)). Many other countries have emissions dominated by harder-to-mitigate sectors such as agriculture (Harmsen et al. 2020), or don't have specific methane emissions goals.

The goal of reducing methane emissions in line with the Global Methane Pledge is to keep the Paris 1.5°C of warming target within reach. The GMP press release claimed that at least 0.2°C of warming could be eliminated by 2050 through its proposed emissions reductions (European Commission 2021). However, it is unclear where this temperature estimate comes from. Shindell et al. (2021) estimated a temperature reduction of 0.15°C in 2040-2070, and 0.2°C of avoided warming in 2070-2100, following a 30% methane mixing ratio reduction (slightly lower than the GMP ambition). They used absolute global temperature potentials: a calculation of the global mean temperature change per kilogram of emission based on an impulse-response function for the climate system from CMIP5 (UNEP / WMO 2011). While this is a useful initial estimate, simulating emissions reductions in a chemistry-climate model gives a fuller picture of the climate response.

Forster et al. (2023) simulated the temperature impacts resulting from 30, 40 and 50% reductions in methane emissions using the FaIR climate emulator. They found that 30% reductions lead to 0.12 (0.08-0.17)°C less warming by 2100, and to get to the predicted temperature impact of 0.2°C, emissions reductions of 50% are necessary. They also performed experiments that combined methane mitigation with coal phase-out and found a large combined impact. Some measures that tackle methane would also reduce carbon dioxide emissions (Nisbet et al. 2020), so these are likely to be conservative temperature estimates, since CO₂ reductions were not included (Forster et al. 2023). The FaIR model used was based on the UKESM1-conc model, parameterised by several equations representing the gas cycle, radiative forcing and climate response. It is a simple climate model calibrated to provide similar results to chemistry-climate models (but much faster

and with lower computational expense), and provides global average results. One limitation is that analysis of zonal or regional effects is not possible using FaIR.

Here, we build on these estimates by simulating the Global Methane Pledge in a fully coupled chemistry-climate model, driven by methane emissions directly, not with a lower boundary condition (LBC). From the ZAME experiments we saw that the methane concentration dropped faster than expected given the methane perturbation lifetime. Therefore, the use of an emissions-driven model is informative in predicting the decreases in methane concentration following mitigation, and from that the temperature impact of these measures.

Reducing methane emissions has benefits beyond temperature decreases: in particular, reductions in tropospheric ozone concentrations and exposure. According to Shindell et al. (2021) and Fiore et al. (2008), the impact of methane emissions is virtually the same regardless of location of emissions; ozone produced from methane oxidation is expected to be independent of the location of the methane emissions. In an experiment where methane emissions over Asia were reduced to zero, Fiore et al. (2008) found that the global response in ozone in all other regions was similar to the equivalent global reduction in methane. However, there were also much larger ozone decreases in the source region. Using UKESM1-ems, it is possible to change the methane emissions in different regions and examine the impacts on methane concentration, ozone concentration, climate, and other metrics. UKESM1-ems enables an estimation of whether countries that sign up to the Pledge will benefit more - through air quality improvements - than those who don't.

In this chapter I estimate the impact of regional emissions reductions in line with a Global Methane Pledge scenario. Chapter 3 included a very large (and unrealistic) perturbation in methane emissions, as an initial experiment to attribute the role of anthropogenic methane. A trajectory following the Global Methane Pledge is much less extreme (in terms of feasibility with respect to current technologies) - but still has a large impact on atmospheric composition. I will test whether the stated 0.2°C temperature impact is achieved - it is unclear whether this perturbation will be enough to show a significant temperature signal in UKESM1-ems (which as shown in Chapter 3, displays a reasonable amount of internal climate variability). While methane emissions

reductions lead to a decrease in the global background methane concentration, do localised emissions decreases lead to local decreases in the methane concentration? And does this extend to further benefits, such as reductions in local ozone concentrations and mortality? This was not possible with previous model configurations due to the LBC, and offline calculation of the methane concentrations from the methane emissions.

5.2 Experiment setup

The SSP2-4.5 scenario is used as the basis for the experiments in this chapter, representative of a realistic future climate pathway. Of all the CMIP6 scenarios, SSP2-4.5 is the closest to the current global emissions trajectory, according to UNFCCC (2021). This was estimated by comparing SSP emissions with the latest Nationally Determined Contributions from all countries, for all greenhouse gases. SSP2-4.5 is a middle of the road scenario, with moderate forcing by the end of the century: lower than the SSP3-7.0 scenario used as a baseline in Chapters 3 and 4 (Gidden et al. 2019; Fricko et al. 2017).

While SSP2-4.5 is a good approximation and baseline for a future climate trajectory (in terms of CO₂), there are more up to date methane emissions inventories available. The methane emissions in the ECLIPSEv6b inventory are based on region-specific estimates from 40 source sectors, using the GAINS model (Höglund-Isaksson 2012; Amann et al. 2011). ECLIPSEv6b was updated in 2019, and takes into account current air pollution policies, to create a current legislation scenario up to 2050. CMIP6 historical emissions only go up to 2014, and from 2015 onwards are based on a range of possible future scenarios, one of which is SSP2-4.5. Anthropogenic methane emissions in SSP2-4.5 increase by 3% between 2015 and 2030 and then start to decline (Riahi et al. 2017; Gidden et al. 2019). This isn't consistent with current policies - emissions in ECLIPSE continue to increase up to 2050 and beyond (see Fig 5.1a, orange vs dashed grey line). Therefore, in order to get more up to date historical (2015-2019) methane emissions, and a future trajectory based on real-world policies, I substituted anthropogenic methane emissions from the ECLIPSEv6b inventory into the SSP2-4.5 scenario (IIASA 2019).

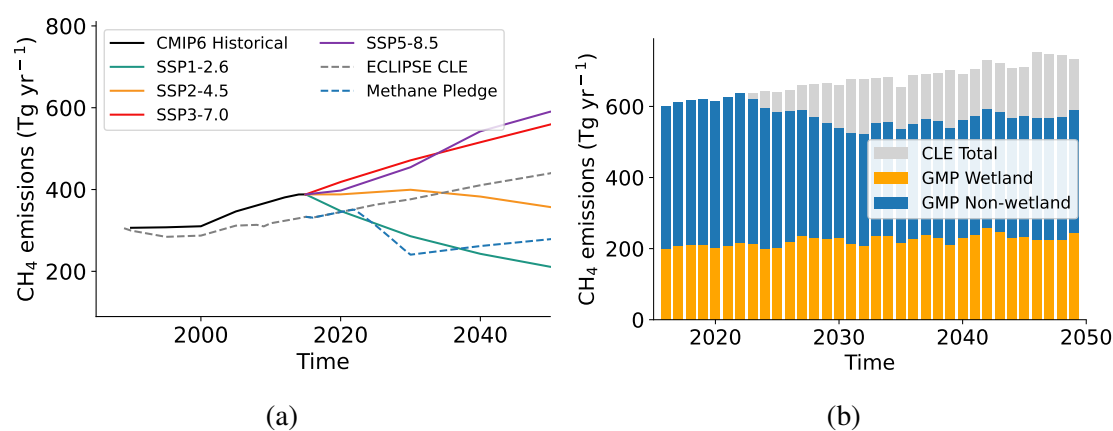


Figure 5.1: (a) Anthropogenic methane emissions from 1990 to 2050 from CMIP6 experiments (for the SSP scenarios) and from the ECLIPSE inventory (grey dashed line). The emissions used for the GMP scenario are shown in the blue dashed line. (b) Model methane emissions for the CLE (grey) and GMP experiments (online wetland emissions in orange, non-wetland emissions in blue).

The historical ECLIPSEv6b methane emissions are lower than the CMIP6 emissions (approximately 15% lower by 2015, see Fig 5.1a). This is likely to increase the anomaly in the methane concentration simulated by UKESM1-ems compared to the observations, as discussed in Chapter 2. However, these methane emissions are more representative of the current best estimate, in terms of magnitude and spatial resolution. In summary, the baseline used in these experiments is the CMIP6 SSP2-4.5 scenario with ECLIPSEv6b methane emissions, with all other emissions following the SSP2-4.5 trajectory, hereafter referred to as CLE (current legislation scenario).

Initial tests included running the CLE scenario directly from the CMIP6 historical run (with methane emissions following the black line in Fig 5.1a up to 2014, grey dotted line from 2015). This step change in methane emissions caused a decrease in the methane surface mixing ratio from 2015 up to 2020, when the mixing ratio started to increase again. Therefore, a spin-up experiment was necessary to get the system into a more steady state, before starting the CLE run from 2015.

To produce a model configuration suitable for these experiments, a perpetual 2014 timeslice spin-up experiment with ECLIPSE methane emissions was run for 10 years. After 10 years, the methane lifetime was stabilised, and the methane concentrations

and burden had reached the minimum values from the non-spun-up run. There is currently still some uncertainty about how long UKESM1-ems takes to spin up, due to the online methane wetland emissions. A fully spun-up 2014 timeslice would also not be representative of the methane state in 2014, since the atmosphere is not in steady-state. An optimal solution would have been a historical simulation from 1990 to 2014 with the ECLIPSE emissions, with CLE continuing directly from the end of it. However, this would have involved a more complex model setup, and more computer time and expense: a 25 year experiment takes around 3 weeks of model runtime, not including setup, fixing errors, and machine problems, which would likely extend the overall experiment time to months. The end of the 10 year timeslice was determined to be a satisfactory starting point for the CLE and GMP runs. Overall, this was a solution to requiring a lower initial methane concentration. Analysis in this chapter focuses on 2020 onwards, so the first 5 years of the experiments following on from the timeslice also provided a buffer for the methane concentrations to stabilise. In hindsight, a better approach would have been to harmonise the ECLIPSE emissions to the CEDS emissions to avoid the need for spin-up simulations.

UKESM1-ems provides an opportunity, for the first time in a fully-coupled Earth system model, to change methane emissions directly and at any given location, rather than perturbing the global emissions or mixing ratio. This enabled me to use different emissions trajectories for Pledge and non-Pledge countries, to make an overall Global Methane Pledge scenario. In this scenario I assume that the non-Pledge countries follow the current legislation (CLE) baseline for methane emissions. This is likely a conservative estimate, as some countries, for example China, have their own methane reduction targets, but are not officially part of the Pledge.

The Pledge countries undertake large methane emissions reductions; in order to bring the global methane emissions down by 30% (compared to 2020), the emissions reduction required by the Pledge countries in 2030 is 63% (relative to CLE). In this scenario, the emissions in Pledge countries decrease linearly from 2023 to 2030, and then stay at the same percentage reduction below the baseline up to 2050. This is a simple idealised trajectory (consistent with (Forster et al. 2023)). See Table 5.1 for a summary of the scenarios and emissions used in this section. Fig 5.1a shows the global methane

emissions trajectory for the Pledge scenario compared to other scenarios. Compared to SSP1-2.6, the scenario with the most mitigation in CMIP6, the methane pledge scenario reductions are similar in scale, but happen on a shorter timescale, and also don't continue after 2030.

The map plots in Fig 5.2 show the spatial distribution of the emissions reductions. Panel (a) shows the methane emissions in 2020, which are the baseline for the emission reduction. Panels (b) and (c) show the change in emissions in the 2030 Global Methane Pledge scenario compared to 2020, in absolute and percentage changes respectively. This shows that in non-Pledge countries, the methane emissions continue to increase up to 2030. Panel (d) shows the percentage reduction in emissions in 2030 compared to the 2030 baseline, i.e. the amount of mitigation required in 2030. This shows which countries are included more clearly: the non-Pledge countries, with no mitigation, are in white. A full list of countries without any mitigation in the GMP scenario can be found in the appendix Table A.1, corresponding to the countries not signed up to the Global Methane Pledge at the time of the experiments.

Scenario	Methane Emissions		
	Global	GMP countries	non-GMP countries
Current legislation (CLE)	ECLIPSE CLE	ECLIPSE CLE	ECLIPSE CLE
Global Methane Pledge (GMP)	30% reduction	63% reduction	ECLIPSE CLE

Table 5.1: Methane pledge experiments and associated methane emissions. Percentage reductions in emissions are by 2030, relative to 2020 values. For the Global Methane Pledge countries, the 63% reduction is sustained from 2030 to 2050.

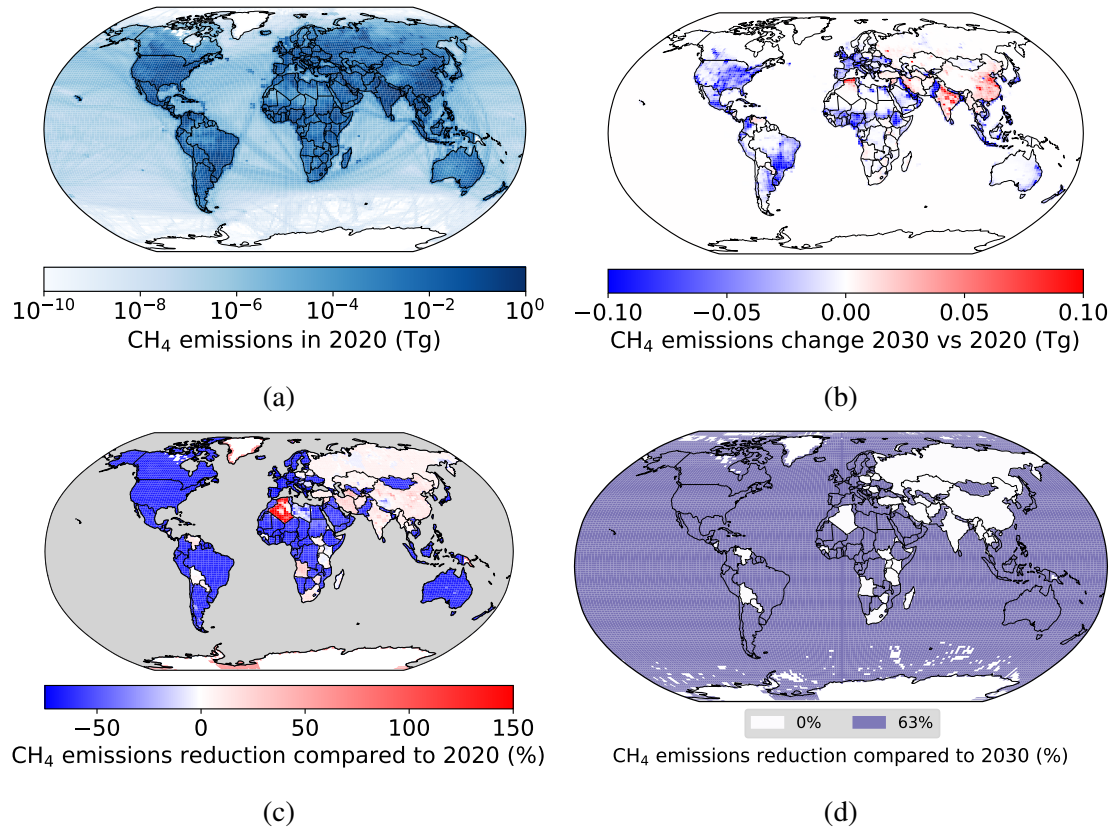


Figure 5.2: Methane emissions in the Global Methane Pledge (GMP) scenario (a) GMP emissions in 2020 (Tg per gridbox), (b) absolute emissions change between 2020 and 2030 (Tg per gridbox, where red = increased emissions), (c) emissions in 2030 as a percentage of 2020 emissions. (d) GMP emissions in 2030 as a percentage of 2030 CLE emissions.

5.3 Atmospheric composition response

Methane mitigation in the Global Methane Pledge scenario leads to widespread impacts on atmospheric composition. In this section I present the results showing changes in methane mixing ratio, OH and ozone, and their spatial distribution. I also explore the production and loss terms for ozone to gain a better understanding of the drivers behind the ozone changes in the GMP scenario.

Following the decrease in methane emissions from 2023 onwards, the global mean surface methane mixing ratio decreases from 2023 up to 2040, then stabilises at 1424 ± 6 ppb (10 year average, see Fig 5.3a). The methane lifetime is between 7-8 years (mainly

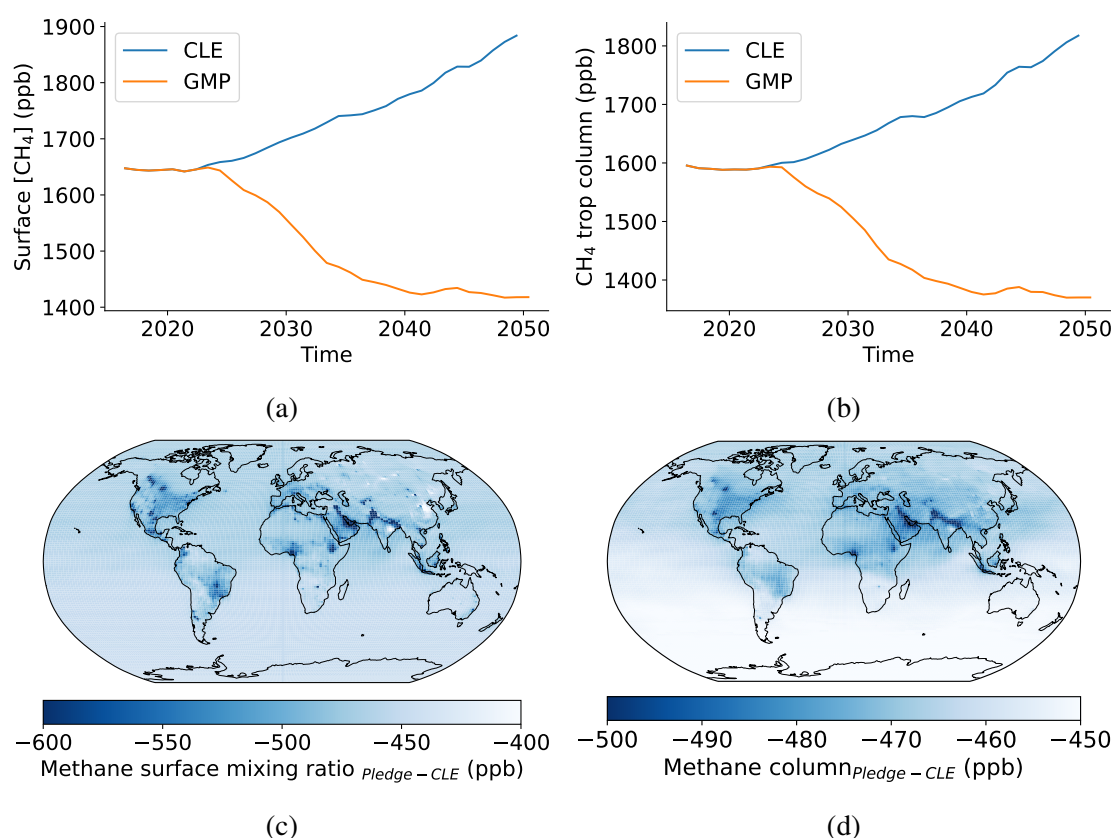


Figure 5.3: Methane response in the Global Methane Pledge (GMP) scenario (a) surface mixing ratio, (b) tropospheric methane column (c) GMP - CLE difference in methane mixing ratio in 2049 (d) GMP - CLE tropospheric average column difference in 2049 .

determined by the sink via OH, Fig 5.4a), so the mixing ratio continues to decrease for a few years after the emissions stabilised (in 2030). Overall, there is a 13% decrease in methane surface mixing ratio compared to 2020. Fig 5.3 also shows the global distributions of surface mixing ratio and tropospheric mean methane column. These are representative of what could be measured using on the ground *in situ* instruments and satellites respectively. The background (60-90°S, 2040-2050 average) tropospheric methane column is 1378 ± 6 ppb, a 13% decrease compared to 2020, or a 22% decrease compared to the 2040-2050 counterfactual scenario.

While methane levels decrease globally, there are regions where the methane concentration decreases by more than the background decrease. Here I define the background decrease as the mean change in methane mixing ratio far away from methane sources, between 60°S-90°S. These larger decreases occur in the northern hemisphere and over land, corresponding to methane source areas - and therefore emissions reductions in this scenario. Country-specific analysis shows that of the top 50 countries with the highest decrease in methane surface mixing ratio, only one is not a GMP member. In the top 100, 87% are part of the Global Methane Pledge. This shows that, while methane levels decrease globally, local methane concentrations also go down by more than the background decrease - with an average $27 \pm 3\%$ decrease in the top 50 countries compared to the CLE scenario. Methane affects air quality through the production of ozone, which is an air pollutant. Since methane decreases globally in the GMP, there are likely to be global ozone and air quality benefits. Furthermore, the larger decline in local methane concentrations in GMP countries suggests that there could also be local air quality benefits - not just global temperature benefits - to reducing methane emissions.

As seen in Chapter 3, with methane mitigation actions and a reduction in methane mixing ratio (and therefore burden), the methane lifetime decreases (Fig 5.4a). In 2045-2050, the GMP methane lifetime is $\sim 7\%$ lower than in the CLE scenario. In this way, there is a double benefit from methane mitigation: a reduction in the methane mixing ratio ($22 \pm 1\%$ lower than CLE), and a decreased residence time for methane in the atmosphere, both of which contribute to reducing the overall warming effect from methane.

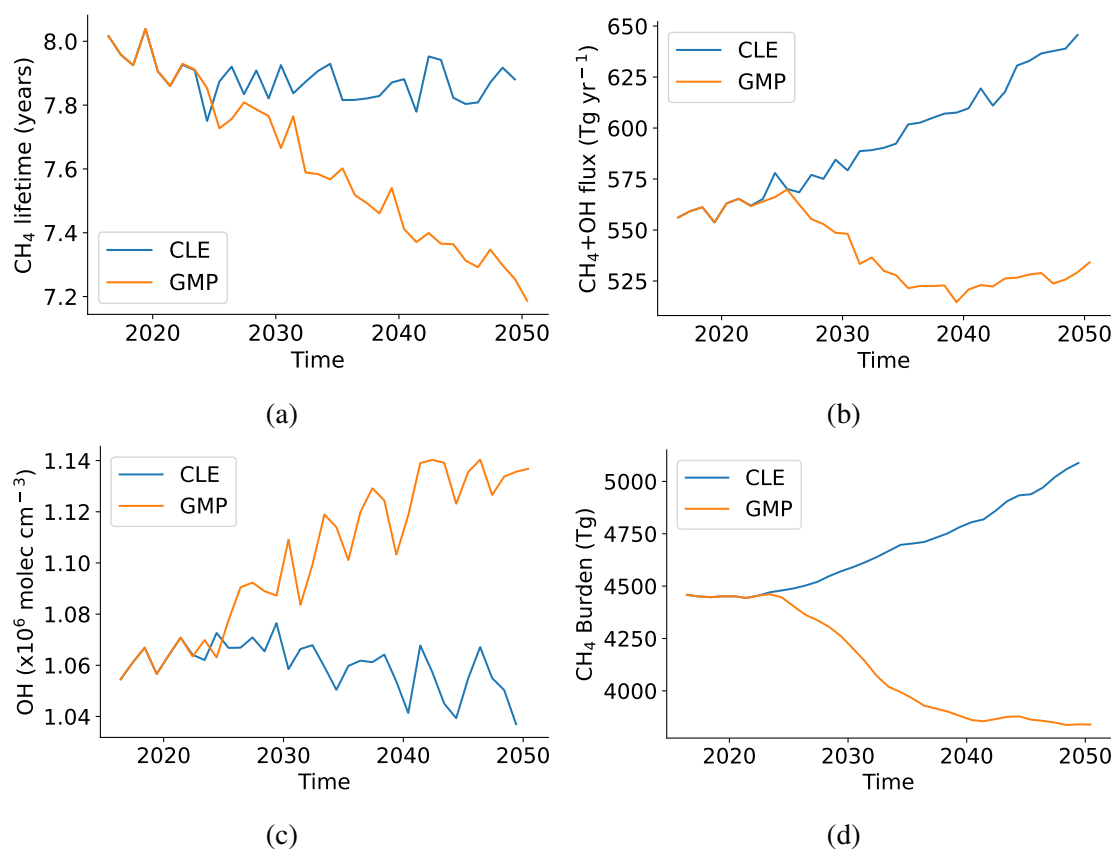


Figure 5.4: Atmospheric composition changes over time for the current legislation scenario (CLE, blue) and the Global Methane Pledge scenario (GMP, orange) (a) methane lifetime, defined as the whole atmosphere methane burden divided by the tropospheric $\text{CH}_4 + \text{OH}$ flux, (b) flux through the $\text{CH}_4 + \text{OH}$ reaction (c) tropospheric mean OH concentration, (d) whole atmosphere methane burden.

Fig 5.4a shows the methane lifetime response. In the current legislation scenario the methane lifetime shows interannual variability, but stays at a similar level, with an average of 7.88 ± 0.06 years (1σ) over the whole time period. In this scenario, the methane burden increases over time, but the $\text{CH}_4 + \text{OH}$ flux also increases correspondingly, leading to a near-constant methane lifetime (and OH concentration). In the GMP scenario, the methane lifetime decreases to 7.28 ± 0.05 years by 2045-2050. Methane burden, OH concentration and $\text{CH}_4 + \text{OH}$ flux all contribute to the methane lifetime. Fig 5.4 shows that the lifetime decrease is a combination of decreased methane burden, and increased OH concentration, which overall leads to a lower $\text{CH}_4 + \text{OH}$ flux (since the burden change is dominant). The flux decreases ($\sim 17\%$) by less than the burden decrease ($\sim 23\%$), and since the lifetime is the whole atmosphere burden divided by the tropospheric flux through the $\text{CH}_4 + \text{OH}$ reaction, the overall effect is a decrease in methane lifetime. By 2050, the methane lifetime hasn't stabilised, likely due to the increasing $\text{CH}_4 + \text{OH}$ flux.

The evolution of methane concentration, burden and lifetime depends on emissions and chemistry in the atmosphere, and is less dependent on climate variability. Therefore, when running multiple ensemble members for a single scenario, these quantities have a very low ensemble member spread. For example, in Fig 3.1b, where the three ensemble members for SSP3-7.0 and ZAME are plotted, they are indistinguishable from the multi-ensemble mean for most of the time series. In the GMP experiment, the emissions perturbation causes large changes in methane, so the difference between GMP and CLE experiments is much greater than the expected ensemble member range (13 ppb in ZAME, 19 ppb in SSP3-7.0). Therefore, when modelling the methane response to such an emissions perturbation, the lack of extra ensemble members is not a limitation.

The modelled OH and ozone concentrations show a slightly larger interannual variability and ensemble member spread, since they are more affected by climate variability. The GMP methane emissions decrease has a significant effect on both OH and ozone, outside of the expected ensemble member spread. However, the significance of the regional differences in ozone and OH is harder to diagnose without more ensemble members (Fig 5.5e, 5.6b).

5.3.1 Ozone response

The ozone response in the Global Methane Pledge (and CLE) scenario is shown in Fig 5.5. The global mean surface ozone concentration decreases by 1.5 ± 0.5 ppb (6%) by 2050. The benefits of methane emissions reduction on ozone are only seen later in the time period, beyond 2030. The global distribution of the difference in surface ozone concentration is shown in Fig 5.5e for the last 5 years of the experiment (2045-2049). Ozone decreases globally, except for a small area of increase over the Phillipine sea.

Fig 5.5b shows the population-weighted global mean surface ozone concentration over time. This combines surface ozone concentrations (Fig 5.5d, 5.5c) with population data from SSP2 (Fricko et al. 2017), to give an indication of the population exposure to ozone over time. In CLE, the population-weighted ozone increases over time, likely due to increasing population in high ozone areas, as seen in SSP3-7.0 in Chapter 3 (Fig 3.2d). In GMP, the population-weighted ozone concentration decreases after 2020, so there are likely to be public health benefits linked to lower ozone exposure. These are discussed further in section 5.4.

Previous studies have suggested that methane emissions reductions act on a globally uniform scale, such that there is no difference in response based on where the emissions are reduced (Fiore et al. 2009; Shindell et al. 2021). In an LBC model, this is the default assumption, since the methane concentrations decrease globally. Here, the large differences in the methane concentration in different regions (see Fig 5.3) are likely to have an impact on tropospheric ozone production locally, depending on the local VOC and NO_x regimes (Archibald et al. 2020b; Monks et al. 2015).

The country-averaged surface ozone concentration decreases in all countries considered (110 countries, naturalearthdata.com). In the top 20 and 50 countries with the highest ozone concentrations in the CLE and GMP scenarios, a similar number are GMP members vs non-members (8/7 and 14/18 respectively in the top 20 and 50): countries with the highest ozone in the CLE scenario remain the countries with the highest ozone in the GMP scenario. However, when looking at the ozone differences, being a Global Methane Pledge member does have local benefits. Of the top 20 and 50 countries with the highest (absolute and percentage) differences in surface mean ozone concentration,

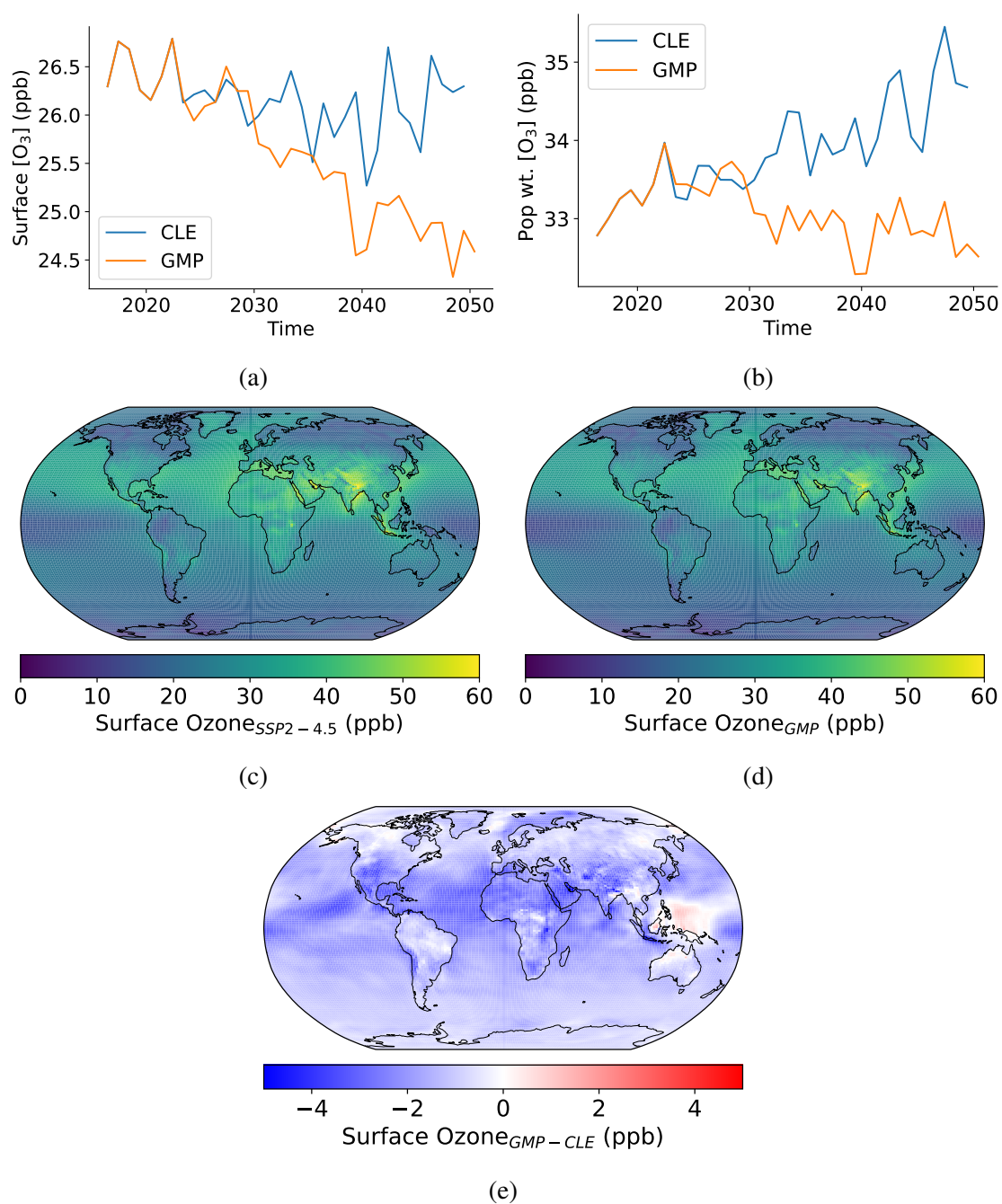


Figure 5.5: Ozone response in the Global Methane Pledge (GMP) scenario (a,b) ozone (area-weighted and population-weighted) surface mixing ratio (c) CLE average surface ozone mixing ratio for 2045-2049 (d) GMP average surface ozone mixing ratio for 2045-2049 (e) GMP - CLE average ozone surface mixing ratio difference for 2045-2049.

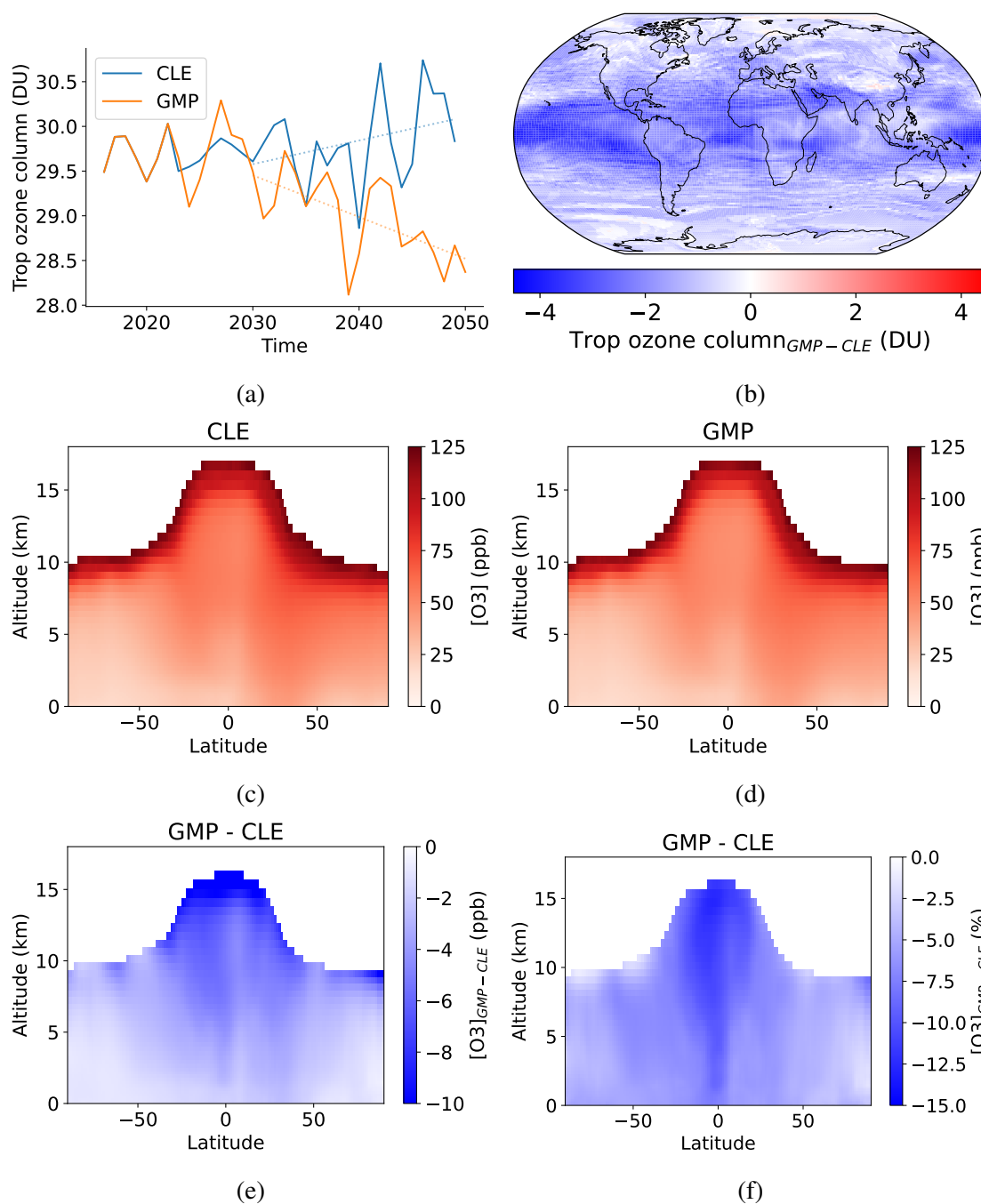


Figure 5.6: Tropospheric ozone column and zonal means in the GMP and CLE scenarios. (a) Global mean tropospheric column ozone (DU) (b) GMP - CLE column ozone average difference in 2045-2049, global distribution (c, d) CLE and GMP zonal mean ozone mixing ratios (e,f) GMP - CLE zonal mean ozone difference in ppb and as a percentage.

80% are GMP members. Table 5.2 shows the countries with the highest ozone in the GMP and CLE scenarios, and those with the greatest ozone decrease following the GMP scenario, with GMP member countries in blue.

Countries with the highest surface mean $[O_3]$ in the GMP and CLE scenarios	Countries with the largest $[O_3]_{GMP-CLE}$ for 2045-2050
Bhutan	Israel
Nepal	Bahamas
Bangladesh	Kuwait
Afghanistan	Jordan
India	Suriname
Iran	UAE
Qatar	Saudi Arabia
Saudi Arabia	Egypt
Sudan	Kyrgyzstan
UAE	Ghana

Table 5.2: Left: countries with the highest ozone concentrations in the CLE and GMP scenarios. Right: Countries with the largest decrease in surface mean ozone concentration in the GMP scenario compared to the CLE scenario in 2045-2049, in ppb and percentage terms. Countries signed up to the Global Methane Pledge at the time of writing are in blue.

Ozone decreases throughout the troposphere: the tropospheric ozone column is shown in Fig 5.6a. Figs 5.6b-f show the distribution of ozone in the troposphere, and the ozone differences between the CLE and GMP scenarios. The zonal mean plots (Figs 5.6c-f) show the longitudinally-averaged ozone mixing ratios, as a function of latitude and altitude. These plots and the global distribution show that ozone decreases most in the tropics, particularly in the tropopause region and extending down to the surface at the equator. This ozone decrease is a balance between the different production and loss terms which make up the ozone budget. Methane decreases affect many different parts of the ozone budget, and these are discussed in the next section.

5.3.2 Reaction fluxes

Looking at the reaction fluxes of production and loss of ozone, as well as related reactions, can help to diagnose the underlying cause for the decrease in ozone in the GMP scenario. The production and loss of ozone in the troposphere can be estimated from the approximate $P(O_3)$ and $L(O_3)$ expressions below (Seinfeld et al. 2016). The $P(O_3)$ reactions lead to ozone production via formation of an NO_2 molecule, which is photolysed to produce ozone.

$$P(O_3) = k_{HO_2+NO}[HO_2][NO] + k_{MeOO+NO}[MeOO][NO] \quad (5.1)$$

$$L(O_3) = k_{O^1D+H_2O}[O^1D][H_2O] + k_{HO_2+O_3}[HO_2][O_3] \quad (5.2)$$

Methane oxidation leads to ozone production (Archibald et al. 2020b; Monks et al. 2015) - the first reaction in this sequence is the $CH_4 + OH$ reaction (1.4). The methyl radical produced via the first oxidation reaction goes on to form a methyl peroxy radical, MeOO, via reaction with molecular oxygen. The reaction of MeOO with NO forms a methoxy radical (CH_3O), and NO_2 . Therefore, the reaction $MeOO + NO$ is a key step in the formation of ozone from methane. Another important reaction for tropospheric ozone production is $HO_2 + NO \longrightarrow OH + NO_2$. Like the $MeOO + NO$ reaction, this leads to ozone production via the formation of an NO_2 molecule.

Reducing methane emissions in line with the Global Methane Pledge likely affects all of the reactions in equations 5.1 and 5.2, through changes in ozone, peroxy radicals, NO_x and HO_x ($OH + HO_2$). Here I investigate these production and loss terms by looking at the zonal distribution of the fluxes and flux changes. My aim is to find out which reactions cause the difference between the CLE and GMP scenarios, both for the overall decrease in tropospheric ozone, and which reaction(s) are responsible for the larger decrease in ozone in the upper tropical troposphere (see Fig 5.6e,f).

The highest flux through the $CH_4 + OH$ reaction is in the tropical lower troposphere, where the methane and OH concentrations are high. The rate constant, k_{CH_4+OH} , is tem-

perature dependent, increasing at higher temperatures (Atkinson et al. 2004; Burkholder et al. 2020). Apart from the heterogeneity at the surface (see Fig 5.3c), the difference in methane mixing ratio across the troposphere is uniform, and so the percentage change in the $\text{CH}_4 + \text{OH}$ reaction flux is uniform throughout the troposphere. The largest absolute decrease is in the tropical lower troposphere, as expected due to the large initial flux there. Therefore, although the decrease in $\text{CH}_4 + \text{OH}$ flux would lead to fewer methyl (and MeOO) radicals produced, and an overall decrease in ozone production, it does not explain the ozone decrease in the mid-upper tropical troposphere.

The MeOO + NO flux in the GMP scenario is much lower than in CLE (see Fig 5.7a). The highest flux is in lower tropical troposphere, extending up into the upper troposphere (likely due to lightning NO_x). The flux difference between GMP and CLE scenarios is largest in the same area (in ppt per hour, Fig 5.7c). The percentage difference in flux is much more zonally homogenous (5.7e) - this links to methane being well-mixed and affecting the flux everywhere. Therefore, while a decrease in the MeOO + NO flux is consistent with lower ozone concentrations, the zonal region where the flux decrease occurs doesn't correspond to the location of the ozone decrease, so this doesn't explain the ozone distribution.

The $\text{HO}_2 + \text{NO}$ flux is lower in GMP than in CLE (see Fig 5.7b). This flux decrease is much less uniform than the MeOO + NO decrease: it is mainly located in the upper tropical troposphere, and extends down to the surface near the equator. The spatial distribution is very similar to that of the change in ozone between the CLE and GMP scenarios. This suggests that the $\text{HO}_2 + \text{NO}$ reaction is responsible for the larger ozone decrease in the upper tropical troposphere. HO_2 decreases in the GMP scenario (as also seen in the ZAME scenario): this is likely due to less secondary production of CO from methane, and subsequent reaction of CO with OH to form HO_2 (the main source of HO_2). Lower secondary production of CO leads to less CO and therefore a lower HO_2 concentration, despite increased OH.

There are also changes in the ozone loss fluxes (not shown). The $\text{HO}_2 + \text{O}_3$ and $\text{O}_1\text{D} + \text{H}_2\text{O}$ fluxes both decrease in the GMP, mainly in the tropical lower troposphere, which would lead to an ozone increase. The net effect of all changes in production and loss is an ozone decrease; the decreased ozone production outweighs the decreased ozone loss.

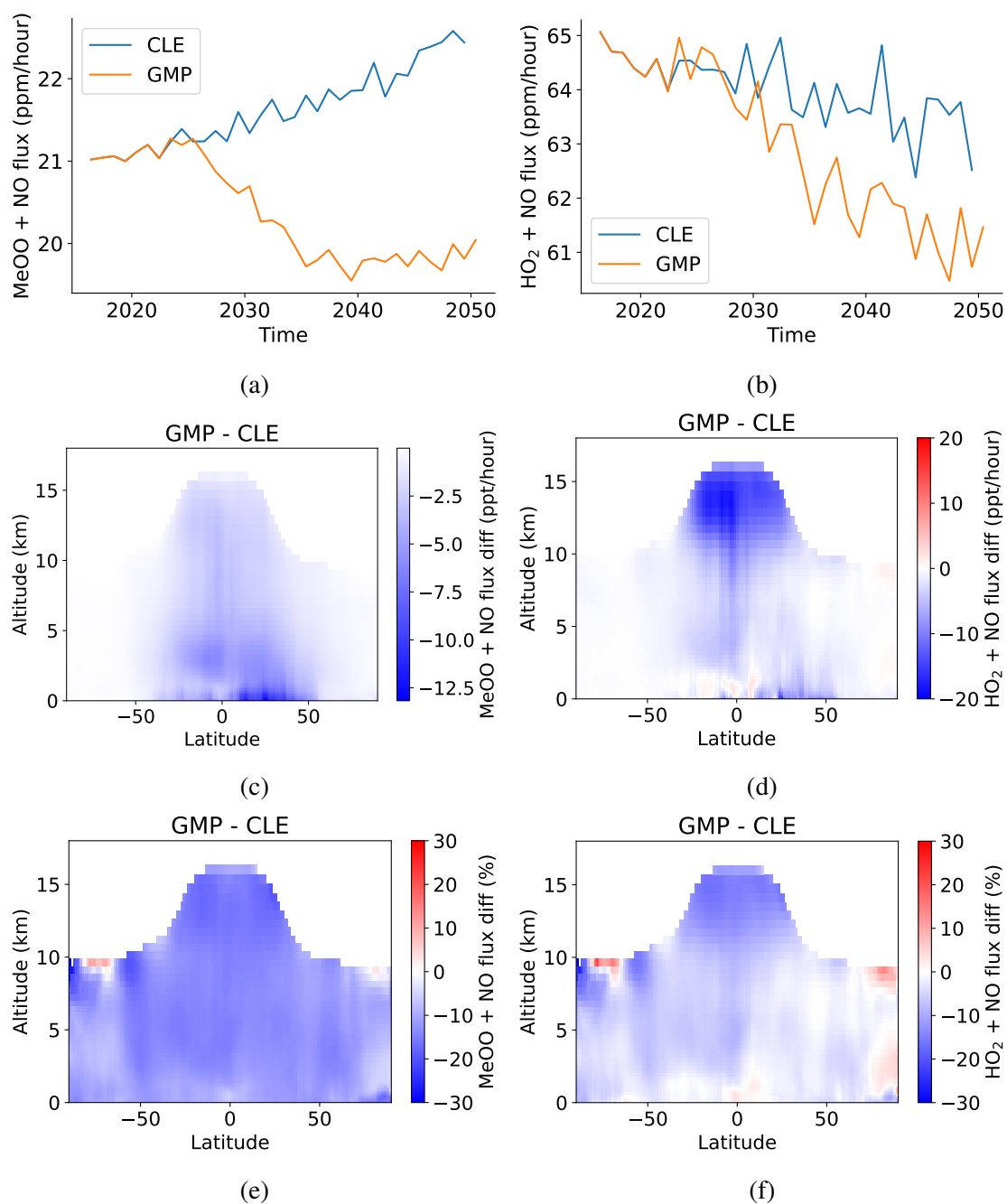


Figure 5.7: Reaction fluxes affecting tropospheric ozone production: MeOO + NO (left) and HO₂ + NO (right). (a,b) global annual mean flux, (c,d) GMP - CLE zonal mean flux difference (ppb/hour), (e,f) GMP - CLE zonal mean flux difference (%).

Overall, the decrease in ozone in the GMP scenario is a combination of changes in the ozone production and loss fluxes (Equations 5.1, 5.2). The main drivers behind the decrease are a lower MeOO + NO flux (throughout the troposphere) and a lower HO₂ + NO flux (mainly in the tropical upper troposphere).

5.4 Health impacts

The air quality impact of the ozone reductions shown in the previous section can be quantified via the calculation of the maximum daily 8 hour average (MDA8h) concentration of ozone at the surface. Here I use the same approach as in section 3.3 to look at the impact of methane changes on ozone exposure and therefore human health, by calculating long-term ozone-related mortality.

The MDA8h concentration was calculated for 2049 and is shown for the CLE and GMP scenarios in Figs 5.8a and c. The maps show the annual mean MDA8h, and so mask the seasonal variation in ozone in different locations. Figs 5.8b and d show the number of days exceeding the WHO recommended limit of 50 ppb. The highest ozone, and number of days that exceed the WHO limit are over Africa, the Middle East and Asia, with lower MDA8h ozone and days exceeding the limit in Europe and North America.

The WHO ozone limit is exceeded in most countries: around 80% have at least 5 days in 2049 where MDA8h [O₃] > 50 ppb in the CLE and GMP scenarios. Section 5.3.1 showed that the Global Methane Pledge countries see a decrease in ozone following GMP compared to CLE. This also translates to the ozone exposure. Of the top 50 countries with the largest decreases in the number of days exceeding MDA8h [O₃] = 50 ppb, 72% are GMP members.

The same method from Malley et al. (2017) was used to calculate the long-term mortality due to ozone exposure in the CLE and GMP scenarios for 2049. Using this method I estimate that the total mortality decreases by 130 [-40-310] 000 deaths per year in GMP compared to CLE (see Table 5.3). There is a large uncertainty in this estimate, which includes an increase in mortality. This is due to the high uncertainty in the mortality

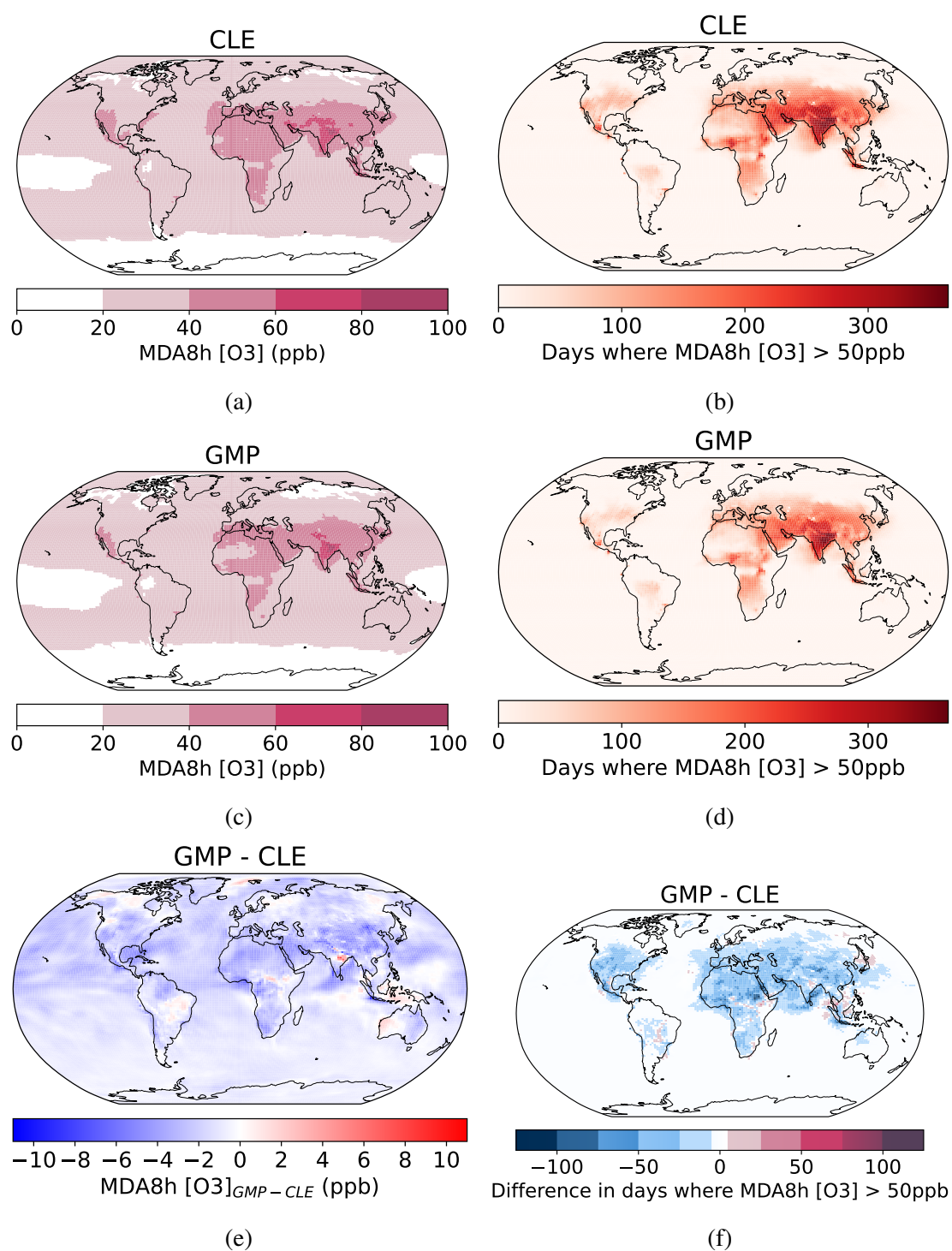


Figure 5.8: Annual mean (2049) maximum daily 8h average ozone concentration (MDA8h) for the (a) current legislation (CLE) and (c) Global Methane Pledge (GMP) scenarios. Number of days exceeding MDA8h = 50 ppb in 2049 in (b) CLE and (d) GMP scenarios. e) GMP - CLE difference in MDA8h [O3] (c - a). (f) GMP - CLE difference in number of days exceeding 50 ppb MDA8h (d - b).

rate in 2050: this depends on many unknowns such as population-health and health-care in 2050. The Global Methane Assessment (Shindell et al. 2021) estimated that a slightly smaller reduction in methane emissions (30% below 2030 values) would prevent $\sim 140,000$ ozone-related deaths per year in 2030. This is very similar to my estimate, even though they use country-specific mortality rates. In section 3.3, I estimated the maximum mortality attributable to future anthropogenic methane emissions as 690 [460-910] 000 deaths per year in 2050, with around 1300 fewer deaths per Tg mitigated. Here, the number of deaths/Tg of mitigation is lower (~ 920) because the scenario is based on SSP2-4.5, which has a smaller total population, different levels of other ozone precursors, and so a lower baseline mortality due to ozone exposure.

Scenario	Mortality due to long-term exposure in 2049 (thousands)		
	CLE	GMP	GMP - CLE
Respiratory mortality	540 [480-570]	480 [430-510]	-60 [-140-30]
Cardiovascular mortality	640 [590-690]	570 [520-600]	70 [-170-10]
Total mortality	1,180 [1,070-1260]	1,050 [950-1,110]	-130 [-310-40]

Table 5.3: Mortality related to long-term ozone exposure in the GMP and CLE scenarios, units = thousands of deaths per year. Calculated using mean, upper and lower estimates of global mortality rates.

While these are global estimates, decreasing methane emissions and therefore ozone concentrations locally (see section 5.3.1) would have benefits for local air quality, and therefore human health and agricultural productivity, as well as climate (Shindell et al. 2021). These advantages could be highlighted to motivate mitigation action in a country, potentially through more targeted studies of local impacts.

5.5 Radiative forcing and temperature response

Although there are many benefits to following a methane mitigation scenario (as discussed in the previous sections), the main motivation behind the Global Methane Pledge is limiting global temperature increase. This section explores the temperature response

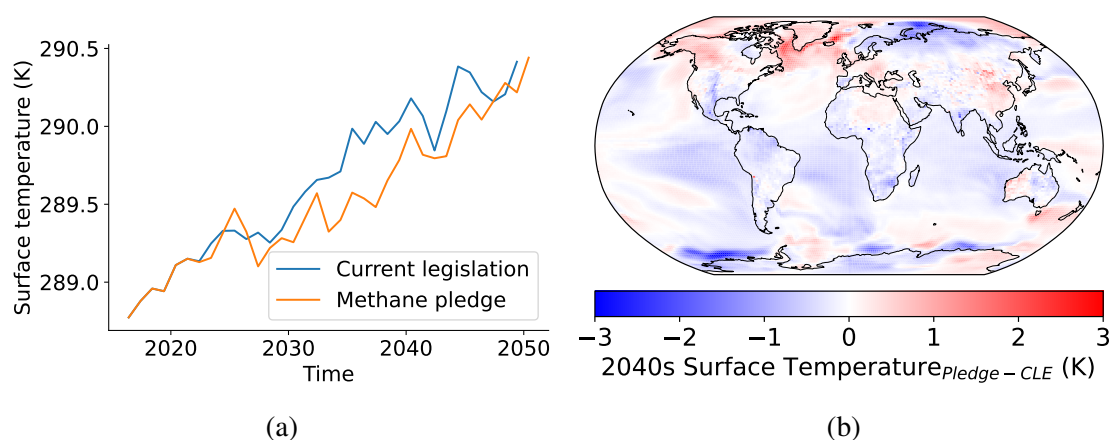


Figure 5.9: Temperature response in the Global Methane Pledge scenario. (a) global mean surface temperature (GMST) over time (b,c) GMP - CLE decadal average surface temperature difference for 2040-2049.

in the GMP scenario by looking at the global mean surface temperature change and calculating the change in radiative forcing from methane.

Fig 5.9 shows the surface temperature response in the CLE scenario and the GMP scenario. In both cases, the global mean surface temperature continues to increase over time up to 2050. For global mean surface temperature, having one ensemble member is a limitation, since the ensemble member spread in global mean surface temperature is larger than that in the atmospheric composition components such as methane and ozone.

The Global Methane Pledge quotes a temperature benefit of 0.2 degrees by 2050 from the 30% methane reductions (source unknown). Using a scenario with slightly less mitigation (30%, but with a 2030 baseline) the Global Methane Assessment estimated a temperature decrease of 0.15 degrees by 2040-2070 and 0.2 degrees from 2070-2100, calculated using Global Temperature Potentials (Shindell et al. 2021).

Here I test whether this expected temperature result would be seen in UKESM1-ems, or whether this magnitude is within the noise and interannual variability of the model. From the experiments in Chapter 3, the ensemble member range in simulated GMST is 0.23 K for SSP3-7.0 and 0.24 K for ZAME. Here, the interannual variability within one ensemble member is around 0.2 K ($2 \times \sigma$, based on a calculation of the standard

deviation from de-trended temperature data). The GMST in the CLE and GMP scenarios overlaps towards the end of the experiment, and it is not possible to calculate a significant temperature difference between these two experiments.

Based on the ensemble member temperature range in SSP3-7.0 and ZAME, and the interannual variability in CLE and GMP, it is unlikely that a significant temperature response could be simulated from the Global Methane Pledge scenario, since the temperature change from the methane perturbation is not large enough.

With three ensemble members, as in ZAME, perhaps an ensemble mean would show different temperature trends in the CLE and GMP scenarios, but the difference in temperature between the two scenarios could still be statistically insignificant. Running a large number of ensemble members would give greater confidence in the ensemble mean temperature outcomes. This is unfeasible using UKESM1-ems, but could be done using an emulator such as FaIR, which simulates the results of UKESM1-ems, and can run hundreds of scenarios in seconds (Leach et al. 2021). Emulation using FaIR is an example of the work being done at the Met Office as part of my collaboration with them on a set of Methane Pledge experiments.

In the real atmosphere, there are also many other factors and emissions changing at the same time that also affect the GMST, and so an individual signal from decreasing methane emissions would not be observable. This doesn't mean that reducing methane emissions in line with the Global Methane Pledge wouldn't have a climate-positive impact on temperature, just that it is unlikely to be observed. The success of the Pledge is likely to be measured based on emissions inventories and top-down inversion models, which look at the evolution of methane emissions over time.

5.5.1 Radiative forcing estimates

In the Global Methane Pledge scenario there is a large decrease in the methane mixing ratio and the methane burden (see Fig 5.3). Although it is difficult to quantify the direct temperature impact here (as discussed in the previous section), this methane reduction would change the radiative forcing from methane. Since this is a coupled (atmosphere-

ocean) experiment, it is not possible to calculate an ERF for methane in these scenarios. However, using a simplified expression for the radiative forcing, it is possible to estimate the radiative forcing resulting from methane and changes in methane concentration (see equation 5.3, Meinshausen et al. (2020)). This expression was used in CMIP6 and updated to include the short-wave component of methane absorption (Etminan et al. 2016; Meinshausen et al. 2020). It gives the radiative forcing from pre-industrial to present day for methane, RF_{CH_4} . $[CH_4]$ is the methane surface concentration, $[CH_4]_0$ is the pre-industrial methane concentration (taken here as 731.41 ppb), $[N_2O]$ is the nitrous oxide concentration, and a , b and d are constants (Meinshausen et al. 2020).

$$RF_{CH_4} = \left(a\sqrt{[CH_4]} + b\sqrt{[N_2O]} + d \right) \cdot \left(\sqrt{[CH_4]} - \sqrt{[CH_4]_0} \right) \quad (5.3)$$

$$\Delta T = \lambda \times RF \quad (5.4)$$

The methane radiative forcing was calculated based on the last 5 years of the CLE and GMP experiments: $0.625 \pm 0.003 \text{ W m}^{-2}$ and $0.420 \pm 0.002 \text{ W m}^{-2}$ respectively. The radiative forcing from methane depends on the square root of the absolute methane concentration (as shown in Fig 5.3). Therefore, the forcing calculated in UKESM1-ems, which is low-biased in methane, will be lower than in a non-biased model. I calculated the radiative forcing for methane concentrations 200 ppb higher than those in the CLE and GMP scenarios, to account for the methane bias. While the RFs calculated were higher, the difference between the CLE and GMP scenarios was the same: $0.192 \pm 0.003 \text{ W m}^{-2}$.

Radiative forcing can be linked by a linear relationship to the equilibrium global mean surface temperature change, ΔT , through the equation 5.4 (Ramaswamy et al. 2001; IPCC 2007). λ is the climate sensitivity parameter, estimated as $0.5\text{-}1 \text{ K / W m}^{-2}$ from current climate models (Ramaswamy et al. 2019). This is a crude but simple method, which gives an initial idea of the climate impact from a change in radiative forcing. Using this method gives an estimated GMST reduction of $0.1\text{-}0.2 \text{ K}$ for the simulated methane concentration difference (and an RF difference of 0.192 W m^{-2}). Calculation of the effective radiative forcing would be a preferred method, however this

is not possible in a coupled simulation such as this one, since it requires a fixed sea surface temperature.

The above is a very simplified estimate of the radiative forcing for methane. It does not include indirect radiative forcing impacts of methane concentration changes such as via ozone and stratospheric water vapour, as described in section 1.2.6. The stratospheric water vapour radiative forcing from changes in methane is very small ($-0.002 \pm 0.003 \text{ m}^{-2}$ for pre-industrial to present day, IPCC (2021a)). However, changes in methane have a large impact on ozone and its radiative forcing. The tropospheric column ozone in GMP decreases by $5 \pm 2\%$ by 2045-50, and ozone in the tropical tropopause region decreases by 5-10 ppb (where ozone is most radiatively active, see Fig 5.6e) (Rap et al. 2015). Taking into account the additional negative radiative forcing from reducing ozone concentrations would increase the temperature impact in the GMP scenario calculated via the RF (i.e. causing a greater temperature decrease).

5.6 Summary

Reductions in methane emissions following the Global Methane Pledge scenario lead to an overall decrease in methane globally. Using the ability to change methane emissions regionally in UKESM1-ems, larger decreases beyond the global background decrease are seen in methane source regions. Therefore, there are likely to be direct benefits to reducing methane emissions locally, as well as on a global scale. The additional methane reductions in GMP countries over the background global decrease are of a high enough magnitude to be observable by satellites or ground measurements.

The methane emissions reduction assumed for GMP countries in this scenario (63%) is above the maximum feasible reduction in global methane emissions (29%). This was calculated using currently available technologies, based on sector emissions and mitigation strategies, which varies between countries (Höglund-Isaksson et al. 2020). The countries with the highest mitigation potential (China and Russia, Höglund-Isaksson (2012)) are not participants in the Global Methane Pledge. This highlights the need for more high-emitting countries to sign up to the Pledge in order to meet its emis-

sions goals. However, there are also further options for methane mitigation beyond the maximum feasible reduction scenario, as outlined in the Global Methane Assessment (2021). These include demand-reduction measures such as behaviour change, which could mitigate an extra 15-20% of methane emissions in 2030 (Shindell et al. 2021).

The main motivation behind the Global Methane Pledge is to limit temperature increase. These experiments using UKESM1-ems have shown that it is unlikely that the initially projected temperature reduction (0.2 °C) would be achieved. 0.2 °C is within the model internal variability of UKESM1-ems, and likely to be within the climate variability. The experiments in this chapter were done in parallel with colleagues at the MetOffice, who are using timeslice experiments for 2020 and 2030 to calculate the radiative forcing impacts of the Global Methane Pledge. The FaIR UKESM1-ems emulator is also being used to investigate different emissions pathways and the resulting radiative forcing and temperature impacts, and provides a large number of ensemble members. Together with my transient experiments, this will provide a more complete picture of the temperature response to the Global Methane Pledge, and its limitations. Overall, while limiting temperature increase is a key goal of the Global Methane Pledge, its success will likely be assessed through tracking emissions estimates over time, rather than by measuring temperature changes.

Although the temperature impacts of the Global Methane Pledge are uncertain, there are huge benefits for air quality and human health. Ozone decreases globally, and the population exposure to ozone also decreases. GMP member countries, where methane emissions reductions take place, see a greater air quality benefit than non-GMP countries. This shows the additional benefits (beyond global temperature decrease) to reducing emissions in line with the Global Methane Pledge, and may provide motivation for more countries to sign up.

Chapter 6

Conclusions and future work

The main aim of this thesis has been to evaluate and explore the new capability of the methane emissions-driven configuration of UKESM1, UKESM1-ems. At the start of this project, UKESM1-ems was a new, untested and unvalidated model; a new tool for studying methane and its impacts on the atmosphere and climate. My first aim was to learn to run the model and use it to compare to observations and previous models, to build confidence in it and understand its limitations. Looking towards the future, the use of a methane emissions-driven configuration is a key target in the development of the next UKESM version, UKESM2, for use in CMIP7 experiments. Therefore, using and understanding UKESM1-ems is essential in informing future model developments in the UKESM and wider Earth system modelling community.

The key differences in UKESM1-ems include emissions at the surface instead of a lower boundary condition, integrating JULES wetland emissions into UKCA, and adding a soil sink for methane. These were implemented by Gerd Folberth at the MetOffice.

By simulating methane sources and sinks directly, UKESM1-ems outperforms UKESM1-conc in modelling the global distribution of methane, with particular improvements in the modelled interhemispheric gradient and latitudinal distribution of methane. The modelled change in methane with altitude is also improved in UKESM1-ems vs UKESM1-conc, compared to observations. The observed trend in methane

mixing ratio is successfully simulated in UKESM1-ems, from 1850 to the present day, including the hiatus period. Post-1920, there is a growing methane bias, and by the present day, the methane mixing ratio is underestimated by around 8% relative to observations. This likely stems from a combination of too low methane emissions and an overestimate in OH, the main methane sink. The OH distributions in UKESM1-ems, UKESM1-conc and other CMIP6 models are very similar. However, there are still gaps in the understanding of the differences between UKESM1-ems and UKESM1-conc, for example the lower pre-industrial ozone concentrations in UKESM1-ems.

UKESM1-ems represents an improvement in the capability for modelling methane at a process level. Its strengths, demonstrated in Chapter 2, include the improved regional distribution of methane, enabled by the ability to change methane emissions on a global and regional scale, compared to using a lower boundary condition. The main limitation of using UKESM1-ems is the low-bias in methane mixing ratio with respect to observations. When looking at trends (rather than absolute values) in emissions, atmospheric composition and temperature over time, the effect of the methane bias is small: a very similar result would likely be simulated in a non-biased model with an 8% higher methane concentration. Most experiments here present the difference between a baseline and perturbation scenario, where the bias is consistent between both experiments. However, there are quantities that depend on the absolute methane concentration and whose results may be different with a non-biased model. These include the ozone concentration and the radiative forcing for methane, which depend on the total methane burden. The ozone concentration in a non-biased model would be higher. While generally methane changes scale linearly with ozone changes - which would yield similar results in a biased and non-biased model - this may not be the case in an emissions-driven model (as shown in section 3.6). The radiative forcing calculation in Chapter 5 was performed for UKESM1-ems and non-biased (200 ppb higher) methane concentrations, to account for the methane bias. While the radiative forcing for the individual scenarios was higher with higher methane concentrations, the resulting difference in radiative forcing (and therefore temperature impact) was the same. In summary, UKESM1-ems represents the new state-of-the-art for methane in Earth system modelling, and is used here with an awareness of its strengths and limitations.

Atmospheric methane is currently increasing at unprecedented rates (Nisbet et al. 2019), and it is vital to understand its future evolution and impacts. The role of future anthropogenic methane emissions in air quality and global temperature change was quantified in Chapter 3. The large decrease in methane mixing ratio to below pre-industrial levels occurred within 15 years of stopping methane emissions, accelerated by the methane self-feedback via OH. I found that by 2050, 1°C of future warming can be attributed to future anthropogenic emissions (upper estimate, SSP3-7.0). Decreased methane concentrations lead to large increases in OH (+30%), and decreases in ozone concentrations (-14%). An estimated ~690,000 premature deaths (due to ozone) per year by 2050 are attributable to anthropogenic methane in the SSP3-7.0 scenario. These ozone and climate changes attributed to future anthropogenic methane emissions represent the upper bound of potential impacts, given my use of the highest emissions scenario for methane and ozone precursors (SSP3-7.0).

The coupling between CO, NO_x, OH and methane in UKESM1-ems was explored and clarified in Chapter 4. The methane emissions reductions simulated in ZAME affected both the total NO_x burden and the NO/NO₂ ratio. The partitioning of NO_y between active NO_x and reservoir species changes with different methane emissions. With less methane, there is less NO_y in reservoir species and more NO_x, increasing the total NO_x burden. Less formation of MeONO₂ - due to a lower concentration of methyl peroxy radicals - was one of the main drivers behind the decrease in NO_y in reservoirs. In the low-methane scenarios, the NO/NO₂ ratio was also higher, with less NO being converted to NO₂. This was due to lower ozone, HO₂ and MeOO in the ZAME scenario, which all react with NO to form NO₂.

The response of global and zonal mean OH to CO, NO_x and methane emissions was investigated. With reduced CO emissions, OH increases globally, consistent with the well-mixed distribution of CO in the troposphere. With lower NO_x emissions, OH decreases, with the largest impact in the northern hemisphere: OH changes the most near NO_x sources. The relationship $[\text{OH}] \propto S_N / S_C$ (where S_N is the NO_x burden and S_C is the CO + CH₄ burden) was found to be applicable across all experiments considered in Chapter 4, including over large changes in methane.

Chapter 5 presents the first study of a Global Methane Pledge scenario in an Earth system model, using the capability of UKESM1-ems to change methane emissions regionally. Methane decreases by 13% globally, and further in countries with local emissions reductions. The 63% emissions reduction required by GMP countries to reach the global 30% target in 2030 is higher than estimated maximum reductions using current technologies. More countries signing up to the Pledge, and demand reduction measures are very likely to be needed to achieve the Global Methane Pledge.

The Global Methane Pledge aims to reduce global warming (by 0.2°C) via methane mitigation. The ZAME experiments showed that a 0.2°C reduction is within the modelled internal variability of global mean surface temperature UKESM1-ems, and likely to be within the climate variability. Therefore, this signal from the GMP scenario is not seen over the interannual variability in temperature.

However, there are also benefits beyond temperature. The global mean surface ozone concentration decreases in GMP, leading to global air quality and human health benefits. Countries where methane emissions decrease (i.e. GMP member countries) see greater reductions in ozone over the global average. This shows the additional local benefits to local methane mitigation.

The use of an emissions-driven model with all chemistry and processes modelled explicitly allows for exploration of the impacts of methane changes without limitations from the non-physical effects of the lower boundary condition. This is key to quantifying the full response of the Earth system to future methane changes, including the methane self-feedback and composition changes.

6.1 Future work

Model bias in methane mixing ratio

The bias in methane mixing ratio in UKESM1-ems provides a challenge, and it is important to understand where this bias is most likely to affect outcomes of this analysis, how we can mitigate its impact, and also how to reduce it. Gerd Folberth and Fiona O'Connor at the Met Office have developed a flux adjustment method to mitigate the bias problem in ongoing experiments. This involves calculating and applying a latitudinally-varying methane flux, to increase the methane mixing ratios up to a level consistent with observations. The advantage of this is that the methane mixing ratio and burden at the starting point is consistent with the present day, or the defined scenario: quantities affected by the absolute methane burden/mixing ratio can be simulated more accurately, such as tropospheric ozone concentration and radiative forcing. This was developed for use in timeslice experiments, and there are limitations with using the flux adjustment method in transient experiments, for example the uncertainty in the required residual flux over time (into the future), leading to increasing uncertainty over time.

CRI-Strat (version 2) is an alternative chemical mechanism also used in UKESM1, but has not yet been implemented in UKESM1-ems. In UKESM1-conc, CRI-Strat led to decreased OH concentrations, comprised of an increase at the surface and a decrease in the upper troposphere compared to StratTrop (used here) (Archer-Nicholls et al. 2021). The $\text{CH}_4 + \text{OH}$ reaction rate coefficient is also slightly faster in CRI-Strat. The impact of these changes on methane in UKESM1-conc is buffered by the use of a lower boundary condition. Implementing CRI-Strat in UKESM1-ems would likely lead to differences in the simulated methane mixing ratio, and may improve the bias.

Methane emissions

Bottom-up emissions estimates currently have around a ~ 50 Tg per year mismatch between total sources and sinks (Saunio et al. 2020; Kirschke et al. 2013), which corresponds to the residual flux required in the present day in UKESM1-ems to correct

the methane bias. Decreasing the uncertainty in methane emissions estimates is an active research area, and a challenge given the diffuse nature of many methane emissions sources, lack of measurements in key regions, and limited/widely varying emissions reporting from industry. Imprecisely known emissions are always likely to cause operational challenges in a methane emissions-driven model. Reducing their uncertainty and updating the emissions may improve the methane bias, or would otherwise highlight other areas for improvement such as the simulated oxidising capacity.

The use of online wetland emissions in particular presents a challenge not encountered in other emissions-driven models, which usually use a wetland climatology or offline emissions. It is important to integrate the latest JULES developments into UKESM1-ems, to continue improving the simulated methane wetland emissions in UKESM1-ems. These include methane flux through trees, and the inclusion of non-wetland freshwater systems such as rivers (Gedney et al. 2019).

Integrating methane isotopes into UKCA and UKESM1-ems would enable better attribution of the methane trend to changes in emissions or sinks. In particular, this would enable the ability to distinguish between different source types using their isotope signatures - for example between biogenic and fossil methane emissions. This would make UKESM1-ems an invaluable tool for understanding the factors behind the historical changes in annual methane growth rate. For example, Nisbet et al. (2016) were able to constrain the drivers behind the post-hiatus (2007-2014) growth in methane, concluding that fossil fuel emissions were not a dominant factor, with biogenic wetland and agricultural emissions being more important. One major challenge in implementing methane isotopes in UKESM1-ems is the very long spin-up time required to simulate isotope fractions accurately, which leads to high computational expense.

Developing further understanding of UKESM1-ems

The analysis done by Folberth et al. (2022) and here represents the first steps in the evaluation of UKESM1-ems. Further work in this area will help in the continuing development of UKESM1-ems, for example in understanding the differences in pre-industrial ozone concentrations between UKESM1-ems and UKESM1-conc.

Quantifying the methane self-feedback in models is a useful metric for comparing their treatment of methane. While Holmes (2018) found that there was no difference in the methane feedback between concentration and emissions-driven versions of GEOS-Chem, this has not been tested in a wide range of models. Performing experiments to calculate the feedback factor in UKESM1-ems is a challenge due to the online wetland emissions, which lead to a high noise level in the emissions. The perturbations required for calculating a feedback factor are larger than the standard (5%), to enable a signal to be seen outside the noise, and the model also requires a longer spin-up time than UKESM1-conc. Potential feedback effects of temperature and CO₂ concentrations on wetland emissions may also complicate the feedback factor calculation. Overall, more work is required to quantify the methane self-feedback in a coupled emissions-driven model with online wetland emissions - e.g. UKESM1-ems.

Global Methane Pledge experiments

Further experiments modelling the Global Methane Pledge are required to constrain the expected temperature response and quantify the effective radiative forcing impact. The use of both timeslice experiments using UKESM1-ems, and a range of GMP-consistent emissions scenarios using the FaIR model (a climate emulator, Leach et al. (2021)) will offer a more comprehensive view on the expected results of achieving the Global Methane Pledge, and the emissions required to achieve the stated temperature target of 0.2°C. These experiments are currently ongoing (by colleagues at the Met Office) and will complement the work presented in Chapter 5.

Resolving the climate crisis requires continual improvements in the understanding of the atmosphere and Earth system, to underpin crucial greenhouse gas mitigation actions. This work has furthered the understanding of the complex interplay between methane, atmospheric chemistry, and climate. It defines the new (emissions-driven) state-of-the-art in modelling methane in the Earth system.

Appendix A

Appendices

A.1 Data and code availability

UKESM1-ems data used in Chapter 3 are archived to the UK Centre for Environmental Data Analysis and are freely available (Staniaszek et al. 2021). Code used for data analysis and producing figures can be found at <https://github.com/zosiast/nzame-scripts>.

A.2 Methane Pledge countries

Countries with no mitigation in the Global Methane Pledge scenario		
China	Angola	Guinea
Russia	Kenya	Madagascar
India	Bolivia	Azerbaijan
Iran	South Sudan	Zimbabwe
Venezuela	Paraguay	Nicaragua
Algeria	Poland	Laos
Turkmenistan	Uganda	Hungary
South Africa	North Korea	Tajikistan
Myanmar	Syria	Haiti
Thailand	Belarus	Sierra Leone
Kazakhstan	Romania	Eritrea
Turkey	Afghanistan	Lithuania
Tanzania		

Table A.1: Countries not signed up to the Global Methane Pledge as of March 2023. These countries' methane emissions follow the CLE trajectory in the Global Methane Pledge scenario. All countries with emissions below 0.1 Tg per year (according to Jones et al. (2023)) also follow the CLE trajectory. Countries are in order of decreasing methane emissions from top-left downwards.

A.3 Experiment suite IDs used in this thesis

Scenario	suite-id	Time span	Model configuration
Historical	u-bc179	1850 - 2015	UKESM1-conc
Historical	u-bn213	1850 - 2015	UKESM1-ems
Historical	u-bl998	1850 - 2015	UKESM1-ems
Historical	u-bl593	1850 - 2015	UKESM1-ems
SSP3-7.0	u-bo797	2015 - 2100	UKESM1-ems
SSP3-7.0	u-ca723	2015 - 2050	UKESM1-ems
SSP3-7.0	u-cb039	2015 - 2050	UKESM1-ems
SSP1-2.6	u-bo812	2015 - 2050	UKESM1-ems
ZAME	u-by186	2015-2050	UKESM1-ems
ZAME	u-bz146	2015-2050	UKESM1-ems
ZAME	u-bz473	2015-2050	UKESM1-ems
SSP370lowCO	u-cq552	2015 - 2030	UKESM1-ems
SSP370lowNOx	u-cq554	2015 - 2030	UKESM1-ems
ZAMElowCO	u-cr272	2015-2030	UKESM1-ems
ZAMElowNOx	u-cr276	2015-2030	UKESM1-ems
SSP2-4.5ECLIPSECH4 spin up	u-cu510	2015-2025	UKESM1-ems
SSP2-4.5ECLIPSECH4	u-cu814	2015-2050	UKESM1-ems
GMP	u-cv430	2015-2050	UKESM1-ems

Table A.2: Model experiments used in this thesis

Bibliography

- Abernethy, S, FM O'Connor, CD Jones, and RB Jackson (2021). "Methane removal and the proportional reductions in surface temperature and ozone". In: *Philos. Trans. Royal Soc. A* 379.2210, p. 20210104.
- Allen, RJ, Larry W Horowitz, Vaishali Naik, Naga Oshima, Fiona M O'Connor, Steven Turnock, Sungbo Shim, Philippe Le Sager, Twan Van Noije, Kostas Tsigaridis, et al. (2021). "Significant climate benefits from near-term climate forcer mitigation in spite of aerosol reductions". In: *Environ. Res. Lett.* 16.3, p. 034010.
- Amann, Markus, Imrich Bertok, Jens Borken-Kleefeld, Janusz Cofala, Chris Heyes, Lena Höglund-Isaksson, Zbigniew Klimont, Binh Nguyen, Maximilian Posch, Peter Rafaj, et al. (2011). "Cost-effective control of air quality and greenhouse gases in Europe: Modeling and policy applications". In: *Environ Model Softw* 26.12, pp. 1489–1501.
- Archer, David, Bruce Buffett, and Victor Brovkin (2009). "Ocean methane hydrates as a slow tipping point in the global carbon cycle". In: *Proc. Natl. Acad. Sci. U.S.A.* 106.49, pp. 20596–20601.
- Archer-Nicholls, S, N Luke Abraham, YM Shin, J Weber, Maria R Russo, D Lowe, SR Utembe, FM O'Connor, B Kerridge, B Latter, et al. (2021). "The Common Representative Intermediates Mechanism version 2 in the United Kingdom Chemistry and Aerosols Model". In: *J. Adv. Model. Earth Syst.* 13.5, e2020MS002420.

- Archibald, A.T., M.A.H. Khan, L.A. Watson, K.C. Clemitshaw, S.R. Utembe, M.E. Jenkin, and D.E. Shallcross (2007). “Comment on ‘Long-term atmospheric measurements of C1–C5 alkyl nitrates in the Pearl River Delta region of southeast China’ by Simpson et al.” In: *Atmos. Environ.* 41.34, pp. 7369–7370. ISSN: 1352-2310. DOI: <https://doi.org/10.1016/j.atmosenv.2007.08.004>.
- Archibald, Alexander T, Fiona M O’Connor, Nathan Luke Abraham, Scott Archer-Nicholls, Martyn P Chipperfield, Mohit Dalvi, Gerd A Folberth, Fraser Dennison, Sandip S Dhomse, Paul T Griffiths, et al. (2020a). “Description and evaluation of the UKCA stratosphere–troposphere chemistry scheme (StratTrop v1.0) implemented in UKESM1”. In: *Geosci. Model Dev.* 13.3, pp. 1223–1266.
- Archibald, AT, JL Neu, YF Elshorbany, OR Cooper, PJ Young, H Akiyoshi, RA Cox, M Coyle, RG Derwent, M Deushi, et al. (2020b). “Tropospheric Ozone Assessment Report: A critical review of changes in the tropospheric ozone burden and budget from 1850 to 2100”. In: *Elementa Sci. Anthropol.* 8.1.
- Atkinson, R., D. L. Baulch, R. A. Cox, J. N. Crowley, R. F. Hampson, R. G. Hynes, M. E. Jenkin, M. J. Rossi, and J. Troe (2004). “IUPAC Task Group on Atmospheric Chemical Kinetic Data Evaluation - Data Sheet HO_x VOC1”. In: *Atmos. Chem. Phys.* 4, pp. 1461–1738. URL: <http://iupac.pole-ether.fr>.
- (2006). “IUPAC Task Group on Atmospheric Chemical Kinetic Data Evaluation - Data Sheet ROO 1”. In: *Atmos. Chem. Phys.*, pp. 3625–4055. URL: <http://iupac.pole-ether.fr>.
- Barret, Brice, JE Williams, Idir Bouarar, X Yang, B Josse, K Law, Mai Pham, E Le Flochmoën, C Liousse, VH Peuch, et al. (2010). “Impact of West African Monsoon convective transport and lightning NO_x production upon the upper tropospheric composition: a multi-model study”. In: *Atmos. Chem. Phys.* 10.12, pp. 5719–5738.
- Bousquet, P., B. Ringeval, I. Pison, E. J. Dlugokencky, E.-G. Brunke, C. Carouge, F. Chevallier, A. Fortems-Cheiney, C. Frankenberg, D. A. Hauglustaine, P. B. Krum-

- mel, R. L. Langenfelds, M. Ramonet, M. Schmidt, L. P. Steele, S. Szopa, C. Yver, N. Viovy, and P. Ciais (2011). “Source attribution of the changes in atmospheric methane for 2006–2008”. In: *Atmos. Chem. Phys.* 11.8, pp. 3689–3700. DOI: 10.5194/acp-11-3689-2011.
- Brewer, AW (1949). “Evidence for a world circulation provided by the measurements of helium and water vapour distribution in the stratosphere”. In: *Q J R Meteorol Soc* 75.326, pp. 351–363.
- Burkholder, JB, SP Sander, JPD Abbatt, JR Barker, C Cappa, JD Crouse, TS Dibble, RE Huie, CE Kolb, MJ Kurylo, et al. (2020). *Chemical kinetics and photochemical data for use in atmospheric studies; evaluation number 19*. Tech. rep. Pasadena, CA: Jet Propulsion Laboratory, National Aeronautics and Space Agency.
- Butz, André, S Guerlet, O Hasekamp, D Schepers, A Galli, Ilse Aben, C Frankenberg, J-M Hartmann, H Tran, A Kuze, et al. (2011). “Toward accurate CO₂ and CH₄ observations from GOSAT”. In: *Geophys. Res. Lett.* 38.14.
- Cain, Michelle, Stuart Jenkins, Myles R Allen, John Lynch, David J Frame, Adrian H Macey, and Glen P Peters (2022). “Methane and the Paris Agreement temperature goals”. In: *Philos. Trans. Royal Soc. A* 380.2215, p. 20200456.
- Callendar, Guy Stewart (1938). “The artificial production of carbon dioxide and its influence on temperature”. In: *Q J R Meteorol Soc* 64.275, pp. 223–240.
- Cao, Mingkui, Keith Gregson, and Stewart Marshall (1998). “Global methane emission from wetlands and its sensitivity to climate change”. In: *Atmos. Environ.* 32.19, pp. 3293–3299.
- Christensen, Torben R, Anna Ekberg, Lena Ström, Mihail Mastepanov, Nicolai Panikov, Mats Öquist, Bo H Svensson, Hannu Nykänen, Pertti J Martikainen, and Hlynur Oskarsson (2003). “Factors controlling large scale variations in methane emissions from wetlands”. In: *Geophys. Res. Lett.* 30.7.

- Chua, Glen, Vaishali Naik, and Larry Wayne Horowitz (2023). “Exploring the drivers of tropospheric hydroxyl radical trends in the Geophysical Fluid Dynamics Laboratory AM4. 1 atmospheric chemistry–climate model”. In: *Atmos. Chem. Phys.* 23.8, pp. 4955–4975.
- Clark, D. B., L. M. Mercado, S. Sitch, C. D. Jones, N. Gedney, M. J. Best, M. Pryor, G. G. Rooney, R. L. H. Essery, E. Blyth, O. Boucher, R. J. Harding, C. Huntingford, and P. M. Cox (2011). “The Joint UK Land Environment Simulator (JULES), model description – Part 2: Carbon fluxes and vegetation dynamics”. In: *Geosci. Model Dev.* 4.3, pp. 701–722. ISSN: 1991-9603. DOI: 10.5194/gmd-4-701-2011.
- Collins, William J, Jean-François Lamarque, Michael Schulz, Olivier Boucher, Veronika Eyring, Michaela I Hegglin, Amanda Maycock, Gunnar Myhre, Michael Prather, D. T. Shindell, et al. (2017). “AerChemMIP: quantifying the effects of chemistry and aerosols in CMIP6”. In: *Geosci. Model Dev.* 10.2, pp. 585–607.
- Crutzen, Paul (1973). “A discussion of the chemistry of some minor constituents in the stratosphere and troposphere”. In: *Pure Appl. Geophys.* 106.1, pp. 1385–1399.
- Crutzen, Paul J (1979). “The role of NO and NO₂ in the chemistry of the troposphere and stratosphere”. In: *Annu Rev Earth Planet Sci* 7.1, pp. 443–472.
- Dalsøren, S. B., C. L. Myhre, G. Myhre, A. J. Gomez-Pelaez, O. A. Søvde, I. S. A. Isaksen, R. F. Weiss, and C. M. Harth (2016). “Atmospheric methane evolution the last 40 years”. In: *Atmos. Chem. Phys.* 16.5, pp. 3099–3126. DOI: 10.5194/acp-16-3099-2016.
- Dalsøren, Stig B and Ivar SA Isaksen (2006). “CTM study of changes in tropospheric hydroxyl distribution 1990–2001 and its impact on methane”. In: *Geophys. Res. Lett.* 33.23.

- Davidson, Nick C, Etienne Fluet-Chouinard, and C Max Finlayson (2018). “Global extent and distribution of wetlands: trends and issues”. In: *Mar. Freshw. Res.* 69.4, pp. 620–627.
- Dean, Joshua F, Jack J Middelburg, Thomas Röckmann, Rien Aerts, Luke G Blauw, Matthias Egger, Mike SM Jetten, Anniek EE de Jong, Ove H Meisel, Olivia Rasiograf, et al. (2018). “Methane feedbacks to the global climate system in a warmer world”. In: *Rev. Geophys.* 56.1, pp. 207–250.
- Dlugokencky, Ed (2020). *NOAA/ESRL*. www.esrl.noaa.gov/gmd/ccgg/trends_ch4/. Accessed 6th May 2020.
- Duncan, BN, I Bey, M Chin, LJ Mickley, TD Fairlie, RV Martin, and H Matsueda (2003). “Indonesian wildfires of 1997: Impact on tropospheric chemistry”. In: *J. Geophys. Res.: Atmospheres* 108.D15.
- Dunne, JP, LW Horowitz, AJ Adcroft, P Ginoux, IM Held, JG John, JP Krasting, S Malyshev, V Naik, F Paulot, et al. (2020). “The GFDL Earth System Model version 4.1 (GFDL-ESM 4.1): Overall coupled model description and simulation characteristics”. In: *J. Adv. Model. Earth Syst.* 12.11, e2019MS002015.
- EIA, US (2012). *Global natural gas consumption doubled from 1980 to 2010*. Last accessed 20th June 2020. URL: <https://www.eia.gov/todayinenergy/detail.php?id=5810>.
- Etheridge, David M, L.P. Steele, RJ Francey, and RL Langenfelds (1998). “Atmospheric methane between 1000 AD and present: Evidence of anthropogenic emissions and climatic variability”. In: *J. Geophys. Res. Atmos.* 103.D13, pp. 15979–15993.
- Etminan, M, G Myhre, EJ Highwood, and KP Shine (2016). “Radiative forcing of carbon dioxide, methane, and nitrous oxide: A significant revision of the methane radiative forcing”. In: *Geophys. Res. Lett.* 43.24, pp. 12–614.

- Europe, WHO (2013). *Review of evidence on health aspects of air pollution—REVIHAAP Project*. Tech. rep. Technical Report. Copenhagen, Denmark: World Health Organization.
- European Commission (Sept. 2021). *Joint EU-US Press Release on the Global Methane Pledge*. Accessed August 2023. URL: https://ec.europa.eu/commission/presscorner/detail/en/IP_21_4785.
- Eyring, V., S. Bony, G. A. Meehl, C. A. Senior, B. Stevens, R. J. Stouffer, and K. E. Taylor (2016). “Overview of the Coupled Model Intercomparison Project Phase 6 (CMIP6) experimental design and organization”. In: *Geosci Model Dev* 9.5, pp. 1937–1958. DOI: 10.5194/gmd-9-1937-2016.
- Feng, Liang, Paul I Palmer, Robert J Parker, Mark F Lunt, and Hartmut Bösch (2023). “Methane emissions are predominantly responsible for record-breaking atmospheric methane growth rates in 2020 and 2021”. In: *Atmos. Chem. Phys.* 23.8, pp. 4863–4880.
- Fiore, Arlene M, FJ Dentener, O Wild, Cornelis Cuvelier, MG Schultz, P Hess, C Textor, M Schulz, RM Doherty, LW Horowitz, et al. (2009). “Multimodel estimates of intercontinental source-receptor relationships for ozone pollution”. In: *J. Geophys. Res. Atmos.* 114.D4.
- Fiore, Arlene M, J Jason West, Larry W Horowitz, Vaishali Naik, and M Daniel Schwarzkopf (2008). “Characterizing the tropospheric ozone response to methane emission controls and the benefits to climate and air quality”. In: *J Geophys. Res. Atmos.* 113.D8.
- Folberth, G. A., Zosia Staniaszek, AT Archibald, N Gedney, PT Griffiths, CD Jones, FM O’Connor, RJ Parker, AA Sellar, and A Wiltshire (2022). “Description and Evaluation of an Emission-Driven and Fully Coupled Methane Cycle in UKESM1”. In: *J. Adv. Model Earth Syst.*, e2021MS002982.

- Forster, Piers, Chris Smith, and Rogelj (2023). *Guest post: The Global Methane Pledge needs to go further to help limit warming to 1.5C*. Last accessed 9 May 2023. URL: <https://www.carbonbrief.org/guest-post-the-global-methane-pledge-needs-to-go-further-to-help-limit-warming-to-1-5c/>.
- Forster, Piers M, Thomas Richardson, Amanda C Maycock, Christopher J Smith, Bjorn H Samset, Gunnar Myhre, Timothy Andrews, Robert Pincus, and Michael Schulz (2016). “Recommendations for diagnosing effective radiative forcing from climate models for CMIP6”. In: *J. Geophys. Res.: Atmospheres* 121.20, pp. 12–460.
- Fricko, Oliver, Petr Havlik, Joeri Rogelj, Zbigniew Klimont, Mykola Gusti, Nils Johnson, Peter Kolp, Manfred Strubegger, Hugo Valin, Markus Amann, et al. (2017). “The marker quantification of the Shared Socioeconomic Pathway 2: A middle-of-the-road scenario for the 21st century”. In: *Glob Environ Change* 42, pp. 251–267.
- Fry, Meridith M, Vaishali Naik, J Jason West, M Daniel Schwarzkopf, Arlene M Fiore, William J Collins, Frank J Dentener, Drew T Shindell, Cyndi Atherton, Daniel Bergmann, et al. (2012). “The influence of ozone precursor emissions from four world regions on tropospheric composition and radiative climate forcing”. In: *J. Geophys. Res. Atmos.* 117.D7.
- Fuglestedt, Jan S, Terje K Berntsen, Odd Godal, Robert Sausen, Keith P Shine, and Tora Skodvin (2003). “Metrics of climate change: Assessing radiative forcing and emission indices”. In: *Clim Change* 58, pp. 267–331.
- Fung, I., J. John, J. Lerner, E. Matthews, M. Prather, L. P. Steele, and P. J. Fraser (1991). “Three-dimensional model synthesis of the global methane cycle”. In: *J. Geophys. Res.* 96, pp. 13033–13065. DOI: 10.1029/91JD01247.
- Gaubert, Benjamin, Helen M Worden, AFJ Arellano, Louisa K Emmons, Simone Tilmes, Jérôme Barré, Sara Martinez Alonso, F Vitt, JL Anderson, F Alkemade, et al. (2017). “Chemical feedback from decreasing carbon monoxide emissions”. In: *Geophys. Res. Lett.* 44.19, pp. 9985–9995.

- Gedney, N, PM Cox, and Chris Huntingford (2004). “Climate feedback from wetland methane emissions”. In: *Geophys. Res. Lett.* 31.20.
- Gedney, N, C Huntingford, E Comyn-Platt, and A Wiltshire (2019). “Significant feedbacks of wetland methane release on climate change and the causes of their uncertainty”. In: *Environ. Res. Lett.* 14.8, p. 084027.
- Ghosh, A, PK Patra, K Ishijima, T Umezawa, A Ito, DM Etheridge, S Sugawara, K Kawamura, JB Miller, EJ Dlugokencky, et al. (2015). “Variations in global methane sources and sinks during 1910–2010”. In: *Atmos. Chem. Phys.* 15.5, pp. 2595–2612.
- Gidden, Matthew J, Keywan Riahi, Steven J Smith, Shinichiro Fujimori, Gunnar Luderer, Elmar Kriegler, Detlef P van Vuuren, Maarten van den Berg, Leyang Feng, David Klein, et al. (2019). “Global emissions pathways under different socioeconomic scenarios for use in CMIP6: a dataset of harmonized emissions trajectories through the end of the century”. In: *Geosci. Model Dev.* 12.4, pp. 1443–1475.
- Granier, Claire, Bertrand Bessagnet, Tami Bond, Ariela D’Angiola, Hugo Denier van Der Gon, Gregory J Frost, Angelika Heil, Johannes W Kaiser, Stefan Kinne, Zbigniew Klimont, et al. (2011). “Evolution of anthropogenic and biomass burning emissions of air pollutants at global and regional scales during the 1980–2010 period”. In: *Clim Change* 109.1-2, p. 163.
- Grant, Aoife, Alexander T Archibald, Mike C Cooke, and Dudley E Shallcross (2010). “Modelling the oxidation of seventeen volatile organic compounds to track yields of CO and CO₂”. In: *Atmos. Environ.* 44.31, pp. 3797–3804.
- Griffiths, Paul T, Lee T Murray, Guang Zeng, Youngsub Matthew Shin, N Luke Abraham, Alexander T Archibald, Makoto Deushi, Louisa K Emmons, Ian E Galbally, Birgit Hassler, et al. (2021). “Tropospheric ozone in CMIP6 simulations”. In: *Atmos. Chem. Phys.* 21.5, pp. 4187–4218.

- Harmsen, JHM, Detlef P van Vuuren, Dali R Nayak, Andries F Hof, Lena Höglund-Isaksson, Paul L Lucas, Jens B Nielsen, Pete Smith, and Elke Stehfest (2019). “Long-term marginal abatement cost curves of non-CO₂ greenhouse gases”. In: *Environ Sci Policy* 99, pp. 136–149.
- Harmsen, Mathijs, Detlef P van Vuuren, Benjamin Leon Bodirsky, Jean Chateau, Olivier Durand-Lasserve, Laurent Drouet, Oliver Fricko, Shinichiro Fujimori, David EHJ Gernaat, Tatsuya Hanaoka, et al. (2020). “The role of methane in future climate strategies: mitigation potentials and climate impacts”. In: *Clim Change* 163.3, pp. 1409–1425.
- Hawkins, Ed and Phil D Jones (2013). “On increasing global temperatures: 75 years after Callendar”. In: *Q J R Meteorol Soc* 139.677, pp. 1961–1963.
- Hayman, Garry D, Edward Comyn-Platt, Chris Huntingford, Anna B Harper, Tom Powell, Peter M Cox, William Collins, Christopher Webber, Jason Lowe, Stephen Sitch, et al. (2021). “Regional variation in the effectiveness of methane-based and land-based climate mitigation options”. In: *Earth Syst. Dynam.* 12.2, pp. 513–544.
- He, Jian, Vaishali Naik, Larry W Horowitz, Ed Dlugokencky, and Kirk Thoning (2020). “Investigation of the global methane budget over 1980–2017 using GFDL-AM4. 1.” In: *Atmos. Chem. Phys.* 20.2.
- Heimann, I, PT Griffiths, NJ Warwick, NL Abraham, AT Archibald, and JA Pyle (2020). “Methane emissions in a chemistry-climate model: Feedbacks and climate response”. In: *J. Adv. Model. Earth Syst.* 12.10, e2019MS002019.
- Hmiel, Benjamin, VV Petrenko, MN Dyonisius, C Buizert, AM Smith, PF Place, C Harth, R Beaudette, Quan Hua, B Yang, et al. (2020). “Preindustrial 14CH₄ indicates greater anthropogenic fossil CH₄ emissions”. In: *Nature* 578.7795, pp. 409–412.

- Hoesly, Rachel M, Steven J Smith, Leyang Feng, Zbigniew Klimont, Greet Janssens-Maenhout, Tyler Pitkanen, Jonathan J Seibert, Linh Vu, Robert J Andres, Ryan M Bolt, et al. (2018). “Historical (1750–2014) anthropogenic emissions of reactive gases and aerosols from the Community Emissions Data System (CEDS)”. In: *Geosci Model Dev* 11.PNNL-SA-123932.
- Höglund-Isaksson, L (2012). “Global anthropogenic methane emissions 2005–2030: technical mitigation potentials and costs”. In: *Atmos. Chem. Phys* 12.19, pp. 9079–9096.
- Höglund-Isaksson, Lena, Adriana Gómez-Sanabria, Zbigniew Klimont, Peter Rafaj, and Wolfgang Schöpp (2020). “Technical potentials and costs for reducing global anthropogenic methane emissions in the 2050 timeframe—results from the GAINS model”. In: *Environ. Res. Commun.* 2.2, p. 025004.
- Holloway, Tracey, Hiram Levy, and Prasad Kasibhatla (2000). “Global distribution of carbon monoxide”. In: *J. Geophys. Res.: Atmospheres* 105.D10, pp. 12123–12147.
- Holmes, Christopher D. (2018). “Methane Feedback on Atmospheric Chemistry: Methods, Models, and Mechanisms”. In: *J. Adv. Model. Earth Syst.* 10.4, pp. 1087–1099. ISSN: 19422466. DOI: 10.1002/2017MS001196.
- Hossaini, Ryan, Martyn P Chipperfield, Alfonso Saiz-Lopez, Rafael Fernandez, Sarah Monks, Wuhu Feng, Peter Brauer, and Roland Von Glasow (2016). “A global model of tropospheric chlorine chemistry: Organic versus inorganic sources and impact on methane oxidation”. In: *J. Geophys. Res. Atmos.* 121.23, pp. 14–271.
- Hu, Haili, Jochen Landgraf, Rob Detmers, Tobias Borsdorff, Joost Aan de Brugh, Ilse Aben, André Butz, and Otto Hasekamp (2018). “Toward global mapping of methane with TROPOMI: First results and intersatellite comparison to GOSAT”. In: *Geophys. Res. Lett.* 45.8, pp. 3682–3689.

Huangfu, Peijue and Richard Atkinson (2020). “Long-term exposure to NO₂ and O₃ and all-cause and respiratory mortality: A systematic review and meta-analysis”. In: *Environment international* 144, p. 105998.

IEA (2020). *Methane Tracker 2020*. accessed July 2023. URL: <https://www.iea.org/reports/methane-tracker-2020>.

— (2021). *Net Zero by 2050: A Roadmap for the Global Energy Sector*. Tech. rep.

IIASA (2019). *Global emission fields of air pollutants and GHGs*. accessed July 2023. URL: <https://iiasa.ac.at/models-tools-data/global-emission-fields-of-air-pollutants-and-ghgs>.

IPCC (2007). “Contribution of Working Group I to the fourth assessment report of the Intergovernmental Panel on Climate Change 2007”. In: *IPCC AR4*. Ed. by SD Solomon, M. Qin, Z. Manning, M. Chen, K.B. Marquis, M. Averyt, Tignor, and H.L. Miller.

— (2013). “Summary for Policymakers”. In: *Climate Change 2013: The Physical Science Basis. Contribution of Working Group I to the Fifth Assessment Report of the Intergovernmental Panel on Climate Change*. Cambridge, United Kingdom and New York, NY, USA: Cambridge University Press. Chap. SPM, pp. 1–30. ISBN: ISBN 978-1-107-66182-0. DOI: 10.1017/CBO9781107415324.004. URL: www.climatechange2013.org.

— (2021a). *Climate Change 2021: The Physical Science Basis. Contribution of Working Group I to the Sixth Assessment Report of the Intergovernmental Panel on Climate Change*. Cambridge University Press.

— (2021b). “Climate Change 2021: The Physical Science Basis. Contribution of Working Group I to the Sixth Assessment Report of the Intergovernmental Panel on Climate Change; Technical Summary”. In: ed. by Paola Arias, Nicolas Bellouin,

Erika Coppola, Richard Jones, Gerhard Krinner, Jochem Marotzke, Vaishali Naik, Matthew Palmer, G-K Plattner, Joeri Rogelj, et al.

IPCC (2022). *Summary for Policymakers. In: Climate Change 2022: Mitigation of Climate Change. Contribution of Working Group III to the Sixth Assessment Report of the Intergovernmental Panel on Climate Change*. Ed. by P.R. Shukla, J. Skea, R. Slade, A. Al Khourdajie, R. van Diemen, D. McCollum, M. Pathak, S. Some, P. Vyas, R. Fradera, A. Hasija M. Belkacemi, G. Lisboa, S. Luz, and J. Malley. Cambridge University Press, Cambridge, UK and New York, NY, USA, pp. 3–24. DOI: 10.1017/9781009157926.001.

— (2023). *Climate Change 2023: Synthesis Report. A Report of the Intergovernmental Panel on Climate Change. Contribution of Working Groups I, II and III to the Sixth Assessment Report of the Intergovernmental Panel on Climate Change*. Ed. by H. Lee Core Writing Team and J. Romero. Cambridge, UK and New York, NY, USA: Cambridge University Press.

Jiang, Zhe, John R Worden, Helen Worden, Merritt Deeter, Dylan Jones, Avelino F Arellano, and Daven K Henze (2017). “A 15-year record of CO emissions constrained by MOPITT CO observations”. In: *Atmos. Chem. Phys.* 17.7.

John, J. G., A. M. Fiore, V. Naik, L. W. Horowitz, and J. P. Dunne (2012). “Climate versus emission drivers of methane lifetime against loss by tropospheric OH from 1860-2100”. In: *Atmos. Chem. Phys.* 12.24, pp. 12021–12036. ISSN: 16807316. DOI: 10.5194/acp-12-12021-2012.

Jones, Bryan and Brian C O’Neill (2016). “Spatially explicit global population scenarios consistent with the Shared Socioeconomic Pathways”. In: *Environ. Res. Lett.* 11.8, p. 084003. DOI: <http://doi.org/10.1088/1748-9326/11/8/084003>.

Jones, Matthew W, Glen P Peters, Thomas Gasser, Robbie M Andrew, Clemens Schwingshackl, Johannes Gütschow, Richard A Houghton, Pierre Friedlingstein, Julia Pongratz, and Corinne Le Quéré (2023). “National contributions to climate

change due to historical emissions of carbon dioxide, methane, and nitrous oxide since 1850". In: *Scientific Data* 10.1, p. 155.

Keeling, C. D., S. C. Piper, R. B. Bacastow, M. Wahlen, T. P. Whorf, M. Heimann, and H. A. Meijer (2001). *Exchanges of atmospheric CO₂ and 13CO₂ with the terrestrial biosphere and oceans from 1978 to 2000*. URL: <http://escholarship.org/uc/item/09v319r9>.

Kelley, Maxwell, Gavin A Schmidt, Larissa S Nazarenko, Susanne E Bauer, Reto Ruedy, Gary L Russell, Andrew S Ackerman, Igor Aleinov, Michael Bauer, Rainer Bleck, et al. (2020). "GISS-E2. 1: Configurations and climatology". In: *J. Adv. Model. Earth Syst.* 12.8, e2019MS002025.

Khalil, MAK and RA Rasmussen (1990). "The global cycle of carbon monoxide: Trends and mass balance". In: *Chemosphere* 20.1-2, pp. 227–242.

Kirschke, Stefanie, Philippe Bousquet, Philippe Ciais, Marielle Saunois, Josep G Canadell, Edward J Dlugokencky, Peter Bergamaschi, Daniel Bergmann, Donald R Blake, Lori Bruhwiler, et al. (2013). "Three decades of global methane sources and sinks". In: *Nat. Geosci.* 6.10, pp. 813–823.

Kleinen, Thomas, Sergey Gromov, Benedikt Steil, and Victor Brovkin (2021). "Atmospheric methane underestimated in future climate projections". In: *Environ. Res. Lett.* 16.9, p. 094006.

Kriegler, Elmar, Nico Bauer, Alexander Popp, Florian Humpenöder, Marian Leimbach, Jessica Strefler, Lavinia Baumstark, Benjamin Leon Bodirsky, Jérôme Hilaire, David Klein, et al. (2017). "Fossil-fueled development (SSP5): an energy and resource intensive scenario for the 21st century". In: *Glob Environ Change* 42, pp. 297–315.

- Krol, Maarten, Peter Jan van Leeuwen, and Jos Lelieveld (1998). “Global OH trend inferred from methylchloroform measurements”. In: *J. Geophys. Res.: Atmospheres* 103.D9, pp. 10697–10711.
- Labrador, Lorenzo J, Rolf von Kuhlmann, and Mark G Lawrence (2004). “Strong sensitivity of the global mean OH concentration and the tropospheric oxidizing efficiency to the source of NO_x from lightning”. In: *Geophys. Res. Lett.* 31.6.
- Lamarque, Jean-François, T.G. Bond, Veronika Eyring, Claire Granier, Angelika Heil, Zbigniew Klimont, David Lee, C. Liou, Aude Mieville, Bethan Owen, M.G. Schultz, D. T. Shindell, S.J. Smith, E. Stehfest, John Aardenne, O.R. Cooper, Mikiko Kainuma, Natalie Mahowald, Joseph McConnell, and Detlef Vuuren (Feb. 2010). “Historical (1850-2000) gridded anthropogenic and biomass burning emissions of reactive gases and aerosols: methodology and application”. In: *Atmos. Chem. Phys.* 10, pp. 7017–7039. DOI: 10.5194/acpd-10-4963-2010.
- Lan, X, K.W. Thoning, and E.J. Dlugokencky (2022). *Trends in globally-averaged CH₄, N₂O, and SF₆ determined from NOAA Global Monitoring Laboratory measurements*. DOI: 10.15138/P8XG-AA10.
- Lawrence, MG, P Jöckel, and R von Kuhlmann (2001). “What does the global mean OH concentration tell us?” In: *Atmos. Chem. Phys* 1.1, pp. 37–49.
- Leach, Nicholas J, Stuart Jenkins, Zebedee Nicholls, Christopher J Smith, John Lynch, Michelle Cain, Tristram Walsh, Bill Wu, Junichi Tsutsui, and Myles R Allen (2021). “FaIRv2. 0.0: a generalized impulse response model for climate uncertainty and future scenario exploration”. In: *Geosci Model Dev* 14.5, pp. 3007–3036.
- Lelieveld, Jos, Sergey Gromov, Andrea Pozzer, and Domenico Taraborrelli (2016). “Global tropospheric hydroxyl distribution, budget and reactivity”. In: *Atmos. Chem. Phys.* 16.19, pp. 12477–12493.

- Lenton, Timothy M, Johan Rockström, Owen Gaffney, Stefan Rahmstorf, Katherine Richardson, Will Steffen, and Hans Joachim Schellnhuber (2019). “Climate tipping points—too risky to bet against”. In: *Nature* 575.7784, pp. 592–595.
- Levy, H (1971). “Normal atmosphere: Large radical and formaldehyde concentrations predicted”. In: *Science* 173.3992, pp. 141–143.
- Levy II, Hiram (1972). “Photochemistry of the lower troposphere”. In: *Planetary and Space Science* 20.6, pp. 919–935.
- Logan, Jennifer A (1983). “Nitrogen oxides in the troposphere: Global and regional budgets”. In: *J. Geophys. Res. Oceans* 88.C15, pp. 10785–10807.
- Lucas, Paul L, Detlef P van Vuuren, Jos GJ Olivier, and Michel GJ Den Elzen (2007). “Long-term reduction potential of non-CO₂ greenhouse gases”. In: *Environ Sci Policy* 10.2, pp. 85–103.
- Lunt, Mark F, Paul I Palmer, Liang Feng, Christopher M Taylor, Hartmut Boesch, and Robert J Parker (2019). “An increase in methane emissions from tropical Africa between 2010 and 2016 inferred from satellite data”. In: *Atmos. Chem. Phys* 19.23, pp. 14721–14740.
- Malley, Christopher S, Daven K Henze, Johan CI Kuylenstierna, Harry W Vallack, Yanko Davila, Susan C Anenberg, Michelle C Turner, and Mike R Ashmore (2017). “Updated global estimates of respiratory mortality in adults \geq 30 years of age attributable to long-term ozone exposure”. In: *Environ. Health Perspect.* 125.8, p. 087021.
- Matthews, H Damon and Kirsten Zickfeld (2012). “Climate response to zeroed emissions of greenhouse gases and aerosols”. In: *Nature Climate Change* 2.5, pp. 338–341.

- McDuffie, Erin E, Steven J Smith, Patrick O'Rourke, Kushal Tibrewal, Chandra Venkataraman, Eloise A Marais, Bo Zheng, Monica Crippa, Michael Brauer, and Randall V Martin (2020). "A global anthropogenic emission inventory of atmospheric pollutants from sector-and fuel-specific sources (1970–2017): an application of the Community Emissions Data System (CEDS)". In: *Earth Syst. Sci. Data* 12.4, pp. 3413–3442.
- Meinshausen, Malte, Zebedee RJ Nicholls, Jared Lewis, Matthew J Gidden, Elisabeth Vogel, Mandy Freund, Urs Beyerle, Claudia Gessner, Alexander Nauels, Nico Bauer, et al. (2020). "The shared socio-economic pathway (SSP) greenhouse gas concentrations and their extensions to 2500". In: *Geosci Model Dev* 13.8, pp. 3571–3605.
- Meinshausen, Malte, Sarah CB Raper, and Tom ML Wigley (2011). "Emulating coupled atmosphere-ocean and carbon cycle models with a simpler model, MAGICC6–Part 1: Model description and calibration". In: *Atmos. Chem. Phys.* 11.4, pp. 1417–1456.
- Melton, JR, Rita Wania, EL Hodson, B Poulter, Bruno Ringeval, Renato Spahni, T Bohn, CA Avis, DJ Beerling, G Chen, et al. (2013). "Present state of global wetland extent and wetland methane modelling: conclusions from a model inter-comparison project (WETCHIMP)". In: *Biogeosciences* 10.2, pp. 753–788.
- Monks, Paul Steven, AT Archibald, Augustin Colette, O Cooper, M Coyle, R Derwent, D Fowler, Claire Granier, Kathy S Law, GE Mills, et al. (2015). "Tropospheric ozone and its precursors from the urban to the global scale from air quality to short-lived climate forcer". In: *Atmos. Chem. Phys.* 15.15, pp. 8889–8973.
- Montzka, Stephen A, Maarten Krol, Edward Dlugokencky, Bradley Hall, Patrick Jöckel, and Jos Lelieveld (2011). "Small interannual variability of global atmospheric hydroxyl". In: *Science* 331.6013, pp. 67–69.
- Murray, Christopher JL, Aleksandr Y Aravkin, Peng Zheng, Cristiana Abbafati, Kaja M Abbas, Mohsen Abbasi-Kangevari, Foad Abd-Allah, Ahmed Abdelalim, Moham-

- mad Abdollahi, Ibrahim Abdollahpour, et al. (2020). “Global burden of 87 risk factors in 204 countries and territories, 1990–2019: a systematic analysis for the Global Burden of Disease Study 2019”. In: *Lancet* 396.10258, pp. 1223–1249.
- Murray, Lee T (2016). “Lightning NO_x and impacts on air quality”. In: *Current Pollution Reports* 2, pp. 115–133.
- Murray, Lee T, Arlene M Fiore, Drew T Shindell, Vaishali Naik, and Larry W Horowitz (2021). “Large uncertainties in global hydroxyl projections tied to fate of reactive nitrogen and carbon”. In: *Proc. Natl. Acad. Sci. U.S.A.* 118.43, e2115204118.
- Myhre, Gunnar, D. T. Shindell, FM Bréon, W Collins, J Fuglestedt, J Huang, D Koch, JF Lamarque, D Lee, B Mendoza, et al. (2013). *Anthropogenic and Natural Radiative Forcing, Climate Change 2013: The Physical Science Basis. Contribution of Working Group I to the Fifth Assessment Report of the Intergovernmental Panel on Climate Change, 659–740.*
- Naik, Vaishali, A Voulgarakis, Arlene M Fiore, Larry W Horowitz, J-F Lamarque, M Lin, Michael J Prather, PJ Young, Daniel Bergmann, PJ Cameron-Smith, et al. (2013). “Preindustrial to present-day changes in tropospheric hydroxyl radical and methane lifetime from the Atmospheric Chemistry and Climate Model Intercomparison Project (ACCMIP)”. In: *Atmos. Chem. Phys.* 13.10, pp. 5277–5298.
- Naus, Stijn, Stephen A Montzka, Prabir K Patra, and Maarten C Krol (2021). “A three-dimensional-model inversion of methyl chloroform to constrain the atmospheric oxidative capacity”. In: *Atmos. Chem. Phys.* 21.6, pp. 4809–4824.
- Nisbet, EG, EJ Dlugokencky, MR Manning, D Lowry, RE Fisher, JL France, SE Michel, JB Miller, JWC White, B Vaughn, et al. (2016). “Rising atmospheric methane: 2007–2014 growth and isotopic shift”. In: *Global Biogeochem Cycles* 30.9, pp. 1356–1370.

- Nisbet, EG, RE Fisher, D Lowry, JL France, G Allen, S Bakkaloglu, TJ Broderick, M Cain, M Coleman, J Fernandez, et al. (2020). “Methane mitigation: methods to reduce emissions, on the path to the Paris agreement”. In: *Rev. Geophys.* 58.1, e2019RG000675.
- Nisbet, Euan G, MR Manning, EJ Dlugokencky, RE Fisher, D Lowry, SE Michel, C Lund Myhre, Stephen Matthew Platt, G Allen, P Bousquet, et al. (2019). “Very strong atmospheric methane growth in the 4 years 2014–2017: Implications for the Paris Agreement”. In: *Global Biogeochem. Cy.* 33.3, pp. 318–342.
- Novelli, PC, KA Masarie, PM Lang, BD Hall, RC Myers, and JW Elkins (2003). “Re-analysis of tropospheric CO trends: Effects of the 1997–1998 wildfires”. In: *J. Geophys. Res.: Atmospheres* 108.D15.
- O’Connor, Fiona M, N Luke Abraham, Mohit Dalvi, Gerd A Folberth, Paul T Griffiths, Catherine Hardacre, Ben T Johnson, Ron Kahana, James Keeble, Byeonghyeon Kim, et al. (2021). “Assessment of pre-industrial to present-day anthropogenic climate forcing in UKESM1”. In: *Atmos. Chem. Phys.* 21.2, pp. 1211–1243.
- O’Neill, Brian C, Claudia Tebaldi, Detlef P Van Vuuren, Veronika Eyring, Pierre Friedlingstein, George Hurtt, Reto Knutti, Elmar Kriegler, Jean-Francois Lamarque, Jason Lowe, et al. (2016). “The scenario model intercomparison project (ScenarioMIP) for CMIP6”. In: *Geosci. Model Dev* 9.9, pp. 3461–3482.
- Ocko, Ilissa Bonnie, Tianyi Sun, D. T. Shindell, Michael Oppenheimer, Alexander N Hristov, Stephen W Pacala, Denise L Mauzerall, Yangyang Xu, and Steven P Hamburg (2021). “Acting rapidly to deploy readily available methane mitigation measures by sector can immediately slow global warming”. In: *Environ. Res. Lett.*
- Palazzo Corner, Sofia, Martin Siegert, Paulo Ceppi, Baylor Fox-Kemper, Thomas L Frölicher, Angela Gallego-Sala, Joanna Haigh, Gabriele C Hegerl, Chris D Jones, Reto Knutti, et al. (2023). “The Zero Emissions Commitment and climate stabilization”. In: *Frontiers in Science* 1, p. 1170744.

- Palmer, Paul I, Liang Feng, Mark F Lunt, Robert J Parker, Hartmut Bösch, Xin Lan, Alba Lorente, and Tobias Borsdorff (2021). “The added value of satellite observations of methane for understanding the contemporary methane budget”. In: *Philos. Trans. Royal Soc. A* 379.2210, p. 20210106.
- Prather, M. J., C. D. Holmes, and J. Hsu (2012). “Reactive greenhouse gas scenarios: Systematic exploration of uncertainties and the role of atmospheric chemistry”. In: *Geophys. Res. Lett.* 39.9.
- Prather, Michael J (1994). “Lifetimes and eigenstates in atmospheric chemistry”. In: *Geophys. Res. Lett.* 21.9, pp. 801–804.
- (1996). “Time scales in atmospheric chemistry: Theory, GWPs for CH₄ and CO, and runaway growth”. In: *Geophys. Res. Lett.* 23.19, pp. 2597–2600.
- (2007). “Lifetimes and time scales in atmospheric chemistry”. In: *Philos. Trans. Royal Soc. A* 365.1856, pp. 1705–1726.
- Price, Colin and David Rind (1992). “A simple lightning parameterization for calculating global lightning distributions”. In: *J. Geophys. Res. Atmos.* 97.D9, pp. 9919–9933.
- Prinn, RG, J Huang, RF Weiss, DM Cunnold, PJ Fraser, PG Simmonds, A McCulloch, C Harth, P Salameh, S O’doherly, et al. (2001). “Evidence for substantial variations of atmospheric hydroxyl radicals in the past two decades”. In: *Science* 292.5523, pp. 1882–1888.
- Prinn, RG, RF Weiss, BR Miller, J Huang, FN Alyea, D Mo Cunnold, PJ Fraser, DE Hartley, and PG Simmonds (1995). “Atmospheric trends and lifetime of CH₃CCl₃ and global OH concentrations”. In: *Science* 269.5221, pp. 187–192.
- Ramaswamy, Venkatachalam, M-L Chanin, J Angell, J Barnett, D Gaffen, M Gelman, P Keckhut, Y Koshelkov, K Labitzke, J-JR Lin, et al. (2001). “Stratospheric temper-

- ature trends: Observations and model simulations”. In: *Rev. Geophys.* 39.1, pp. 71–122.
- Ramaswamy, Venkatachalam, W Collins, J Haywood, J Lean, Natalie Mahowald, G Myhre, V Naik, Keith P Shine, B Soden, G Stenchikov, et al. (2019). “Radiative forcing of climate: the historical evolution of the radiative forcing concept, the forcing agents and their quantification, and applications”. In: *Meteorological Monographs* 59, pp. 14–1.
- Rap, A, NAD Richards, PM Forster, SA Monks, SR Arnold, and MP Chipperfield (2015). “Satellite constraint on the tropospheric ozone radiative effect”. In: *Geophys. Res. Lett.* 42.12, pp. 5074–5081.
- Rhodes, Rachael H, Xavier Faïn, Christopher Stowasser, Thomas Blunier, Jérôme Chappellaz, Joseph R McConnell, Daniele Romanini, Logan E Mitchell, and Edward J Brook (2013). “Continuous methane measurements from a late Holocene Greenland ice core: Atmospheric and in-situ signals”. In: *Earth Planet. Sci. Lett.* 368, pp. 9–19.
- Riahi, Keywan, Detlef P Van Vuuren, Elmar Kriegler, Jae Edmonds, Brian C O’neill, Shinichiro Fujimori, Nico Bauer, Katherine Calvin, Rob Dellink, Oliver Fricko, et al. (2017). “The shared socioeconomic pathways and their energy, land use, and greenhouse gas emissions implications: an overview”. In: *Glob Environ Change* 42, pp. 153–168.
- Rigby, Matthew, Stephen A. Montzka, Ronald G. Prinn, James W.C. White, Dickon Young, Simon O’Doherty, Mark F. Lunt, Anita L. Ganesan, Alistair J. Manning, Peter G. Simmonds, Peter K. Salameh, Christina M. Harth, Jens Mühle, Ray F. Weiss, Paul J. Fraser, L. Paul Steele, Paul B. Krummel, Archie McCulloch, and Sunyoung Park (2017). “Role of atmospheric oxidation in recent methane growth”. In: *Proc. Natl. Acad. Sci. U.S.A.* 114.21, pp. 5373–5377. ISSN: 10916490. DOI: 10.1073/pnas.1616426114.

- Rogelj, Joeri, Alexander Popp, Katherine V Calvin, Gunnar Luderer, Johannes Emmerling, David Gernaat, Shinichiro Fujimori, Jessica Strefler, Tomoko Hasegawa, Giacomo Marangoni, et al. (2018). “Scenarios towards limiting global mean temperature increase below 1.5 C”. In: *Nat Clim Chang* 8.4, pp. 325–332.
- Rubino, Mauro, David M Etheridge, David P Thornton, Russell Howden, Colin E Allison, Roger J Francey, Ray L Langenfelds, L Paul Steele, Cathy M Trudinger, Darren A Spencer, et al. (2019). “Revised records of atmospheric trace gases CO₂, CH₄, N₂O, and $\delta^{13}\text{C}$ -CO₂ over the last 2000 years from Law Dome, Antarctica”. In: *Earth Syst. Sci. Data* 11.2, pp. 473–492.
- Ruppel, Carolyn D and John D Kessler (2017). “The interaction of climate change and methane hydrates”. In: *Rev. Geophys.* 55.1, pp. 126–168.
- Saunois, Marielle, Ann R Stavert, Ben Poulter, Philippe Bousquet, Josep G Canadell, Robert B Jackson, Peter A Raymond, Edward J Dlugokencky, Sander Houweling, Prabir K Patra, et al. (2020). “The global methane budget 2000–2017”. In: *Earth Syst. Sci. Data* 12.3, pp. 1561–1623.
- Schumann, Ulrich and Heidi Huntrieser (2007). “The global lightning-induced nitrogen oxides source”. In: *Atmos. Chem. Phys.* 7.14, pp. 3823–3907.
- Seinfeld, John H and Spyros N Pandis (2016). *Atmospheric chemistry and physics: from air pollution to climate change*. John Wiley & Sons, pp. 175–196.
- Sellar, Alistair A., Colin G. Jones, Jane P. Mulcahy, Yongming Tang, Andrew Yool, Andy Wiltshire, Fiona M. O’Connor, Marc Stringer, Richard Hill, Julien Palmieri, Stephanie Woodward, Lee de Mora, Till Kuhlbrodt, Steven T. Rumbold, Douglas I. Kelley, Rich Ellis, Colin E. Johnson, Jeremy Walton, Nathan Luke Abraham, Martin B. Andrews, Timothy Andrews, Alex T. Archibald, Ségolène Berthou, Eleanor Burke, Ed Blockley, Ken Carslaw, Mohit Dalvi, John Edwards, Gerd A. Folberth, Nicola Gedney, Paul T. Griffiths, Anna B. Harper, Maggie A. Hendry, Alan J. Hewitt, Ben Johnson, Andy Jones, Chris D. Jones, James Keeble, Spencer Liddicoat,

- Olaf Morgenstern, Robert J. Parker, Valeriu Predoi, Eddy Robertson, Antony Siahhaan, Robin S. Smith, Ranjini Swaminathan, Matthew T. Woodhouse, Guang Zeng, and Mohamed Zerroukat (2019). “UKESM1: Description and Evaluation of the U.K. Earth System Model”. In: *J. Adv. Model. Earth Syst.*, pp. 4513–4558. ISSN: 19422466. DOI: 10.1029/2019MS001739.
- Shindell, D. T., N Borgford-Parnell, M Brauer, A Haines, JCI Kuylenstierna, SA Leonard, V Ramanathan, A Ravishankara, M Amann, and L Srivastava (2017a). “A climate policy pathway for near-and long-term benefits”. In: *Science* 356.6337, pp. 493–494.
- Shindell, D. T., Greg Faluvegi, Nadine Bell, and Gavin A. Schmidt (2005). “An emissions-based view of climate forcing by methane and tropospheric ozone”. In: *Geophys. Res. Lett.* 32.4, pp. 1–4. ISSN: 00948276. DOI: 10.1029/2004GL021900.
- Shindell, D. T., J. S. Fuglestvedt, and W. J. Collins (2017b). “The social cost of methane: theory and applications”. In: *Faraday Discuss.* 200, pp. 429–451.
- Shindell, D. T., A. R. Ravishankara, Johan C.I. Kuylenstierna, Eleni Michalopoulou, Lena Höglund-Isaksson, Yuqiang Zhang, Karl Seltzer, Muye Ru, Rithik Castelino, Greg Faluvegi, Vaishali Naik, Larry Horowitz, Jian He, Jean-Francois Lamarque, Kengo Sudo, William J. Collins, Chris Malley, Mathijs Harmsen, Krista Stark, Jared Junkin, Gray Li, Alex Glick, and Nathan Borgford-Parnell (2021). *Global Methane Assessment: Benefits and Costs of Mitigating Methane Emissions*. Nairobi: United Nations Environment Programme.
- Shine, Keith P (2009). “The global warming potential—the need for an interdisciplinary retrieval”. In: *Clim Change* 96.4, pp. 467–472.
- Shoemaker, Julie K, Daniel P Schrag, Mario J Molina, and Veerabhadran Ramanathan (2013). “What role for short-lived climate pollutants in mitigation policy?” In: *Science* 342.6164, pp. 1323–1324.

- Smith, KA, KE Dobbie, BC Ball, LR Bakken, BK Sitaula, S Hansen, R Brumme, W Borken, Søren Christensen, Anders Priemé, et al. (2000). “Oxidation of atmospheric methane in Northern European soils, comparison with other ecosystems, and uncertainties in the global terrestrial sink”. In: *Glob Chang Biol* 6.7, pp. 791–803.
- Solomon, Susan, John S Daniel, Todd J Sanford, Daniel M Murphy, Gian-Kasper Plattner, Reto Knutti, and Pierre Friedlingstein (2010). “Persistence of climate changes due to a range of greenhouse gases”. In: *Proceedings of the National Academy of Sciences* 107.43, pp. 18354–18359.
- Spivakovsky, CM, JA Logan, SA Montzka, YJ Balkanski, M Foreman-Fowler, DBA Jones, LW Horowitz, AC Fusco, CAM Brenninkmeijer, MJ Prather, et al. (2000). “Three-dimensional climatological distribution of tropospheric OH: Update and evaluation”. In: *J. Geophys. Res. Atmos.* 105.D7, pp. 8931–8980.
- Staniaszek, Zosia, Paul T Griffiths, Gerd A Folberth, Fiona M O’Connor, and Alexander T Archibald (2021). *UKCA-CH4 output for methane emissions-driven and methane LBC-driven future climate projections under SSP3-7.0 and SSP1-2.6 scenarios*.
- Staniaszek, Zosia, Paul T Griffiths, Gerd A Folberth, Fiona M O’Connor, N Luke Abraham, and Alexander T Archibald (2022). “The role of future anthropogenic methane emissions in air quality and climate”. In: *NPJ Clim Atmos Sci* 5.1, pp. 1–8.
- Stein, O, Martin G Schultz, Idir Bouarar, H Clark, V Huijnen, A Gaudel, Maya George, and Cathy Clerbaux (2014). “On the wintertime low bias of Northern Hemisphere carbon monoxide found in global model simulations”. In: *Atmos. Chem. Phys* 14.17, pp. 9295–9316.
- Stevenson, David S, Richard G Derwent, Oliver Wild, and William J Collins (2022). “COVID-19 lockdown emission reductions have the potential to explain over half of the coincident increase in global atmospheric methane”. In: *Atmos. Chem. Phys.* 22.21, pp. 14243–14252.

- Stevenson, David S, Alcide Zhao, Vaishali Naik, Fiona M O’connor, Simone Tilmes, Guang Zeng, Lee T Murray, William J Collins, Paul T Griffiths, Sungbo Shim, et al. (2020). “Trends in global tropospheric hydroxyl radical and methane lifetime since 1850 from AerChemMIP”. In: *Atmos. Chem. Phys.* 20.21, pp. 12905–12920.
- Stockwell, DZ, C Giannakopoulos, P-H Plantevin, GD Carver, MP Chipperfield, KS Law, JA Pyle, DE Shallcross, and K-Y Wang (1999). “Modelling NO_x from lightning and its impact on global chemical fields”. In: *Atmos. Environ.* 33.27, pp. 4477–4493.
- Stohl, A., B. Aamaas, M. Amann, L. H. Baker, N. Bellouin, T. K. Berntsen, O. Boucher, R. Cherian, W. Collins, N. Daskalakis, M. Dusinska, S. Eckhardt, J. S. Fuglestvedt, M. Harju, C. Heyes, Ø. Hodnebrog, J. Hao, U. Im, M. Kanakidou, Z. Klimont, K. Kupiainen, K. S. Law, M. T. Lund, R. Maas, C. R. MacIntosh, G. Myhre, S. Myriokefalitakis, D. Olivie, J. Quaas, B. Quennehen, J.-C. Raut, S. T. Rumbold, B. H. Samset, M. Schulz, Ø. Seland, K. P. Shine, R. B. Skeie, S. Wang, K. E. Yttri, and T. Zhu (2015). “Evaluating the climate and air quality impacts of short-lived pollutants”. In: *Atmos. Chem. Phys.* 15.18, pp. 10529–10566. ISSN: 1680-7324. DOI: 10.5194/acp-15-10529-2015.
- Stolarski, Richard, Rumen Bojkov, Lane Bishop, Christos Zerefos, Johannes Staehelin, and Joseph Zawodny (1992). “Measured trends in stratospheric ozone”. In: *Science* 256.5055, pp. 342–349.
- Stone, Daniel, Lisa K Whalley, and Dwayne E Heard (2012). “Tropospheric OH and HO₂ radicals: Field measurements and model comparisons”. In: *Chem. Soc. Rev.* 41.19, pp. 6348–6404.
- Sun, Haitong Zhe, Pei Yu, Changxin Lan, Michelle WL Wan, Sebastian Hickman, Jayaprakash Murulitharan, Huizhong Shen, Le Yuan, Yuming Guo, and Alexander T Archibald (2022). “Cohort-based long-term ozone exposure-associated mortality risks with adjusted metrics: a systematic review and meta-analysis”. In: *The Innovation*.

- Tarasick, David, Ian E Galbally, Owen R Cooper, Martin G Schultz, Gerard Ancellet, Thierry Leblanc, Timothy J Wallington, Jerry Ziemke, Xiong Liu, Martin Steinbacher, et al. (2019). “Tropospheric Ozone Assessment Report: Tropospheric ozone from 1877 to 2016, observed levels, trends and uncertainties”. In: *Elementa: Science of the Anthropocene* 7.
- Task Force on Hemispheric Transport of Air Pollution (2010). *Hemispheric Transport of Air Pollution*.
- Thiery, Wim, Stefan Lange, Joeri Rogelj, Carl-Friedrich Schleussner, Lukas Gudmundsson, Sonia I Seneviratne, Marina Andrijevic, Katja Frieler, Kerry Emanuel, Tobias Geiger, et al. (2021). “Intergenerational inequities in exposure to climate extremes”. In: *Science* 374.6564, pp. 158–160.
- Thornhill, Gillian, William Collins, Dirk Olivié, Ragnhild B Skeie, Alex Archibald, Susanne Bauer, Ramiro Checa-Garcia, Stephanie Fiedler, Gerd Folberth, Ada Gjermandsen, et al. (2021a). “Climate-driven chemistry and aerosol feedbacks in CMIP6 Earth system models”. In: *Atmos. Chem. Phys.* 21.2, pp. 1105–1126.
- Thornhill, Gillian D, William J Collins, Ryan J Kramer, Dirk Olivié, Ragnhild B Skeie, Fiona M O’Connor, Nathan Luke Abraham, Ramiro Checa-Garcia, Susanne E Bauer, Makoto Deushi, et al. (2021b). “Effective radiative forcing from emissions of reactive gases and aerosols—a multi-model comparison”. In: *Atmos. Chem. Phys.* 21.2, pp. 853–874.
- Treat, Claire C and Steve Frohking (2013). “A permafrost carbon bomb?” In: *Nat Clim Chang* 3.10, pp. 865–867.
- Turner, Alexander J, Christian Frankenberg, Paul O Wennberg, and Daniel J Jacob (2017). “Ambiguity in the causes for decadal trends in atmospheric methane and hydroxyl”. In: *Proc. Natl. Acad. Sci. U.S.A.* 114.21, pp. 5367–5372.
- UNEP / WMO (2011). *Integrated assessment of black carbon and tropospheric ozone*.

UNFCCC (2015). *The Paris Agreement*. Last accessed August 2023. URL: <https://unfccc.int/process-and-meetings/the-paris-agreement/the-paris-agreement>.

— (2021). *Nationally determined contributions under the Paris Agreement, Synthesis Report*. <https://unfccc.int/news/full-ndc-synthesis-report-some-progress-but-still-a-big-concern>.

US EPA (2019). *Global Non-CO2 Greenhouse Gas Emission Projections & Mitigation 2015-2050*.

Van Marle, Margreet JE, Silvia Kloster, Brian I Magi, Jennifer R Marlon, Anne-Laure Daniau, Robert D Field, Almut Arneth, Matthew Forrest, Stijn Hantson, Natalie M Kehrwald, et al. (2017). “Historic global biomass burning emissions for CMIP6 (BB4CMIP) based on merging satellite observations with proxies and fire models (1750–2015)”. In: *Geosci Model Dev* 10.9, pp. 3329–3357.

Van Vuuren, Detlef P, Elke Stehfest, David EHJ Gernaat, Jonathan C Doelman, Maarten Van den Berg, Mathijs Harmsen, Harmen Sytze de Boer, Lex F Bouwman, Vassilis Daioglou, Oreane Y Edelenbosch, et al. (2017). “Energy, land-use and greenhouse gas emissions trajectories under a green growth paradigm”. In: *Glob Environ Change* 42, pp. 237–250.

Virtanen, Pauli, Ralf Gommers, Travis E. Oliphant, Matt Haberland, Tyler Reddy, David Cournapeau, Evgeni Burovski, Pearu Peterson, Warren Weckesser, Jonathan Bright, Stéfan J. van der Walt, Matthew Brett, Joshua Wilson, K. Jarrod Millman, Nikolay Mayorov, Andrew R. J. Nelson, Eric Jones, Robert Kern, Eric Larson, CJ Carey, İlhan Polat, Yu Feng, Eric W. Moore, Jake VanderPlas, Denis Laxalde, Josef Perktold, Robert Cimrman, Ian Henriksen, E. A. Quintero, Charles R Harris, Anne M. Archibald, Antônio H. Ribeiro, Fabian Pedregosa, Paul van Mulbregt, and SciPy 1.0 Contributors (2020). “SciPy 1.0: Fundamental Algorithms for Scientific Computing in Python”. In: *Nat. Methods* 17, pp. 261–272. DOI: 10.1038/s41592-019-0686-2.

- Voulgarakis, A, V Naik, J.-F Lamarque, D T Shindell, P J Young, M J Prather, O Wild, R D Field, D Bergmann, P Cameron-Smith, I Cionni, W J Collins, S B Dalsøren, R M Doherty, V Eyring, G Faluvegi, G A Folberth, L W Horowitz, I A Mackenzie, T Nagashima, D A Plummer, M Righi, S T Rumbold, D S Stevenson, S A Strode, K Sudo, S Szopa, and G Zeng (2013). “Sciences ess Atmospheric Chemistry and Physics Climate of the Past Geoscientific Instrumentation Methods and Data Systems Analysis of present day and future OH and methane lifetime in the ACCMIP simulations”. In: *Atmos. Chem. Phys* 13, pp. 2563–2587. DOI: 10.5194/acp-13-2563-2013.
- Wang, Xuan, Daniel J Jacob, Sebastian D Eastham, Melissa P Sulprizio, Lei Zhu, Qianjie Chen, Becky Alexander, Tomás Sherwen, Mathew J Evans, Ben H Lee, et al. (2019). “The role of chlorine in global tropospheric chemistry”. In: *Atmos. Chem. Phys.* 19.6, pp. 3981–4003.
- Wang, Yuhang and Daniel J Jacob (1998). “Anthropogenic forcing on tropospheric ozone and OH since preindustrial times”. In: *J. Geophys. Res. Atmos.* 103.D23, pp. 31123–31135.
- Wayne, Richard P. (Richard Peer) (2006). *Chemistry of atmospheres : an introduction to the chemistry of the atmospheres of Earth, the planets, and their satellites / Richard P. Wayne*. 3rd ed. Oxford University Press, pp. 50–63. ISBN: 9780198503750.
- West, J Jason, Arlene M Fiore, and Larry W Horowitz (2012). “Scenarios of methane emission reductions to 2030: abatement costs and co-benefits to ozone air quality and human mortality”. In: *Clim Change* 114.3-4, pp. 441–461.
- Wofsy, SC, S Afshar, HM Allen, E Apel, EC Asher, B Barletta, J Bent, H Bian, BC Biggs, DR Blake, et al. (2018). *ATom: Merged Atmospheric Chemistry, Trace Gases, and Aerosols, ORNL DAAC, Oak Ridge, Tennessee, USA*.
- Wolfe, Glenn M, Julie M Nicely, Jason M St Clair, Thomas F Hanisco, Jin Liao, Luke D Oman, William B Brune, David Miller, Alexander Thames, Gonzalo González

- Abad, et al. (2019). “Mapping hydroxyl variability throughout the global remote troposphere via synthesis of airborne and satellite formaldehyde observations”. In: *Proc. Natl. Acad. Sci. U.S.A.* 116.23, pp. 11171–11180.
- Yurganov, Leonid N, Thomas Blumenstock, EI Grechko, Frank Hase, EJ Hyer, ES Kasischke, M Koike, Y Kondo, Isabell Kramer, F-Y Leung, et al. (2004). “A quantitative assessment of the 1998 carbon monoxide emission anomaly in the Northern Hemisphere based on total column and surface concentration measurements”. In: *J. Geophys. Res.: Atmospheres* 109.D15.
- Zhang, Zhen, Etienne Fluet-Chouinard, Katherine Jensen, Kyle McDonald, Gustaf Hugelius, Thomas Gumbrecht, Mark Carroll, Catherine Prigent, Annett Bartsch, and Benjamin Poulter (2021). “Development of the global dataset of Wetland Area and Dynamics for Methane Modeling (WAD2M)”. In: *Earth Syst. Sci. Data* 13.5, pp. 2001–2023.
- Zhang, Zhen, Benjamin Poulter, Andrew F Feldman, Qing Ying, Philippe Ciais, Shushi Peng, and Xin Li (2023). “Recent intensification of wetland methane feedback”. In: *Nat Clim Chang*, pp. 1–4.
- Zhang, Zhen, Benjamin Poulter, Sara Knox, Ann Stavert, Gavin McNicol, Etienne Fluet-Chouinard, Aryeh Feinberg, Yuanhong Zhao, Philippe Bousquet, Josep G Canadell, et al. (2022). “Anthropogenic emission is the main contributor to the rise of atmospheric methane during 1993–2017”. In: *Natl. Sci. Rev.* 9.5, nwab200.
- Zhang, Zhen, Niklaus E Zimmermann, Andrea Stenke, Xin Li, Elke L Hodson, Gaofeng Zhu, Chunlin Huang, and Benjamin Poulter (2017). “Emerging role of wetland methane emissions in driving 21st century climate change”. In: *Proc. Natl. Acad. Sci. U.S.A.* 114.36, pp. 9647–9652.